UNIVERSITÄT ZU LÜBECK
INSTITUTE OF COMPUTER ENGINEERING

From Institute of Computer Engineering
of the University of Lübeck
Prof. Dr.-Ing. Erik Maehle

SEMBIO - An Energy Efficient Micro Underwater Robot for Swarm Applications

Dissertation
for Fulfillment of
Requirements
for the Doctoral Degree
of the University of Lübeck

from the Department of Computer Sciences

Submitted by

Ammar Amory

from Aleppo, Syria.

Lübeck, August 31, 2018

1. First referee: Prof. Dr.-Ing. Erik Maehle
2. Second referee: Prof. Dr.-Ing. Andreas Schrader

Date of oral examination August 29, 2018

Approved for printing. Lübeck, August 31, 2018

Acknowledgements

Without the support of a number of people, it would not have been possible for the research in this thesis successfully. First and foremost, I would like to convey my humble gratitude to my principal supervisor, Prof. Dr.-Ing. Erik Maehle, who over time became my guide in the world academia during this project. Thank you for engaging me intellectually; for teaching me about the current state of robotics research; for believing in me throughout this research; and for having a true sense of patience, honesty, and support. I would also like to thank Marek Litza and Dr. Thomas Tosik for their invaluable assistance in all aspects of my research. Thank you to my colleagues at the Institute of Computer Engineering for their continuous support, along with the fantastic and friendly environment they maintained. I extend special thanks to the intelligent, dynamic, and positive Dipl.-Ing. Ulrich Behrje. I was a blessing to work with him, and we spent many fun hours conducting robotics research and experiments within the institute. I am grateful for him offering to continue supporting me and my research, especially in the field of control systems.

I would also like to thank Dr. Ahmad Al-Homsy for engaging me in interesting discussions over lunch, and more generally the friendly atmosphere that has made these years an enlightening and enjoyable experience. I am sincerely thankful to Dr. Bashar Altakrouri for all the support given during my research and thesis preparations; your advice has been extremely helpful during these stressful times. I would also like to thank Dr. Patrick Weiß for special support during this work. Many Thanks go to Ines Schieban for supporting me and proofreading. Moreover, thanks to the students I have worked with for their effort and diligence, especially Sönke Hennings.

I owe my deepest thanks to my family for their unconditional and selfless support. This thesis certainly would not have existed without them. Special thanks, my highest appreciation, and respect go to the people who are dearest to my heart: my mother and father. They have provided a constant source of support and encouragement during these years. They were the first to teach me the noble and exciting meanings of asking questions and searching for answers, and the first to teach me what patience really means. To them, I dedicate this thesis. Moreover, to my lovely brothers and sister, I am grateful for having had you by my side during this long journey.

From the depths of my heart, I would like to give my special thanks to my dear wife, Khansaa Alyosif for her love, patience, and understanding. The ideal partner in life, my wife has been always my strength and guiding light. Thank you for tolerating

me, for caring for me, and making sure that I had the best possible environment in which to finish this work. My sons, Mohammed, Yamaan, and Abdulrahman, who have filled my heart with love, have always been present as inspiring candles, lighting the world with happiness and joy. To my friend in Lübeck, Radwan Hamdoun and his family, thank you for making my stay in Germany a smooth, enjoyable, and unforgettable experience.

Last, but by no means least, I thank all those who supported and contributed to the completion of my research work and thesis.

Erklärung

Ich versichere, die vorliegende Arbeit selbstständig und nur unter Benutzung der angegebenen Hilfsmittel angefertigt zu haben.

Lübeck, August 31, 2018

Zusammenfassung

In den letzten Jahren zielten sowohl praktische als auch wissenschaftliche Initiativen darauf ab, die Fähigkeiten von autonomen Unterwasserfahrzeugen (AUV) auszunutzen, sie zu verbessern und weiterzuentwickeln. Zum großen Teil wurden diese Initiativen durch die zunehmende Tendenz zur Unterwasser-Erkundung vorangetrieben. Da AUVs als Instrumente der Datenerfassung unentbehrlich sind, sieht ihre Fortentwicklung zu einem fundamentalen Schlüssel zur weiteren Erkundung der Unterwasserwelt vielversprechend aus. Gegenwärtig werden AUVs zur Erforschung der Weltmeere, egal ob flach oder tief, konzipiert. Zudem dienen sie der Verfolgung der Verbreitung von Verschmutzungen, der Untersuchung von Algenblüten und der Kontrolle der Wasserqualität. Eine der bemerkenswertesten Entwicklungen der letzten Jahre ist die Zusammenstellung und der Einsatz von AUV-Schwärmen.

AUV-Schwärme sind besonders vorteilhaft, wenn sie in relativ großen Unterwasserregionen eingesetzt werden. In solchen Situationen sammeln AUV-Schwärme Daten mit einer Rate, die weit über dem liegt, welche ein einzeln agierender AUV erreichen kann. Zusammen mit Forschungen, die bereits zu Entwicklungen im Bereich der Schwarm-Parallelität geführt haben, beinhalten weitere bemerkenswerte Weiterentwicklungen einfache Kontrollalgorithmen, welche zum auftretenden kollektiven Verhalten beitragen. Erwähnenswert ist, dass die lokal interagierenden Teilnehmer den Einsatz preiswerter Sensoren und Ausstattungen erlauben, welche sich vorteilhaft auf die Kosteneffektivität des einzelnen AUVs auswirken. Eine Mission kann auch bei auftretenden Problemen bei einem oder mehreren Robotern erfüllt werden.

Die vorliegende Arbeit hat nun das Ziel, das Potential im Zusammenhang mit dem Einsatz kostengünstiger Micro-AUVs SEMBIO mit der Fähigkeit zur Schwarmbildung auszuschöpfen, die sich durch ihre Agilität, Kompaktheit, Zuverlässigkeit, Wirtschaftlichkeit, Robustheit und Energieeffizienz auszeichnen. Für dieses Projekt ist ein überschaubarer Rahmen vorgesehen und seine Entwicklung zielt auf den Einsatz eines AUV Schwarms zur Überwachung und Umweltmonitoring in küstennahen und Binnengewässern ab. In Bezug auf die verwendete AUV-Konstruktion und Entwicklung verwendet dieses Projekt ein mechanisches und elektrisches System basierend auf dem Stromversorgungs-System, der Rechnerarchitektur und der Sensorik. Zudem wurden weitere Teilsysteme in den Entwurfs- und Entwicklungsprozess eingebunden. Die abgeflachten und stromlinienförmigen Micro-AUVs sind im Wesentlichen der Natur nachempfunden. Durch eine hydromechanische Analyse ist es möglich, den Widerstandsfaktor zu minimieren und dadurch die Energieeffizienz während der Bewegung (besonders in einer Unterwasserumgebung) zu maximieren. Darüber hinaus schlägt diese Arbeit ein Energiemanagementsystem vor und imple-

mentiert dieses. Sein Zweck besteht darin, die begrenzten bordseitigen Energieressourcen zu überwachen und zu kontrollieren und dadurch die Energieeffizienz zu steigern.

In Bezug auf die Systemidentifizierung, welche ausgeführt wird, um Modelleinschränkungen für die beabsichtigte vertikale Bewegung des AUVs zu erkennen und damit die Tiefenregelung des Fahrzeugs zu verbessern und zu entwickeln, wird in dieser Arbeit ein dynamisches Model angewandt, für das wiederum Daten mit Hilfe der bordseitigen Sensoren gesammelt werden, um die zugehörigen Parameter zu ermitteln.

Ein naheliegender Leader-Follower-Algorithmus wurde für den Zweck der Simulation und Visualisierung des Verhaltens mehrerer AUVs implementiert. Hinzu kommt ein Lastbalancierungskonzept, um die Vorteile bezüglich des Teamverhaltens zu maximieren, damit die Gesamtmissionszeit erhöht, die Fehlertoleranz positiv beeinflusst und die Energieeffizienz maximiert wird.

Abstract

In recent years, both practical and academic initiatives have sought to capitalize on, improve, and further develop many of the capabilities of Autonomous Underwater Vehicle (AUV). In large part, these initiatives have been promoted by the increasing trend towards underwater exploration. Since AUVs are invaluable as data-gathering instruments, their ongoing development is one of the fundamental keys to further illumination of the underwater world. AUVs are currently being created to investigate the Earth's oceans, shallow and deep alike, and they are usefully tracking the proliferation of pollution, investigating harmful algal blooms, and monitoring water quality. One of the most notable developments in recent years has been the construction and deployment of AUV swarms.

Swarm AUVs are particularly advantageous when deployed in sizeable underwater territories. In these situations, swarm AUVs gather data at a rate that far outpaces an AUV operating in isolation. With research already having contributed to developments in the domain of swarm parallelism, other notable advancements include simple control algorithms, which contribute to emergent collective behavior. It is worth noting that participants' local interaction permits the employment of low-cost sensors and equipment, which is benefit for promoting the cost-effectiveness of single AUVs; a mission can be maintained even if there are problems with one or more robots.

The present thesis is now seeking to exploit the potential associated with the use of an inexpensive micro AUV SEMBIO with swarm capability that is characterized by agility, compactness, reliability, cost-effectiveness, robustness, and energy-efficiency. This project is intended to be hand-sized, and its task is focused towards deploying swarm AUVs for observation and environmental monitoring in coastal and inland aquatic areas. In terms of the proposed AUV's design and development, this project implemented a mechanical and electrical system based on the power system design, computer architecture, and sensor considerations. Additionally, other subsystems were integrated into the design and development process. For the most part, the flattened and streamlined micro AUV was designed under the aspects of natural principles. Conducting a hydrodynamic analysis enabled the minimization of the drag factor, thus maximizing energy efficiency when in motion (especially in submarine environments). Furthermore, this thesis proposed and implemented an energy management system, the purpose being to monitor and supervise restricted on-board energy resources and, thus, further heightening energy efficiency.

With respect to the system identification conducted to identify model constraints for the proposed micro AUV's vertical motion in order to improve and develop the

vehicle's control system, this thesis applied a dynamic model and, in turn, collected data using on-board sensors to identify related parameters.

A straightforward leader–follower approach was implemented to simulate and illustrate multiple AUVs' behavior. In addition, a load-balancing approach was applied to maximize the advantages associated with the leader–follower approach, thereby augmenting the overall mission time, favorably impacting fault-tolerance, and maximizing energy efficiency.

Contents

1 Introduction

The field of autonomous robotics has become increasingly important in our lives over the last decade. An Autonomous Underwater Vehicle (AUV) is an untethered robotic device that operates underwater and moves through the water using a propulsion system. It is typically powered by batteries and has no physical link or any external cable to the surface [100]. Vehicles such as AUVs are provided with actuators, sensors, and a control system by an on-board computer and are maneuverable in three dimensions to successfully complete surveys and gather data from the environment without human supervision. The missions undertaken by AUVs are typically preprogrammed and permit the AUV to follow trajectories wherever and whenever required [219].

1.1 Motivation

More than two-thirds of the earth's surface is covered with water. This water environment, which includes oceans, seas, rivers, coasts and shores, is a priceless resource and has a significant effect on the future existence of human beings. Thus, exploring our marine environments, protecting water resources from pollution, tracking harmful algal blooms and pollution spread, and monitoring the water quality are prerequisites when utilizing water resources for human welfare. Furthermore, the water environment represents an important and valuable site for scientific research and investigation across a wide variety of areas [98, 115, 186].

Obtaining underwater data within biological, chemical, and physical parameters is currently an expensive and time-consuming activity [114]. In order to obtain underwater data, understand this environment, and model and track the involved phenomena, large amounts of accurate spatial and temporal dispersion data are required [122, 156, 163]. In other words, a large range of precise in-situ sensors is required to track physical variables (such as a Conductivity Temperature Depth (CTD) profiler, oxygen measurements, salinity, and flow), chemical variables (such as pH, nitrate, and hydrocarbons), and biological parameters (such as chlorophyll and dissolved organic matter). This means that sensors are important elements that are usually deployed over a large field to periodically collect data. For instance, meteorologists seek to monitor a set of physical variables, such as temperature and air pressure, to study the weather and to forecast its behavior.

Over the past few decades, underwater measurements have typically been achieved by either professional divers or manually by lowering a probe from a ship or fixed moorings. However, the dangers of water environments restrict the capabilities of human divers, who cannot access hazardous or deep underwater regions. Moreover, the fixed moorings or probes lowered from a ship are available at very few spots and, thus, the amount of spatial data that can be collected is limited.

Therefore, to meet these data requirements, present-day remote sensing techniques are typically used and supported by local fixed monitoring stations. On a global scale, satellite techniques are used [115, 190, 237], while on a local scale, manual and automated sampling is performed. These techniques can be extremely difficult and often limit data collection, especially during bad weather conditions. Furthermore, local scale sampling is often costly, and it is difficult to maintain persistent sampling. However, sensor networks, which are commonly used on land and have emerged as a new tool to collect spatially dense information in real time from the natural world, are not as effective when they are used in water environments. Moreover, because sensor networks are distributed and fixed in specific locations, they can only provide fixed monitoring points without the ability to adjust to changes in the surrounding environment.

Increasing requirements to utilize underwater resources to the fullest extent have led researchers to contemplate how to increase data collection efficiencies, especially in harsh environments. Marine scientists and oceanographers believe that the Underwater Vehicle (UV) is a promising tool with the capacity to improve their current capabilities to explore, understand, monitor, and collect data about natural processes or phenomena at enormous spatial and temporal scales [43, 140, 242].

Oceanographers have been at the forefront of the earth sciences in using underwater robots to survey the deep ocean and seafloor [227]. Most commercially available underwater vehicles are tethered and can be remotely operated, making them the ideal choice in underwater exploration. These vehicles are referred to as Remotely Operated Vehicle (ROV). As ROVs are controlled by a human being with communication links on the base of the tether (cable, fiber optics, etc.), and because of the high operational costs of the mother vessels, operator fatigue, and safety issues, the use of ROVs is currently limited to just a few applications. This has led to the emergence of a variety of research efforts that have increased the autonomy of marine robotic vehicles and minimized the need for the participation of human operators in order to obtain a self-contained, intelligent, decision-making autonomous robotic vehicle.

Many scientists have indicated in their research that AUVs are currently the most important tool in obtaining large amounts of underwater environment data [24, 29, 34, 53, 56, 95, 127, 232, 236]. In fact, the AUVs that are increasingly being employed as data gathering tools by scientists have already been in use for many years to explore our marine environments; monitor and survey coasts, shores, deep oceans, and seas, which carry sonar sensors; and to extend the reach of these instruments.

In addition, the many capabilities of AUVs have enabled their use for a wide range of underwater applications. For example, AUVs can scan large areas of the seafloor and take samples autonomously. Oil and gas industries use the capabilities of AUVs not only to inspect pipelines, but also to carry out maintenance on their undersea equipment, while the military utilizes the benefits of AUVs to detect and destroy mines without jeopardizing human life.

Due to advancements in technology, AUVs now feature new and better sensors, along with smart algorithms to enable them to work more autonomously, especially in highly unstructured environments such as deep oceans [228]. However, these requirements are special and very precise and, therefore, need very expensive sensors for accurate orientation. Such costs mean that the price of an AUV can range from \$50,000–\$5,000,000 per AUV, which is very expensive [147].

Furthermore, commercial AUVs have a mission duration on average of less than 10 hours, and their average speed in the water is about two knots. These vehicles require a correspondingly long time to execute an investigation mission. In addition, the majority of operators can often afford only one AUV, which reduces the volume of water that can be explored within a specific time frame. During environmental monitoring, some natural phenomena can change drastically over time and space, and, thus, measurements taken in a single spot, or by only one AUV, are insufficient. Moreover, due to their size and very high costs, the researchers that typically use AUVs mostly work in oceanography and sometimes in limnology and environmental monitoring applications [25].

A much better scenario for environmental monitoring applications can be obtained by measuring using many sensors at many places simultaneously using a fleet of AUVs featuring actuated sensor platforms that might behave independently or in cooperative swarms and which can cooperatively obtain high resolution water quality measurements of natural water bodies, coasts, or shores. Of course, the use of several AUVs would decrease the time of the mission, but that would certainly lead to an increase in investment costs. Thus, the big question is: How can the use of several AUVs be made cost effective?

As most research labs and companies working in the field of AUVs are focused on large-sized underwater vehicles for use in oceanography, there is a demand for a reduction in the costs of AUVs to increase their application, especially in shallow water. In addition, due to the development of more advanced processing capabilities of tiny chips and micro-sensing systems, the creation of a small or micro, portable, and cost-effective AUV is progressing more and more. Thus, a micro AUV would most likely be the next generation of underwater vehicles, and could contribute strongly to the establishment of a swarm at a lower cost while offering many additional advantages.

Instead of a single expensive, complex, and limited AUV, a swarm of inexpensive, simple, and small AUVs offers very great advantages, especially in the area of environmental monitoring. Having cooperating AUVs that create a swarm increases the

service area and provides redundancy when solving complex underwater tasks [197]. The natural concept of the swarm and its emergence behavior results in very simple control algorithms. It is sufficient to provide each member of the swarm with basic sensors without the need for great accuracy or a wide range [63, 180]. Through self-organization, the swarm is able to search a large area using only a simple algorithm. In addition, there are other advantages, such as redundancy by data acquisition, allowing the swarm to continue to operate even if one or more members of the swarm fail.

1.2 Research Objective and Overview

The objective of this research is to develop and design an inexpensive, small (portable in one hand), and streamline-shaped AUV that can be employed in swarm robotics research, particularly for environmental monitoring applications in most inland and coastal waters. One important point that has to be highlighted during this research is the energy consumption. This is considered by using a streamlined AUV shape centered around reducing hydrodynamic resistance. In addition, an energy management system is created to monitor and manage the power resources in the robot to prolong the mission time. Still, the environmental monitoring of water bodies, coasts, and shores remains challenged by several pressing issues, some of which are discussed in the scope of this thesis. The following is a brief listing of the objectives of this work:

- As will be outlined in Chapter 2, traditional AUVs are too large to be used in swarm applications, meaning a new, smaller vehicle is required. Thus, one of the most important objectives of this research is to establish and construct a mechanical design for a micro AUV and related provisions for mobility, power systems, and motion control that are suitable for the swarm application. The AUV is designed so that it can be produced cost-effectively in large quantities.

- The energy consumption of the streamline-shaped micro AUV (named SEMBIO) will be improved by optimizing the vehicle's hull design to achieve satisfactory hydrodynamic coefficients.

- We will analyze the SEMBIO model to obtain hydrodynamic properties data and to calculate fluid flow parameters, such as velocity and pressure distributions.

- The SEMBIO model will be provisioned with mobility, electrical and power systems, and motion control, and we will identify, model, and analyze the preliminary controller of SEMBIO.

- A solar and energy management system able to measure the power consumption of the AUV's elements will be established in order to control energy resources.

- This work will demonstrate a simulation of the load-balancing behavior concept that uses a swarm of AUVs to prolong the overall mission time.

This work is divided into three phases. The first phase is concerned with the design and construction of the micro AUV, including not only the mechanical system, but also the electrical system of the AUV. The second phase involves the identification, modeling and preliminary control analysis, and energy management of the vehicle. The third phase involves the load-balancing behavior when employing a swarm of AUVs.

1.3 Thesis Structure

Every chapter starts with a brief introduction and general and theoretical survey of the subject, which covers the background, methodology developed during the research, experimental results and analyses, extensions, and conclusions. This thesis is structured as follows:

Chapter 1 - Introduction

This chapter describes the motivation for and aims of this work.

Chapter 2 - Mechatronic Requirements and Related Work

This chapter begins by outlining the mechatronic requirements for this work that are related to the AUV design. It highlights and reviews existing state-of-the-art underwater vehicle technology and presents the classification of the AUVs according to length, weight, and application. It concludes by identifying which systems may be of interest to this project.

Chapter 3 - Dynamic Model and Parameters Estimation

This chapter describes the fundamental equations and associated notations that will be applied in whole chapters. It also provides a general discussion about the kinematic and dynamic models of an AUV. In addition, another major objective of the this chapter is to identify and to briefly discuss the most important factors that require consideration during the process of designing an underwater vehicle.

Chapter 4 - Propulsion Systems of a Micro AUV

This chapter reviews and compares many different propulsion systems that are used in underwater vehicles to provide both vertical and horizontal movements. Many factors are considered by selecting the propulsion systems such as energy consumption, size, thrust, mechanical complexity, and cost. The most suitable propulsion system is selected after several comparisons between multiple option.

Chapter 5 - Mechanical Design of the Micro AUV SEMBIO

Chapter 5 focuses on the design of the proposed underwater vehicle, SEMBIO. The chapter addresses the processes of mechanical design, such as drawing, construction, and 3D printing along with SEMBIO assembly and its electrical design. In addition, this chapter covers electrical design, such as sensing capacity, and embedded systems. CFD and SolidWorks permitted a hydrodynamic analysis of SEMBIO to identify potential hull improvements, and a comparison of the CFD results of SEMBIO and MONSUN is conducted.

Chapter 6 - Vertical Motion Control for SEMBIO

This chapter presents the development of the control systems for vertical motion of the SEMBIO AUV using system identification tools in MATLAB. The controller was implemented on the SEMBIO prototype and experiments were conducted at facilities both within the university and in a swimming pool.

Chapter 7 - Solar and Energy Management System

In this chapter, an energy management system for SEMBIO's energy consumption is presented. This system attempts to reduce the energy consumption and prolong the mission time by controlling the restricted on-board energy source. Emergency and solar systems are presented to facilitate retrieval of the vehicle in emergency situations.

Chapter 8 - Load Balancing Approach to Increase Mission Time of Multiple AUVs

Chapter 8 illustrates a leader–follower approach for a multiple AUVs. The algorithm is conducted using the MARS simulator to illustrate the behavior

of the multiple of AUVs. A load-balancing approach is proposed to prolong the overall mission time with consideration of energy and fault-tolerance.

Chapter 9 - Conclusion and Future Work

This final chapter summarizes the general conclusions of this thesis. This work's achievements and contributions to the field of underwater robotics are concluded. Finally, an outlook for future challenges and possible improvements are presented.

2
Mechatronic Requirements and Related Work

As mentioned in Section 1.1 and Section 1.2, environmental monitoring applications in shallow water are more effective when using swarm robotics, which in turn requires the use of a simple, inexpensive, and small or micro AUV that can be produced cost-effectively in large quantities.

Lakes and shallow waters, such as coasts, cover relatively small area compared with oceans, where traditional AUVs are used. This leads to the first point, namely, that the size of the vehicle has to be appropriately scaled down. The second point is that the design of the AUV has to be energy-efficient to increase the mission time of the swarms and reduce the operating costs. The third point is that AUVs must be cost-effective to be produced in large quantities.

The size, cost-effectiveness, and energy efficiency of the AUV that has been developed in this research are what differentiates it from traditional designs.

2.1 Mechatronic Requirements

There are several design-related mechatronic requirements that are universal across different applications. Therefore, some of the mechatronic requirements for this work are essential with regard to the AUV design, while other requirements are application-specific. The mechatronic requirements for this work are summarized as follows:

- Our design goals were to develop an AUV that was small enough to be carried with one hand in order to minimize the costs to transport the vehicle to the mission place. The low weight of the vehicle makes it easily deployable by hand, from a shore or a boat.

- The AUV has to be able to move at least in three Degrees Of Freedom (DOF), the surge, heave, and yaw being most important to maneuver the vehicle into any position in the vertical and horizontal planes [75]. However, using four or five DOFs is preferred when the maneuverability is a key requirement (as shown in Figure 2.1). The environmental monitoring in shallow waters requires an AUV that can move in hard-to-reach and unstructured areas; a small AUV with greater maneuverability should be suitable for this application.

- The vehicle should also be able to move each DOF bi-directionally, unlike the traditional AUV technology (that can not move bi-directionally), such as GUANAY-II [80] or Tethys [31], that includes a ballast system or buoyancy saddles, enabling a change of buoyancy and carrying out of vertical immersions; however, there are several recent vehicles that use bi-directional movement, such as Girona 500 [173].

- The AUV has to provide an on-board power supply to run several hours independently (it is very important to be able to work with its energy sources one workday), unlike the ROVs that use tethers to control which also provide them with power, which is the main reason why they are unsuitable for swarm applications. In addition, the AUV has to be rechargeable after the power supply has been depleted.

- To build a swarm of AUVs, the construction of individual vehicles should be undertaken by using low-cost means, so that the whole swarm can be commercially viable.

- The vehicle must be large enough to house all the sensors, drive electronics, processors, batteries, and other equipment.

- The capability, sensors, propulsion, mechanical design, and all components related to the properties of the vehicle have to be commensurate with the working conditions in the water environment in which it will be operating.

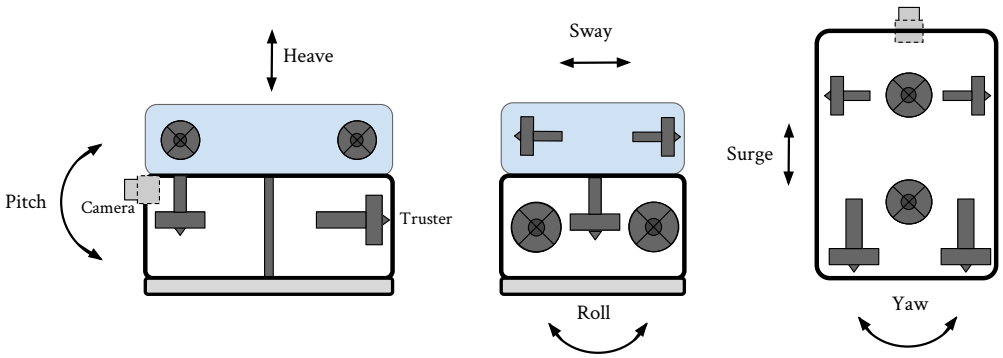

Figure 2.1 Vehicle degrees of freedom

The scope of this thesis has been established to meet all of the mechatronic requirements.

2.2 Unmanned Underwater Vehicles UUV

Apart from AUVs and ROVs, a wide range of other marine equipment is available for ocean observation and research, including manned submersibles, Unmanned Surface Vehicles (USV), and underwater gliders and wave gliders. What makes Unmanned Underwater Vehicles (UUV) particularly advantageous and useful is the fact that they do not need to be operated by human beings on board, who can thus avoid exposing themselves to the dangerous and hazardous conditions of the underwater environment that can be life-threatening. By contrast, UUVs can withstand such conditions without any problems [116]. Actuality the family of UUVs contains both the AUVs and ROVs.

In addition to facilitating a more comprehensive understanding of various issues and problems associated with the ocean and with the environment in general, UUVs can also contribute to protect the ocean resources against pollution and ensure that they are rationally and effectively used for human well-being.

Before proceeding to the main point of discussion, it is necessary to provide some clarification of the variety of acronyms that are employed with reference to underwater vehicles. ROV refers to a remotely operated vehicle, which, as its name suggests, is managed and receives its power supply through a tether. UUV stands for unmanned underwater vehicle and is usually used by the US Navy. Although this term is applicable to both ROV and AUV, in most cases, it is used with reference to an AUV.

Current AUVs are highly relevant as unmanned survey platforms as they enable data to be collected for various purposes by carrying sensor payloads along trajectories established beforehand to gather data for a variety of applications [148]. These vehicles also facilitate the performance of spatial and time series measurements as the sensors they are equipped with sample the ocean while moving through it. Geospatial and temporal references about the high-quality sensor data supplied by the AUVs are produced automatically [219].

2.3 AUV vs ROV

As previously indicated, ROVs and AUVs are the two major types of UUVs that have been employed with equal success in various industrial applications. The choice between these two UUV types for the purposes of a specific mission depends on their inherent dissimilarities. Both types present strengths as well as weaknesses and are suitable for different tasks to greater or lesser degrees. What distinguishes them most significantly is that the ROV is tethered to the base station, but the AUV is not. Through the tether, the ROV is controlled in its movements and has its status monitored by a human operator. Furthermore, based on how the vehicle

is configured, the tether powers its actuators, sensors, and other internal electronic components as well [116].

A brief outline of the key differences between AUV and ROV is provided in the following.

- On the one hand, the AUV allows for greater maneuverability because it is not tethered. On the other hand, it may not be possible for an ROV to operate in every kind of environment due to the fact that it is attached with a tether, which could get caught on various structures in the underwater environment and could also have a negative impact on the vehicle's maneuvering performance by causing drag on its motion.

- The ROV cannot be used in many applications at the moment due to the fact that the mother vessels are highly expensive to operate, human operators can become fatigued, and due to safety concerns.

- The tether restricts what can be done in particular applications, such as swarms, that require the vehicle's location to be shifted and changed.

- The range of the ROV from the base station is determined by the length of the tether.

- In some cases, AUV operations can diminish the number of vessels necessary for the performance of a survey. Two vessels are commonly employed in the majority of commercial deep-tow operations, for towing and for locating the tow-body, respectively.

- Interaction by a human operator is minimally or not at all required by the AUV as it carries out its established tasks or mission. Staff at the base station do not need to intervene due to the fact that the aims and goals of the mission are pre-programmed into the vehicle, and, therefore, the vehicle already knows what it is supposed to do after it is launched. Such an approach is highly useful because it makes it less likely for human error to occur during the process of vehicle operation.

- The AUV is capable of "intelligent" behavior in the form of sensing and automatic decision-making. This is made possible by the fact that the vehicle is pre-programmed with particular tasks and operations, thus enabling it to act independently of a human operator.

The robotic vehicle has become much more autonomous as a result of the extensive research endeavors that have been made. One major outcome of the greater autonomy of the robotic vehicle has been a minimization or elimination altogether of the necessity for the presence of human operators and the emergence of a self-contained and autonomous robotic vehicle demonstrating intelligence and the capability of making decisions on its own. As outlined above, the AUV clearly has more advan-

tages compared to the ROV, which is why it is the preferred choice of UUV for use in survey missions conducted in dynamic and hazardous underwater environments of great complexity. For all these reasons, the present study focuses on the AUV.

2.4 A brief History of Underwater Exploration Vehicles

The commercial introduction of AUV technology has enjoyed tremendous success and has consequently sparked an ample amount of research on AUVs.

Research on oceans and marine environments has barely scratched the surface and there is still a vast amount of knowledge to be accumulated and many phenomena and aspects require clarification and comprehension. However, a great obstacle to this research and advancement in knowledge, particularly with regard to the investigation of seafloors, is the enormous volume of water contained in oceans and the challenges it poses to human exploration.

From the 1900s onwards, ocean exploration usually entailed the study and analysis of samples that had been collected from the ocean with the use of some sort of trawl. This approach did not produce data that were too rich and detailed, but they were still sufficiently noteworthy to fuel research for a long period of time. It was not until the 1930s that the first endeavors to take human beings into the ocean depths were made by Otis Barton and William Beebe, who made use of a vessel attached to a tether for this purpose [40]. This vessel technology made it possible for explorers to experience the ocean depths directly and at close quarters. By the 1950s, innovations in electronics and engineering technology and materials paved the way for the creation of the first manned submersibles that were not tethered, the most famous of which was ALVIN [119].

The introduction of floats of neutral buoyancy made it possible for development to commence towards the end of the 1950s on what may be considered the first "true" AUV [81]. This was undertaken by Stan Murphy, Bob Francois, and subsequently Terry Ewart of the Applied Physics Laboratory at the University of Washington in recognition of the necessity to acquire oceanographic data along accurate trajectories. The efforts made by these researchers materialized in 1957 with the creation of the self-propelled underwater research vehicle (SPURV) [219], which is illustrated in Figure 2.2. With a weight of 454 kg, a length of 3.1 m, and a speed of 2.2 m/s, the SPURV was capable of operating for five and a half hours at a depth of up to 3 km. The control of the vehicle from the surface was acoustic-based. After this achievement, AUV innovation did not progress at a fast pace during the 1970s and the 1980s, with EAVE and SKAT, respectively developed by the University of New Hampshire and the Russian Shirshov Institute of Oceanography, being among the only few of vehicles that were created with success [225]. This setback in research can be attributed to insufficient technological capacity with regard to processing power and power storage.

Figure 2.2 The first true AUV, the SPURV, was introduced in 1957 and was an achievement of the Applied Physics Laboratory at the University of Washington [20].

To aid the search for sunken ships and aircrafts, the development of the Advanced Unmanned Search System (AUSS) was initiated by the Naval Ocean System Center, today known as SPAWAR, in 1973 [208]. It was only ten years later, in 1983, that the vehicle was deployed, and during the following decade, related reports and publications were still in press. With a weight of 907 kg, the AUSS was equipped with silver zinc batteries that could provide 20 kw-hours of energy and could dive to a depth of 6 km. Furthermore, it achieved video image transmission through the water with the help of an integrated system of acoustic communication at a rate up to 4800 bits per seconds. The vehicle was deployed more than 114 times. What is more, this technology has provided the basis for the subsequent development of the concept of enhancing system performance by employing more than one free-swimming vehicle. This research reached completion in the early part of the 1980s [66].

In 1976, Epulard was developed by IFREMER, followed by assembly two years later and deployment in 1980. This was the first 6 km-rated AUV based on acoustic control that enabled not only imaging of the deep ocean but also bathymetric surveys. At the surface, the vehicle used a cable to drag and ensure that it stayed at a fixed altitude above the ocean floor. During the period from 1970 to 1990, Epulard was deployed 300 times, sometimes to a depth of 6 km [141].

Academic researchers began to pay increasing attention to AUVs during the 1990s. This research interest led to the development of a number of six Odyssey vehicles by the Sea Grant AUV Laboratory of the Massachusetts Institute of Technology (MIT). Weighing 160 kg and with a speed of 1.5 m/s, these vehicles were capable of up to six hours of operation and could go to a depth of 6 km. In 1994, they were deployed under ice and in the next year, they were operated for three hours at a depth of

1.4 km [30]. Furthermore, experiments designed to demonstrate the Autonomous Ocean Sampling Network benefited from the use of the Odyssey vehicles as well [59]. In addition, further advancements included the Remote Environmental Monitoring Units (REMUS) that were the outcome of a collaboration between the MIT, the Woods Hole Oceanographic Institution (WHOI) [166], and the Autosub, which was created by the Southampton Oceanography Center [219]. It was also during the 1990s that AUVs began to become commercially available.

Figure 2.3 Odyssey II class AUV developed at MIT Sea Grant's AUV Lab [143]

There was a significant intensification in the development of AUVs for commercial use at the beginning of the twenty-first century. By the year 2009, the number of AUVs in use at global level was more than 600 and by the year 2016 already 930 units. The AUV market is expected to increase and is predicted to rise to about 1400 units by the year 2019 [147, 221]. They are employed for a wide range of purposes, such as surveys and research or military use [221, 226].

2.5 The Main Classes of AUVs

In keeping with factors like size and weight, there are four major categories of AUVs that can be discerned [39, 203]. In spite of the fact that they differ from one another in terms of various aspects, every one of these four categories except the first one considers solely the standard type of AUVs characterized by a torpedo-shape. The four categories are outlined in the following part:

- **The category of man-portable AUVs**: With a weight between 10 and 45 kg, the vehicles in this category can operate continuously for a duration of 10-20 hours and they do not present any particular hull shape.

- **The category of light-weight vehicles (LWVs)**: **Displacing** more than 200 kg, these vehicles usually have a diameter of about 32 cm. By comparison to man-portable AUVs, the payloads of these vehicles are designed to be between six and twelve times larger, while their duration of operation has been designed to be twice as long.

- **The category of heavy-weight vehicles (HWVs)**: **Displacing** around 13.5 tons, the vehicles in this category usually have a diameter of about 54 cm. By comparison to the category of LWVs, these vehicles are designed to have a capability twice as high. Submarine-compatible vehicles are one example of heavy-weight vehicles.

- **The category of large vehicles**: Fully-developed, these vehicles are intended to **displace** about 10 tons and will be able to be employed not only with submarines, but also with surface ships.

Table 2.1 below provides an overview of the main features of each of the four categories of AUVs presented above.

Class	Diameter (cm)	Displacement (kg)	Endurance-High Hotel Load (hours)	Payload (m^3)
Man-portable	7-23	< 45	<10	<0.007
LWV	32	$\sim$225	10-20	0.028-0.084
HWV	54	$\sim$1350	20-50	0.113-0.170
Large	>90	$\sim$9000	100-300	0.424-0.844

Table 2.1 Vehicle Classes from the 2004 UUV Master Plan (SOURCE: U.S. Department of the Navy, 2004, Table 5-1, p. 67) [203]

2.6 AUV Market Classification

As far as possible, a large number of AUVs are organized using the four classes mentioned in Section 2.5. Nevertheless, commercial and scientific AUVs that may serve as the basis for military AUVs tend not to fall exactly under these four classes. A number of vehicles currently in development (e.g. "flying wing" glider AUVs without a distinct fuselage), biomimetic AUVs (e.g. robotic lobsters), and hybrid UUVs do not fit into this classification scheme either.

The AUV market has enriched the classification of AUVs by dividing them into a wide range of categories according to type (e.g. Shallow Water Survey AUVs, Mid-

water AUVs, and Deep-water AUVs), application (e.g. Environmental Monitoring, Military, Defense, Coastal Security, Oil and Gas, Oceanography, and Scientific), and technology (Autonomy, Energy, Collision Avoidance, Communication, Navigation, Propulsion, Sensors, and Imaging) [28, 32, 100, 201, 226, 236, 243]. The previous references have also been used to categorize the AUVs in Section 2.6.1, Section 2.6.2, and Section 2.6.3, although additional sources were employed as well.

2.6.1 Classification by Type

Depth ratings of most existing AUVs fall into three categories: vehicles designed for depths on the order of 100 m (Shallow-Water), vehicles designed with ratings of up to 1000 m (Mid-Water), and vehicles designed with maximum ratings between 1000 and 6000 m (Deep Water).

- **AUVs Shallow Water Survey (Depth of up to 100 meters)**

  Operational at depths of up to 100 m, this type of AUV is employed in the performance of both oceanographic and non-oceanographic surveys at a depth not far from the surface. Due to the fact that they are not subjected to significant water pressure, these AUVs usually have a small size. On the other hand, they are capable of maneuverability in high current areas because their thrust-to-drag ratio is high. Furthermore, these AUVs have a considerably high operating speed of a couple of knots per hour, since the surveys for which they are employed are generally conducted over an extensive area but with a relatively low resolution. One of these types of AUV is the REMUS-100 (Figure 2.4), which measures 1.7 m in length, 19 cm in diameter, and 39 kg in weight and is operational at a depth of up to 100 m [10, 157].

Figure 2.4 REMUS-100 is a 100 meter rated AUV, used with permission from Kongsberg Maritime [117]

- **Mid-water AUVs (Depth of up to 1,000 meters)**

  Operational at depths of up to 1000 m, this type of AUV is employed in the performance of mid-water column surveys or surveys of the sea floor in areas that are not too deep. Since they have to be able to withstand the high pressure

associated with the greater depth, these AUVs usually have a considerable bulk and their size is further expanded due to the fact that they require a greater amount of power and more thrust. At the same time, their thrust-to-drag ratio is not that high, because currents are not intense at those depths. There is some variation in their operating speed, according to the nature of the application for which they are employed. For example, AUVs used for a photographic survey have a speed of less than one knot per hour, whereas AUVs used for a multibeam or side-scan survey can reach a couple of knots per hour.

The Gavia Surveyor AUV was discussed in [92]. With a length of 2.7 m and a weight of less than 80 kg, this AUV is of the type employed for data collection at a depth of up to 1000 m. Another example is the REMUS 600 as shown in Figure 2.5, which was created by the Oceanographic Systems Laboratory of the WHOI, presenting a diameter of 32.39 cm, a length of 2.7 m, and a weight of 220 kg. This AUV stands out because it is equipped with mine countermeasure sensors [198].

Figure 2.5 REMUS-600 AUV, used with permission from Kongsberg Maritime [117]

- **Deep-water AUVs (Depth above 1,000 meters)**

  Operational at depths greater than 1000 m, this type of AUVs is large and bulky in size so as to be able to withstand the high oceanographic pressures associated with such depths. Another reason for their large size is they need to store greater amounts of power to prolong the missions as much as possible, given the long duration it takes to reach the depths for which these vehicles are designed. Meanwhile, their thrust-to-drag ratio is not that high in order to increase their power efficiency and avoid further size expansion. Furthermore, AUVs of this type have to be capable of maneuvering at reduced speeds because they are typically employed near the ocean floor to ensure the high resolution of the surveys. Deep-water AUVs present a multi-hull design with more than one thruster but also a lack of control surfaces for maneuvering. One example of AUVs of this type capable of operating at depths of up to 3000 m is the HUGIN 3000, which has a length of 5.5 m and a weight of 1,400.00 kg.

Figure 2.6 The HUGIN 3000 AUV was developed by Norway's Kongsberg A/S for C & C Technologies [134]

2.6.2 Classification by Application

The AUVs are used for a variety of applications to gather data about the oceans. The diverse and large numbers of applications that use AUVs increase the discovery and understanding of marine and other environmental issues. Some AUVs have been provided with a variety of equipment to be used for multiple applications. The most important applications are related to the following major fields:

- **Military and Defense**: A significant driver of AUV research and development have been military applications, which benefit from the covert nature of AUVs, the elimination of risk to manned vessels, and other advantages of AUVs. For example, mine warfare makes good use of AUV characteristics to provide covert, rapid, controlled, and efficient surveys of a potential minefield without risking a human operator. Much of today's successful AUV technology was initially government-funded for military applications. The military HUGIN 1000 AUV has been developed by the Norwegian Defence Research Establishment (FFI) to counter the threat from sea mines [85].

- **Oil and Gas**: One specific hydrographic application of AUV technology is undersea exploration and production of oil and gas. The International Submarine Engineering (ISE) built a torpedo-shaped AUV called Eagle Ray [61], which has additional operational requirements and tasks to collect background data and understand the process of natural oil and gas seeps.

- **Environmental Protection and Monitoring**: The ARCS AUV developed by ISE has been used to measure a chemical (Dimethyl sulphide) plume using a CTD sensor and underwater mass spectrometer (called In-Spectr) [149, 159].

- **Oceanography**: The need to obtain high-quality oceanographic data has prompted the South Hampton Oceanography Center to develop the Autosub AUV to provide scientists with the capability to monitor the oceans [82, 219].

- **Archeology and Exploration**: The ARROWS EU project [12] has used three different low-cost AUVs, MARTA [11], U-CAT [46], and A_Size AUV to complete archaeological autonomous missions.

- **Search and Salvage Operations**: After Air France Flight 447 crashed in 2009, REMUS-6000, as shown in Figure 2.7, was the key equipment in the successful search for plane wreckage that was detected using the AUV side-scan sonar [168]. It has a maximum diameter of 0.68 m and a length of 4 m. The vehicle weight is approximately 880 kg.

Figure 2.7 The REMUS-6000 AUV was developed by the Oceanographic Systems Laboratory at WHOI, used with permission from Kongsberg Maritime [117]

2.6.3 Classification by Technology

Some AUVs can be classified according to the technology that they use. AUVs require many subsystems to provide the desired capability [243]. No single type of AUV will solve all problems related to ocean research [142]. Complex, multi-dive science missions are likely to require a mix of several AUVs that are provided and loaded with different technologies. The capabilities and subsystems of an AUV to survey and conduct studies in deep water are different from those used in shallow water. The main technologies employed are as follows:

- **Sonars**

- **Communication**

- **Navigation**
- **Propulsion**
- **Imaging**
- **Energy**
- **Operator Software**
- **Autonomy and Behaviors**
- **Collision Avoidance**

2.7 Gliders

Autonomous Underwater Gliders (AUG) is which belong also to the UUV family use wings and buoyancy changes for propulsion, in a manner analogous to glider aircraft, by converting vertical motion into forward motion (controlling buoyancy generates the profile for vertical moving and the wings are used to move horizontally). These buoyancy systems achieve much more efficiency than the electric thrusters that are typically used in AUVs, which leads to a significant increase in their range to an order of thousands of kilometers. Gliders are capable of deployments lasting weeks to over a year, due to their energy-efficient design and slower speeds (approximately 0.3 m/s forward speed for gliders, compared to over 1.0 m/s for many AUVs). Gliders have been optimized for long-range and endurance missions. This class of vehicles typically operates in the upper water column and is usually rated for less than 1000 meters [108, 148, 204].

The typical vehicle trajectory is a saw-tooth pattern called a "yo", which consists of a dive (buoyancy engine retracted to make the vehicle negatively buoyant) and a climb (buoyancy engine extended to create positive buoyancy). It has been proven that it is possible to perform vertical zigzag maneuvers in the ocean with little energy consumption for many days and even up to a month or more in cases where obtaining temperature and salinity measurements as a function of depth is of key interest.

The Naval Research's Autonomous Oceanographic Sampling Network (AOSN) developed three underwater gliders, Slocum, Spray, and Seaglider [108, 178].

The first example of buoyancy-driven vehicle is the Slocum glider shown in Figure 2.8(c) which is produced by Teledyne Webb Research [202]. The Webb Research Corp (WRC) has developed Slocum to be suitable for missions in shallow water environments to enable fast movement and turning [178] as well as to run in missions of long duration [234]. The glider is 180 cm long and weighs around 70 kg [224].

(a) Spray [204]

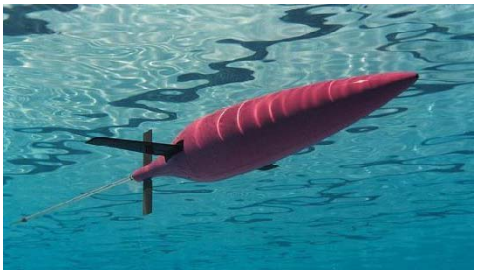

(b) Seaglider [204]

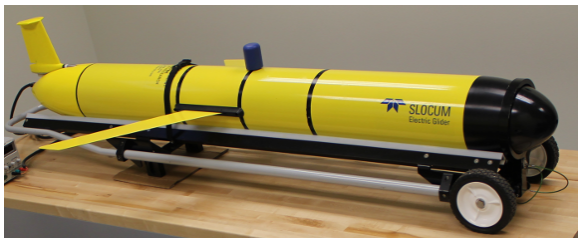

(c) Slocum [235]

Figure 2.8 Examples of gliders

The second example of buoyancy-driven vehicle is the Spray glider shown in Figure 2.8(a), which was developed by the Scripps Institute of Oceanography at UC San Diego [191]. Spray is 2 m in long and weighs 50 kg.

The third example is Seaglider (Figure 2.8(b)), which was designed at The University of Washington and is enclosed in hydrodynamic fiberglass that supports wings, vertical stabilizer, and tailing antenna [67, 204]. The Seaglider fairing is 1.8 m long, its wing span is 1 m, the antenna mast is 1.4 m long, and its weight is 52 kg.

As a new concept of underwater vehicle, hybrid AUVs or Gliders such as Multifunctional Hybrid Glider (MHG) can be regarded as a new type combination of underwater vehicles [204].

2.8 Torpedo and Non-torpedo Shaped AUVs

Another method of classification available for the majority of AUVs that are currently employed in scientific and industrial fields is according to whether they present a torpedo or a non-torpedo shape. The torpedo defines the same structure of the design in Figure 2.9 supplies a sleek, hydrodynamic form that includes components in a high structural safety, cylindrical hull. Power consumption is a minimum due to the use of one thruster located on the stern. The non-torpedo shape is contrary to what is mentioned above.

This method of classification has a decisive influence on many features and capabilities of the AUVs and, are therefore, of great significance. The main difference between a torpedo shape and a non-torpedo shape is the fact that, by comparison to a conventional AUV with a single hull and a non-torpedo shape, an AUV with a single hull and a torpedo shape does not have as much drag and its speed is much higher. Furthermore, the movement of an AUV with a torpedo shape is controlled by an aft thruster and fins. The basic design configuration of this type of AUV [22, 131, 133, 166] has been applied in the development of the REMUS and SPARUS AUV that are shown in Figure 2.4 and Figure 2.9 respectively. As the vehicle moves forward, the drag is minimized thanks to its streamlined and torpedo shape. Moreover, the streamlined hull is intended to improve the energy efficiency of the vehicle by reducing the drag (more details in Chapter 5). Another advantage of the torpedo-shaped AUV is that it has an extensive range and is operational in areas with moderate currents. On the downside, it is quite difficult for this type of vehicle to control itself autonomously.

Figure 2.9 Sparus AUV, created in the underwater robotics laboratory at the University of Girona [133]

In general, the AUV with a non-torpedo shape is designed in a way that affords full control at a significantly lower speed. On the other hand, this type of vehicle has a considerable drag due to its larger form factor, and therefore it is not easy to deploy in areas with high currents.

Some non-torpedo shaped AUVs are small in size, but they are most suitable for shorter operations carried out in areas of coast or extensive water bodies like dams [175], as well as for inspection of ship hulls [155]. This category of AUVs with a non-torpedo shape and a small size includes the Ictinea AUV [37, 174] and the HAUV [212, 223] as shown in Figure 2.10.

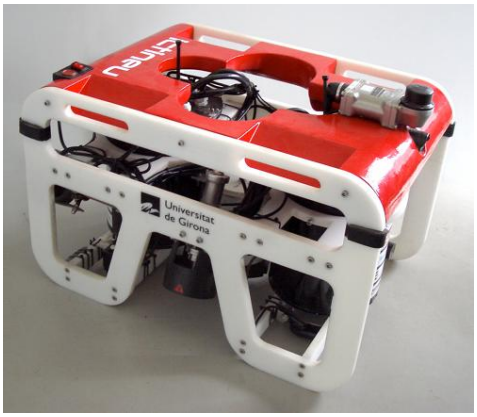

(a) Ictineu AUV, developed by the Underwater Robotics Laboratory of the University of Girona [174]

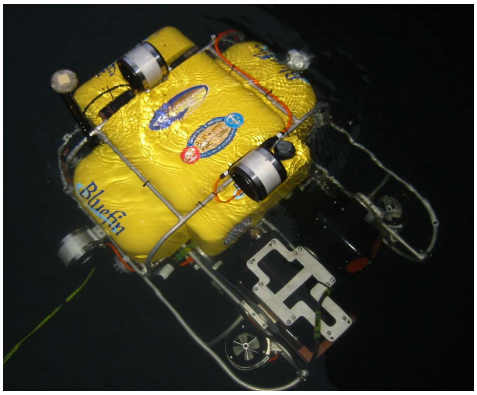

(b) HAUV, developed by Bluefin Robotics in collaboration with MIT [212]

Figure 2.10 AUVs with a non-torpedo shape

2.9 Micro AUVs and Swarming Applications

In the following part, the discussion focuses on micro AUVs, which are characterized by low payload capacity and high cost-effectiveness. They were often designed by researchers with the intention of operating together as a swarm to increase the efficiency and success of a given mission.

Actually, there is no clear definition of the micro AUVs that defines the specification or dimension. In [33] it is concluded that the micro AUVs are smaller, lighter and cheaper to acquire and maintain. In [189] it is mentioned that micro AUVs refer to less than a meter of dimensional size and have the capabilities to perform an underwater task. More clarification is detailed in [69] which defines that a micro AUV is small enough such that it can resolve many of the problems that face the large AUVs such as reduce the cost of the AUV itself and maintenance costs, transport difficulty and cost to perform underwater experiments, explore and navigate in small spaces and areas, and minimize the financial risk in the event that one of these AUVs is lost. By review of some researches of micro AUVs [33, 93, 101, 112, 154, 189], we can conclude that a micro AUV is a vehicle that is inexpensive, small (portable in one hand), it has less than 1 m length and 10 kg weight and in addition, it makes launching and retrieval very simple and efficient.

2.9.1 The Advantages of Micro AUVs

The first question comes to mind: Why small or micro AUVs are beautiful?
To answer this question, a brief introduction is required.

Over the last five decades, a wide variety of AUVs of different size have been developed, including portable lightweight AUVs and AUVs with a large diameter and a length of more than 10 m. However, despite these advancements, AUVs are not available for purchase from many companies [1, 35]. Moreover, functional micro AUVs are still not produced on a large scale for either commercial or academic purposes.

Despite the fact that they are clearly advantageous as far as endurance and sensor payload capacity are concerned, AUVs of large size are not cost-effective enough for many of the various operations they are compatible with, due to the high complexity of their mechanical and electrical systems as well as due to the high expenditure that their transportation, deployment, and recovery involve. For example, the use of the ABYSS AUV [124], which weighs 880 kg and is around 4 m long, entails significant costs in terms of operation and equipment, therefore making the process of data collection more complex. Furthermore, AUVs of large size are particularly inadequate for use in smaller areas, like wrecks, subterranean rivers, or coral reefs, because they are unable to maneuver in such tight spaces.

In theory, it is possible to apply the principle of swarming with most types of AUVs, although significant limitations in terms of handling specifications and expenditure are posed by the use of multiple vehicles. At the moment, the market cost of a small AUV like REMUS 100 is between $50,000 and $250,000, whereas an AUV of larger size could cost up to $5 million [147]. Given these figures, the majority of research projects struggle to find the funds for even one or two AUVs, let alone twenty or thirty, which completely lacks feasibility in terms of costs. The deployment of an AUV weighing 300 kg, for example, relies on the input of several individuals and, requires the use of a crane and a large boat, as well as favorable sea conditions. Aside from being extremely challenging, the successful deployment of twenty AUVs is significantly time-consuming. However, the difficulties do not end after the launch; the process of recovering the vehicles upon completion of the mission is equally challenging, with affixing a crane hook to the AUVs being a particularly risky procedure.

On the other hand, the logistics associated with the use of micro AUVs (e.g. support vessel footprint, deployment, and recovery processes) are more manageable, due to the fact that the small size of the vehicles makes it easier to overcome or to avoid problems that may occur with larger vehicles. A crane is usually needed to deploy and recover an AUV with a length of more than 1 m and a weight of more than 30 kg. By contrast, an AUV smaller than this could be deployed by one individual or several individuals working together. The processes of deployment and recovery are greatly simplified with vehicles that are less than 1 m long and weigh less than 10 kg, as they can be easily handled with just one hand. In addition to being operational in areas where present AUVs cannot navigate, such micro AUVs are much less expensive, so their loss or damage will not have a significant financial impact.

Commercial companies are aware of the fact that a vehicle of larger size is needed in order to attain the range and endurance necessary to optimize AUV efficiency and performance. Recent innovations in underwater vehicle technology have made it possible to develop micro AUVs that are smaller in size, have lower resistance, are more flexible and cost-effective, and have a higher efficiency. An additional advantage that micro AUVs have over AUVs of standard size is the fact that they are equipped in a more convenient manner, thus enabling more missions to be carried out as well as broadening the range of applications with which underwater vehicles are compatible. On the basis of all of these considerations, the assembly of a fleet or swarm of inexpensive, simple, and micro AUVs that can perform better than AUVs of large size is legitimate and feasible with strong encouragement and motivation.

2.10 State-of-the-Art Micro AUV

As mentioned in the previous section, if the AUV has less than 1 m and 10 kg, handling with only one hand is possible, making launching and retrieval very simple and efficient. Of the available vehicles, Serafina [112] from the Australian National University, MONSUN AUV from the University of Luebeck [152, 154], RANGON from Nekton Research, LLC. [93], and the CoCoRo project [185] are the best known.

There are a number of other micro AUVs which have been designed purely as an academic exercise and have not been implemented. Due to this, the next section will concentrate on the well-documented vehicles Serafina, MONSUN, RANGER, and CoCoRo.

There is an AUV of one cubic inch [101, 223], but it is not suitable for carrying the sensors and the thruster, and, therefore, it cannot be used for environmental monitoring.

2.10.1 Serafina

The Serafina Project that was active at the Australian National University until 2009 is one of the best known AUV swarm projects. The project focused on the potentials of multiple, robust, small, fully autonomous, but organized underwater vehicles [246]. A school of these underwater vehicles offers possibilities far beyond any individual submersible for fault-tolerant, scalable coverage of ocean spaces [112, 184].

The aim of the Serafina project was to investigate the possibility of using a swarm of small, autonomous underwater vehicles for exploration, mapping, and monitoring of ocean spaces using relative localization with respect to their neighborhood as well as dynamic communication based on dynamic routing protocols [118]. The Serafina AUV is 45 cm long and has a diameter of 10 cm. It is equipped with five

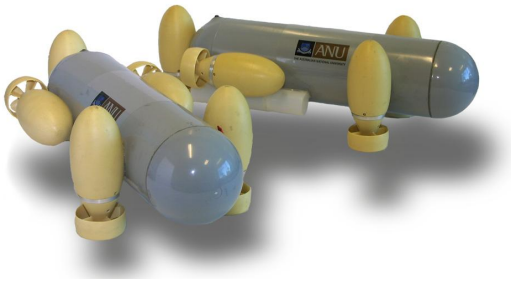

Figure 2.11 Prototypes of Serafina AUVs [184]

Size	0.45m x 0.21m with 3-4 kg
DOF	5: Surge, Heave, Roll, Pitch and Yaw
Power Supply	Unknown Batteries
Propulsion Systems	5 x Propeller-Based Thrusters
Sensing Capabilities	Sonar, Acceleration, Compass, and Pressure Sensor
Control Algorithms	Unknown
Testing	in Pool

Table 2.2 Serafina Review

thrusters to move around, as shown in Figure 2.11, making it highly maneuverable and able to swim against moderate ocean currents. The vehicle's capabilities are shown in Table 2.2.

It detects movement and location with an acceleration sensor, a compass, as well as a pressure sensor. The sensor data are processed with a 40 MHz PowerPC processor. The propulsion is conducted with two horizontal and three vertical thrusters.

The payload consists of a sonar sensor module, compass, pressure sensor, and linear accelerometers. The data of the sensors are processed with a PowerPC processor with 40 MHz. The propulsion is conducted with two horizontal and three vertical thrusters. The AUVs cannot recharge their power source so, once the power is low, they have to be retrieved and recharged.

The main focus was on the development of the algorithms and less on the hardware. In the foreground were aspects like fault tolerance and scalability. The functionality of each AUV should be able to adjust according to the current position in the swarm. Therefore, determining the positioning and the distance in relation to the neighbors is very important.

Another focus of the project was on the efficient communication within the swarm, due to the limited bandwidth of communication underwater to obtain the rela-

tive position information. Once the position and distance were determined, it was possible to conduct simulations demonstrating simple formations, such as a triangle-formation of a small group of AUVs as well as polygonal formations [113].

2.10.2 MONSUN

Researchers at the University of Lübeck have created a micro AUV called MONSUN, which is applicable in a robotic swarm [137, 152, 154]. In keeping with the characteristics and specifications associated with swarm robots, this AUV possesses various sensors, such as camera and obstacle avoidance sensor that permit sensing over a restricted range. As illustrated in Figure 2.12, the vehicle is 80 cm long, has a diameter of 10 cm, and weighs around 8 kg. It also has six motors, of which four are mounted in a vertical orientation and two are mounted in a horizontal orientation. These motors permit the vehicle to dive dynamically as well as to rotate around the roll and pitch axis to make up for the pose in rough water and the robot's yaw angle. In addition, MONSUN is equipped with a modular expansion set suitable for adaptation to a broad range of missions [139]. Table 2.3 lists the capabilities of MONSUN.

Figure 2.12 The small AUV MONSUN

Size	0.8m x 0.1m x 0.3m with 8 kg
DOF	5: Surge, Heave, Roll, Pitch, and Yaw
Power Supply	Lithium Polymer Batteries
Propulsion Systems	6 x Propeller-Based Thrusters
Sensing Capabilities **Communication**	CTD, IMU, Compass, Pressure Sensor, and Acoustic Modem
Control Algorithms	PID
Testing	in Pool, Lakes, and Baltic Sea

Table 2.3 MONSUN Review

The MONSUN project differs from the Serafina project in that it does not incorporate solely relative localization in the swarm, but integrates absolute and relative localization to cover the area intended for survey as best as possible.

Consequently, due to the fact that expensive sensors are not needed, the vehicle is highly cost-effective. Furthermore, because it is so small, the vehicle can be used in areas that are not easily accessible to other vehicles of larger size. The results of preliminary tests have revealed that, even when a vertical thruster stops functioning properly, MONSUN can still maneuver and dive. Within a swarm, MONSUN uses its incorporated acoustic modem to communicate with other members, thus enabling collaborative operations. Two cooperating MONSUN have already successful been used for eddy measurements in the Baltic sea [138], and a V-formation of three MONSUN has been tested at Lake Ratzeburg [27].

2.10.3 Ranger

A new series of micro AUVs called Ranger has been created by Nekton Research and is distinguished by the commercial, multi-parameter water sensor arrays it contains [93]. With a diameter of 90 mm, these AUVs collaborate in multiple groups to facilitate multi-agent, distributed sensing of inshore and near-shore waters up to 100 m deep. By diving and operating together in groups of 4-12 members, these vehicles can help to shed light on a variety of phenomena, such as chemical plume geometry, small-scale mixing, as well as three-dimensional flow dynamics [187]. The Ranger vehicles are also effective when they operate on their own, but their efficiency and capability increase significantly when they work together in the form of a coordinated group.

The aim of Nekton Research in creating the Ranger Micro AUVs has been to eliminate the obstacles of AUV costs and complexity that have hindered the execution of coordinated tasks [94]. Capable of a speed of 3 knots, the vehicles have a storage capacity of 150,000 data points associated with a wide range of aspects, including conductivity, temperature, depth, dissolved oxygen, pH, and turbidity sensors. What is more, the WHOI Micro-Modem that is incorporated in the Ranger AUVs enables not only communication but also long baseline localization [77, 78]. Regrettably, the most recent publications and information related to this project date back to 2005.

2.10.4 CoCoRo

Another project in the area of underwater swarm robotics is the CoCoRo project, which was founded in 2011 [185]. The aim of the project is the development of a swarm of interacting, cognitive AUVs. The purpose of the interaction with neighbors is to ensure a balanced distribution of tasks. Therefore, systems found in

Figure 2.13 Ranger micro AUV [94]

Size	0.92m x 0.1m with 4.5 kg
DOF	3: Surge, Heave, and Pitch
Power Supply	Lithium Ion Batteries
Propulsion Systems	2 x Propeller-Based Thrusters
Sensing Capabilities	Acoustic Modem, Conductivity, Dissolved O_2, Temperature, and Pressure Sensor
Control Algorithms	Unknown
Testing	in River

Table 2.4 Ranger Review

nature, such as fish shoals, bee swarms, or the immune system, constitute models that can be emulated and combined.

Figure 2.14 The Lily platform developed in the CoCoRo project [170]

The swarm itself is divided into three groups and is partially heterogeneous. For the external communication and absolute positioning via GPS or UTMS, there should be floating base stations on the water surface. They are to receive global commands

Size	0.13m x 0.1m x 0.07
DOF	3: Surge, Heave, and Yaw
Power Supply	Lithium Polymer Batteries
Propulsion Systems	2 x Differential Propellers and 1 Buoyancy System
Sensing Capabilities	Blue-light based Optical Systems and Pressure Sensor
Control Algorithms	Bio-inspired Algorithm
Testing	in Pool

Table 2.5 'Lily' underwater swarm platform

and relay them to the underwater swarm or rather to transmit data of the swarm, such as status messages or information about the environmental situation. This system differs from other swarm participants in that it does not provide a diving possibility. The underwater swarm member consist of homogeneous robots, such as the prototype shown in Figure 2.14. This swarm is divided into two groups. The first group, the 'ground swarm', performs the main task, while the second group, the 'relay swarm', joins a chain between the ground swarm and the base station. This situation arises because the single participants communicate only optically through blue LEDs and, therefore, they have a poor communication range. The relay swarm serves as a communication chain.

2.11 Special AUVs

2.11.1 The Solar-Powered AUV

It has been proposed that the efficiency of AUV platforms, particularly those operating continuously or over a long period of time, could be markedly increased through on-station recharging of the vehicles on the basis of solar cells. Developed for operations over a long duration of weeks or months, the solar-powered AUV (SAUV) [107] does not need to be retrieved to be serviced, maintained, or recharged during its operation period. It is functional both at the surface of the water and at a depth of up to 500 m. Furthermore, the vehicle maintains its high endurance even when there is little solar radiation, owing to the fact that it incorporates rechargeable lithium ion batteries.

The SAUV (Figure 2.15) has been deployed for the purpose of environmental monitoring on the Hudson River and Lake Pontchartrain as part of the RiverNet project, which was initiated as a collaboration between the RPI, Autonomous Undersea Sys-

tems Institute, Technology Systems Inc., Falmouth Scientific Inc., and the Naval Undersea Warfar Center [158, 243].

Figure 2.15 The Solar Powered AUV (SAUV) [32]

2.11.2 AQUA

Owing to the munificent support of the Canadian Institute for Robotics and Intelligent Systems (IRIS), the AQUA vehicle was developed with the purpose of creating a platform and computer-vision system that could map coral reefs in 3D [64, 164]. In addition to being operational in water and diving into a depth of 10 m, the platform was also designed to operate on land. Thus, the AQUA vehicle constitutes a new type of aquatic vehicle design, which is dependent on legged locomotion, instead of thrusters and control surfaces. As shown in Figure 2.16, the vehicle either walks or swims by using its six actuators together with the specially developed legs and/or fins.

Size	0.65m x 0.50m x 0.13m with 18 kg
DOF	5: Surge, Heave, Roll, Pitch, and Yaw
Power Supply	NiMH Batteries
Propulsion Systems	6 x Actuators coupled to legs
Sensing Capabilities	Cameras for Visual Servoing
Control Algorithms	Visual Servo Control
Testing	Coral Reefs

Table 2.6 AQUA Review

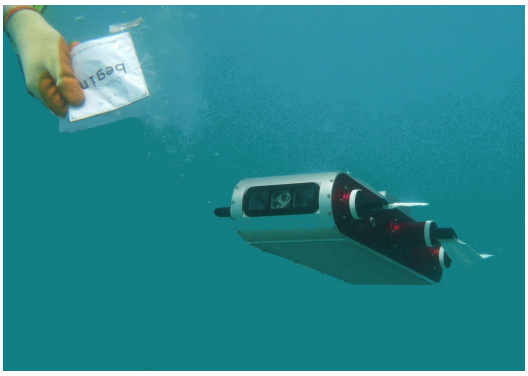

Figure 2.16 AQUA is an amphibious vehicle which can propelling itself on land or through the water [183]

2.12 Summery of the Chapter

The present chapter has focused on two key aspects. The first key aspect was the mechatronic requirements associated with the current project regarding the development of an AUV design suitable for swarms. The second key aspect was the UUVs based on the most cutting-edge technology, particularly AUVs and how they differ from ROVs. As discussed in Section 2.9.1, the majority of existing AUV technologies are intended primarily for oceanographic research and their size and absence of maneuverability make them inadequate for use in swarm applications for various tasks, such as environmental monitoring. There are various methods of classification of AUVs, such as by length, weight, and application. These categories have been explored and particular types of AUVs have been discussed in detail. Particular attention has been paid to the technologies considered to be of greatest relevance to the purposes of the present project, as outlined in Section 2.10. However, none of those examined technologies were compatible with the applications presented in Section 2.1, despite the fact that a few of them met some of the stated requirements.

3
Dynamic Model and Parameters Estimation

The purpose of the present study is to provide a comprehensive and detailed examination of underwater robots, with particular emphasis on their mechanical properties and control system. In order to provide a full description of underwater robots, a number of models are presented in the current chapter alongside the research requirements. Among the various existing models, the most important ones are those that demonstrate how underwater robots behave kinematically and dynamically. To achieve its objectives, the study draws on Fossen's book [75] and other relevant studies on the topic. The calculation of the hydrodynamic coefficients and other parameters will be addressed and discussed in Chapter 5.

The present section focuses on the mathematical model of an underwater vehicle, which complies with the laws of rigid body motion, as it is typically a body with six degrees of freedom. The system dynamics are characterized by their significant non-linearity. The kinematic model of the underwater vehicle is also described in the following part.

3.1 Kinematics

The formulation of AUV kinematic equations requires the development of the following three premises,

- The submersion of the AUV takes place at a significant distance from the bottom, walls, and water surface in a non-heterogeneous liquid;
- Underwater currents are neglected;
- The AUV is a body that displays rigidity and a mass that does not change.

The kinematic model of the system is characterized by the fact that the equations of motion do not include the actual forces that underpin the movement and the dynamic features of the vehicle. The main advantage of this model is that it enables the dynamics of the vehicle to be separated from the motion of the vehicle. Furthermore, the non-linear nature of the kinematic model is the source of the non-holonomic character of the AUV.

As illustrated in Figure 3.1, the body-fixed reference frame ($x_b y_b z_b$) and the earth-fixed frame ($x_e y_e z_e$) are the two coordinate frames that indicate how the AUV moves in six DOFs.

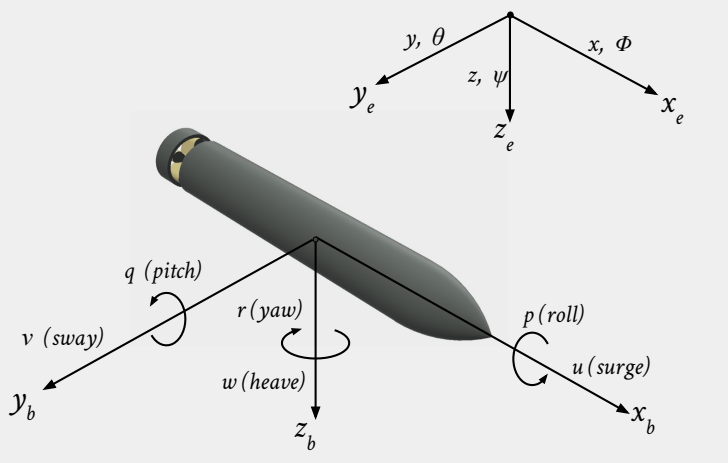

Figure 3.1 The two reference frames and the DOFs of the AUV

The earth-fixed reference frame constitutes the basis for the description of the position and the orientation of the vehicle, whilst the body-fixed reference frame helps to establish the linear velocities and the angular velocities of the vehicle (Table 3.1) [75].

6 motion components	**forces and moments**	**linear and angular velocities**	**positions and Euler angles**
surge (motions in the x-direction)	X	u	x
sway (motions in the y-direction)	Y	v	y
heave (motions in the z-direction)	Z	w	z
roll (rotation about the x-axis)	K	p	ϕ
pitch (rotation about the y-axis)	M	q	θ
yaw (rotation about the z-axis)	N	r	ψ

Table 3.1 Notation used for underwater vehicles [75]

In keeping with the above notation, the following vectors can be used to describe the general movement of an AUV in six DOFs.

$$
\begin{aligned}
\boldsymbol{\eta} &= \begin{bmatrix} \boldsymbol{\eta}_1 \\ \boldsymbol{\eta}_2 \end{bmatrix} \qquad \boldsymbol{\eta}_1 = \begin{bmatrix} x \\ y \\ z \end{bmatrix} \qquad \boldsymbol{\eta}_2 = \begin{bmatrix} \phi \\ \theta \\ \psi \end{bmatrix} \\
\boldsymbol{\nu} &= \begin{bmatrix} \boldsymbol{\nu}_1 \\ \boldsymbol{\nu}_2 \end{bmatrix} \qquad \boldsymbol{\nu}_1 = \begin{bmatrix} u \\ v \\ w \end{bmatrix} \qquad \boldsymbol{\nu}_2 = \begin{bmatrix} p \\ q \\ r \end{bmatrix} \\
\boldsymbol{\tau} &= \begin{bmatrix} \boldsymbol{\tau}_1 \\ \boldsymbol{\tau}_2 \end{bmatrix} \qquad \boldsymbol{\tau}_1 = \begin{bmatrix} X \\ Y \\ Z \end{bmatrix} \qquad \boldsymbol{\tau}_2 = \begin{bmatrix} K \\ M \\ N \end{bmatrix}
\end{aligned} \tag{3.1}
$$

The position and orientation vector based on the earth-fixed coordinates frame is given by η. In accordance with [75], Euler angles (ϕ, θ, ψ) are employed to describe the orientation η_2. Meanwhile, the linear and angular velocity vector based on the body-fixed coordinate frame is given by ν and the forces and moments that the vehicle is subjected to in the body-fixed frame are denoted by τ. A correlation between η and ν is established by the Euler angular transformation in Equation 3.2. This provides the kinematic transformation between the two reference frames, which makes of use a transformation matrix $J(\eta)$ [75]:

$$
\dot{\eta} = J(\eta)\nu = \begin{bmatrix} J_1(\eta_2) & 0 \\ 0 & J_2(\eta_2) \end{bmatrix} \nu \tag{3.2}
$$

where the linear velocity transformation is given by

$$
J_1(\eta_2) = \begin{bmatrix} c\psi c\theta & -s\psi c\phi + c\psi s\theta s\phi & s\psi s\phi + c\psi c\phi s\theta \\ s\psi c\theta & c\psi c\phi + s\phi s\theta s\psi & -c\psi s\phi + s\theta s\psi c\phi \\ -s\theta & c\theta s\phi & c\theta c\phi \end{bmatrix} \tag{3.3}
$$

and the angular velocity transformation by

$$
J_2(\eta_2) = \begin{bmatrix} 1 & s\phi t\theta & c\phi t\theta \\ 0 & c\phi & -s\phi \\ 0 & s\phi/c\theta & c\phi/c\theta \end{bmatrix} \tag{3.4}
$$

Note that, *sin*, *cos*, and *tan* are respectively denoted by s, c, and t.

3.2 Dynamics

The dynamic model is characterized by the fact that it takes into consideration the actual forces and, implicitly, the motion and dynamic features of the vehicle. Newton's law is applied to derive the translation and rotation equations.

The AUV achieves submersion into water by relying on its buoyancy. The underlying mechanism involves increasing the weight of the vehicle by drawing water into its body. The vehicle begins to submerge when the weight is higher than the buoyant force that acts upon it. The change in the weight of the vehicle that this mechanism determines simultaneously leads to a change in the position of its center of gravity (CG) as well. By contrast to the CG, the center of buoyancy (CB) does not fluctuate, but is constant and is dependent on the volume of the AUV. The calculation of the CB is straightforward, as it represents the CG of the volume of the water bubble that the AUV takes up. Consequently, the CB can be considered as the inertial center of the body frame that is attached to the vehicle.

The form of the dynamic model that describes the motion in 6 DOFs of an AUV can be expressed by the following equation [75]:

$$M\dot{\nu} + C(\nu)\nu + D(\nu)\nu + g(\eta) = \tau \tag{3.5}$$

where

$M = M_{RB} + M_A$ is the inertia matrix of the rigid body M_{RB} and hydrodynamic added mass M_A;

$C(\nu) = C_{RB}(\nu) + C_A(\nu)$ describes the Coriolis and centripetal forces for the rigid body including added mass;

$D(\nu) = D_{\text{lin}}(\nu) + D_{\text{quad}}(\nu)$ is a damping term consisting of linear and quadratic drag;

$g(\eta)$ is the vector of restoring hydrostatic forces and moments (gravitational and buoyancy forces);

τ is the vector of control inputs.

It is possible to simplify the dynamic equations that are associated with a rigid body in the following way:

$$M_{RB}\dot{\nu} + C_{RB}(\nu)\nu = \tau_{RB} \tag{3.6}$$

The CG in the body-fixed reference frame is denoted by $r_G = \left[x_G, y_G, z_G\right]^T$, while the inertia tensor associated with the body-fixed reference frame is denoted by I_0.

Thus the inertia matrix M_{RB} of the rigid body is expressed as:

$$M_{RB} = \begin{bmatrix} mI_{3\times3} & -mS(\boldsymbol{r}_G) \\ mS(\boldsymbol{r}_G) & I_0 \end{bmatrix} \tag{3.7}$$

The rigid-body Coriolis and Centripetal matrix is expressed as:

$$C_{RB}(\nu) = \begin{bmatrix} 0_{3\times3} & -mS(\boldsymbol{\nu}_1) - mS(\boldsymbol{\nu}_2)S(\boldsymbol{r}_G) \\ -mS(\boldsymbol{\nu}_1) + mS(\boldsymbol{r}_G)S(\boldsymbol{\nu}_2) & -S(I_0\boldsymbol{\nu}_2) \end{bmatrix} \tag{3.8}$$

The skew-symmetric matrix function described in [75] is denoted by S.

The generalized vector of external forces and moments is denoted by $\tau_{RB} = \begin{bmatrix} X, Y, Z, K, M, N \end{bmatrix}^T$.

3.3 External Forces and Moments

In keeping with [75], the external forces and moments τ_{RB} (it represents the right-hand side of the Equation 3.6) that act on the AUV can be defined as:

$$\tau_{RB} = \tau_H + \tau_E + \tau \tag{3.9}$$

where

τ_H represents the hydrodynamic forces and moments (restoring forces and hydrodynamic forces);

τ_E represents the environmental forces (ocean currents, waves, and wind);

τ represents the propulsion forces and moments (thruster forces and control forces);

In general, the environmental forces are associated with floating objects. In the context of underwater operation of an AUV, it is possible to disregard the environmental forces or consider them as interference. The thruster forces can be addressed separately because they constitute the inputs to the AUV. The hydrodynamic forces and moments τ_H can be described in the following equation [75]:

$$\tau_H = \underbrace{-g(\eta)}_{\text{restoring forces}} \underbrace{- M_A\dot{\nu} - C_A(\nu)\nu}_{\text{added mass}} \underbrace{- D(\nu)\nu}_{\text{damping}} \tag{3.10}$$

3.3.1 Restoring Forces and Moments

The expressions describing the weight (the force of gravity) of the AUV and the buoyancy force, are $W = mg$ and $B = \rho V g$ respectively. In these expressions,

the mass of the AUV is denoted by m, the liquid volume displaced by the AUV is denoted by V, while g and ρ respectively denote the gravity acceleration and the liquid density. Based on the East, North, Up, referred as ENU (geographical coordinate system for representing state vectors) rotation, it is possible to convert the weight and buoyancy force to the body-fixed reference frame in the following way:

$$f_G(\boldsymbol{\eta}_2) = J_1^{-1}(\boldsymbol{\eta}_2) \begin{bmatrix} 0 \\ 0 \\ W \end{bmatrix}, f_B(\boldsymbol{\eta}_2) = -J_1^{-1}(\boldsymbol{\eta}_2) \begin{bmatrix} 0 \\ 0 \\ B \end{bmatrix} \tag{3.11}$$

In accordance with Equation 3.10, it is necessary to modify the sign of the restoring forces and moments $g(\eta)$ because this notation is placed on the left-hand side of Newton's second law. Therefore, within the body-fixed reference frame, the expression of the restoring force and moment vector is as follows:

$$g(\eta) = - \begin{bmatrix} f_G + f_B \\ \boldsymbol{r}_G \times f_G + \boldsymbol{r}_B \times f_B \end{bmatrix} \tag{3.12}$$

In the above equation, the CB in the body-fixed reference frame is denoted by $\boldsymbol{r}_B = [x_B, y_B, z_B]^T$.

3.3.2 Hydrodynamic Damping

Hydrodynamic damping forces constitute the principal forces that act against the direction in which the body moves through the water.

The inertial and viscous characteristics demonstrated by the liquid are the factors that influence the hydrodynamic forces and moments that act upon a body as it moves through real incompressible liquid. Based on the premise that the liquid is ideal (i.e. lacks viscosity), it is possible to measure the inertial forces and moments to some extent, as well as the forces and moments associated with viscosity.

Hydrodynamic damping refers to the forces and moments that are related to the viscous nature of the liquid. Potential damping, wave drift damping, skin friction, and vortex shedding are the primary factors that determine hydrodynamic damping in the case of ocean vehicles [75]. An AUV with six DOFs typically exhibits damping that is coupled and demonstrates a high non-linearity. These damping effects cannot be measured on their own.

3.3.3 Added Mass Estimation

The hydrodynamic forces and moments associated with the inertial nature of the liquid that a body is exposed to during acceleration or deceleration are defined

on the basis of added mass. The assumption underlying the standard model is that velocity does not fluctuate. Movement of a body through a liquid causes displacement of the liquid in its surrounding fluid. By comparison to air, the density of water is much higher, and, therefore, greater additional force is necessary for displacement of the surrounding liquid. It is possible to model this additional force as an added mass to the body, in other words, each rigid body in fluid has an inertia matrix $M = M_{RB} + M_A$ where the inertia matrix for the rigid body and added mass is denoted by M_{RB} and M_A respectively. The best way to interpret added mass is as forces and moments that are triggered by pressure and are equivalent to the body acceleration.

3.4 Factors with Effects on Underwater Vehicles

During the process of the design of an underwater vehicle, a number of forces other than those discussed above have to be taken into account as they affect the vehicle as well. A playground seesaw is a good example to illustrate the correlation between weight and mechanical force or moment; thus, the greater the distance between the weight and the fulcrum point,the higher the mechanical force or moment needs to be (in order) to be able to overcome the weight. The ability of an overturned object to innately bring itself back to a steady state is known as 'positive stability'. In the case of an underwater vehicle, a combination of low weight center and high buoyancy center on the vehicle can easily help to attain positive longitudinal and lateral stability. The outcome of such an approach is a vehicle that demonstrates inherent stability on the pitch and roll axis. In the case of the majority of observation-class underwater vehicle systems, the vehicle can be more effectively and easily controlled the more stable it is. On the other hand, control is more difficult to achieve when the static stability is less than optimal. However, it must also be borne in mind that stability could seem to be diminished due to the external forces acting on the vehicle when it is in the water. The key design factors that must be considered during the process of designing an underwater robot are addressed more comprehensively in the following part.

3.4.1 Buoyancy

As shown in Figure 3.1, all vehicles move with around six degrees of freedom. To ensure that a system is as stable as possible, its high buoyancy center is balanced out by a low gravity center. The physical law of buoyancy, known as Archimedes' principle, states that when a body is either partly or completely submerged in a liquid, it is acted upon by a buoyancy force that is the same as the weight of the liquid that has been displaced by the body. No movement would occur if it were possible to extract the body and immediately introduce liquid in the empty space left behind that is the same as the surrounding liquid. This is because there would

be no difference whatsoever between the weight of the body and the weight of the liquid that had been displaced. The 'center of gravity' CG within the body represents the point where the totality of the entirety of weight forces acting on the displaced liquid converges. In other words, this constitutes the totality of all the forces that the body is exposed to by gravity. Meanwhile, as shown in Figure 3.2, the 'center of buoyancy' CB refers to the totality of buoyant forces that oppose the gravitational pull that acts in an upward direction via the CG of the displaced liquid. In order to make sure that, in the event of problems with power supply, the vehicle is not lost and can still come back to the surface, the standard approach is to have the vehicle positively buoyant while it is in operation.

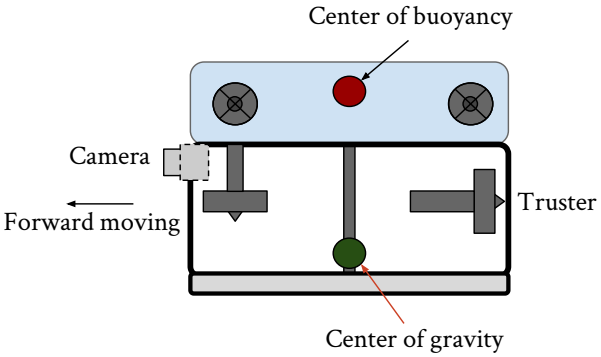

Figure 3.2 Illustration of how the positive stability of an underwater water can be achieved

3.4.2 Stability

The stability of an underwater vehicle is understood in the same way as the buoyancy. If it is assumed that there is no water movement, then the positions of the CG and the CB are the main determinants of how stable a static body is underwater. The CB represents the centroid of the body's volumetric displacement [75]. It is essential that a vertical alignment exists between the CG and the CB in the longitudinal direction or the lateral direction, otherwise a non-zero moment will be created, resulting in a loss of stability (Figure 3.3).

To avoid the vehicle becoming sensitive to disruptions, the CB and the CG must not be in the same position. The optimal situation that ensures the best bottom-heavy setting with inherent stability is when there is a vertical alignment between the CB and CG with some distance between them and with CG being under CB.

Figure 3.4 provides an illustration of the righting moment, R_M that results from the above-mentioned setting, when the vehicle rolls or pitches in direct proportionality not only to the perpendicular distance between the two centroids, but also to both

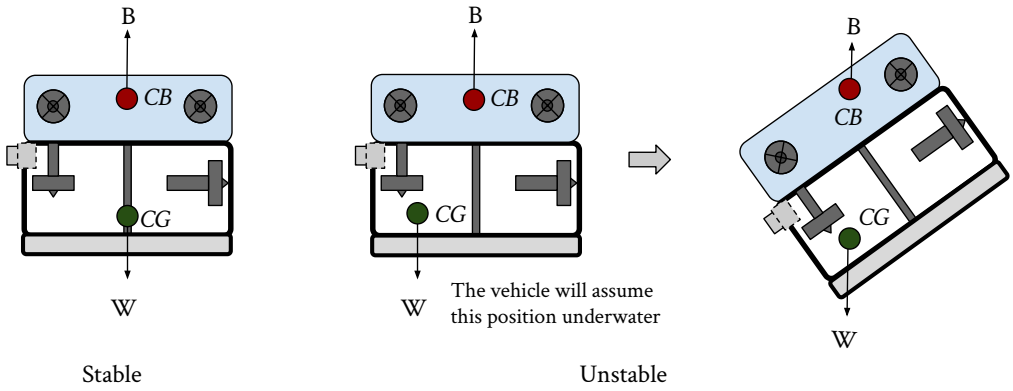

Figure 3.3 The setting in which an underwater body is in a state of stability

B and W. This R_M helps to maintain the vehicle stable by serving as a passive roll and pitch control system, and it is expressed as shown in Equation 3.13.

$$R_M = \frac{1}{2} l(B + W) sin\alpha \tag{3.13}$$

where l represents the distance between CG and CB, and α is the angle of the vehicle's heel.

External forces and centers of drag are also among the factors that have an impact on the stability of a dynamic underwater body, alongside the center of mass and the center of buoyancy. There must be an alignment between the centers of drag, which are established by the centroids of the vehicle's effective surface areas and the centers of the forces applied from the exterior, in order to enhance the dynamic stability as much as possible. This will prevent the vehicle from manifesting less-than-optimal attributes as it moves.

3.4.3 Drag Force

A drag force or water resistance is the force that opposes an underwater vehicle as it moves through the water and that consequently has to be surmounted. This forces can be expressed as drag forces F_d which have a common formula used to calculate force of drag experienced by an object due to its movement through a fully enclosing fluid domain. The expression for modeling the drag force is provided below [135]:

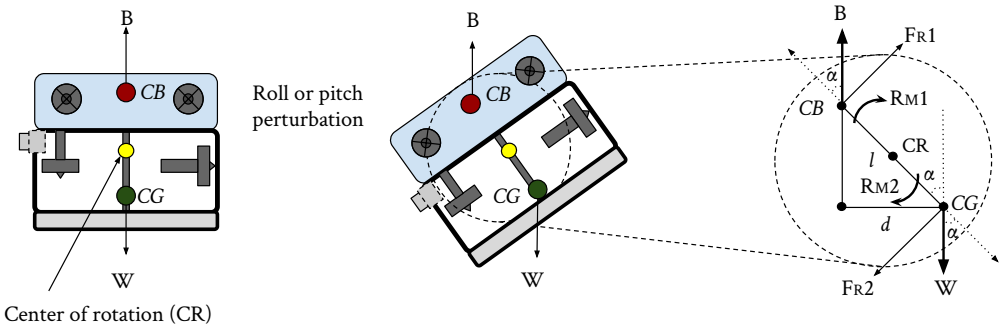

Figure 3.4 Illustration of the righting moment that occurs as a result of the roll or pitch of the vehicle

$$F_d = \frac{1}{2}\rho v^2 A C_d \tag{3.14}$$

In the above equation, the drag force or water resistance is denoted by F_d, it is equal to thrust force F_T, the density of the liquid is represented by ρ, the velocity of the body is denoted by v, the reference area (the cross-sectional area) is denoted by A, and the drag coefficient is represented by C_d which is an important factor to measure the drag force of the interactions between a vehicle and fluid, and thus determines hydrodynamic parameters of the vehicle [135].

The thrust force is the same as the drag force, provided that the velocity, v, does not fluctuate. The drag coefficient lacks dimensionality and its function is to measure and quantify the drag or the resistance that is generated by a body in a liquid, it uses to model all of the complex dependencies of shape, inclination, and flow conditions. There are two types of liquid drag whose effects are encompassed by the drag coefficient. These two types are the skin friction or frictional drag, which represents the friction of the liquid against the surface of the body, and the form drag or pressure drag, which is the drag that is produced by the form of the body.

The value of the drag coefficient can be derived from existing tables in the case of geometric forms that are not very complicated, such as the disk or sphere. However, this is not the case with the majority of underwater vehicles, which present a form of considerable complexity, as a result of which the theoretical calculation of the drag coefficient and of the reference area is not possible. Nevertheless, it is possible to calculate the drag coefficient and the reference area with the help of experimental methods or instruments of numerical analysis. In order to achieve this, several premises have to be formulated. One such premise is that the speed should be kept at a minimal level, due to the fact that the increase in the drag is directly proportional to the square of the velocity. In fact, in the context of a small AUV, a high speed is actually not advantageous because of the performance of other tasks at the same time, such as object recognition. By designing an AUV with a streamlined

shape, it is possible to diminish both the reference area and the drag coefficient. In order to achieve this, smooth transitions and forms that are not very bulky should be used.

One of the most important parameters in fluid flows that determine the C_d is Reynolds number (Re) [96], which means that the drag coefficient can be estimated by the relationships of $C_d = f(Re)$ [96]. The following equation enables the calculation of the Re [220].

$$Re = \frac{\varrho v L}{\mu} = \frac{vL}{\nu} \tag{3.15}$$

In the above equation, the density and dynamic viscosity of the fluid are denoted by ϱ and μ respectively, characteristic length is denoted by L, the velocity of the fluid is denoted by v, and the kinematic viscosity is denoted by ν.

Re is the Reynolds number which gives an impression about the flow characteristics, in addition, Re is the ratio of inertial (resistant to change or motion) forces to viscous forces for given flow conditions. Re is also a dimensionless number, high values of Re (on the order of 10 million) reference that viscous forces are very small and the flow is basically an ideal fluid.

The magnitude of quantity of Re determines the flow characteristics (laminar or turbulent). For example, to evaluate the Re numbers in a circular pipe, the pipe diameter that is denoted by d represents the characteristic length, while the mean velocity over the cross section represents the velocity of the flow. The results illustrate that if Re < 2000 the flow through the pipe can be considered as laminar, if Re > 4000 the flow can be considered as turbulent.

After the calculation of the drag coefficient has been solved, it is possible to apply Equation 3.14 to determine the drag force.

3.4.4 Pressure

The pressure that acts upon an underwater vehicle during its submersion increases in direct proportion with the level of depth at which the vehicle dives. The pressure in a non-compressible liquid can be calculated with the following equation:

$$p = p_a + \rho g h \tag{3.16}$$

In the above equation, the atmospheric pressure is denoted by p_a, the density of the liquid is denoted by ρ, the acceleration of gravity is denoted by g, and the height of the column of water is indicated by h [135].

The atmospheric pressure has a value of 10^6 Pa or 1 atm at sea level. When an underwater vehicle is closed airtight, this pressure is maintained within the hull. The rise in pressure is 1 atm for every 10 m of descent into the depths. It is vital that the hull of the underwater vehicle is capable of resisting this pressure. At the same time, it is not only the hull that must demonstrate resistance to pressure, but also every through-hull connection, such as cables or shafts, which constitute the least strong areas of the AUV structure. However, in the context of AUV of shallow water depth, the underwater vehicle is not subjected to extremely high pressure, due to the fact that the depths do not usually exceed 100 m. Nevertheless, the rise in pressure facilitates the measurement of the level of depth with the help of a pressure sensor.

3.5 Summary of the Chapter

With the purpose of reviewing the fundamental equations and associated notations that will be applied in the following chapters of the thesis, the present chapter has provided a general discussion about the kinematic and dynamic models of an AUV. Furthermore, the chapter has also addressed the hydrodynamic coefficients and added mass. In addition, another major objective of the current chapter has been to identify and to briefly discuss the most important factors that need to be considered during the process of designing an underwater vehicle.

4
Propulsion Systems of a Micro AUV

Vehicle design depends, to a great extent, on the propulsion system used. Compared to other elements, greater importance is generally afforded to the type, configuration, and power source of the thrusters. The on-board battery is the principal power source for the majority of AUVs, with the greatest amount of the total energy being used by the motors. In keeping with the aim of prolonging mission time by developing a more energy-efficient micro AUV, as Chapter 2 highlighted, the present chapter concentrates on the selection and optimization of the propulsion system. More specifically, the objective is to identify the ideal motor and propeller, as well as the ideal combination of the two.

Current aquatic vehicles employ a wide variety of propulsion systems. However, owing to physical size and power specifications, numerous systems associated with vehicles of larger dimensions are not compatible with the applications that were discussed in Section 2.1. On the other hand, some systems are too small and, therefore, cannot supply the propulsive thrust needed to permit the movement of the body through water. Furthermore, as was also specified in Section 2.1, decoupling the vertical and horizontal motion (i.e., movement of the vehicle is possible in the vertical plane but not in the horizontal plane) is among the key requirements.

4.1 Propulsion Systems Types

Vehicle submersion can be achieved in one of two ways: dynamic diving, which is the case with numerous model submarines, and static diving, which is the case with every military submarine [89]. Vehicles that are submerged through dynamic diving are characterized by the fact that they possess constant positive buoyancy, meaning that they float innately. In this case, diving is achieved based on the vehicle speed combined with the dive planes, coercing the vehicle to go underwater. This mechanism bears close similarities to the mechanism underpinning an airplane flying. By contrast, vehicles that are submerged through static diving alter their positive buoyancy to negative buoyancy ratio by permitting water to enter the ballast tanks, thus causing them to submerge. Unlike dynamic diving vehicles, static diving vehicles can submerge without reliance on speed.

The least complex existing submarine models are fully dynamic diving boats. What makes them particularly advantageous is the fact that, in the event of loss of control,

the innate positive buoyancy that these vehicles possess allows them to float back to the surface.

Some underwater vehicle applications integrate both dynamic and static diving. In such cases, submersion is achieved by permitting water to enter the main ballast tanks, followed by the precise adjustment of the buoyancy with the trim tanks. After submersion, the hydroplanes control the depth of the vehicle.

Artificial and biomimetic propulsion systems are the two major types of propulsion systems. The former are human-designed (e.g., propellers or water jets), while the latter replicate propulsive mechanisms occurring in nature, like the propulsive mechanisms of various aquatic creatures.

Five propulsion systems, four of which are artificial and one which is biomimetic, have been distinguished as promising choices, namely, piston ballast tank, mechanical oscillator, propellers, and water jets.

In the following section, each of the four propulsion systems will be discussed in terms of their functioning mechanisms, the types of vehicles in which they are incorporated, and an approximation of their force generation and power consumption.

4.1.1 Piston Ballast Tank

An artificial static diving method, the piston ballast tank resembles a syringe of large proportions, being made up of a cylinder and movable piston (Figure 4.1). The piston tank is driven by a Direct Current (DC) motor and consists of a power screw that is connected to a movable plate at one end and coupled with the gear affixed to the DC motor at the other end. The external end of the cylinder is in direct contact with the water. There is no air in the piston ballast tank. Similar to the flexible tank, filling the piston tank with water causes a rise in the pressure within the vehicle. Therefore, clockwise rotation of the motor directs the power nut to move outward, enabling the ballast to be filled with water as the blast tank generates suction pressure. This increases the general weight of the system and submersion is subsequently accomplished. Likewise, anti-clockwise rotation of the motor directs the power nut to move inward, with the water within the ballast tank being eliminated due to the injection pressure that is generated.

Precise adjustment of vehicle buoyancy can be achieved based on the measurement of the cylinder position with, for instance, a linear potentiometer linked to the thread. These kinds of ballast tanks are usually fitted horizontally because the piston stroke is of a large dimension. Consequently, there is an effect on the axial center of gravity of the vehicle when the tank is filled. For instance, the vehicle angle is no longer zero with an empty tank if the vehicle is balanced in such a way as to ensure it runs in a horizontal manner with a full ballast tank. The use of two piston tanks in the aft and bow part of the vehicle is a potential solution for this

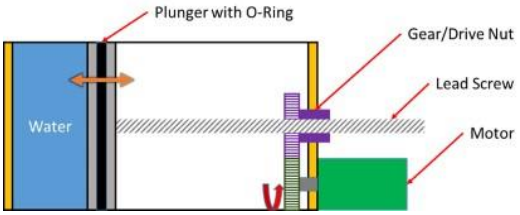

Figure 4.1 General representation of a piston tank without control components [42]

issue. Nevertheless, the piston tank still poses problems because the design is so mechanically complex and the controller demonstrates significant oscillation.

Among the most affordable and least complex existing systems is the ballast tank based on a tube pump mechanism. The system volume can be expanded or diminished by pouring water into rubber bags with the help of tube pumps, thus enabling the adjustment of the water flow within the ballast tank. However, this mechanism reduces the accuracy of the water flow control and protracts the flood time.

An AUV employing a piston ballast tank is presented in [7]. Ballast motor actuation requires 10-12 W of power for the test system with an operational range of 0.85-1.0 Amps and 12 V supply voltage.

4.1.2 Mechanical Oscillators

Frequently demonstrating greater maneuverability, stability, and quietness compared to conventional propeller-based AUV designs, biomimetic mechanical oscillators replicate the propulsive motion of fish. They are equipped with mechanically actuated oscillating fins that are responsible for enabling motion [50]. MIT's Robotuna is one example of this kind of propulsion system [18]. Meanwhile, systems of greater complexity can achieve multi-stage fin oscillation by employing more than one joint and linkage.

In [125], an experiment was carried out with a biomimetic underwater vehicle weighing 20 kg capable of generating sufficient forces; in the 17 V mode and the 12 V mode the power consumed was 34 W and 18 W, respectively.

However, backward swimming or on-the-spot rotation are motions that the majority of fish cannot perform and, therefore, neither can the mechanical models mimicking them. Although there is the possibility to use more than one fin and control surface to surmount this problem, it is not a feasible solution, especially in comparison to other potential propulsion systems under assessment. Therefore, for the purposes of the current study, mechanical oscillators are not a practical option because they are poorly maneuverable, have a highly complex design, and consume a high amount of power.

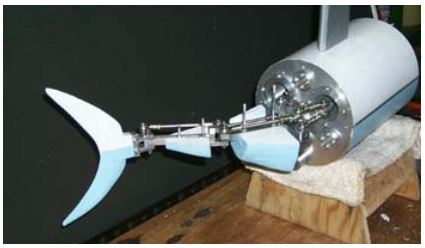

Figure 4.2 A prototype fish robot PF-600 developed to facilitate the investigation of propulsion performance [146]

4.1.3 Propellers

Categorized as artificial propulsion systems, propellers are incorporated in numerous underwater and surface vehicles. They are affixed to the motor and afford bi-directional thrust while consuming reasonable power. The use of more than one propeller/motor unit helps to improve maneuverability.

As was discussed in Section 2.10, the majority of existing AUVs relies on propellers for propulsion purposes. Ample knowledge and documentation exist on propeller-based propulsion technology. However, in the case of electric motors and propellers of extremely small size, the analytical analyses and characterization of such technologies are somewhat problematic. Nonetheless, this issue can be addressed by careful selection of the propeller and by running the motors in the efficiency work area.

The results of force tests in the Section 4.5 carried out with a few combinations of small DC motors/propellers provided in the efficiency zone a thrust estimate in the range of 200-1,100 mN, while the amount of power consumed was in the range of 2.5-16 W.

4.1.4 Water Jets

Water jets are not usually employed for underwater vehicles, despite the fact that they are a well-known and widely applied type of artificial propulsion. The underlying mechanism involves sucking in the water through a pump, accelerating it, and finally ejecting it through a nozzle. Due to the fact that more thrust is generated by the water output jet when ejected in the air compared to under the water, in the case of standard water jet systems, water ejection takes place above the water line and into the air.

Current AUVs that employ water jets as a primary form of propulsion were discussed in [165], where the target size of the initial vehicle was not very different from that in the present work. However, the system did not have fine motion control, even though preliminary evaluation suggested that the system could potentially be

highly maneuverable. Furthermore, the thrust that the water jets were capable of producing at an input voltage of 11.1 V was 1.2 N, and, overall, 16 W could be drawn up by the propulsion system.

4.2 Comparison of Propulsion Systems

As previously highlighted, a wide range of propulsion systems that are compatible with micro AUVs are available, and all of them present both weak and strong points. The four propulsion systems that were discussed above are compared in Table 4.1, with an overall weighted score being provided. A number of weighting factors were used to characterize each system, thus enabling a comparative analysis, with weightage being assigned to several criteria, as follows: controllability, mechanical complexity, volume utilization, thrust and power, and bi-directionality. A score between 0 and 3 was accorded, with 0 denoting bad or unsupported and 3 denoting the ideal case. The results of the comparative analysis indicated that, of all the propulsion systems, only propellers attained the highest weighted score and, therefore, were deemed the best option for movement in both horizontal and vertical planes.

As previously mentioned, the piston ballast tank is static systems, in which the adjustment of vehicle density requires water to be either added or eliminated. The piston ballast tank was chosen as the diving system in [14], revealing that the controller was highly complex and demonstrated a great deal of instability. Therefore, every static propulsion system was excluded as being less suitable.

Mechanical oscillators allow movement in a single direction, meaning that the vehicle cannot move in the reverse direction. Furthermore, mechanical oscillators present additional limitations in that they are either too large in size and have a high power consumption or are too small in size and fail to supply sufficient force.

Propulsion systems based on water jets cannot orientate and steer the water current to control the force without extra equipment. Moreover, their size is too large, they have a high power consumption, and the thrust they are capable of supplying diminishes as the vehicle submerges to deeper levels.

As is seen in Table 4.1 above, among the four propulsion systems, the highest total score was obtained by the propellers, reflecting the fact that they are a well-developed technology that is the most popular propulsion method. They are advantageous primarily because they afford thrust in both directions and have relatively low power consumption. However, the difficulties still remain securing optimal defining data and a run operating area for components of small size.

The various available options have been subjected to a more thorough analysis, as discussed in the following section.

		Piston Ballast Tank		**Mechanical Oscillators**		**Propellers**		**Water Jets**	
	Weightage	Rating	Wtd. Rating	Rating	Wtd. Rating	Rating	Wtd. Rating	Rating	Wtd.Rating
Controllability	0.2	**1**	**0.2**	**2**	**0.4**	**2**	**0.4**	**3**	**0.6**
Mech. Complexity	0.2	**2**	**0.4**	**3**	**0.6**	**2**	**0.4**	**2**	**0.4**
Volume Utilization	0.2	**1**	**0.2**	**1**	**0.2**	**3**	**0.6**	**1**	**0.2**
Trust and Power	0.3	**2**	**0.6**	**1**	**0.3**	**3**	**0.9**	**2**	**0.6**
Bi-Directional	0.1	**3**	**0.3**	**0**	**0**	**3**	**0.3**	**0**	**0**
	Total Weighted Score		**1.7**		**1.5**		**2.6**		**1.6**

Table 4.1 Comparative analysis of the different propulsion systems

4.3 Forces Acting on the Vehicle

A number of preliminary aspects must be addressed prior to beginning analysis the propellers. During submersion, a vehicle is subject to a number of forces, namely, the buoyancy force F_b, the gravitational force F_g, the drag force F_d, and the external thrust force F_T, as shown in Figure 4.3. The working assumption is that z has a positive value in the downward buoyancy force as direction.

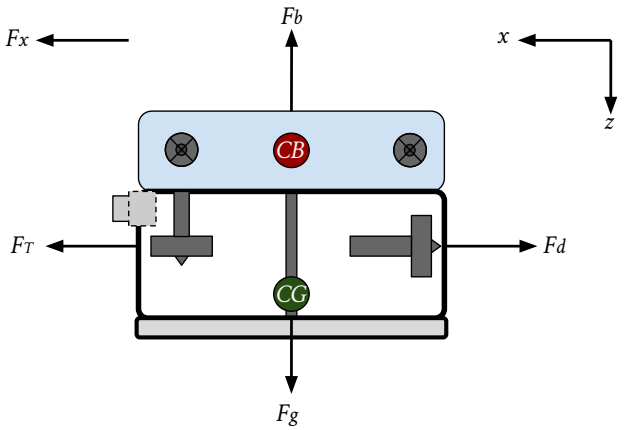

Figure 4.3 The forces a submerged vehicle is subjected to

The buoyancy force and the gravitational force are the two forces that act on a submerged vehicle in the vertical plane. The vehicle is considered to be neutrally buoyant if the two forces are equivalent, that is, the density of the vehicle and the density of the surrounding water are the same. This is illustrated by Equation 4.1 below:

$$\begin{aligned} F_b &= F_g \\ \rho g V &= mg \end{aligned} \tag{4.1}$$

Although the water density depends on depth, it undergoes alterations solely at depth values greater than 100 m. This does not apply to the current work because, as mentioned in Chapter 2, the designed vehicle is planned for deployment in shallow waters with depths not exceeding 100 m.

A neutrally buoyant vehicle will hover at a depth where the density of the water and that of the vehicle are equal, if it lacks vertical momentum. On the other hand, in order to be able to hover, a non-neutrally buoyant vehicle will necessitate an external thrust force that is equal to but opposite of the imbalanced buoyancy force.

The external thruster units would need to be constantly activated to neutralize the positive buoyancy and thus make dynamic diving possible. Although the complexity of the control system would be limited, the buoyancy force might give rise to steady-state errors [75]. Furthermore, since the thruster units would be constantly activated, dynamic diving would consume a great amount of power.

Sole movement in dimension x is taken into account in the horizontal plane. Owing to the assumption that the vehicle is neutrally buoyant, no mass flow occurs because the gravitational force and the buoyancy force counteract one another.

$$F_x = F_T - F_d \tag{4.2}$$

4.4 Propulsion System Components

The remaining option for analysis is propellers, as indicated in Section 4.2. Marine vehicles of various sizes, from ocean liners to AUVs, incorporate propellers. The major components of the electric propulsion system underpinning a propeller-based thruster unit are the battery, motor controller (also called Electronic Speed Controller (ESC)), electric motor, and propeller (Figure 4.4). Occasionally, a gear system is integrated between the motor and propeller, but most often it is a part of the motor.

The degrees of freedom that can be controlled depend on the motor location (later on, Chapter 5 will illustrate the location of the vertical and horizontal thrusters of the proposed vehicle), which also has implications for noise interference with on-board electronic components and propeller-to-hull and propeller-to-propeller interactions. These two types of interactions can affect AUV dynamics in an undesirable way. The combination of the thrusters and the hull of the vehicle are illustrated in detail in Chapter 5. During movement at a constant speed, the motor-generated thrust and the vehicle's friction or drag are the same; in other words, the thrust is equivalent to that exhibited by Equation 3.14. Hence, the increase in vehicle speed causes a significant increase in the amount of power consumed by the propulsion system, due to the fact that the thrust power is equivalent to the product of thrust and speed. Consequently, thrust power is a function of speed cubed:

$$Thrust\ Power = F_d \times v = \frac{1}{2}\rho v^3 A C_d \tag{4.3}$$

The energy supply of an AUV is limited, meaning that it must move at a speed that does not require excessive power consumption while ensuring an acceptable mission time. Hence, determining the ideal speed is a matter of optimization.

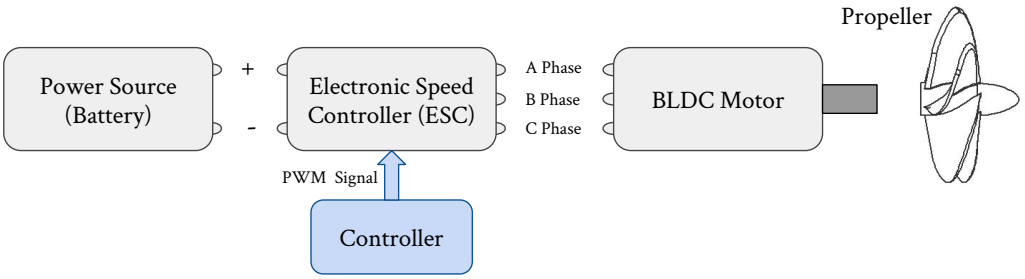

Figure 4.4 The components of a standard electric propulsion system

The optimization routine will exclude the design of the ESC, as it would go beyond the scope of the current study. Nonetheless, an efficiency coefficient is included because of the effect determined by various brands and types of speed controllers. Likewise, the battery is also excluded from the optimization routine because it does not directly impact the propulsion system, provided that a suitable type is chosen with consideration given to its continuous discharge rate. Furthermore, at this stage, the weight of the components is ignored because it is only relevant during the performance of a complete vehicle optimization with the propulsion system included. Instead, the current chapter focuses on the choice of motor and propeller.

4.4.1 Electric DC Motor and its Driver Selection

Electric motors are electromechanical machines capable of generating mechanical output power from electrical input power. DC is the power supply usually used in AUVs. There is a variety of electric motor shapes, sizes, and technologies that are all associated with different functions. Brushed and brushless motors are the most frequently used types. They respectively rely on mechanical and electronic commutation to change the electric current direction and produce a pulling magnetic force between the stator and the magnets. Compared to brushed motors, brushless motors, or BLDC, are advantageous because they are more efficient, have a longer lifespan, are less noisy, and have a higher power-to-weight ratio, making them more reliable for AUV applications. In-runners and out-runners are the two types of brushless motors, which differ in that the former have the magnets positioned on the motor shaft and the windings are on the external motor side, while the latter have the magnets rotating around the stator. In contrast to out-runner motors, in-runner motors can attain higher rotation speeds due to the low inertia of the

motor shaft. Nonetheless, out-runner motors are more popular because they run cooler and have high torque specifications.

According to the requirements outlined in Chapter 2, the complete thruster unit must have a low power consumption and a small size, but be capable of generating enough force for both horizontal and vertical thrust.

Based on the examination of a dozen different DC motors, the ROXXY BL Out-runner 2220-20 three-phase brushless motor was chosen for this project due to its long-term use in the MONSUN project [154], which is relevant to the current study as it has satisfied performance to thrust a 6-kg vehicle, it is affordable, small in size, and has a long and stable lifespan.

Category	Brushless DC motor
KV (RPM per volt)	1300
Output power	60 W
Max. current	8.5 A
Shaft	2 mm
Length and diameter	22 mm x 20 mm
Weight	28 g

Table 4.2 The main characteristics of ROXXY BL Out-runner 2220-20 brushless motor

To ensure compatibility, the ESC, namely the ROXXY BL-Control 918, was chosen from the same company. The ROXXY BL-Control 918 is a motor driver board that is suitable for the chosen motor because it enables the bi-directional control of brushless DC motors.

4.5 Propeller Selection

Aside from the motor, the propellers are also important for maximizing propulsion system performance. The two components are interdependent and their optimization represents an iterative process. In fact, interdependence exists between all components, although they can be modified separately.

Propellers are responsible for transferring power to the water, a process known as thrust. More specifically, generated thrust occurs when water is pulled by the propellers in front of them (the vehicle side) before being pushed out at the back. This pull–push effect of the blades and the low-to-high pressure differential engender this momentum change, which underpins the thrust generation. Although the basic components are the same in all propellers, they differ considerably in terms of diameter, rotation, and number of blades, giving rise to different reactions.

Various propellers were analyzed with a developed prototype using propeller-based thruster units, as presented in Figure 4.5. In order to make sure that there was

optimal performance compatibility with the DC motor, six Graupner propellers were analyzed. Graupner is a leading manufacturer of small boat propellers. This type of propeller was chosen because they were in the appropriate diameter range and were available off-the-shelf. Numerous projects using micro or small AUVs [94, 154, 184] specified that the diameter should be in the range of 30-50 mm with a 50 mm diameter generating a force of up to 17 N [103]. Several propellers of different sizes and blades were assessed, as indicated in Figure 4.5, to determine which one was the best to provide sufficient thrust to move the vehicle hull bi-directionally. As will be discussed in detail in Chapter 5, the requested thrust to move the vehicle hull of a micro AUV in the vertical direction is around 6 N for 1 m/s, and in the horizontal direction is around 2 N for low-speed diving.

Figure 4.5 The tested propellers with different sizes and blades

4.5.1 Experimental Setup

Figure 4.6 illustrates an actual thruster experiment. For affordability reasons and due to a lack of complexity, the carbon fiber-reinforced propellers with M5-threaded brass inserts were selected. To link the propeller via the M5-thread nut, the M5-threaded screw was developed on the motor shaft axis, in the manner illustrated in Figure 4.7. To protect the DC motor against damage caused by water, the thruster was coated in lacquer. According to the control signal Pulse Width Modulation (PWM) generated by the micro-controller (Arduino board), the thruster received a value of 0-11.1 V from the output of the ESC to which it was connected. Simultaneously, the ESC input was connected to an 11.1 V Lithium-Polymer (Li-Po) battery that powered the DC motor. The PWM represented the input control signal of the ESC that was emitted by the "servo library", according to the microseconds function incorporated in every Arduino board (see Figure 4.8 for simple code), with 1100 μs giving max. reverse, 1500 μs stopped, and 1900 μs max. forward of the DC motor, as can be seen in Figure 4.9. Furthermore, the deadband on which the DC motor did not run was in the range of 1440-1545 μs.

The ESC generated a series of pulses at 32 kHz with a pulse width producing 0-11.1 V to the DC motor and driving it. The current consumption of the thruster for every PWM value was determined with the use of a multimeter.

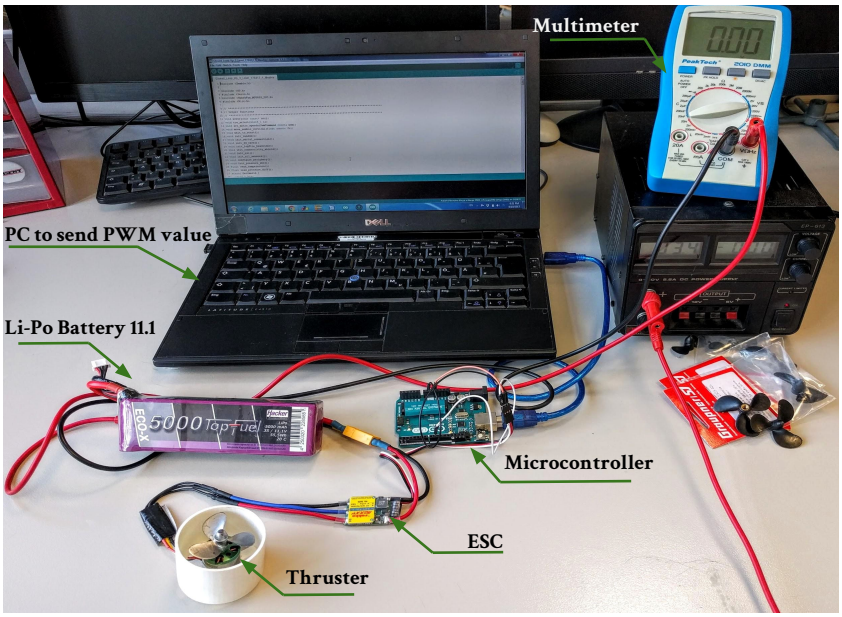

Figure 4.6 The actual experimental setup for measuring the thrust of the propellers

Figure 4.7 The connection between the DC motor and the propeller

The forward propeller is a right-handed propeller in the case of a counter-rotating set. In order to attain more thrust in the diving direction while the positive buoyancy allows the AUV to float to the surface, only left-handed propellers were analyzed. However, the assumption that followed was that the performance curves produced by a left-handed propeller would be the same as by a right-handed propeller.

The digital force gauge Sauter FH500 was used to measure the thruster force of every propeller to determine performance (Figure 4.10) within a precision of 0.1 N. In the present case, the force sensor was employed with the sole reason of measuring the magnitude of the thruster's force. When the thruster was completely under water, it was connected to the force sensor through a long axis, as can be seen in Figure 4.10.

```
#include <Servo.h>
Servo mythruster;  // create servo object to control a servo
int val;     // variable to read the value from the analog pin

void setup() {
mythruster.attach(9);  // attaches the thruster on pin 9 to the thruster object
servo.writeMicroseconds(1500); // send "stop" signal to ESC
}

void loop() {
val = map(val, 1500, 1900, 0, 100);      // scale it to use it with the thruster
mythrustrr.write(val);                   // sets the servo position according to the
      scaled value
delay(10);                               // waits for the thruster to get there
}
```

Figure 4.8 A simple code for thruster driving

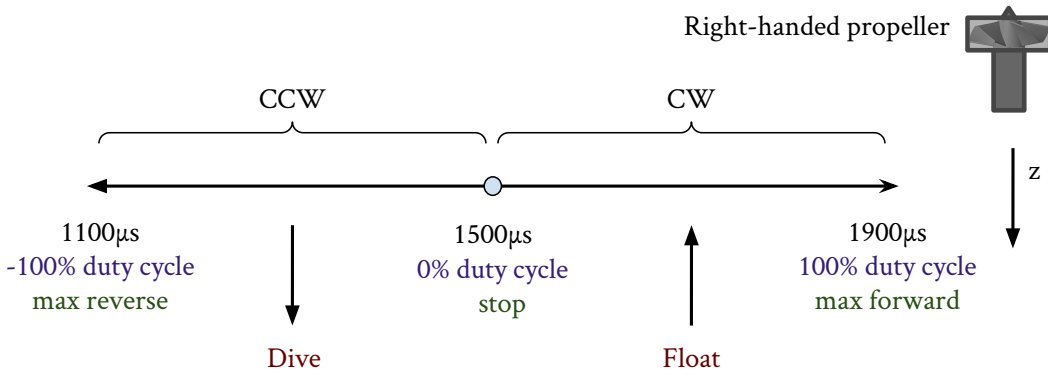

Figure 4.9 The reference direction of the thruster and the scale range associated with the dive and float movement

4.5.2 Propeller Analysis and Results

As discussed in Section 4.2, the propellers were considered to be the most viable option of the various propulsion systems tested. They are used on a broad basis in marine vehicles of every size, from ocean liners to AUVs.

To determine the impact of the thruster on efficiency, a nozzle test was carried out in the beginning. According to the results, the efficiency factor could be increased by covering the thruster with a nozzle in order to produce more force, as illustrated in Figure 4.11.

Figure 4.12 and Figure 4.13 present the results from the experiments carried out on the different propellers without nozzle. Based on those results, it was deduced that the increase in the thruster force and the current were nearly linear with the duty cycle. The duty cycle, otherwise known as the speed control, of the PWM

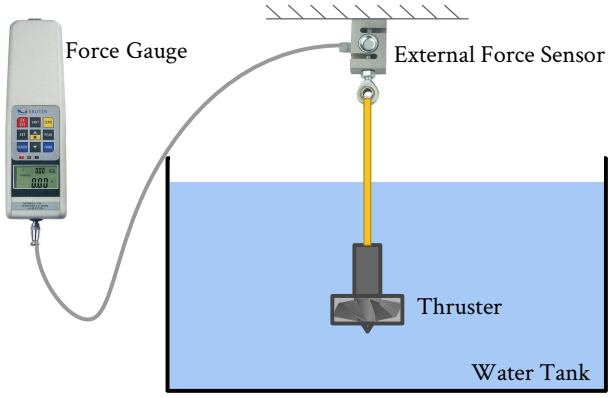

Figure 4.10 Overview of the experiment setup for the measurement of the propeller thrust

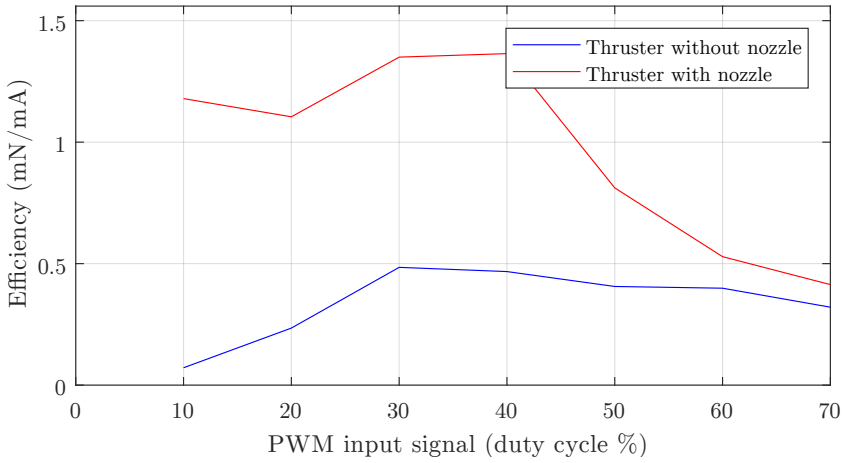

Figure 4.11 The impact of the nozzle on the thruster

signals driving the DC motor increased from 0% to 80%, with a spacing of 10%. The Arduino board received the code from the computer and sent back the PWM value through the serial monitor. Furthermore, the ESC received the PWM from the Arduino board and, in turn, transmitted a voltage value to the DC motor.

A dead zone was displayed by the DC motor, wherein the propellers only started to turn at 13% and began to provide a measurable thrust at 13-15%. The friction of the shaft seals was the main reason for the occurrence of this dead zone.

The results of the force analysis suggests that the worst performance was associated with the 2310-47 propeller with four blades, as can be seen in Figure 4.12. This type of propeller generated a low force that was less than 1,000 mN, despite the

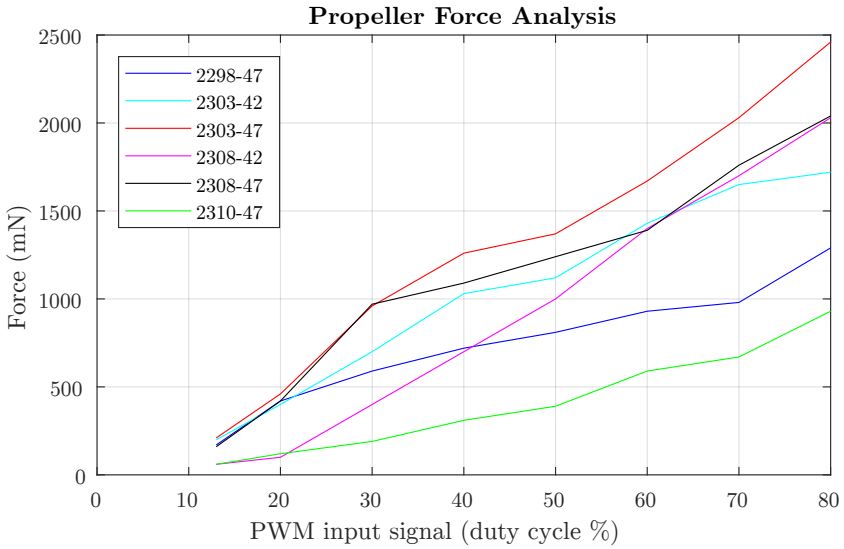

Figure 4.12 The analysis of the force of the different propellers

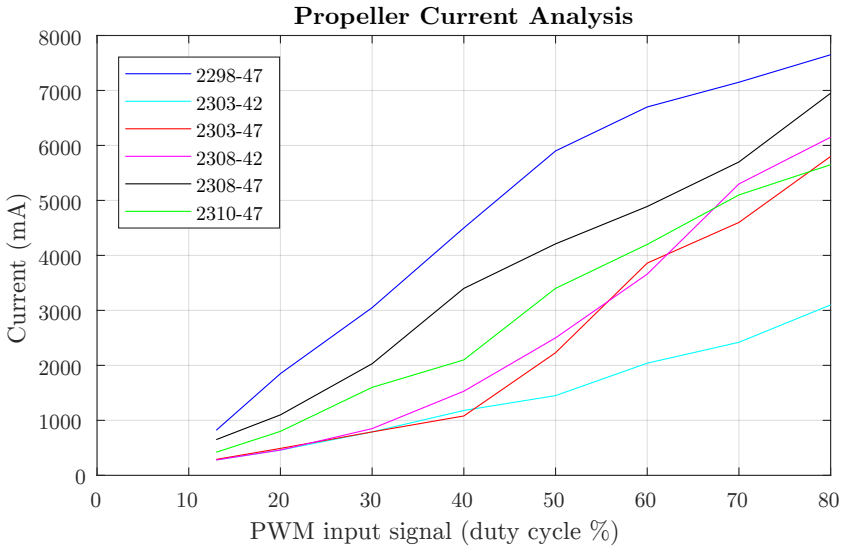

Figure 4.13 Current analysis conducted on the different types of propellers

high signal input (it used 80% of the input signal or speed). Similarly, the 2298-47 propeller with five blades required over 70% of the input signal to provide a force of 1,000 mN. Between these two types of propellers, the 2308-42 propeller with three blades performed better, as it was able to exceed the 1,000 mN threshold with the use of 50% of the input signal. Meanwhile, the remaining three propellers generated sufficient force of more than 1,000 mN with less than 50% of the input signal. The propeller that produced the greatest amount of force was the 2303-47. On the basis

of these results, the propellers that generated over 1,000 mN at less than 50% of the input signal were selected, while the propellers that did not satisfy this condition, namely, the 2298-47 propeller and the 2310-47 propeller, were eliminated.

However, as is illustrated in Figure 4.13, the types of propellers that were tested presented additional points of differences and similarities. For example, the diameter of propellers 2298-47, 2308-47, and 2310-47 were the same, but these three types of propellers exhibited the worst performance when it came to the amount of current consumed. By contrast, in view of current consumption, the 2303-42 propeller demonstrated optimal performance, consuming the least amount of current. Therefore, based on the results obtained from the analysis of current performance, the 2298-47, 2308-47, and 2310-47 propellers were eliminated as unsuitable candidates.

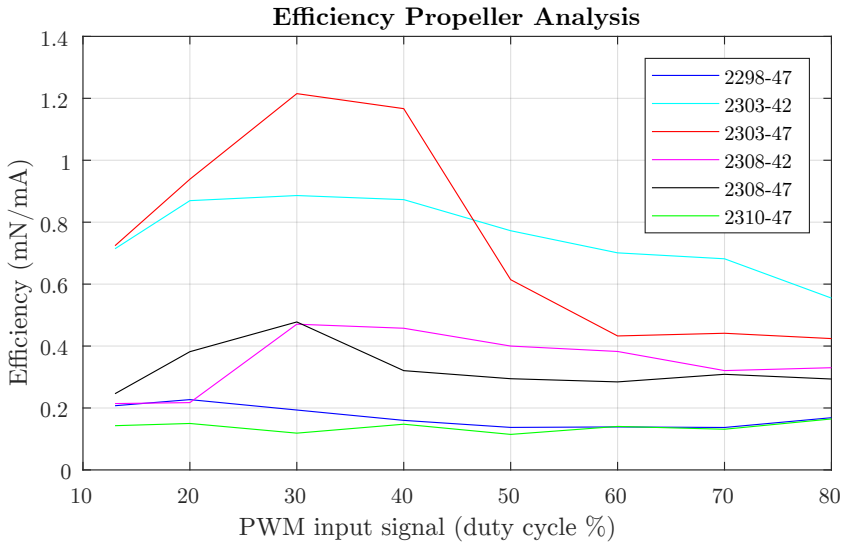

Figure 4.14 The levels of efficiency demonstrated by the different propellers under consideration

An additional comparative analysis was conducted on the selected types of propellers focusing on their efficiency. The results revealed that the propellers that exhibited a low efficiency factor were 2298-47, 2308-47, 2310-47, and 2308-42. Therefore, these propeller types were removed from the list of potential candidates. After the elimination of the propellers as described above, the two that were left were the 2303-42 and 2303-47 propellers. These propellers were similar in that both of them were equipped with two blades; on the other hand, they differed in terms of size. Another point of difference between the 2303-42 propeller and the 2303-47 propeller was that the latter had a higher efficiency factor until approximately 50% of the input signal. Compared to the 2303-42 propeller, the 2303-47 propeller provided a much longer battery life. Given that, as mentioned in Chapter 2, a major aim of the present study was to develop a micro AUV that consumed a limited

amount of energy, the 2303-47 propeller was chosen to be integrated in the thruster as the most viable propeller for the purposes of this study. Despite the fact that the thruster, under normal working conditions, was run only at a low speed, the 2303-47 propeller succeeded in avoiding the low efficiency factor zone. Furthermore, to improve the efficiency of the chosen propeller even more, a number of aspects of the thruster were refined and developed. The results obtained with the use of the chosen propeller are detailed in the following section.

4.5.3 Experiments Conducted on the Chosen Propeller

It is of great importance to be able to take the measurement of the output force of the thruster units, particularly with regard to the control systems. The PWM should be as low as possible so that the propeller spins with minimal speed, which helps to maximize the efficiency of the system. As was discussed in the preceding section that focused on the comparative analysis of the different propellers, the type of propeller that demonstrates the highest efficiency is the one equipped with two blades. Consequently, the two-bladed propeller allows for a propeller design of greater efficiency and, implicitly, a system of greater overall efficiency. However, despite the importance of the propeller efficiency, it is not the only parameter that needs to be considered; all the other aspects of the propulsion system are important as well, and, therefore, must be taken into consideration. For instance, the closer to the zone of maximum efficiency that the thruster operates, the greater the force that it is capable of producing and the lower the amount of energy consumed.

The results related to the performance of the chosen propeller are outlined and discussed in the following section. The chosen 2303-47 propeller has the following characteristics: it is M5-threaded, equipped with two blades, and is classified as a left-handed propeller. The nozzle diameter was expanded by a couple of millimeters. Chapter 5 provides details about how the nozzles that contained the thrusters were used and how they were combined together for the vehicle. Further, Chapter 7 focuses on running the thruster in the efficient band.

For the purposes of implementing a propeller-based thrust that can be controlled, the velocity of the motor was subjected to manipulation so that it changed within the same range that the duty cycle of the PWM signals changed. In the experiment conducted, the precise output was reflected in the fine range of the PWM input signal that was used. An additional use of this fine range was to define the deadband of the thruster so as to avoid it whilst the vehicle was in motion. The correlation between the thrust and the velocity and the variation experienced by the latter, according to the duty cycle of the PWM input signals, was explored in Equation 4.3. Furthermore, to attain thrust control, experiments related to the thrust measurement of one propeller were carried out to accurately determine how the duty cycle of the PWM input signals and the thrust of the propeller were correlated.

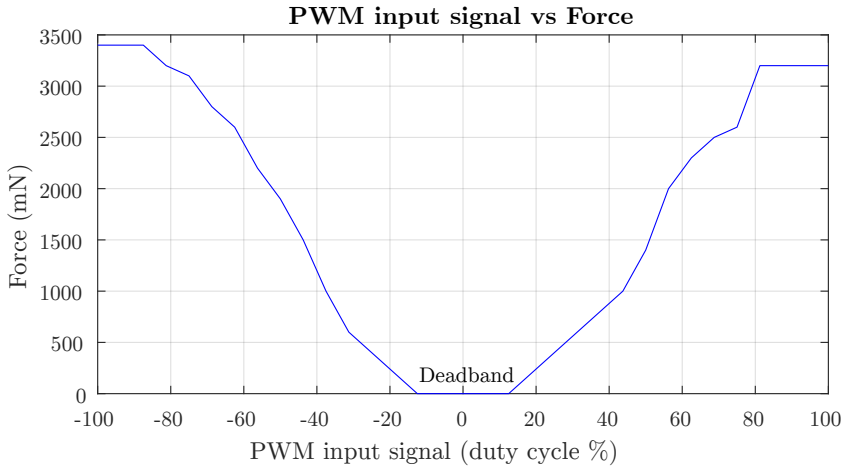

Figure 4.15 The performance of the propeller in terms of force

As can be derived from the results presented in Figure 4.15, the increase in the thrust of the propeller is a function of the duty cycle of the PWM input signals. The same figure indicates that the maximum thrust was 3,400 mN, which is a considerably high force in comparison to that used in [123], where the maximum force of a vehicle of a round shape with a diameter of 25 cm was approximately 180 mN at a duty cycle of 100%, with every actuating unit functioning in a horizontal plane. An additional aspect that can be observed in Figure 4.15 is that the generated force was more or less symmetrical in the forward and reverse directions. The saturation band began at approximately 82% of the input signal, while the deadband of the thruster was in a range from 0% to 17%. Figure 4.16 presents the experiments that were carried out in relation to the power and current, and Figure 4.17 shows the efficiency of the thruster depending on the duty cycle.

4.6 Summary

This chapter identified a range of different candidate propulsion systems that could be used to support the movement of the vehicle in the horizontal plane as well as in the vertical plane and subjected them to a comprehensive analysis and comparison. The conclusion derived from this process was that the most appropriate and practical option for the horizontal and vertical planes are propeller-based thruster units that make use of small electrical motors.

Propeller-based thruster units present a number of advantages, such as being capable of providing the required thrust, enable bi-directional movement due to their relatively small power consumption, and are relatively simple in terms of mechanics and the control system. Furthermore, to ensure that the thruster performed optimally, an adequate selection propulsion system components was made, especially

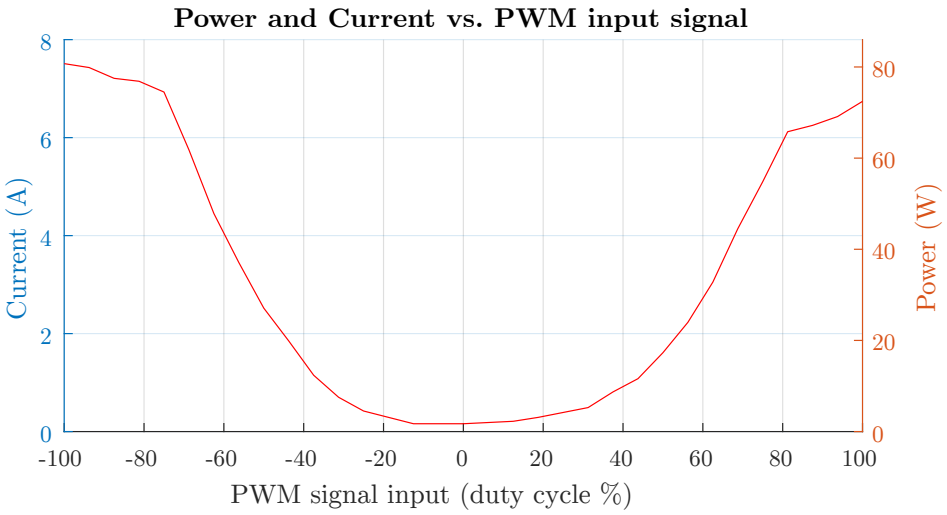

Figure 4.16 The performance in terms of current and power

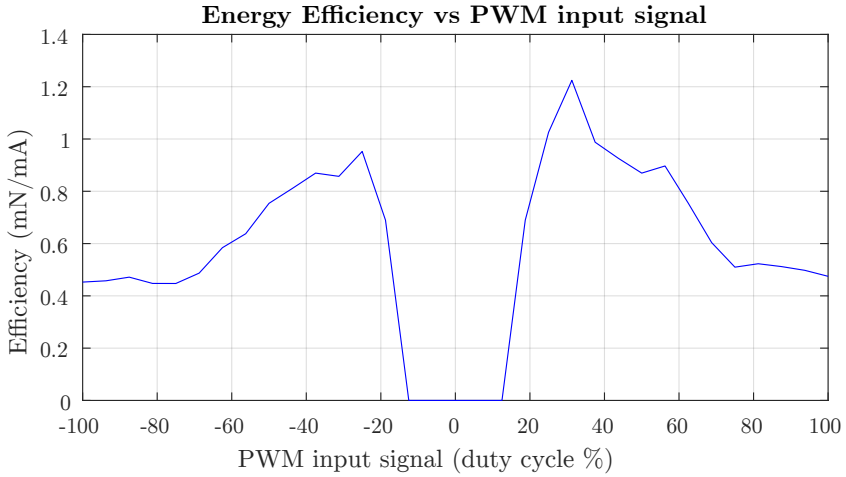

Figure 4.17 The energy efficiency

with regard to the propeller component. Chapter 5 and Chapter 7 will provide a comprehensive discussion with respect to the experiments conducted to test the chosen propeller with the vehicle.

5
Mechanical and Electrical Design

Putting the mechanical design into practice was among the key priorities of the project. This required the construction of a prototype vehicle with the complete five DOF movement capabilities discussed in Chapter 2. This chapter addresses this construction and presents the streamlined design of the pressure hull, which constitutes the main vehicle body in which every component and electronic device is enclosed, the design of each internal component of the AUV, and the 3D drawings created with the CAD software SolidWorks. Furthermore, the outcomes of the hydrodynamic analysis of the vehicle conducted on the basis of Computational Fluid Dynamics (CFD) are provided in this chapter.

Chapter 2 discussed in detail existing AUV designs of different sizes that may have been relevant to the current project. Not many existing AUVs, for both commercial or research purposes, were found to be appropriate for environmental monitoring and swarm applications, and the few that were appropriate had a design that disregarded energy consumption. Therefore, the design of a new vehicle was necessary to achieve this vision. To this end, the optimal approach was the integration of nature-inspired design ideas and the alteration of an existing design relevant to the project rather than coming up with an entirely new design.

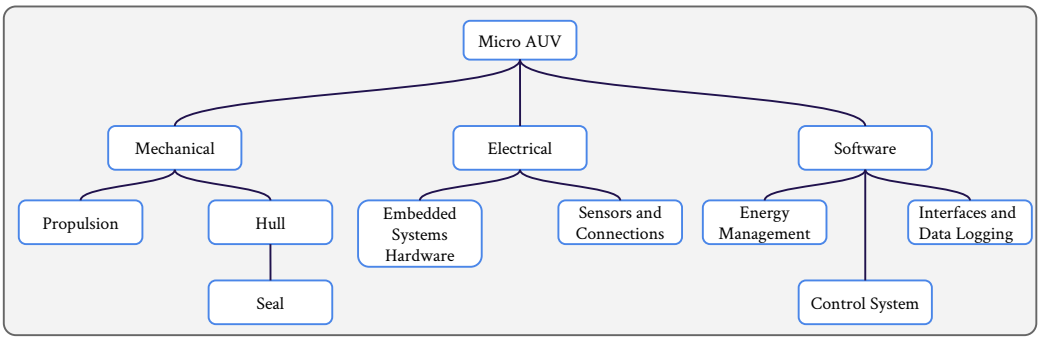

Figure 5.1 Illustration of each technical area of a micro AUV

As outlined in Chapter 2, an electrical system capable of controlling the vehicle using software underpinned by Embedded System Hardware (ESH) was envisioned for the design of the prototype micro AUV. Several functions had to be fulfilled by the ESH, including interfacing with the input sensors, applying the control algorithms, and recording input and output data. Section 5.6 describes the modular

approach that was adopted for the design. Such an approach enabled the addition of extra circuitry, including a digital signal processor to support the interface with the acoustic modem.

The envisioned sensor suite consisted of a pressure sensor to enable depth measurements, a digital compass and gyroscope to measure angular positions and velocities, and a Global Positioning System (GPS) for surface navigation and location. Staff at the Institute of Computer Engineering undertook the task of creating the acoustic modem and communication system. Moreover, the energy and recharging system was taken into account, as discussed in Chapter 7.

The separation of the design into particular technical areas is illustrated in Figure 5.1. The work that was performed in each area is reviewed in the following parts of this chapter.

5.1 Background and Design Idea

The natural world has been the main inspiration for the development and design of a streamlined micro AUV with a streamline shape called SEMBIO. A number of concepts associated with conventional micro AUVs were included in the design as well. The vehicle was strengthened in several ways by its combination design. The discussion in the following part focuses on the justification of the importance of biological inspiration for AUV design, what the initial source of inspiration was, and why that particular source was selected.

5.1.1 Biomimetics and Biological Inspiration

A major source of innovative ideas is biomimetics and bio-inspired design. The purpose of biomimetics is to create engineered systems that have the same properties or that look and work in the same way as living systems [217]. More specifically, in the context of the robotics field, biomimetics aims to create machines replicating how living organisms utilize their body shape by drawing inspiration from the biological world.

By incorporating innovative features from nature into engineered systems, the biomimetic approach attempts to advance technology. Biomimetics may help engineered systems to perform better through imitation of the biological properties that afford living organisms a higher performance than human-made devices [72]. Thus, ingenious technological solutions can be formulated more rapidly by taking advantage of the wide range of specialized features demonstrated by organisms that can be incorporated into technology.

In the case of aquatic systems, the biomimetic approach has been mostly focused on the exploration of the locomotion specializations of living organisms that have

Figure 5.2 The manta ray belonging to the eagle ray family *Myliobatidae*

a higher energy efficiency. Over a period of more than 500 million years, fish and other animals have evolved features that allow them to live in a liquid environment with a density and dynamic viscosity that exceed those of air 800-fold and 60-fold, respectively [73]. Aquatic engineered systems are subject to the same physical forces as aquatic organisms in an environment governed by Archimedes' Principle and where movement must overcome the opposition of drag. The imitation of natural features and the knowledge of independent convergence with animal designs have enabled new developments in engineered systems intended to operate in an aquatic environments [38]. Biomimetics may help the development of innovative technologies to be streamlined on the basis of investigations of processes that can facilitate the adaptation of aquatic organism designs to human-made devices [73].

With regard to the design of AUVs, an increasing amount of attention has been paid to determine how the development of such machines could benefit from biological inspiration. This has prompted studies to comprehend how marine organisms behave and how they are shaped [179]. The development of AUVs that can be launched rapidly and can be used for different missions is highly important at the moment. The general consensus is that next-generation AUVs must be efficient, maneuverable, stable in environments of high disturbances, operational both in areas near the coast and in the open ocean, and can hold a position. Meanwhile, the most desirable properties to be achieved in the design process include a rigid hull, low drag, and efficient energy use. These properties are demonstrated by several organisms in the animal kingdom, which, therefore, may afford potential solutions. One such organism is the manta ray of the family *Myliobatidae*. The development of the Biomimetic Autonomous Undersea Vehicle (BAUV) has included an attempt to replicate the biological properties and kinematics of *Myliobatidae* rays [84]. There are consistencies between the biological properties of *Myliobatidae* rays, including the manta (Figure 5.2) and the design space of a BAUV. This type of vehicle could be produced to consume less energy and be more maneuverable by investigating the

properties of aquatic organisms [44, 188]. It must be noted that, from a biological perspective, the concept of design refers to the fact that the structure and function of a particular feature of an organism are correlated.

To summarize, robotic systems for aquatic deployment could be made to perform better by modelling them on living organisms [71, 74, 207] with relevant properties. Since the ultimate goal is to create engineered systems that can move effectively without consuming a great amount of energy, nature-inspired design solutions may be useful in the development of novel technologies. In particular, biomimetic mechanisms may support the improvement of engineered system shapes and propulsion. Additional advantages that human-made aquatic systems could obtain from biological innovations include speed, stealth, reduced energy consumption, and better maneuverability [97].

5.1.2 Shovelnose Guitarfish

The research organism selected to help the development of the batoid body shape was the Atlantic or shovelnose guitarfish *Rhinobatos lentiginosus (Batoidea: Rhinobatoidei)*. This species of fish belongs to the *Chondrichthyes* class, which also includes skates and sharks, the order *Rajiformes* (e.g., electric ray, sawfish, skate, stingray), and the family *Rhinobatos productus ray* [120, 231]. Its swimming motion is supported by median paired fins, and its body is flat and has the shape of a diamond (Figure 5.3). It has pectoral fins of considerable size that merge with the head and the gill slits are situated ventrally [52, 177]. The species of smallest size display great agility and swiftness. The largest species are also agile, capable of significant maneuverability (e.g., turn-on-a-dime maneuvers), and can swim over distances of significant length and at high speed. They are also very strong. The fluid-dynamics of their propulsion mechanism has been the focus of some studies [32, 128]. Owing to these characteristics and features, the guitarfish can inspire the development of biomimetic aquatic engineered systems, such as AUVs and ROVs.

5.1.3 Design Inspiration of Guitarfish

When biological designs are replicated, exact practical outcomes are not usually achieved, which can even be detrimental to the development of engineered systems [71, 218]. For instance, the idea of flight and early wing design were inspired by birds [106], but birds' wing flapping for concomitant production of lift and thrust is not replicated by aircrafts, owing to drawbacks such as scaling and the incredibly high speeds at which commercial and military aircrafts can travel. Research currently aims at understanding the agility displayed by birds during the performance of aerial maneuvers of high complexity. This agility cannot be demonstrated by any human-made machine, as birds' cognitive processes control the sophisticated mechanical connections while simultaneously sensing and adjusting the airflow over

Figure 5.3 The shovelnose guitarfish [230]

the propulsor surfaces cannot be replicated. From this perspective, birds obviously perform better than any human-made aircraft. Despite the great potential and attraction of drawing inspiration from animal performance to create more advanced technological designs, it has not yet been achieved.

Based on the considerations discussed above, this research restricts itself to imitating the hydrodynamic geometry and flattened streamlined shape of the guitarfish to design engineered systems that can move underwater effectively and rapidly, with minimal thrust force.

In recent times, biologists and engineers have directed their attention to the potential of batoid fish (e.g., electric ray, sawfish, guitarfish, skate, and stingray) as a source of inspiration for the development of next-generation BAUVs [144]. In this study, the selection of the guitarfish as a bio-inspired model is justified on the following grounds:

- The guitarfish differs from other species of fish in that it does not need to move its body as it swims, owing to the flatness and large size of its body (its swimming thus resembles an underwater flight); this makes it a good model for the design of a surface that can carry various instruments such as sensors (i.e., payload) for exploring the aquatic environment.

- The guitarfish has a highly effective forward propulsion thanks to the geometric shape of its front part, particularly the shovel-shaped nose, as well as a low-drag profile, as its body and fins have a streamlined shape (see Figure 5.3) [70, 218].

- Its size also makes the guitarfish a suitable inspiration for the modelling of a BAUV, which is usually between 75 cm (similar to the size of a micro AUV of $<$ 1 m) and 170 cm long. The size and speed of the guitarfish are compatible with AUV design and operation, which is why matters of scaling can be disregarded. From the perspective of the key variables of Re and Strouhal number (St), an

equivalence exists between the hydrodynamics of the biological and engineered systems.

- A high Re denotes the ratio of inertial to frictional forces and indicates whether the flow conditions surrounding a submerged body are laminar or turbulent. The Re value associated with batoid fish swimming at one body length is more than 3 million, while the Re value associated with the cownose ray [88] is around 90,000. The dominance of inertial forces can be deduced from such high Re values.

Figure 5.4 The real size of a shovelnose guitarfish [229]

5.2 Mechanical Structure Design

To ensure a successful design, a number of aspects related to the electrical and mechanical design of an AUV must be taken into account (Figure 5.1). The design of any AUV requires background knowledge, basic concepts, and theoretical frameworks regarding the processes and physical laws that a vehicle is subjected to in the aquatic environment. Hence, hull design, propulsion, submersion, and electric power are the main aspects of design that require attention.

Investigations into the design of an underwater pressure hull were conducted earlier and a major limitation was identified to be its resistance to collapse. The purpose of the present investigation is to create an affordable and safe design encompassing all the relevant components and to replicate the flattened streamlined shape of the guitarfish. In the remainder of this section, several aspects are addressed, including the correlation between shape and drag and the choice of the hull shape, the prototype design requirements, a vehicle representation in 3D, and end closures design meeting the hull and design requirements.

5.2.1 Drag of the Hull and Selected Shape

Drag reduction based on the selection of a suitable hull shape for UUVs has been the focus of several recent studies [13, 128]. A significant savings in thrust requirement can be achieved through even a small decrease in drag. Nonetheless, further research is required to improve the hull shape design and, thus, reduce the drag and enhance the propulsion efficiency [111].

The laminar flow body benefits from its bulbous shape in maintaining laminar flow over the greater part of its length, and, thus, ensures a low drag. Thus, in terms of drag minimization, the ideal option is a shape promoting laminar flow within the boundary layer. Laminar flow is characterized by the movement of fluid particles in layers and a significantly lower skin friction drag compared to turbulent flow, in which the movement of fluid particles is more irregular, causing greater inter-layer shear stresses. As previously mentioned, the Re is indicative of the flow conditions (i.e., laminar or turbulent). A low Re is associated with a laminar flow with regular and smooth fluid movement. By contrast, a high Re is associated with a turbulent flow with arbitrary flow fluctuations, such as eddies and vortices. As can be seen in Figure 5.5, the maintenance of the laminar flow requires a hull design whereby there is a progressive increase in diameter from the nose to give rise to a positive pressure gradient over the forward 60-70% of the hull. In this area, there must not be any irregularities on the surface and hydrodynamics must be maximal. Since the laminar flow is disrupted by forward-mounted hydroplanes, the fitting of every hydroplane must be on the boom. Furthermore, to make sure that the laminar flow is not affected by any apertures and protuberances, the positioning of the acoustic payload and the communication and navigation transducers must be located as far aft as possible. However, this singular form of the laminar flow body also presents a major limitation, specifically the fact that it restricts the possibility of modular expansion because that would make it difficult to curtail or elongate the length of the vehicle [192].

Figure 5.5 The frontal part of the shovelnose guitarfish [230]

In keeping with the preceding discussion and the aspects addressed in Section 5.1.3, the conventional torpedo shape and the shape of the shovelnose guitarfish will serve

as inspiration for the suggested micro AUV. The Myring hull [145] possesses the smallest drag coefficient profile for a particular fineness ratio of body length to a maximum diameter [121], which is why it is the most popular hull form for torpedo-shaped AUVs. Thus, the vehicle hull has been designed on the basis of the Myring hull, which is made up of a nose-section (a), a middle-section with a constant radius (b), and a tail-section (c) (Figure 5.6). The second fundamental shape for the micro AUV is the shape of the shovelnose guitarfish (Figure 5.7).

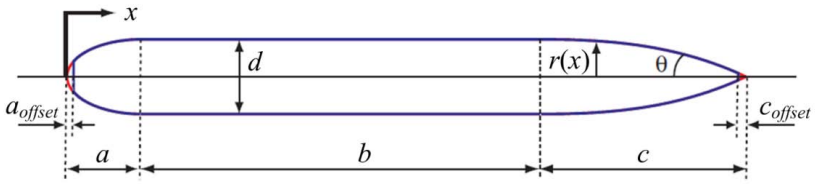

Figure 5.6 The profile of the Myring hull and indication of geometric parameters

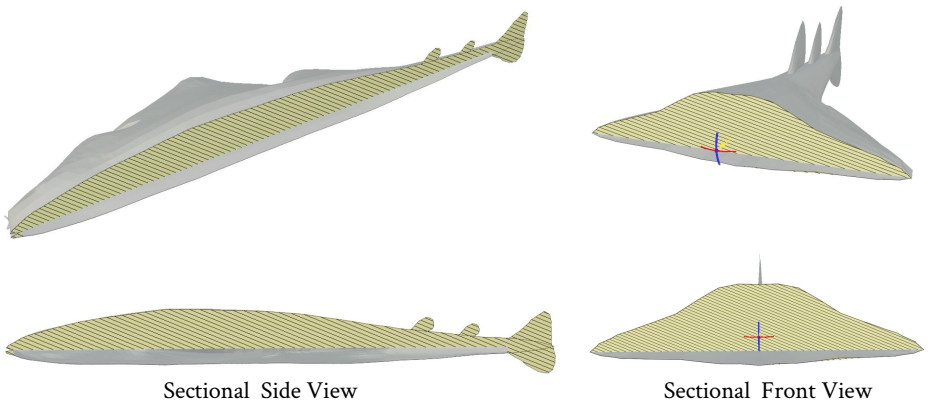

Figure 5.7 Sectionals view of guitarfish seen

5.2.2 Requirements on the Prototype Design

Size and shape are the main features of an AUV. The initial stage in the design of an AUV is determining its shape, with all other features being adjusted accordingly. The shape of the AUV dictates how it can be used, how efficient it is, and the range of which it is capable.

As discussed in Section 2.9.1, a micro AUV is an AUV that does not exceed 1 m in length and 10 kg in weight, thus being easily manageable with a single hand. Furthermore, the avoidance of scaling problems is essential for replicating the shape of the guitarfish (see Section 5.1.3). Hence, the concept underpinning the design of

the AUV proposed in this project is a vehicle of small size and low weight that does not require special equipment to deploy, recover, and operate, and that is functional at snorkeling depth.

The present project applies the following design specifications:

- Resistance to hydrodynamic forces created by currents, swell, waves, and vehicle propulsion, without getting damaged, flexing too much, or undergoing other types of deformation that may impair the function of its components;
- The vehicle must be maneuverable and easy to control;
- Strong but not exceeding 10 kg in weight;
- Maximum length of 1 m;
- Cost efficient;
- Propulsion by propeller-based thruster for both vertical and horizontal motion;
- Streamlined shape for minimization of drag forces on the hull of the vehicle (subject to restrictions related to hydrodynamic properties);
- The internal components of the vehicle must be easily accessible;
- A horizontally flat shape to make the vehicle more maneuverable in the horizontal plane, which is necessary in missions concerned with environmental monitoring;
- The manufacturing process must be straightforward and the materials used must be easy and inexpensive to procure.

5.2.3 3D Drawing of SEMBIO

In the above sections, the inspiration sources for the development of the proposed vehicle and the guitarfish-inspired design have been presented, and the design specifications were also outlined. The following stages involve the execution and the field deployment of the micro AUV.

As previously mentioned, the name of the proposed micro AUV is SEMBIO, which is an acronym that reflects the aim of the project, namely, the development of a Swarm for Environmental Monitoring with a BIOlogically inspired AUV.

The 3D modelling of SEMBIO from the first drawing to the end-outcome was achieved with the help of the SolidWorks software, which is useful, as it allows alterations to be brought to the model, such as adding, removing, or changing different features in accordance with a particular application. The development of the 3D model usually starts with 2D drawings or mating components comprising parts or sub-assemblies for the creation of 3D assemblies. Furthermore, 3D assemblies can be illustrated in 2D as well.

The benefits provided by the shape of the guitarfish and Myring were integrated in the creation of a torpedo-shaped, streamlined body with a frontal part similar to the nose of the guitarfish.

In keeping with the Myring design, key features, such as the variability in cross parts over the length of the body, were replicated in the model. The production of vorticity depends greatly on the nose-section. The development of the 3D model was based on a subjective "resemblance" to capture the main features and measurements of the guitarfish morphology. Thus, the SEMBIO model was given the same dimensions as a guitarfish of small size at 70 x 27 x 10 cm, as can be seen in Figure 5.4.

Improvement and optimization of the 3D shape model were achieved via CFD simulations, which were useful for the assessment of the hydrodynamic properties of the proposed vehicle and also provided guidelines for enhancing the design of the vehicle. Furthermore, to obtain feedback regarding the improvements for alterations and optimizations of the 3D model, as discussed in detail in Section 5.3, a simple method was adopted (Figure 5.11). Meanwhile, the investigation and analysis of MONSUN (see Section 5.3) was also significantly beneficial for the SEMBIO design in terms of ensuring that design errors and ambiguities were avoided.

The first version of the SEMBIO design is presented in Figure 5.8. The final version was achieved after extensive effort and work, and is illustrated in Figure 5.9. This form was attained after numerous versions, corrections, and amendments to obtain the final 3D model drawing. The final version of SEMBIO consisted of an overall number of 230 components. A comparison between Figure 5.8 and Figure 5.9 clearly shows the various changes and modifications that were made, particularly with regard to the position of the thruster, which is discussed more comprehensively in Section 5.5.

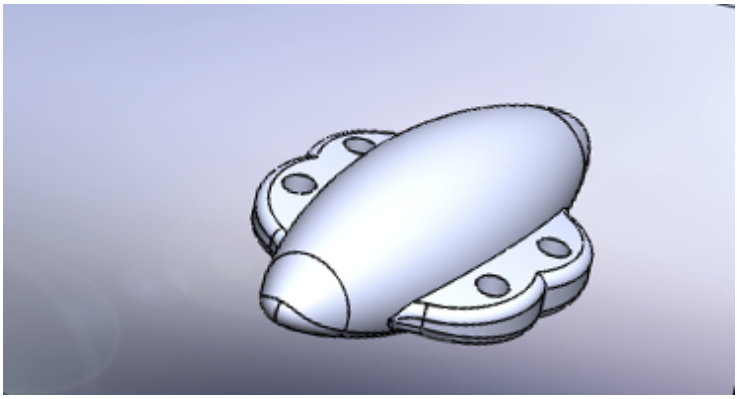

Figure 5.8 The first version of the SEMBIO design

As previously mentioned, the SEMBIO model was designed to imitate the streamlined shape of the guitarfish, with its nose and front part expanding smoothly

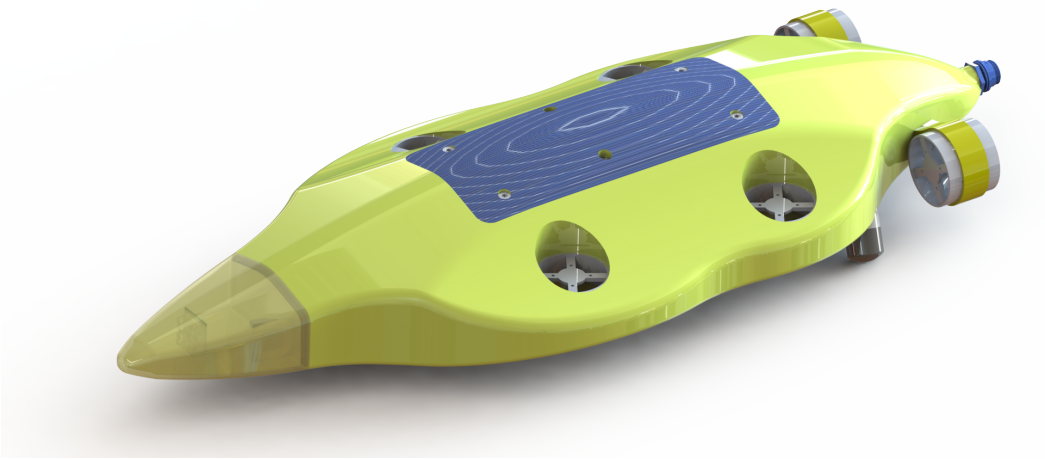

Figure 5.9 Representation of the SEMBIO model in 3D based on SolidWorks

towards the middle of the body before gradually decreasing towards the tail. Furthermore, to ensure smooth movement underwater, the model was created without any sharp edges.

The lateral and frontal perspectives in Figure 5.7 and Figure 5.10 show how similar SEMBIO and the guitarfish are in terms of flow shape and smooth edges.

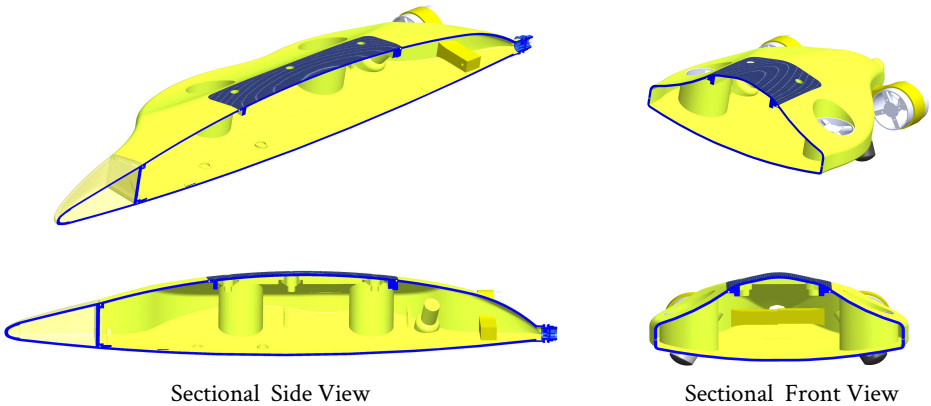

Figure 5.10 The SEMBIO model shown from the side and from the front

5.3 Hydrodynamic Analysis of SEMBIO

5.3.1 Introduction and Background

Robot autonomy is restricted by weight and battery capacity, which is why a major difficulty in creating an AUV for swarm and environmental monitoring applications was to ensure that it was energy efficient. Given that improvements of energy use and endurance depend on drag estimation and shape optimization of the AUV hull [79], the drag had to be estimated accurately due to its impact on power requirements. In general, hydrodynamic efficiency of AUVs is achieved through the adoption of streamlined hulls and designs that focus on the body are preferred because they improve hull drag, pressure-bearing capability, and use of internal space.

The hydrodynamic properties of AUVs have been the focus of extensive research, due to the benefits of a streamlined hull. This research has produced a variety of shapes (e.g., fish-like, dish-shaped, spherical underwater robots) to achieve the desired hull-shaped design. For instance, the robotic fish called RoboTuna served to show the correlation between the hull shape and the power needed for underwater propulsion of the fish-like body [23]. Another aspect highlighted by the results was that the AUV's drag reduction raised the energy efficiency factor, which in turn improved the endurance and diminished the power requirements [8, 9, 162]. Furthermore, the findings obtained prompted two studies to conclude that the thrust requirement could be considerably reduced and the vehicle cruising speed could be significantly increased by slight improvements in the drag coefficient, which is connected to a shape improvement [8, 9].

There are two major categories of methods that can help to calculate hydrodynamic coefficients, namely, test-based methods and predictive methods. The former involve the performance of a wind-tunnel or towing-tank model tests and the testing of full-sized vehicles to determine the hydrodynamic parameters [2, 239]. These methods must be carried out in a special laboratory and necessitate considerable resources for testing facilities. On the other hand, predictive methods are based on CFD and are becoming increasingly amenable for hydrodynamic coefficient determination thanks to the development of CFD packages and computer technology innovations.

Computer technology advances have led to the broad application of CFD for the analysis of the hydrodynamic performance of AUVs with the visualization of flow field, which is challenging and time-consuming to undertake via field experiments. In addition, CFD simulation allows for a range of hull shape models to be tested and validated prior to the production of the first prototype model for testing. CFD is also advantageous because it makes analyses for the achievement of shape optimization more cost and time efficient.

As indicated earlier, the characteristics of the guitarfish and Myring served as inspiration for the 3D model, and a simple method was adopted to improve and optimize the SEMBIO shape. The stages of this method are outlined in Figure 5.11, alongside the techniques and procedures employed, such as software for solid modeling (SolidWorks), meshing, and flow analysis (ANSYS).

The sections below present the final results of SEMBIO, which were considered acceptable enough to proceed to the construction phase of the hull for the first SEMBIO prototype. Furthermore, to ensure that the underwater flow of SEMBIO was as smooth as possible and to enhance the hull design, an analysis of MONSUN was conducted to observe its flow and hydrodynamic performance. In the process of designing the model, a number of essential aspects were taken into account, including robustness, ease of manufacture, and assembly.

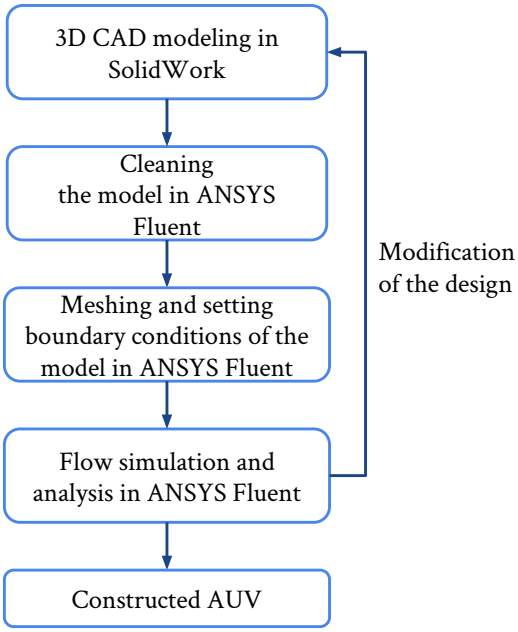

Figure 5.11 The stages of the method adopted for improvement and optimization of the SEMBIO shape design

5.3.2 Preprocessing and Geometry for the CFD Analysis

Upon completion of the design process of the SEMBIO 3D model, which was constructed and modeled entirely with SolidWorks (see Section 5.2.3), the full-scale geometrical 3D SEMBIO model was imported into ANSYS Fluent in the SolidWorks format. The chosen CFD solver was ANSYS Fluent to afford a central role to ANSYS in the AUV design, enabling the execution and visualization of recent CFD results [83, 104, 214, 240]. The next step was cleaning the imported model

based on the fusion of the undesirable edges and surfaces that might have interfered with mesh production. Furthermore, the ANSYS Fluent setting permitted the adjustment of every setup associated with fluid flow experiment simulations (e.g., suitable parameters and boundary conditions).

Regarding the hydrodynamics analysis, the flow field was constructed on the basis of the 3D model of the robot, since the main concern was the effect of the robot's flow field. The flow field had to be sufficiently large to make sure that the outcomes of the hydrodynamics analysis were unaffected by the flow field wall and that ground effects were avoided [215, 240]. In ANSYS Fluent, SEMBIO was fixed in a rectangular domain, which was built and added for a water flow field. The dimensions of the pool were 1 x 1 x 2 m to ensure that there was sufficient space for a dynamic fluid flow (see Figure 5.12). MONSUN was also examined in the same context for comparative purposes (see Figure 5.13). The real MONSUN dimensions were of course transferred and drawn using SolidWorks.

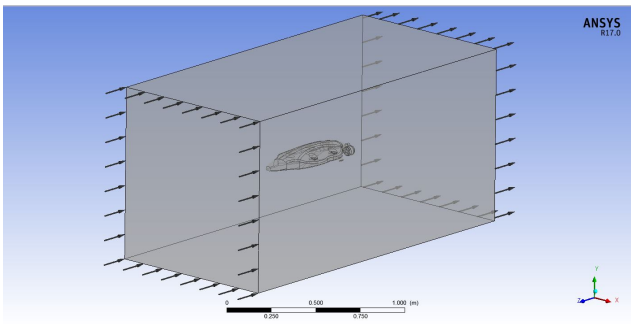

Figure 5.12 Computerized representation of the flow domain associated with SEMBIO

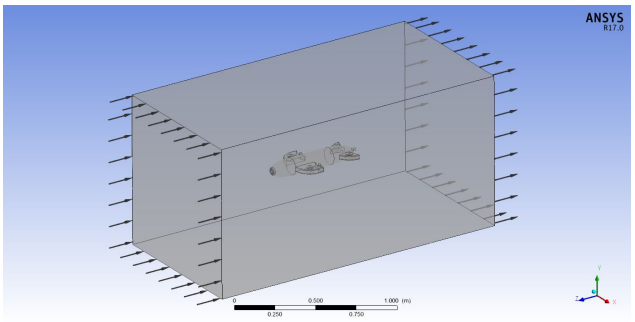

Figure 5.13 Computerized representation of the flow domain associated with MONSUN

As can be seen in Figure 5.12 and Figure 5.13, a flow speed was indicated at the inlet boundary. From a physical perspective, the upstream flow was homogeneous and set to be normal to the plane.

5.3.3 Meshing

It must be noted that the analysis of CFD was performed solely in the horizontal forward direction of SEMBIO. The decision was made for two reasons. The first was due to the fact that SEMBIO was afforded a horizontally flat design to make it more maneuverable in the horizontal profile (guitarfish-inspired). The second reason, due to the fact that, since the main application of SEMBIO was for environmental monitoring, the vehicle had to move vertically to reach a specific depth and subsequently commence its mission and move horizontally. Hence, the purpose of the application required SEMBIO to be capable of greater movement in the horizontal plane rather than the vertical plane. Nonetheless, vertical diving with a high pitch angle ensured that SEMBIO could reach the intended depth.

No other factor is more important in hydrodynamics analysis than the flow field mesh. This is because the amount of mesh determines how well the hydrodynamics analysis performs and how complex the computation is. As such, prior to commencing the analysis, mesh smoothing was undertaken and the 3D model was simplified prior to meshing. For instance, to make the mesh simpler and to improve its quality, elements such as motors and bolts were disregarded.

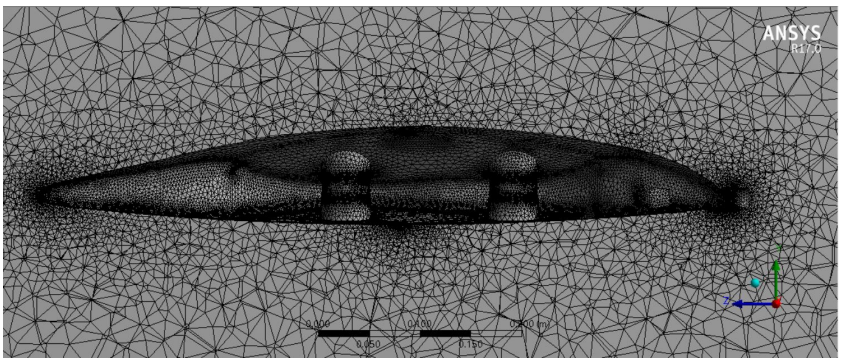

Figure 5.14 The SEMBIO mesh represented in 3D

As illustrated in Figure 5.14, ANSYS Fluent with CFD-Mesh was employed to carry out the meshing procedure. Prior to initiating the CFD simulation, it was necessary to define the face spacing that dictated the surface area of the mesh that came into contact with the surface of SEMBIO. The dimensions of face spacing had to be sufficiently small to capture the SEMBIO geometry. Furthermore, on the SEMBIO surface, the number of inflation layers rose.

The above figure shows that there is an exponential increase in the size of mesh away from the SEMBIO surface. Achieving a lower number of meshes at a distance from the body and at the same time maintaining the meshes fine close to the body is essential.

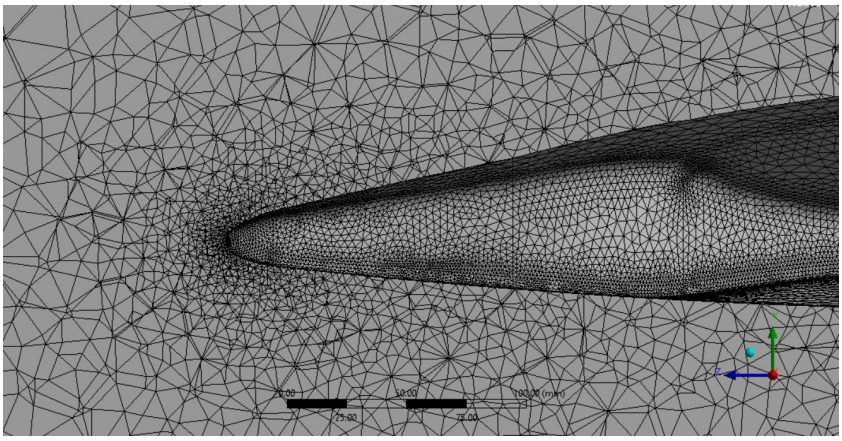

Figure 5.15 The side view of the magnified representation of the results of meshing of the front part of SEMBIO

A close-up view of the inflation layers is shown in Figure 5.15. A thin layer in the proximity of the body contains the boundary layer. Hence, the inflation layer plays a central role in capturing the flow close to the boundary layer, as it supplies a finer mesh in that area. More specifically, the boundary layer elements surrounding the SEMBIO body were produced with the help of layered meshes, whereas the area at a distance from the body contained unstructured (tetrahedral) meshes, which are inappropriate for resolving the boundary layers close to the solid body.

Before starting the computation, each variable must be allocated an initial value. In the case of steady-state calculation, the initial variable values provide a flow field for the ANSYS CFD Solver to begin the calculations. If the initial values that are allocated are reasonable, then convergence will occur faster. Nonetheless, the initialization should have no impact on the converged results. The automatic initial guess should be ideally employed, if no data regarding turbulent eddy dissipation exists.

For the earlier setting, the fluid domain surrounding SEMBIO consisted of an overall number of nodes and elements of 334,157 and 1,819,692, respectively.

The same earlier work was suitably applicable to MONSUN, with the results being presented in Figure 5.16 and Figure 5.17.

5.3.4 Setup and Solving

ANSYS Fluent includes a CFD analysis module that is straightforward to use and enables a rapid generation of solutions through iteration time regulation. Besides being easy to use, this tool can yield acceptable results of reliability analysis with the intended degree of convergence.

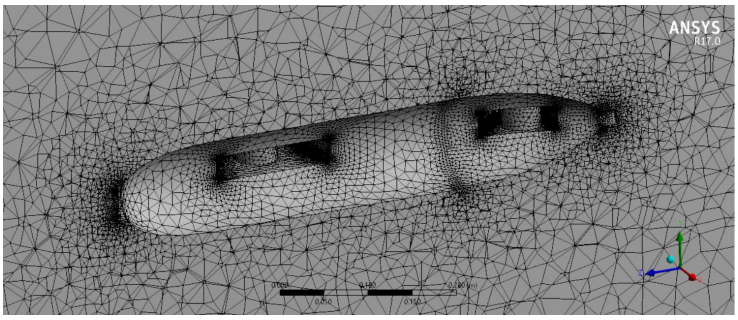

Figure 5.16 The MONSUN mesh represented in 3D

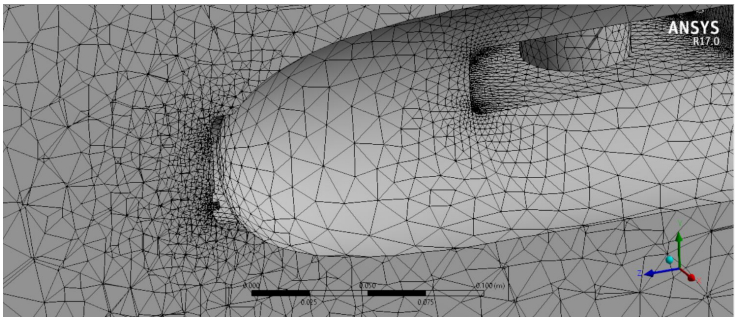

Figure 5.17 Magnified representation of the meshing results associated with the MONSUN nose

The run can be stopped once the results of a particular value are deemed satisfactory, and post-processing can be initiated to visualize the results. The monitoring step of the solve process during the operation of the ANSYS Fluent solver observed that it took almost 20 iterations for convergence of the value of the Z-direction drag force of the AUV hull to be achieved. Hence, to save CPU time, the number of iterations for convergence and cessation can both be set.

The commercial CFD analysis code (CFD solver) was employed to model and solve the fluid flow surrounding the SEMBIO on the basis of ANSYS Fluent. For the purpose of these calculations, the flow field and water pressure surrounding the SEMBIO body were determined based on the motion modeling of the fluid with the incompressible, isothermal Reynolds-averaged Navier-Stokes (RANS) equations. These equations are employed in the majority of studies due to the fact that, by comparison to the potential flow theory, they provide a better treatment of viscous effects and do not require as many computer resources as the Large Eddy Simulation (LES). The equations comprise a standard solution of the ensemble-averaged, steady-state, and 3D Navier-Stokes equations characterizing the properties of the flow, like velocity, pressure, temperature, and density. In the present case, to enable the closure of the RANS system of equations by ANSYS Fluent, the $k - \omega$ turbulence model was selected, with k and ω respectively denoting the turbulence kinetic

energy and the viscous dissipation rate. This model helps to anticipate how the turbulence and flow behave around the hull, and its selection for the purposes of the project was justified, as it is a widely employed turbulence model for engineering simulations that is robust and can be applied to different flows. Furthermore, the computation time was cut by using the symmetry condition.

The speed variations for the fluid were in the range of 0 - 1 m/s, which was an estimation of the general speed at which an AUV operates. For the surge translational direction, a speed interval of 0.25 m/s was chosen.

The vehicle was axisymmetric along the Z-axis, which represented the longitudinal axis for the proposed model.

Table 5.1 presents an overview of the requirements for the pre-processing stage, including mesh generation.

Object name	Mesh
Water domain size	1000x1000x2000 mm^3
Turbulence model	$k-\omega$ model
Reynolds number	22.47×10^5
AUV dimensions	$0.7m \times 0.1m \times 0.27m$
Total no. of elements (nodes)	1819692 (334157)

Table 5.1 The main specifications applied in the numerical computation

5.3.5 CFD Analysis and Results

The kinematic relationship between the fluid and the vehicle can be characterized via two methods. The first method of dynamic mesh is based on the settings for static and movement of the water and the vehicle wall, respectively. By contrast, the second method is based on the assumption of movement at 1 m/s speed for the water and static vehicle wall. The latter was the method selected in this project due to its straightforward nature and ease of use [86, 109]. Given that the vehicle and fluid were moving relative to one another, they were respectively set as a static wall and constant velocity of flow.

The hull design was improved many times, with the final results being based on a forward direction at a speed of 1 m/s. The streamline of the SEMBIO shape and the movement and contact of the fluid flow within the domain were presented in Figure 5.18. For comparison purposes, Figure 5.19 presents the fluid flow of MONSUN.

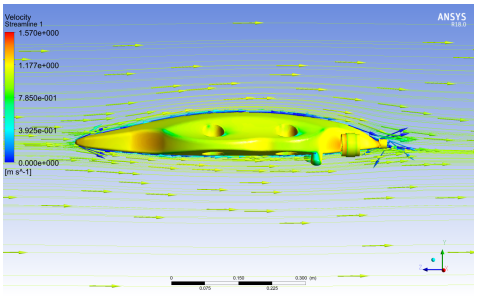

(a) Side View

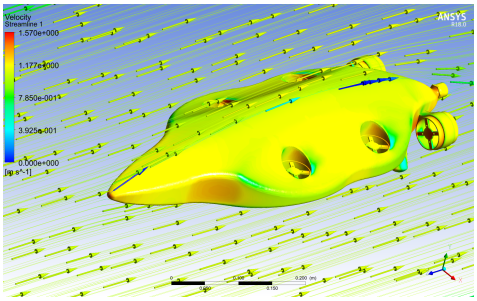

(b) 3D View

Figure 5.18 Illustration of the fluid flow during the CFD analysis of SEMBIO

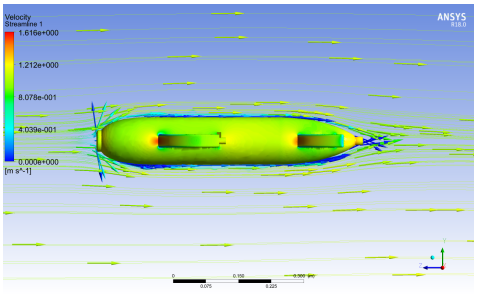

(a) Side View

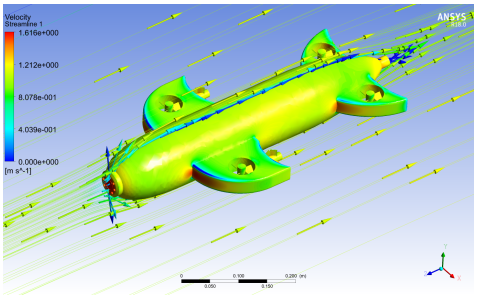

(b) 3D View

Figure 5.19 Illustration of the fluid flow during the CFD analysis of MONSUN

ANSYS Fluent was employed to perform every step of the vehicle's hull analysis. Hence, CFD post-processing from ANSYS Fluent supplied comprehensive data related to the velocity and pressure distribution surrounding both SEMBIO and MONSUN.

As is shown in Figure 5.20, the pressure distribution surrounding SEMBIO is homogeneous, apart from the tiny points. The interaction between the fluid and SEMBIO is the reason for the occurrence of maximal pressure, denoted by the red color, at the tip of the nose of the vehicle and on the side edge of each thruster ring. Such areas of maximal pressure are so few that they are almost insignificant. In the other parts of the SEMBIO surface, the pressure is not as high and is more or less uniform due to the smooth flow. Thus, SEMBIO demonstrates a good hydrodynamic performance thanks to the smooth streamline and balanced pressure distribution.

The pressure distribution surrounding MONSUN is shown in Figure 5.21. It can be seen that maximal pressure occurs over the whole tip of the nose, while minimal

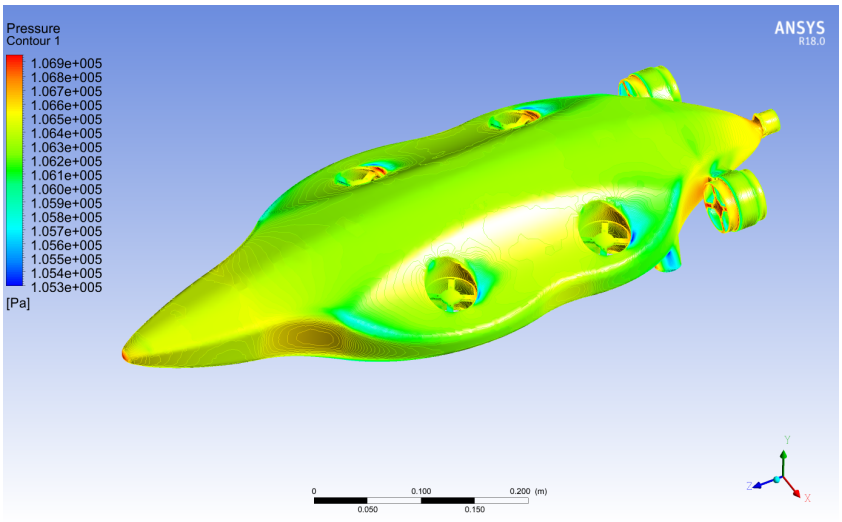

Figure 5.20 The distribution of pressure on the surface of the hull of SEMBIO

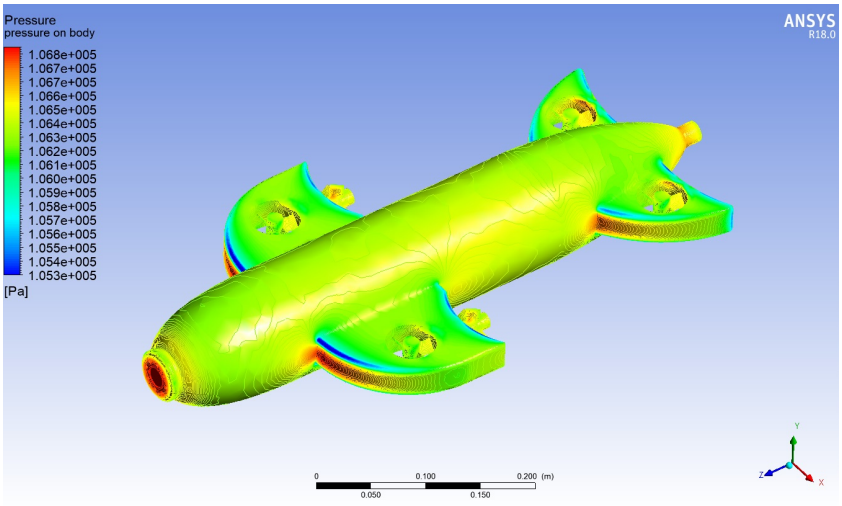

Figure 5.21 The distribution of pressure on the surface of the hull of MONSUN

pressure, denoted by the blue color, occurs at the edge of the windward side of each fin. A compression dysfunction is generated by the pressure difference on the fins.

As presented in Figure 5.22, the velocity associated with SEMBIO was measured over the entire cross-section of the hull. It decreased slightly at the tip of the nose and subsequently increased and was maintained to the end of the hull, where it decreased again at the starting point of the tail curve. The velocity is presented from

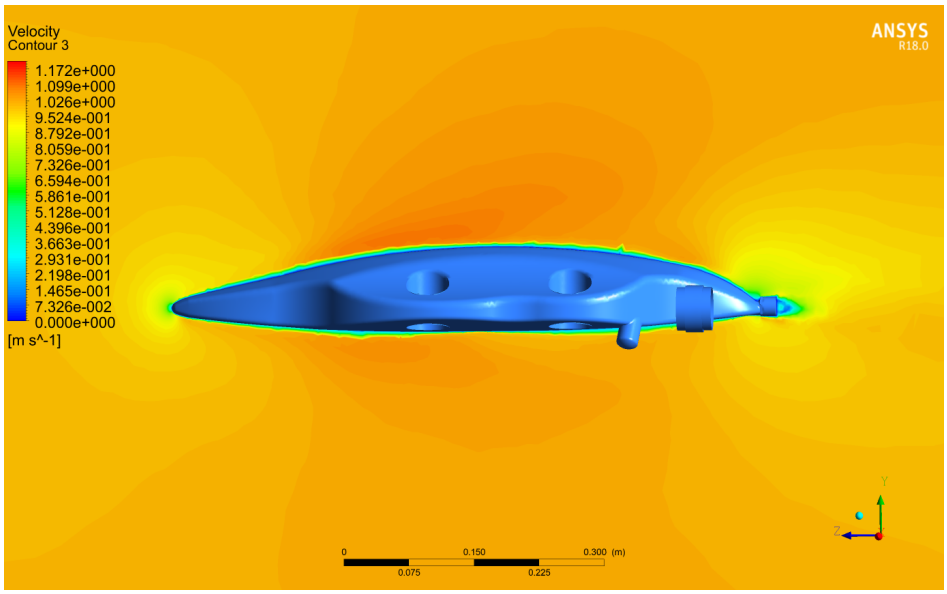

Figure 5.22 The velocity contour around SEMBIO at a speed of 1 m/s in side view

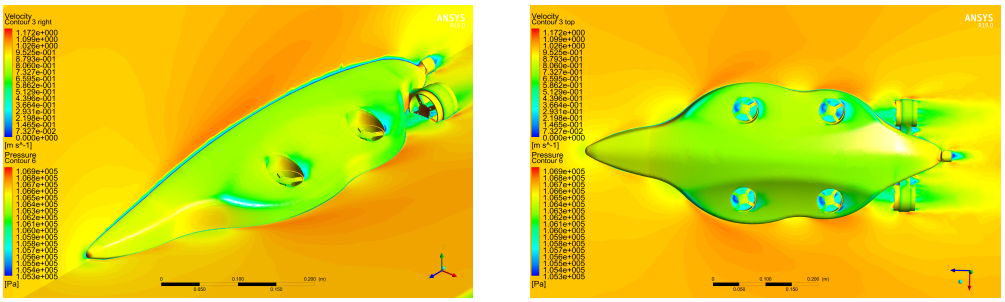

(a) The 3D view

(b) The top view

Figure 5.23 The velocity contour of SEMBIO represented in 3D

different views in Figure 5.23(a) and Figure 5.23(b) (for comparison, Figure 5.25(a) and Figure 5.25(b) presents the results of MONSUN).

According to the velocity results, by comparison to MONSUN, the velocity of SEMBIO around the hull was greater (1.164 vs 1.172). An analysis of the effect on the MONSUN fins was conducted in this study. Figure 5.24 shows the flow after each fin, which was not present in SEMBIO, the latter generating a greater proportion of drag due to its higher velocity. The velocity is presented from different views in Figure 5.25(a) and Figure 5.25(b). An identical pattern of an increasing velocity across the bow curvature and the curve of the tail section as well as a reduction in velocity at the bow tip and tail end was exhibited by every type of hull. The

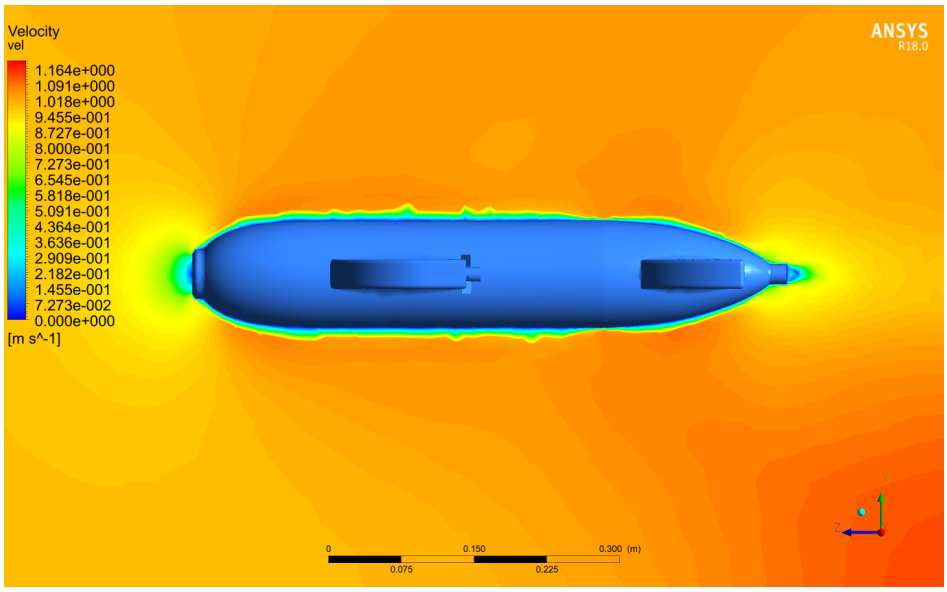

Figure 5.24 The velocity contour around MONSUN at a speed of 1 m/s in side view

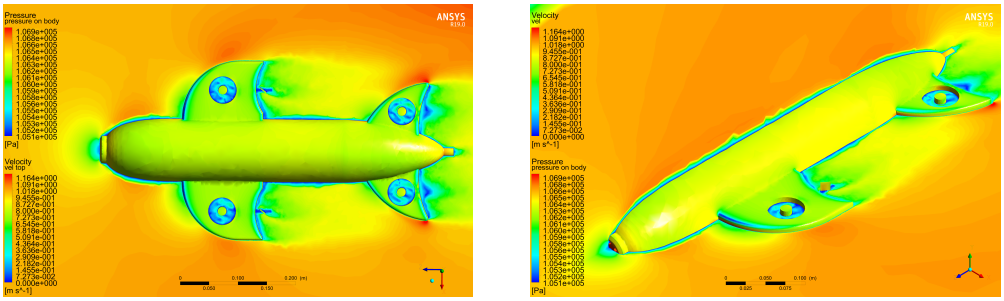

(a) The 3D view

(b) The top view

Figure 5.25 The velocity contour of MONSUN seen from different views

vehicle noses differed significantly between the two models, the spot being greater on MONSUN compared to SEMBIO and most likely causing a rise in drag.

Drag Coefficient

As was discussed in Section 3.4.3, the shape and speed of a body moving underwater determines the drag forces acting on that body. The F_d can be simulated and determined by ANSYS Fluent based on a given velocity for movement in the

horizontal direction. More specifically, the amount of force needed by a vehicle to attain a particular speed can be determined by ANSYS Fluent.

The following equation permits the calculation of the drag coefficient C_d, which represents a key hydrodynamic feature (the drag coefficient is defined using Equation 3.14):

$$C_d = \frac{F_d}{\frac{1}{2}\rho v^2 A} \tag{5.1}$$

The value obtained for the drag coefficient associated with the horizontal movement following the removal of the acoustic transducer was 0.12. This value suggested that SEMBIO had a more streamlined shape than MONSUN, as the latter's C_d was 0.48.

Drag force-CFD results (N)	1.95	3.41	4.48	5.44	6.52
Speed (m/s)	0.25	0.5	0.75	1.0	1.25

Table 5.2 Drag force data obtained from CFD results of SEMBIO

Drag force exp. results (N)	1.0	1.5	2.0	2.5	3.0	4.9	5.8
Speed (m/s)	0.20	0.32	0.41	0.52	0.60	0.72	1.0

Table 5.3 Drag forces obtained from experimental results of SEMBIO

ANSYS Fluent was also used to determine the drag force F_d associated with movement in a horizontal direction, which in turn was needed to obtain the thrust force F_T for SEMBIO (Table 5.2). In addition to theoretical calculations, the determination of F_T also required empirical work on the SEMBIO hull. Thus, the empirical work involved the submersion of SEMBIO at a depth of 0.5 m in a swimming pool and a simple and approximate method was employed to issue a detected value of the force required to thrust SEMBIO in a forward direction, with subsequent measurement of the speed. Table 5.3 provides the values of the drag force yielded by the empirical work.

The drag force and velocity results produced by CFD and the empirical work are presented in Figure 5.26. It is clear that they were not identical, and there was no significant difference between the results. However, there were two factors that may have impacted the results: the fact that the method employed was simple and possibly prone to computational errors and the waves in the swimming pool.

The stage of the propulsion system design depended on the determination of the drag or thrust force needed to thrust SEMBIO in a horizontal direction. According to the drag force results, to reach a speed of 1 m/s, a minimum of 5.8 N had to

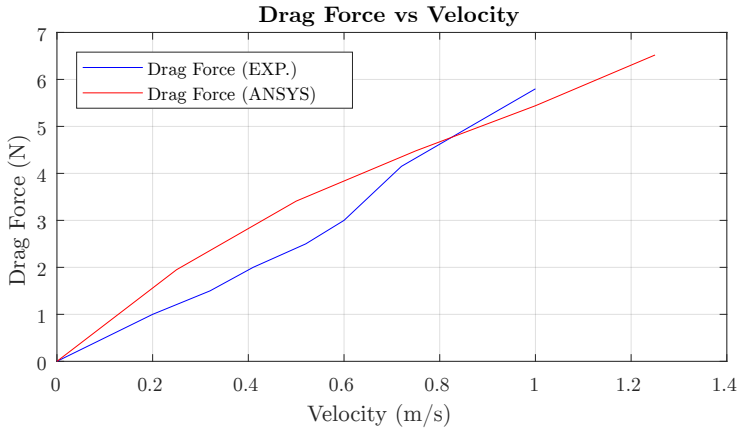

Figure 5.26 The drag force and velocity demonstrated by SEMBIO

be generated by the horizontal thruster. Meanwhile, to thrust the SEMBIO in a vertical direction, the vertical thrusters had to generate a thrust that exceeded the buoyancy force F_b (0.2 - 1.0 N) and the gravitational force F_g. Practically, stable movement in a vertical direction up to a depth of 4 m could be achieved with a force of 2 N. The diving speed reached by SEMBIO at 1.4 N was 0.1 m/s.

In the case of MONSUN, a drag force value of 7.06 N was indicated by ANSYS Fluent as being necessary to move the vehicle in a horizontal direction at a speed of 1 m/s. Although this value may not seem very different from that calculated for SEMBIO, it could still have a significant effect, particularly in the case of missions of lengthy duration. However, it is not very reasonable to compare the two vehicles from this perspective, since they differ in terms of cross-section (SEMBIO = 0.01685 m^2; MONSUN = 0.015531 m^2) and 3D surface area (SEMBIO = 0.34 m^2; MONSUN = 0.29 m^2). In other words, by comparison to MONSUN, SEMBIO had a volume that was 1.2 times larger, yet the results still turned out in favor of SEMBIO. What is more, MONSUN was transferred from real life into SolidWorks, and the real MONSUN was closely approximated in the drawings; furthermore, MONSUN was drawn on the basis of a Myring form that does not exist in reality, meaning that the drawn MONSUN is not an accurate reflection of the real MONSUN. In spite of these considerations, however, the comparative analysis still highlighted that the SEMBIO design was more advantageous and superior compared to MONSUN.

5.4 Vehicle Construction

After the finalization of the design of the SEMBIO 3D model, making the robot come to life is the next step. The construction of SEMBIO involves the selection of materials, determining the hull thickness, and 3D printing the model.

5.4.1 Selection of Materials for the Designed Vehicle

The material used to construct the pressure hull should ideally possess the following properties: low density (kg/m^3), high strength (up 1 MPa, where is 1 MPa= 1000,000 Pa), resistance to corrosion, and an appealing shape. Titanium is one such material that exhibits these properties, but it is not cost-effective and it is not easy to process.

In the selection process for the SEMBIO construction material, the conditions of work were taken into account. In general, the depth at which a vehicle is expected to dive is known at the beginning of a mission. As indicated in Chapter 2, the vehicle was not intended to dive at a depth greater than 100 m, and, therefore, it was neither necessary nor worth the resources to use a material of such a high strength as titanium.

A search for market alternatives produced a number of materials with properties relevant to an underwater vehicle, as indicated in Table 5.4.

Material	**Density (kg/m^3)**	**Yield strength (MPa)**	**Elastic modulus (GPa)**	**Corrosion resistance**
Aluminum (6061)	2700	275	69	Good
PVC (extruded)	1360	46	1.9	Excellent
ABS	1050	37-110	2.2	Excellent
Polycarbonate	1200	67	2.4	Good
PLA	1300	50-80	3.5	Excellent

Table 5.4 Materials with properties relevant to an underwater vehicle

Materials were assessed to see whether they could effectively withstand corrosion, were not very dense, could resist high external pressure, were widely available, not very expensive, and could be machined and manufactured without difficulty. According to these criteria, a suitable material for designing the pressure vessel would have been aluminum. However, this material was disadvantageous from the perspective that it was not cost-effective and not easy to machine and manufacture in the available laboratory facility. Plastics have the advantage of being highly appropriate for 3D printing and effectively withstanding corrosion. On the downside, they are not very strong. Marine structures (e.g., ships) are usually made out of Fibre-glass Reinforced Plastic (GRP), but this material is distorted by molding and formation processes. An acceptable mixture can be obtained by combining plastics and GRP, the former being used for vehicle molding and the latter for strengthening and consolidating the vehicle. Hence, the chosen material consisted of a plastic layer covered with GRP on the internal sections, demonstrating acceptable strength, good resistance to corrosion, broad availability, affordable costs, and easy machining and manufacture.

Based on the features summarized in Table 5.4, the plastic material that was chosen was Poly Lactic Acid (PLA). This material is widely employed due to the fact that it does not warp as much as other materials (e.g., Acrylonitrile Butadiene Styrene (ABS)) during the printing process, and the emissions it releases during printing are not so pungent [196]. In addition, PLA does not generate toxicity, it is biodegradable, and is produced through a sustainable process that does not damage the environment because is composed of corn-based resin [205].

5.4.2 The Analysis of Hull Thickness

The fact that the SEMBIO's hull is manufactured through a combination of PLA and GRP, the aim of this combination material was to effectively maintain levels of hydrostatic pressure to avoid a structural disintegration or buckling (for the 10 m depth referenced in this work). From the design of the prototype, the thickness of the wall was 3 mm of PLA and 2 mm of GRP, comprising an overall thickness of approximately 5 mm. In order to enhance the safety of this process, the presumption was made that the analysis' thickness is 3 mm of PLA.

To evaluate the structural integrity of the SEMBIO hull, this analysis has the objective of utilizing Finite Element Analysis (FEA). This was crucial in creating innovative structures and scrutinizing marine structures that are currently present. Additionally, there was also a desire to investigate the structure's buckling dimensions [194]. The evaluation placed its emphasis on the modeling elements using FEA to analysis the effect of the water pressure on the surface of the SEMBIO hull, these effects are illustrated by the stress and displacement results of SEMBIO hull.

Figure 5.27 illustrates the finite element mesh of SEMBIO hull, in excess of 43,198 (63,409 nodes) finite solid elements are then interconnected from the geometrical model in order to generate the finite element model to obtain more precise results. SolidWorks was used to generate this model.

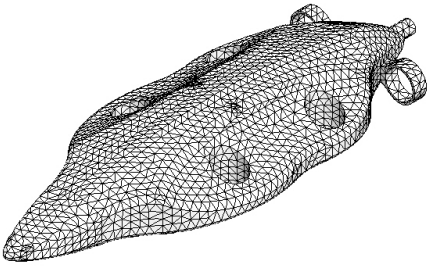

Figure 5.27 The finite element mesh of the SEMBIO hull generated by SolidWorks

In SolidWorks software, the 3D model of SEMBIO hull is imported, all conditions of the evaluation are set up, the model is meshed, the definitions of material properties are selected, and then the analysis of the model is solved. After the solving step, the post-processing solver of SolidWorks illustrates all the FEA results such as stresses and displacement of the hull. Von Mises stress method is selected to illustrate the stress distribution results, which is a method that widely used by designers and programs to calculate the stress of an object to proof whether the object will resist a specific load condition.

Tow level of water pressure are applied to the SEMBIO hull, the first level is 10 m of the water which is 98,066 Pa or 0.098 MPa, the second level is 100 m of the water which is 980,664 Pa or 0.98 MPa. The inside of the hull subjected to normal atmospheric pressure (1 atmospheric pressure $\approx$ 10 m of water). The hull is subjected to a uniform pressure loading.

After loading all conditions and conducting FEA processes, Figure 5.28 and Figure 5.29 illustrate distributions of stress and displacement for the SEMBIO hull at 10 m.

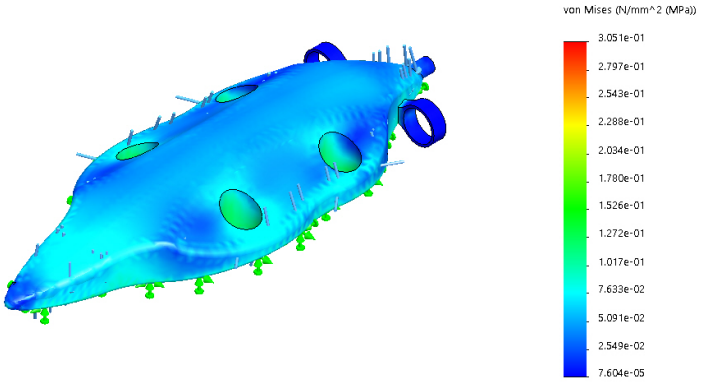

Figure 5.28 The stress distribution (Von Mises) on the hull at 10 m of water

At the begging, the SEMBIO hull structural integrity was defined by a stress safety factor of 3 (more than 1 is safe enough). Figure 5.28 presents the Von Mises stress distribution. The stress is very small on the hull and the maximum level of stress possible is 0.3051 MPa (less 1% of maximum strength of PLA). The maximum stress tends to be at the nuzzle of the vertical thrusters.

The displacement or the deformation results of the SEMBIO hull are illustrated in Figure 5.29. The maximum displacement is 0.004 mm which occurs at the top of the vehicle.

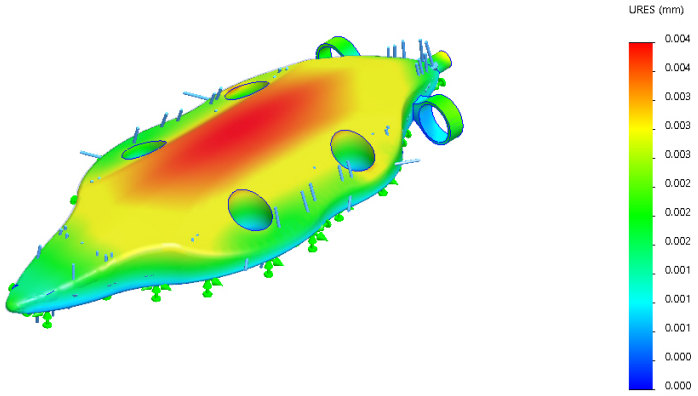

Figure 5.29 The displacement vector on the hull at 10 m of water

For comparison purposes, Figure 5.30 and Figure 5.31 present the results at 0.980 MPa (100 m of water). It should be noted that the results are still acceptable. The deformation of the hull is enlarged 700 time to be more clear in the Figure 5.31.

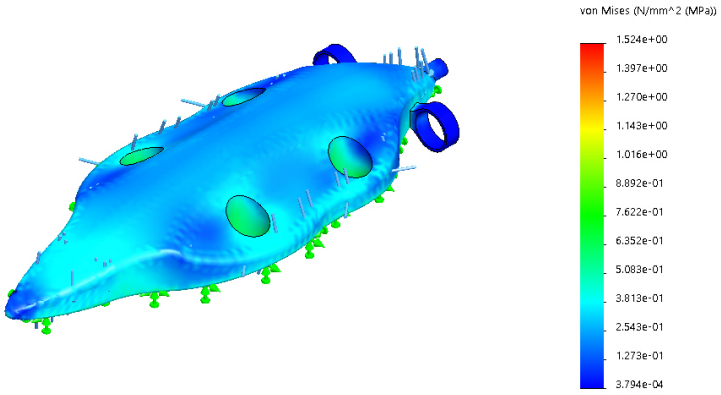

Figure 5.30 The stress distribution (Von Mises) on the hull at 100 m of water

5.4.3 3D Printing and Assembling of SEMBIO

There were six separate components that made up SEMBIO model, as can be seen in Figure 5.32. As discussed in Chapter 2, to enable the construction of a swarm of micro AUVs that is acceptable from a financial perspective, micro AUV manufacture must not be too expensive. Thus, every component of SEMBIO was produced with the help of a 3D printer, which was more than 75% cheaper compared to other alternatives available on the market [160]. The reason why the process of

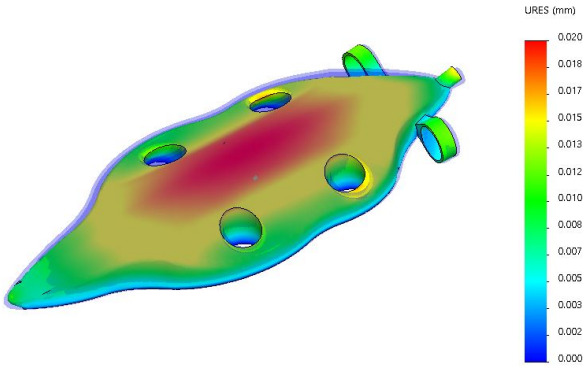

Figure 5.31 The displacement vector on the hull at 100 m of water, the transparent body represents the original hull size before the deflation

manufacturing is so cost-effective when a 3D printer is used is that such a device can achieve production without any marked difficulty.

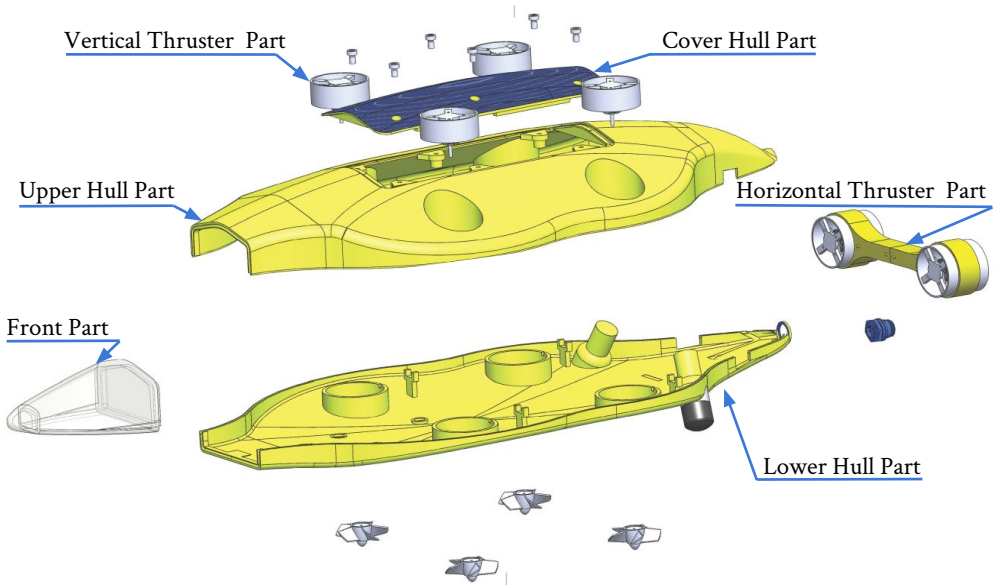

Figure 5.32 The key components in the construction of SEMBIO

The Ultimaker 3D printer was used to perform the 3D printing process. However, there were some difficulties (due to small size of the 3D printer) that arose during this process. The dimensions of the components of the SEMBIO model, particularly the lower and upper parts of the hull, and the build volume (i.e., the physical space within the printer employed for 3D printing components) of the 3D printer were

not the same. More specifically, the build volume of the printer had dimensions of 34 x 36 x 39 cm, whereas SEMBIO had dimensions of 70 x 27 x 10 cm. To address this issue, every part of the SEMBIO model was cut and exported as printer items with the help of SolidWorks in order to ensure compatibility with the build volume of the 3D printer. The work time was significantly lengthened by this solution, as the parts had to be glued back together again, as shown in Figure 5.33.

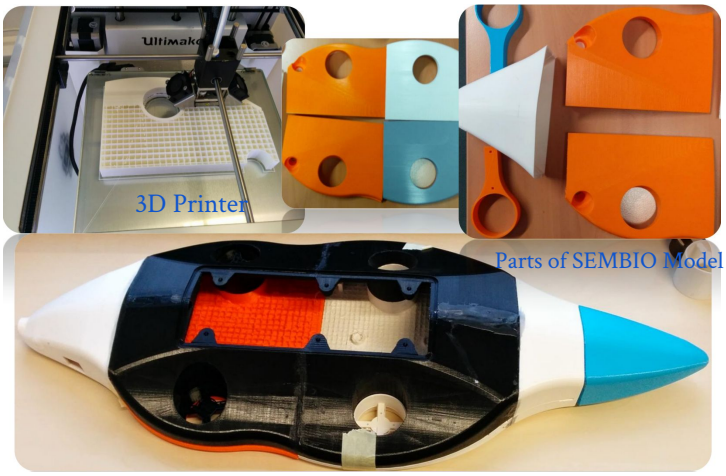

Figure 5.33 3D printer with the components of the SEMBIO model

After uploading the exported printer items into the Cura software (Ultimaker) [210], a record was made of the resulting data related to estimated print time, item weight, and length of the filament used. Furthermore, the filament that was chosen was a 3 mm PLA, due to the fact that it was a widely used 3D printing material that was stocked by the majority of 3D printing suppliers.

For all components that were printed for the SEMBIO construction, the average cost of the filament was determined to be 60 € (30 €/kg).

The next step after the completion of the 3D printing process was assembling the components of SEMBIO to create the hull of the vehicle. In order to attach the various components together, epoxy adhesive mixed with fine lead shot was used and covered the bottom to create a flat layer in which the electrical components could be set. Furthermore, to ensure the positive stability of the vehicle, the lead shot also served as ballast and nose weights (the center of mass should be minimal to enhance stability, and it must be adjusted in the center of the vehicle, see Section 3.4.2). In addition, to avoid the need to trim with extra weights to achieve and calibrate the positive buoyancy of the vehicle, the overall weight should be similar to the buoyancy force. Further, to improve the safety factor of the hull pressure (see Section 5.4.1), the inner walls of the hull were coated with a mixture of GRP and epoxy adhesive, which made the hull more rigid and cohesive.

Preventing water from coming in (whilst at the same time allowing for access to the equipment) is a major challenge in the process of constructing a pressure hull. Underwater vehicles are usually sealed through the installation of O-rings or hydraulic seals, which are pieces of elastic material, such as rubber that produce a watertight seal when they are positioned in a groove and wedged between smooth surfaces. Six short screws based on O-rings were used to fix the cover of the hull, as shown in Figure 5.34. Furthermore, a watertight seal was produced by wedging rubber of high flexibility between the hull and the cover. In this way, the cover was insulated and the hull was protected against any leakage caused by contact between the cover and the hull, thus making the whole hull impermeable. Additionally, the gaps between cables and the holes for the connection of the external thruster units and for mounting the lenses of the camera and sensor units were filled with a waterproof methacrylate adhesive (Technicoll 9403) to create a watertight seal between the vehicle's hull body and the control, charger, and motor cables.

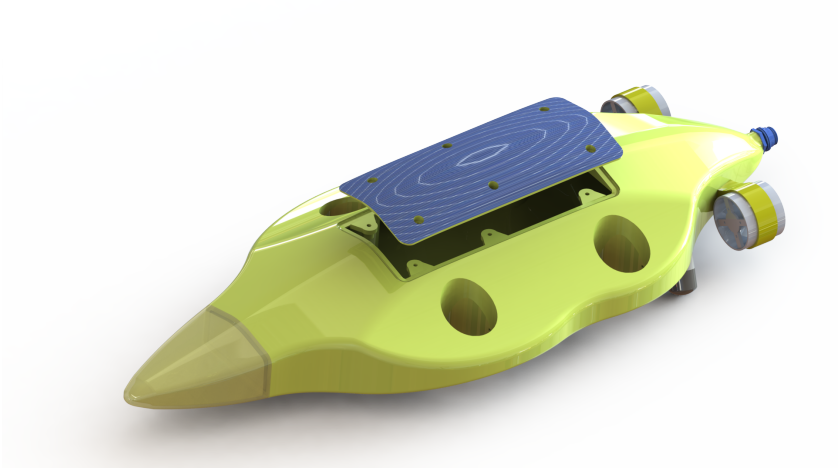

Figure 5.34 The contact between the cover and the hull of SEMBIO

The SEMBIO construction process was finalized with the painting of the vehicle (Figure 5.35). The reason for painting the hull was to protect it from the effects of external elements such as the sun and water salinity. The steps followed to achieve this were the same as those involved in painting a car. The process commenced with cleaning and taping the surface of the hull, after which the surface was smoothed and flattened with the help of the sander machine and made even with the use of the filler. The next step was priming the hull with a primer of good quality in order to ensure that the hull and its components did not come into direct contact with the paint as well as in order to create a smooth and uniform surface to which the paint could adhere. The last step was selecting and applying the paint color, after which the hull was introduced in the paint booth at a temperature of 160 ℃ for a quarter of an hour to help the paint to dry and bind to the surface.

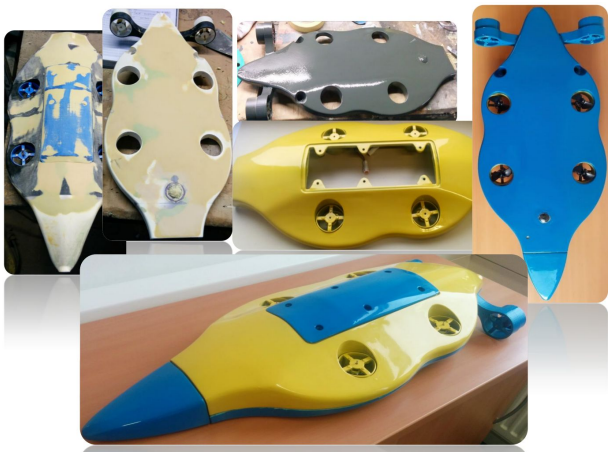

Figure 5.35 The painting steps and SEMBIO after painting was completed

5.5 Propulsion Configuration

The design of an underwater vehicle depends to a great extent on the propulsion system. Indeed, few components are of more importance than the type of thrusters, how they are configured, and the power source that propels them.

The propulsion system of an AUV consists of one or more thrusters that drive the vehicle in a way that enables navigation to the work site. The thrusters must be positioned on the vehicle in such a way that adequate maneuverability and control are permitted by the moment arm of their thrust force in relation to the central mass of the vehicle. Chapter 2 outlined the maneuverability specifications of the proposed vehicle, while the chosen type of propulsion system was discussed in Chapter 4. The present chapter focuses on the configuration of the thruster units.

5.5.1 Vertical Thrusters

It is essential for an AUV employed for purposes of environmental monitoring to be maneuverable (see Section 2.1). Therefore, to afford SEMBIO good maneuverability, the propulsion system was designed with a number of four vectored vertical thrusters to enable vertical movements (heave) as well as pitch and roll movements.

In the case of MONSUN, the vertically mounted thrusters are positioned on all four fins. As discussed in Section 5.3, CFD was used to conduct the analysis of the thrusters associated with the MONSUN design, which revealed that the manner in which the thrusters were positioned created a turbulent flow behind the vehicle, affecting the flow of the vehicle (e.g., increased the drag force). Based on these

observations, the analysis results of CFD once again illustrated the advantages of the SEMBIO design, where the vertical thrusters of SEMBIO design are located not on the fins but within the hull of the vehicle. This decision improved the SEMBIO design and led to a diminished drag force and, implicitly, lower energy use. Also, this decision was motivated by the need to make the upper and lower hull more robust and easy to assemble; the upper and lower hull parts made up four columns within the hull to serve as nozzles or rings (Figure 5.36), increasing the resistance to pressure.

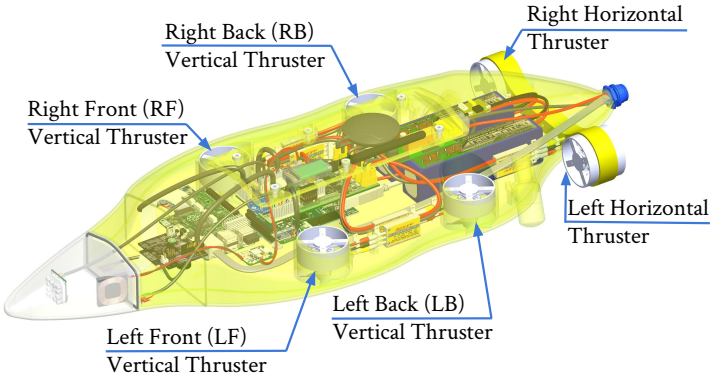

Figure 5.36 Illustration showing the positioning of the thrusters within the hull

Every thruster was positioned on the individual nozzles (see Section 4.5.3 for further information regarding the implications of the nozzle use). The nozzles were subsequently incorporated into the hull of the vehicle. The purpose of the nozzles was to direct water to the thrusters in a particular direction in relation to the vehicle's main axis. Furthermore, as they surrounded the propeller blades and served as a base for the thrusters, the nozzles minimized the likelihood of external objects getting access to the thruster propeller and decreased the amount of propeller vortices produced during the high-speed turning of the propeller. The construction of the vehicle was greatly simplified by the integrated thrusters, which also ensured innate watertight integrity. Moreover, the removal of the thrusters to inspect, maintain, or replace them was facilitated by a plastic tube containing the motor cables that was thread through a small pierced hole. Figure 5.37 shows how the nozzle and thruster were correlated with the base of the horizontal thruster. A cross-sectional view of the vertical and the horizontal thrusters is provided in Figure 5.38.

As illustrated in Figure 5.39, the thrusters were orientated with the propellers below the line of the inferior half of the vehicle, facing down to make sure that they were the first to go into the water when the vehicle was submerged.

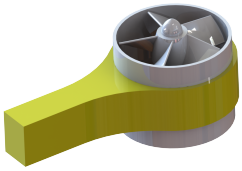

Figure 5.37 The horizontal thruster with the nozzle fixed to the base

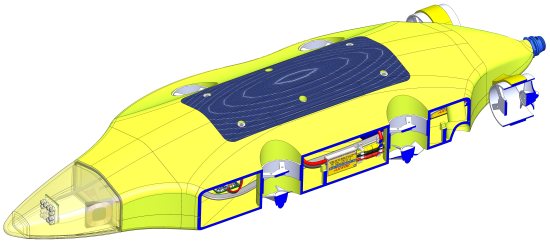

Figure 5.38 The nozzles facilitated the positioning of the vertical thrusters within the hull; the four vertical thrusters were connected to the body, serving as four support columns for the hull

5.5.2 Horizontal Thrusters

In the case of MONSUN, the horizontal thrusters are located at the posterior part of the frontal fins in the middle of the vehicle. Consequently, water perturbation is intensified because the current flow of water rushing from the vertical nozzle is orthogonal to the horizontal nozzle (see Section 5.3).

With regard to the guitarfish, all perturbations and vortices take place behind the body, due to the thrust force that the movement of the tail creates to propel the body forward. Taking these aspects into account, the horizontal thruster was positioned at the back of the designed SEMBIO vehicle.

Figure 5.39 The vertical thrusters were positioned in such a way as to ensure they were immersed in the water first

To produce the yaw and surge motion in SEMBIO, two horizontal thrusters of the propulsion system were created and installed at first, affording the vehicle five DOFs and a high level of maneuverability. As shown in Figure 5.40, the horizontal thrusters were placed at the tail end of the hull and each one of them was vectored.

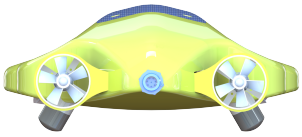

Figure 5.40 Illustration showing how the horizontal thrusters were positioned

Torque steer is a notable issue related to the use of more than one horizontal thruster along the same axis in the absence of counter-rotating propellers. When at least two thrusters operate on the same motion plane, this engenders a counter-reaction to this turning moment. To prevent the torque of the thrusters from rolling the vehicle in the opposite direction in which the propeller rotates, the AUV must be equipped with counter-rotating thruster propellers, just like a helicopter propeller has to be countered by the tail rotor or a counter-rotating main rotor. In the absence of such rolling, course deviations referred to as "torque steering" may be caused by the ensuing asymmetrical thrust and drag loading.

As outlined in Section 4.5.3, every thruster was positioned on separated nozzles, which were then incorporated into the hull of the vehicle. The construction of the vehicle was greatly simplified by the integrated thrusters, which also ensured innate watertight integrity. Moreover, the removal of the thrusters to be inspected, maintained, or replaced was facilitated by a plastic tube containing the motor cables and going through a small pierced hole.

Similar to the vertical thrusters, nozzles were installed on the arm of every horizontal thruster to enhance the torque (moment arm of thrust force), as illustrated in Figure 5.37 and Figure 5.40.

Prior to the installation of the electrical components, an experiment was carried out to make sure that the vehicle did not leak after the thrusters, cover, connectors, and camera lenses were installed. The experiment involved keeping SEMBIO submerged in a swimming pool at a depth of 4 m for several hours. The results confirmed that the hull was indeed completely watertight.

Chapter 6 discusses in detail the force tests that were conducted in relation to the horizontal and vertical thrusters combined within SEMBIO.

5.5.3 Setting the Buoyancy

As specified in Section 5.3, for horizontal movement at a speed of 1 m/s, SEMBIO needed a force of 5.8 N, while for vertical movement at a speed of 0.1 m/s, the vehicle required a force of around 1.4 N, with F_b being 0.7 N. To ensure the positive buoyancy of the vehicle, the vertical force had to exceed F_b, because diving would not have been possible if the thrust had been less than F_b.

To achieve positive buoyancy, F_b plays a central role in balancing the vehicle at the surface and supporting its stability prior to diving. This ensures that the vehicle can float to the surface in the event of power failure. A fixed value of 700 mN was established for F_b, which would help the vehicle to float to the surface at a speed of 0.06 m/s.

5.6 Electrical Design and Embedded System Hardware

When designing a micro AUV, the control electronics board needs to be as compact as possible. This means that the on-board control system must be custom-designed. From a structural perspective, SEMBIO exhibits a modular design in its control electronics system. Hence, the system can be expanded to incorporate extra modules with the interfaces reserved on the primary control board.

Owing to its structural integrity and shape, the hull of the SEMBIO vehicle can accommodate electronic components. In addition, the shape of the hull ensures that the existing space can be efficiently used since the majority of components and systems have a rectangular form. The protection of the entire electrical system is ensured through its incorporation within the hull, including battery, sensors, processors, cameras, and the ESC of the thrusters. A layered view of the electrical components integrated within the vehicle is provided in Figure 5.41.

The ESH includes all the necessary units to allow SEMBIO to attain its mission, including the control of the six thruster units (see Chapter 4) and the interface with the relevant input sensors. There are five different parts to the ESH, namely, processing, sensing, communication, power, and actuation. The first four are discussed in the following section, while actuation was already addressed in Chapter 4.

5.6.1 Communication

An AUV swarm is a major goal of SEMBIO. In a swarm, communication among members or a host station is essential. The communication strategy that is most widely applied in the field of underwater robotics and which was inspired by the communication of whales and dolphins is acoustic communication. Modems available on the market are usually intended for long-range communication and have high energy and space requirements. In addition, they are typically used for point-

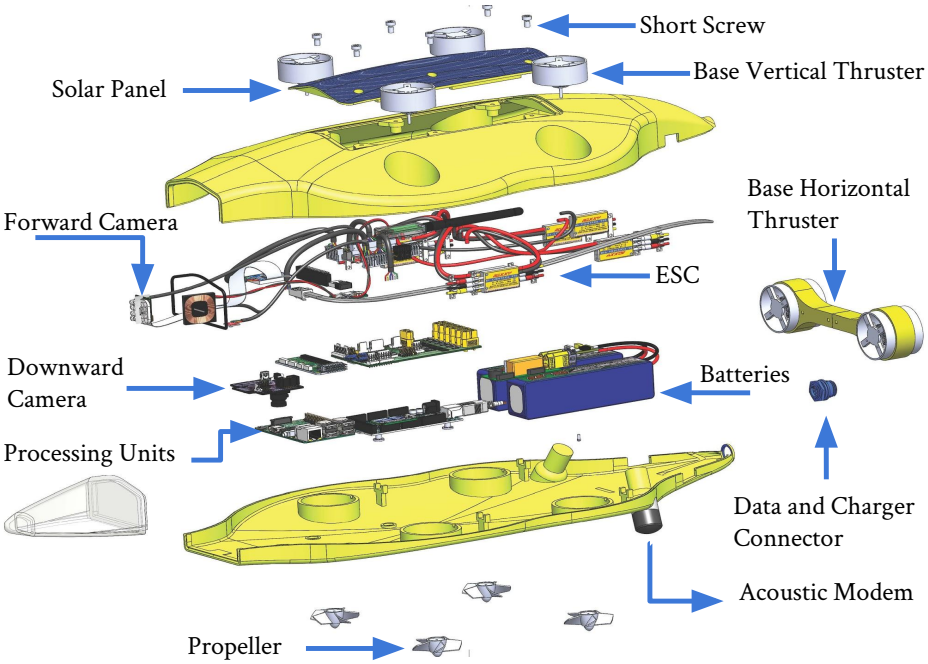

Figure 5.41 Exploded representation of the mechanical and electrical components of SEMBIO

to-point communication, which has implications for the communication protocol, medium access control, and addressing. For these reasons, such modems are not appropriate for use in micro AUVs. Instead, acoustic modem deemed to be adequate for the present project was a custom design created initially for MONSUN [154, 171]. Since the design was unrelated to the current work, it is described only in general terms. Although the design was unavailable at the time the project was undertaken, it should soon become available [171].

The acoustic modem prototype presents a number of significant advantages, such as small size, which means it is suitable for micro AUVs; low energy consumption, which means that it does not reduce the operation time of the host; affordable costs (< 600 €); and capability of communication at distances of 50 m or greater [172].

To accommodate this type of acoustic modem into the mechanical design of the SEMBIO vehicle, two holes for hydrophones to transmit signals among the members of the swarm were created, as shown in Figure 5.41. Indeed, the SEMBIO design can be altered without difficulty to accommodate any modifications in the shape and size of the acoustic modem or its transducers.

Wireless communication is useful for changing programs on the controller, transmitting sensor data from the AUV, and for remote driving of the AUV. Bluetooth adapters are not very costly and can be affixed to the RX/TX port of the primary controller without difficulty. In the air and underwater, Bluetooth has a range of

less than 30 m and less than 30 cm, respectively. However, it is highly advantageous in that the program on the AUV can be changed with no need to open it. The Bluefruit EZ-Link module [4] is connected to the primary controller. A Bluetooth USB dongle can then serve a notebook, enabling communication, such as from the side of the pool. What is more, to facilitate the communication between the energy management system and the GUI mission on PC, the XBee [62] (ZigBee/IEEE 802.15.4 compliant) was selected. XBee has a variety of features, operates transparently and displays a high-level API. In this project, a low-power model was used with a range of 100 m, corresponding to a class-2 Bluetooth. Furthermore, the XBee Pro variation would permit signal transmission across a 1 km range without the hardware or software needing to be modified (Figure 5.42).

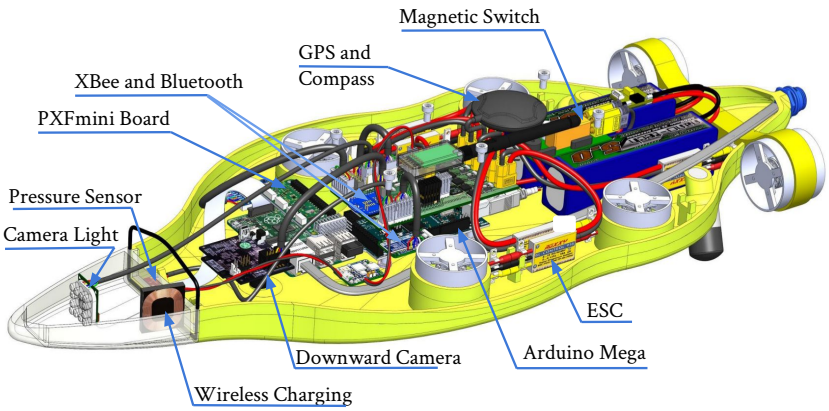

Figure 5.42 This view illustrates the position of the electrical system elements

5.6.2 Sensors

As discussed in an earlier section, SEMBIO possesses five DOFs, which are surge, roll, heave, yaw, and pitch. Therefore, input sensors are required to allow for a combination of acceleration, velocity, and/or position to ensure that the movement in each degree can be controlled with precision. The sensors employed in this project are discussed in the following section.

The Pressure Sensor

The rise in water pressure is directly proportional to depth, which means that pressure can be used to determine the exact vertical position. For the purposes of the present project, the MS5803-14BA [54] miniature module was the chosen pressure sensor, since it is a high-resolution pressure sensor with Serial Peripheral

Interface (SPI) and Inter-Integrated Circuit or I square C (I2C) bus interfaces optimized for systems of depth measurement with a water depth resolution of 1 cm and less.

The components making up the sensor module are a highly linear pressure sensor and an ultra-low power 24-bit ADC with internal factory-calibrated coefficients. It offers not only an accurate digital 24-bit pressure and temperature value, but also a range of operation modes enabling optimization according to conversion speed and current use. Furthermore, no extra sensor is needed to implement a depth measurement system and thermometer function, owing to the high-resolution temperature output.

The gel membrane and anti-magnetic stainless-steel cap affording resistance to a water pressure of 30 bar are features singular to the MS5803-14BA. In the case of SEMBIO, the location of the pressure sensor is beneath the hull, as shown in Figure 5.42.

Inertial Measurement Unit

To determine how an AUV is orientated in relation to the earth, the Inertial Measurement Unit (IMU) was integrated. The IMU modules available on the market often exhibit a large size and high power requirements [99]. For the system used in SEMBIO, the PXFmini [68] with the MPU9250 IMU was chosen, comprising a 3-axis accelerometer, a 3-axis magnetometer, and a 3-axis gyro (Figure 5.42). The PXFmini was considered a suitable choice because of its design. It is intended for drone platforms comparable to the underwater vehicle concept with considerations of power use, cost, and weight, and also because it possesses an open autopilot mini board for the Raspberry Pi (RPi) that ensures accurate measurement owing to the robust underlying code.

GPS and Digital Compass

The uBlox Neo-M8N GPS module with an HMC5883L digital compass kit was chosen that delivers and provides location and time information outdoors in all weather conditions. It combines high sensitivity with low power consumption. The kit requires the following ports: UART port for GPS and I2C for a compass. This kit can also connect to the PXFmini, which supports it through strong software. This kit features active circuitry for the ceramic patch antenna, rechargeable backup battery for warm starts, and I2C EEPROM for configuration storage. The kit is located on the cover of the SEMBIO hull so it is on the top and highest point of the vehicle in order to keep the GPS above water if the vehicle is floating on the surface, which will aid quick communication between the satellites and the GPS (see Figure 5.42).

5.6.3 Processing

To ensure a successful mission accomplishment, the SEMBIO vehicle has been equipped with two main processors (Figure 5.43). Arduino Mega is the first processor, being originally intended for projects of greater complexity, like robotics. Because the Arduino Mega represents a microcontroller rather than an actual computer, it presents a number of strengths and weaknesses. A microcontroller is advantageous mainly because it is capable of task performance at hard real-time interfacing and execution without difficulty. Another strong point of a microcontroller is that it provides direct interaction with a broad range of sensors and actuators via on-board analog-to-digital converters, PWM generators, and pin interrupts for quick encoder reading. The ATmega2560 chip is the core of the Arduino Mega 2560 microcontroller board. It consists of 54 digital input/output pins, 15 of which can serve as PWM output, an 8-bit system, 16 analog inputs, one I2C, four Universal Asynchronous Receiver/Transmitter (UART), a 16-MHz crystal oscillator, and a USB connection. The ATmega2560 is also advantageous because it relies on specialist PWM driver modules to run six DC motors concomitantly, signifying that all six thruster units of the SEMBIO vehicle could be controlled with a single microcontroller (Figure 5.41).

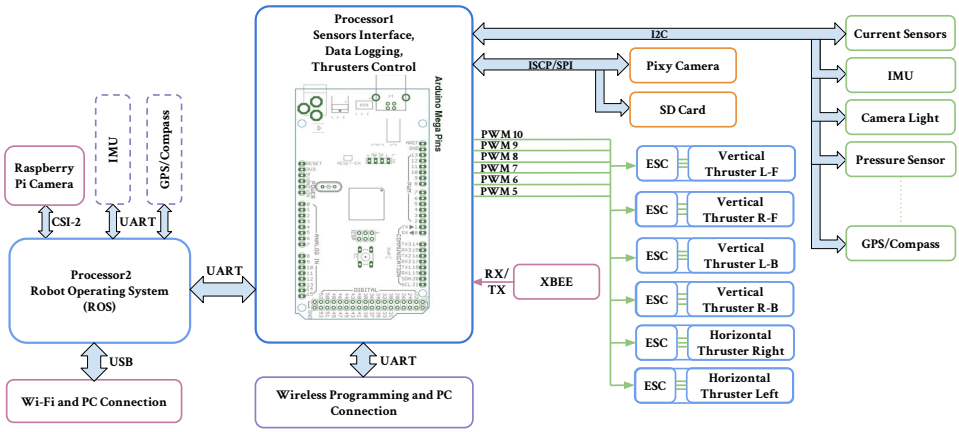

Figure 5.43 The configuration of the embedded system hardware

The other processor employed in SEMBIO is the RPi, which differs from Arduino Mega because it is a minicomputer based on the Linux operating system. RPi2 possesses a quad-core processor of 900 MHz and RAM of 1 GB. Sensors without high update data requirements could connect to this processor to alleviate the load on Arduino.

Several Arduino tasks are made possible by the synergy between RPi and Arduino, including the management of real-time control execution, sensor signal reading, and the transmission of the PWM signal to the ESC. Meanwhile, the RPi supplies the Robot Operating System (ROS) [22], Wireless Networking Technology (Wi-Fi)

connection, and extra computational power for components like cameras and sensors that do not require real-time execution.

The storage of the input and output data employed by the ESH was necessary for the experiment analysis. One suitable storage option of such data is the non-volatile memory on external flash memory devices.

5.6.4 Power

The power system of an underwater vehicle has to be capable of fulfilling a number of objectives at the same time. Furthermore, the storage capacity of the source of power must be sufficiently large to ensure that the vehicle can carry out its tasks effectively. Power has to be supplied at a constant voltage in order to make sure that the on-board electronic circuits are functioning as intended. Additionally, the functions of different components must not be disrupted by noise and power glitches created by one circuit component.

The most widely employed source of power in AUVs is batteries. To be considered ideal, a battery must demonstrate two main properties: a high density of energy and the ability to preserve a voltage that does not fluctuate during discharge. Additional features that a battery should exhibit include the ability to resist extremely high and extremely low temperatures, a shelf life that is not limited, the ability to recharge, and cost-effectiveness. However, so far, there is no battery that displays all of these properties.

When it comes to choosing a battery, the type of battery that is most widely employed is the Li-Po battery. The main strength of this type of battery is the fact that its internal resistance is low. As a result, the voltage does not decline significantly when drawing a high current. This is why this type of battery is suitable for the application pursued in this project. Thus, SEMBIO was equipped with a primary powerful 11.1 V battery block with a 10 Ah capacity.

In order to ensure that the specifications of SEMBIO were met, two voltage levels were added as well, namely, 5 V and 3.3 V for the sensors and the processors, while 11.1 V were linked straight to the thrusters via ESC. A Printed Circuit Board (PCB) was included in the design of the power board, with a more comprehensive discussion about the power system being provided in Chapter 7. SEMBIO was also equipped with a set of current sensors geared towards measuring the main current draw of the vehicle, and thrusters and sensors to keep track of and to estimate how much power was consumed by the electrical system on the whole.

5.6.5 Additional Electronic Components

A number of extra electronic components was selected to ensure that the supplementary functions that were set in the function structure could be performed.

Cameras

SEMBIO was equipped with two cameras. One camera was a forward-facing camera that was positioned at the front of the hull, while the other camera was a downward-facing camera that was positioned at the bottom of the vehicle's hull. The purpose of both of these cameras was to support the vision system of the vehicle, see Figure 5.42.

There are three reasons why two distinct types of cameras were used to support the SEMBIO vision system. The first reason was to ensure an effective vision for the vehicle. The second reason was that RPi could only connect with a single camera. The third reason was to expand the range of missions that SEMBIO could fulfil concomitantly, such as an obstacle detection algorithm and pipeline tracking algorithm on the basis of the forward-facing camera and downward-facing camera, respectively.

A frequently encountered problem in the case of microcontrollers is the fact that they lack the computational power necessary for processing, in real-time, incoming video streaming signals, which constitute extensive volumes of data typically in Mb/s, from a vision sensor. The Pixy CMUcam5 is an inexpensive, rapid vision sensor equipped with the omni-vision image sensor 1280 x 800 [45], which can be connected straight to Arduino and additional controllers. It can also monitor a number of seven distinct color objects simultaneously with up to 50 Hz. The ability of Pixy to perform image processing tasks like the real-time detection of colored objects is due to its on-board processor. The detection results can be transmitted by the camera in the ASCII text format through SPI, UART, or I2C. For all these reasons, the Pixy sensor was chosen for the SEMBIO project.

The Pixy served as the downward-facing camera of SEMBIO in order not only to enable the vehicle to monitor and identify objects such as pipelines, but also to provide the visualization of the area beneath it.

The purpose of the RPi camera module is to the ensure connection to RPi via the Camera Serial Interface (CSI) connector. The video modes supported by the camera are 1080p30, 720p60, and 640x480p90. Due to the fact that the image process does not occur as Pixy but in RPi, the output basic image of the camera is processed with the open source computer vision (OpenCV) software. This type of camera is advantageous because it is not large in size, offers good technical assistance, and it is not expensive.

The RPi camera was established as SEMBIO's front camera to allow the vehicle to identify and follow other members of the swarm.

To equip the vehicle with a night vision device, the RPi camera that was used was the Bright Pi breakout, which enables visualization not only in visible bright white light, but also in infrared light. Connected to the I2C interface, Bright Pi made it

possible to control the brightness of Light-Emitting Diodes (LED) on the basis of the on-board LED driver chip.

Magnetic Switch

A magnetic switch was introduced within the hull of SEMBIO to make it possible to turn the power system on or off, thus making this system safer. Such a magnetic operating switch permits the main power system to be easily activated or deactivated based on a magnet. More specifically, the main power system can be switched on or off by moving a magnet on the external part of the hull corresponding to the internal area where the magnetic switch is located in the opposite direction.

Owing to this magnetic switch, it is not necessary to open the watertight hull in order to turn SEMBIO on or off. A "peep" sound is made when the main power supply of 16 A is switched, as is shown in Figure 5.41.

Wireless Charging

The wireless charging system used for SEMBIO allows the batteries of the power system within the vehicle to be charged by induction, with no need for a physical connection. The charger was positioned at the rear of the forward-facing camera, on the left side, as can be seen in Figure 5.42.

The wireless charging system was assessed by charging a battery of 2700 mAh, which was quite a small capacity in comparison to the main battery. However, the main battery could not be successfully charged. There are a number of reasons why the main battery charge failed, including the fact that the wireless charger was slower than a wired charger, its efficiency was not as high, and there was a significant loss of energy due to heat. In relation to this aspect, the research was not continued, as additional developments and empirical work are required to enable the use of this technology underwater on the basis of a special base charger embedded in a particular underwater region.

5.6.6 Software

The MONSUN project adopted a software architecture [137, 154] demonstrating a hierarchic structure with an emphasis on adaptability and modularity (see Figure 5.44). This architecture was borrowed for SEMBIO. In the following section, the architecture is described without going into too much detail because this is not a major priority of this study. A key advantage of the software architecture is that it contains ROS and it consists of three levels, namely the task level, the behavior level, and the sense/act level. The definition of the tasks is conducted at the highest level and the tasks draw on data from the behavior level and the robot

system. The behavior (e.g., diving or adjusting depth) transmits its parameters to the controller, which asks the sensors to provide the necessary data and adjusts the speed of the motors according to the controller computation. The controller informs the top behavior on whether or not the intended task has been accomplished. The sense/act level interacts with the other levels and supplies them with data on the basis of its connection to the driver of the sensors and actuators.

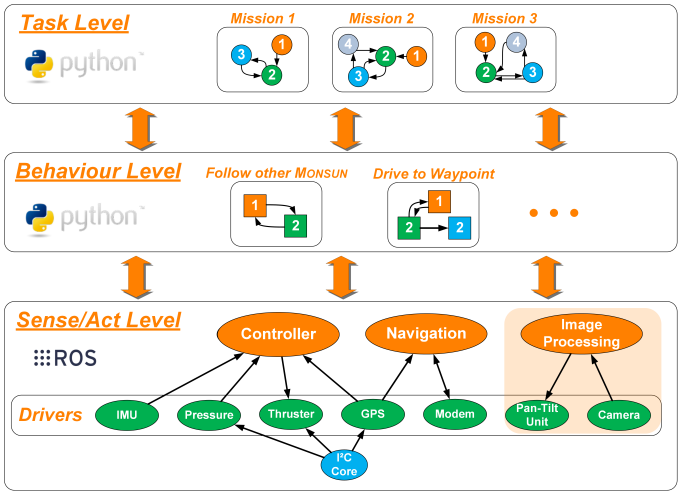

Figure 5.44 The MONSUN software architecture borrowed of SEMBIO

5.7 Summary

In the present chapter, the discussion focused on how the design of the proposed underwater vehicle SEMBIO was developed. The importance of the natural world as a source of inspiration for creating ingenious ideas for the development of engineered systems was highlighted. An explanation regarding the choice of the guitarfish as the organism that inspired the flattened and streamlined shape of the designed vehicle was also provided.

The discussion addressed the processes of mechanical design, drawing, construction, and 3D printing and assembly of SEMBIO, along with a detailed description of the development of a working prototype with the designed propeller-based thruster. CFD and SolidWorks permitted a hydrodynamic analysis of SEMBIO to identify potential hull improvements, and a comparison of the CFD results of SEMBIO and MONSUN was conducted. The discussion also covered SEMBIO's electrical design, sensing capacity, and embedded system.

6 Vertical Motion Control for SEMBIO

The previous chapter presented the creation of a complete prototype micro AUV SEMBIO allowing formulation of motion control algorithms. In the present chapter, the control systems employed in other AUVs are explored and the fundamental SEMBIO model based on which the controller will be developed is characterized.

The movement of a vehicle between two points is made possible by motion control systems. For instance, vertical motion control systems rely on software hard coding to move the vehicle from the water surface to a particular depth. In the case of three-dimensional movement, the control system can be separated into several independent controllers for heave, sway, yaw and surge, pitch, and roll. The overall concept of a motion control system can be grasped if one of these controllers is understood. Additionally, the development and testing of each controller can be undertaken separately prior to their integration.

The heave DOF was selected to underpin the control system design, due to the reliability and stability of the input sensor (pressure sensor, see Section 5.6.2), especially as the input sensors associated with yaw are significantly affected by noise and drift. Heave DOF was also selected because of the simplicity of the heave model, without any cross-coupling terms with other DOFs. Furthermore, the heave controller is theoretically appropriate for surge and sway control as well.

This chapter presents the work conducted on the development of a heave controller using the SEMBIO prototype vehicle. For this, the basic SEMBIO model underpinning controller development is described. The controllers considered to be particularly relevant to the present project are the Proportional Integral Derivative (PID) and Sliding Mode Control (SMC) controllers. This work was done together with U.Behrje and partly published in [26].

6.1 Introduction and Background

Exploration of underwater environments depends significantly on AUVs, which carry sensor payloads along pre-determined trajectories for different applications, as mentioned in Chapter 1 and Chapter 2 [34, 53, 148, 236]. Micro AUVs, due to their high maneuverability, possess particular efficiency for environmental monitoring applications when they are used to form a swarm. To make vehicles as maneuverable

as possible, they must be able to move autonomously in both horizontal and vertical planes.

Monitoring enclosed processes requires measurements to be taken at specific points and locations. Consequently, all AUVs categorized as sensor platforms must be capable of remaining stationary at a particular series of 3D coordinates.

Conventional AUVs are incompatible with small-scale environments because they are usually large in size and expensive [176] (see Chapter 2). The design of such AUVs frequently entails coupled movements in the vertical and horizontal planes, meaning that AUV movement in the vertical plane necessitates forward momentum [10, 75]. By contrast, the SEMBIO design can effectively serve as a small-scale sensor platform and can hold stationary at any point because it does not require forward motion or coupling of movements in the two planes.

Vertical control frequently figures among the main feedback control loops of micro AUVs. Measurement tracks can be taken thanks to the capability to dive to a particular depth and maintain that depth for a period of time. Since the pressure of the surrounding water rises linearly with depth and its sampling is straightforward and precise, it can be used as the input. Besides being the most fundamental movement, the vertical movement is among the key movements of an underwater robot as well. The underwater robots that are powered by solar cell panels [107] have to return to the surface prior to power loss, and after the charging process is complete, they have to return to their previous location. Meanwhile, GPS-incorporating AUVs have to rise for communication and positioning purposes, as GPS is not functional underwater [200]. Vertical movement can be achieved via two approaches, as discussed in Chapter 4, namely, static diving based on the adjustment of robot buoyancy and dynamic diving, which relies on the propulsion system supplying propulsive force in the vertical direction and necessitates a high-response speed to establish a balance between buoyancy and other disturbance forces. The latter approach is employed in SEMBIO.

To change its buoyancy and reach the target depth, the AUV relies on its propulsion system as well as on a variable buoyancy system, if present. The buoyancy must be reduced to zero to enable the vehicle to maintain the required depth.

6.2 State-of-the-Art

This section reviews related works on small or micro AUVs intended for use in swarm applications (e.g., environmental monitoring), their vertical control systems, and techniques employed for small form factor.

The Serafina project was created to investigate the potential of using a swarm of small AUVs for mapping and monitoring the ocean spaces [118], but no data was provided regarding the control algorithms associated with vertical movement.

At the German Research Centre for Artificial Intelligence (DFKI), Hanff and colleagues [87] created a micro AUV called μAUV2 which was intended for applications of navigation and inspection. A non-linear model is used to describe and model the thruster dynamics, while the system model draws on the work conducted by Fossen [75]. To enable experimental determination of coefficients, simplifications were brought to this system model. For each DOF, heuristic PD controllers were implemented and fine-tuned in a water basin.

Compatible with robotic swarm applications [152, 154], MONSUN has six thrusters, four orientated vertically and two horizontally, allowing not only dynamic diving but also rotation around the roll and pitch axes to offset the pose in rough water and the yaw angle of the vehicle. Vehicle depth is controlled by standard PID controller with manual parameter tuning [65].

Additional control system applications were described in [161], where identification methods for non-linear models defining the pitch and yaw movement for small AUVs were also provided. There is significant complexity involved in the use of non-linear models for characterization of AUV movements based on mathematical equations in the dive plane. The above-mentioned work permitted simplification of the theoretical and practical assumptions underpinning the highly non-linear AUV dynamics, while also theoretically and practically justifying the use of linear second-order AUV pitch-axis models for system identification.

6.2.1 Control Systems: A General Summary

As illustrated in Figure 6.1, there are two major components to the standard feedback control system, namely, the controller (C) and the plant (G). The latter represents a model of the dynamics of a real-world system and its form has a direct impact on the selection of the control system.

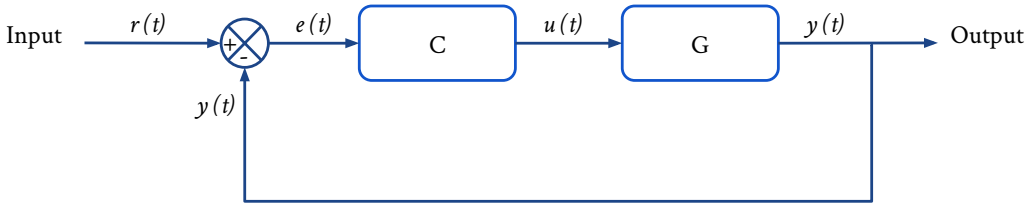

Figure 6.1 The general classic feedback control loop, where $r(t)$ is the input signal, $y(t)$ is the output signal, $u(t)$ is the control output, $e(t)$ is the error which is the deference between $r(t)$ and $y(t)$

The classification of control systems is based on the number of inputs and outputs, which include Single Input Single Output (SISO), Single Input Multiple Output (SIMO), Multiple Input Single Output (MISO), and Multiple Input Multiple

Output (MIMO) [209]. The complexity of the control system increases with the number of inputs or outputs. In many cases, it is preferable to transform multiple input or multiple output systems into several single input or single output systems that can be merged [105].

The SEMBIO depth controller is a SIMO system that has depth and four vertical motors serving as input and outputs, respectively, or a SISO system, if the working premise is that roll and pitch are zero during the dive. The ballasting negates the roll and pitch, which enables modelling of the force generated by the four thrusters as a point force exerted along the center of the vehicle. Consequently, the controller is SISO. That is, controlling all thrusters and the buoyancy system with a single feedback controller can result in a SISO controller. The current depth and the buoyancy or vertical force exerted on the vehicle are input and output, respectively, of the depth controller. The force established by the depth controller must be attained by a cascade control loop. This enables significant control structure simplification, and the controller and propulsion system are decoupled.

Sensor noise and external interferences and disturbances affect all real systems. Disturbances influencing underwater vehicles include waves and flowing water, the measurements of which are challenging. In particular, interferences frequently occurring in large lakes or at open sea constitute limiting factors for small AUVs in terms of control performance.

There are two types of flow around an object, namely, laminar flow and turbulent flow. From a mathematical perspective, water fluid dynamics constitute a difficult matter. The main difference between laminar flow and turbulent flow is that the former is underpinned by linear dynamic models, while the latter is associated with highly non-linear dynamics. If identification of a dynamic model is desirable, a Taylor approximation of second order is frequently employed.

6.3 Controller Types

A variety of controllers have been employed for AUVs. The AUV control systems adopted most often are a reasonable point of departure when selecting the control methodology for a micro AUV. As mentioned above, of particular relevance for the purposes of the present project are the PID and SMC controllers.

A widely employed approach is to avoid the issue of identifying a model and employing a fixed-structure controller, such as a PID controller, and establishing parameters based on heuristic methods (e.g., Ziegler-Nichols) followed by manual tuning. It is assumed that the movement in various DOFs is uncoupled and each DOF is associated with its own controller. This affords acceptable control performance, but it is an arduous process as it requires numerous experiments. In addition, the system must be secured, because the control loop may be unstable during the tuning phase.

6.3.1 PID Control

The control system most frequently employed is the PID controller, which represents about 90% of industrial controllers [21]. This controller derives its name from its elements, namely, Proportional (P), Integral (I), and Derivative (D).

The expression of PID controllers typically takes the form of a Transfer Function (TF) in the Laplace domain, because the primary usage of these controllers is for Linear Time Invariant (LTI) SISO systems. The TF of a standard PID is either the ideal or parallel form [21]. This project employed the parallel form (Equation 6.1) because it is flexible. The proportional gain, integral gain, and derivative gain are, respectively, denoted by K_p, T_i and T_d.

$$C(s) = K_p + \frac{1}{T_i s} + T_d s \tag{6.1}$$

The variety of controller structures mirrors the variety of tuning rules applicable to the system. Several methods can be employed for tuning purposes, such as step responses and frequency responses. The Ziegler-Nichols method enjoys the greatest popularity [245]. The system design specifications, including performance criteria or robustness, determine the tuning type that can be used [150].

Conventional tuning methods may be inadequate in cases where a PID controller is employed alongside a non-linear plant.

6.3.2 Sliding Mode Control

An appropriate control law that has the ability to override control problems to fulfill the required performances of closed loop system stays an interesting challenge. A method that uses PID controllers may be restricted to achieve the desired performance, especially in robotics applications that have nonlinear models [47]. Therefore, it is recommended to employ robust control methods such as SMC, which are able to solve many control problems [193]. However, the so-called chattering problem is the most obstacle and handicap issue in sliding mode control applications. This problem is created by the switching term of the control input when applying it to real systems, which can damage in some cases the mechanical system.

The precision of the model underpinning the plant to be controlled is a major issue in the context of control system design. Parametric uncertainties (e.g., vehicle drag underestimation) and unmodeled dynamics (e.g., treating the vehicle drag not as quadratic but as linear) [195] are the main sources of imprecision in plant modelling.

Disturbances, parameters exhibiting rapid variability, and unmodeled dynamics can be most effectively addressed through robust control, while uncertainties in

parameters that are constant or vary slowly can be addressed through adaptive control.

The SMC [213] is a type of robust control approach that is widely employed. Numerous AUVs have been successfully equipped with this controller type, as detailed in [222, 238]. As a variable structure control system, SMC is highly stable, robust, and is in general straightforward to tune and implement. For previous reasons and advantages, SMC was selected to be the final controller for SEMBIO.

6.4 Method and Modeling Approach

The experience of using and creating swarm AUVs inspires the adopted method. The applied premise is that the propulsion system of inexpensive AUVs allows independent movement in each DOF, and that they can withstand inclination away from their steady state in roll and pitch. As explained at the beginning of this chapter, a dynamic model with decoupled sub-models for each DOF is made possible by this premise.

Owing to limitations of cost and energy consumption/source, the microcontroller of an inexpensive AUV is inexpensive as well. Hence, advanced feedback control methods requiring extensive computational resources (e.g., model predictive control) are disregarded, and a straightforward controller scheme compatible with an 8-bit microcontroller must be identified.

A pressure sensor for depth measurement and a GPS receiver for surface navigation are among the sensors employed for inexpensive AUVs. A compass and an IMU can also be incorporated, but these sensor inputs are not useful for the heave model.

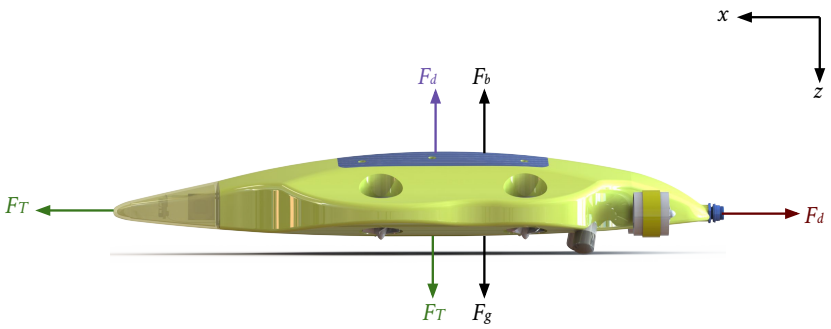

Figure 6.2 The forces that SEMBIO is subject to in the water, where F_d is drag force, F_b is buoyancy force, F_g is gravitational force, and F_T is thrust force

By comparison to a non-linear system, a linear system is easier to understand, and the design of its control system is more straightforward as well. In the case of certain

non-linear systems, dynamics can be adequately estimated through linearization and can be subsequently controlled. The highly non-linear dynamics frequently presented by AUVs comprise a multitude of disturbances and interferences that are difficult to measure. The heave DOF was subjected to linearization. The premise that linear models are appropriate for characterizing the dynamics of every DOF underpins the chosen approach. For this purpose, the propulsion system structure is not included into those models, alternatively, it is assumed that the inputs of the motion of a rigid body represent the resulting external forces and moments (see Figure 6.2).

Accurate control performance is still possible because the errors introduced by overlooking the non-linear effects and propulsion system dynamics are negligible. Only the static model of the propulsion system on the other hand has to be modeled explicitly.

6.5 System Identification

The AUV-related issue of movement control can be addressed via different approaches, which distinguish themselves through the method employed for control law formulation, the computational power required for the control loop, the measurement equipment for identification of model parameters, and the configuration of the dynamic movement model. The selected control system must be able to deal with the fact that linear equations do not permit precise modelling of AUV non-linear behavior and the fact that the system is subject to unidentified disturbances that cannot be dismissed.

In essence, the different movement directions can be modelled individually if the AUV design permits the vehicle to dive without forward momentum. The impact of the rolling angle on the vertical movement and other potential coupling effects can be ignored. However, the AUV behavior is characterized adequately by such models only if there are no movements with strong coupling. In addition, an AUV dynamic model with six DOFs can be deduced and worked out as well. To avoid excessive complexity, quadratic terms can be used to model non-linear dynamics, but establishing model parameters requires non-linear identification. For this purpose, it is essential to employ advanced measurement tools. Factors like inherent measurement noise, unmodeled dynamics, and non-linear model structure make the determination of model parameters challenging. The difficulties and efforts involved in creating a precise non-linear AUV model with six DOFs are beyond the lab capabilities and time available to small workgroups, it requires additional expensive devices and a swimming pool for testing, and is very time-consuming.

6.5.1 Dynamic Model/Heave Model

Formulating differential equations defining the plant is the starting point for control system development and implementation. The general movement equations for an n-DOF AUV have been provided by many studies. For instance, Equation 3.5 (from the Chapter 3) provides the dynamic model underpinning AUV movement [19, 51, 75, 76].

$$M\dot{\nu} + C(\nu)\nu + D(\nu)\nu + g(\eta) = \tau$$

$$\dot{q} = B\nu \tag{6.2}$$

The inertial matrix is denoted by M. Meanwhile, the Coriolis and centripetal matrix C can be disregarded and negated due to the low speed of the vehicle. The drag matrix and translational drag are respectively indicated by D (it is usually modeled with the term $D_l(\nu)+D_q(\nu)$ consisting of linear and quadratic drag), while the vector of restoring forces and moments is given by g. The vector of thrust forces is denoted by τ, while a Jacobian matrix associated with the earth fixed velocities ν and the body fixed velocities $\dot{q}$ is given by B.

The integrative behavior in connection with the buoyancy force make the heave DOF open-loop unstable, signifying that the heave control system cannot be switched off to hold stationary at a particular depth, and neither can the thrusters. The vehicle mission time will be reduced as a result of this, but there is no other option. The addition of an extra term to the thrust output helps to offset the steady-state (SS) error determined by the buoyancy force in the control system [75].

The matrices M, C, D, and g represent diagonal matrices in the uncoupled model, signifying that the various movement directions in this reduced model are uncoupled. This enables individual determination of the matrix parameters for every DOF, reducing the complexity of model parameter identification. However, it is important to make sure that the premises underpinning this kind of uncoupled model are valid throughout the identification experiments and subsequent missions.

The simplified model of SEMBIO can be found by the following assumptions. The movement of vehicles at higher speed is characterized with precision by linear and quadratic drag [87]. It is enough to consider linear drag in applications with low speed or dynamic positioning of the vehicle, such as in the context of depth control [76]. Same as previous consideration is possible for the $C(v)$ term. Hence, trimming the vehicle has to be done in a manner that roll and pitch are insignificant. This leads to a simplified buoyancy term, where the g term includes restoring forces and moments, gravitational forces, and lift forces.

Taking into account the previous assumptions, Equation 6.3 provides the heave motion (z-direction) given by

$$m_t \dot{v}_z + d_l v_z + m_i g = \tau_z \tag{6.3}$$

where the discrepancy between the gravitational and buoyancy forces is denoted by $m_i g$, which has a negative value if the AUV has a positive buoyancy. The velocity in the vertical direction (z-direction) is denoted by v_z, the mass of the rigid body (m_{rb}) including the hydrodynamic added mass (m_a) is denoted by m_t, the linear drag term is denoted by d_l, and g is the gravity of earth. As we do not take winds and waves for a submerged vehicle into account, this is the resulting force applied by the propulsion system τ_z without any external disturbances.

The outcome of a Laplace transformation is:

$$v(s) = \frac{\tau_z(s) - m_i g}{s\, m_t + d} \tag{6.4}$$

Since the AUV weight remains constant throughout a mission, the term of $m_i g$ represents a constant force. The addition of an integrator allows for a description of the depth z rather than the heave velocity v:

$$z(s) = \frac{\tau_z(s) - m_i g}{s(s\, m_t + d)} \tag{6.5}$$

The influence of the buoyancy can be reduced using $+m_i g$ to bias the thruster force:

$$\tilde{\tau_z} = \tau_z - m_i g \tag{6.6}$$

A small deviance would trigger a small constant force acting as an interference, which should be compensated by the feedback loop. The transfer function can be used to characterize the heave movement (open loop) by using a thruster force offset to make up for the buoyancy:

$$G_o(s) = \frac{z(s)}{\tilde{\tau_z}} = \frac{1}{s(s\, m_t + d)} \tag{6.7}$$

6.5.2 Depth Sensor

There is a linear increase in the hydrostatic pressure in a fluid as a vehicle is immersed deeper and deeper, and inexpensive sensors are adequate for measuring pressure. Thus, AUV depth can be practically measured with a pressure sensor. A measurement of the surrounding air pressure serving as offset for depth measurement should be undertaken as a reference point outside the water during the process of starting up the vehicle. The pressure sensor selected for SEMBIO was the inexpensive temperature compensated pressure sensor MS5803-14BA (see Section 5.6.2), which displays a 0.2 hPa resolution and up to $14{\cdot}10^5$ Pa operating range, which is equivalent to a water depth of around 140 m.

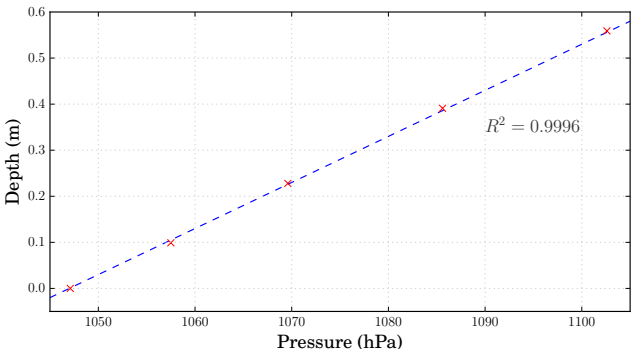

Figure 6.3 The sampled pressure output data for testing the linearity of the pressure sensor

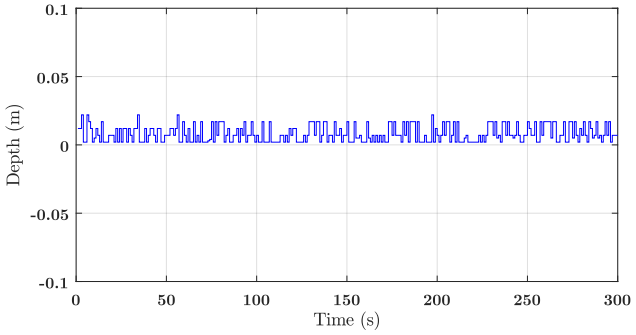

Figure 6.4 The steady state response associated with the pressure sensor

An uncomplicated experiment was conducted to confirm that this depth measurement sensor was appropriate. The experiment involved manual submersion of SEMBIO to various depths in a tank. The depth measurement was undertaken with both the pressure sensor and a measuring tape. As indicated in Figure 6.3, the measurements were precise, with less than 6 mm error, while the curve displayed

linearity, the coefficient of determination R^2 is 0.9996. Sensor noise was also tested by submerging the AUV to a constant depth, and multiple measurements were then taken one after the other. The measurements exhibited a 0.60 cm standard deviation (Figure 6.4). Furthermore, no delays or transient responses were noticed in the measurements.

6.5.3 Propulsion System

The diving force τ_z was derived from the propulsion system presented in Chapter 4. The mechanical structure of the propulsion system and the defining curve of every thruster gave a ratio of τ_z and the thruster rotational speed. Additionally, the correlation between the input signal and generated force was established by the defining thruster curve as well. The generated thruster force represents a non-linear function of propeller revolution, fluid speed, and input torque, which are influenced by density of the fluid, diameter of propellers, length of tunnel (nozzle), and tunnel cross-sectional area, among other parameters [19]. Computation of this force is challenging, however. The approach adopted in this project was to determine the force of every thruster and combine it with the vehicle body for the static case, and perform an estimation based on those values. Given the slow AUV speed, such simplification is legitimate.

The use of an ESC means that every input value is associated with a rotational speed. The generated force achieves constancy after the propellers have attained the target speed and a constant flow around the propellers has been established. Thus, obtaining the static gain of all thrusters for the entire operating range is sufficient.

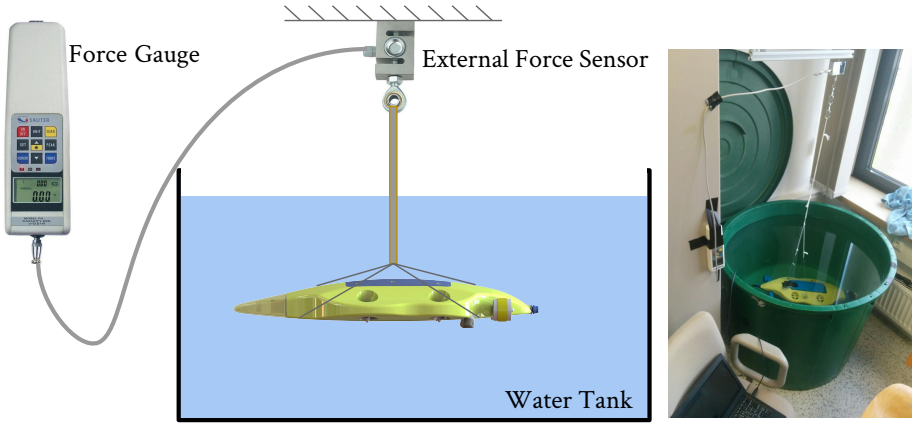

Figure 6.5 The configuration of the experiment for measuring a propeller thrust in combination with the vehicle's body

The back Electromotive Force (EMF) was measured for use in the commutation of the three phases, since the BLDCs are not equipped with hall sensors. Hence, the feasibility of this measuring principle depends on a minimal rotational speed.

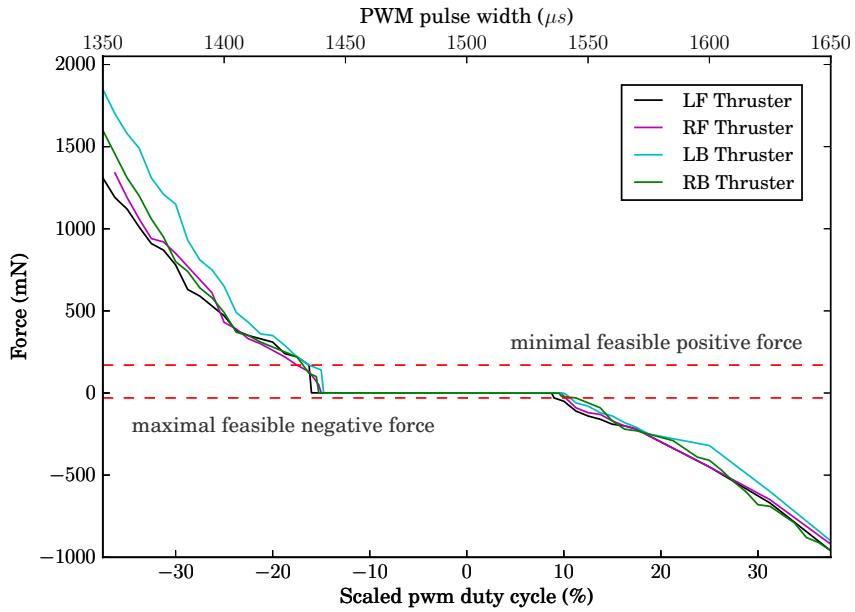

Figure 6.6 Characteristic curves of vertical the thrusters

The defining curve of the thrusters was determined through several experiments. As illustrated in Figure 6.5, the configuration of these experiments was identical to the experiment for measuring the force of a single thruster (see Section 4.5.1). A water tank with a volume of 1,000 l was used to conduct the experiments for determining the transfer behavior. SEMBIO was immersed in the water with a minor negative trimming and multiple tethers to keep it in place. The digital force gauge SAUTER FH500 was employed to measure the vertical force on the tethers. This configuration enabled the measurement of the extra force exerted by the thruster. The procedure was applied and repeated for all four vertical thrusters and both directions. Figure 6.6 provides the results of the measurements. As can be observed, one of the thrusters could not exert a force of less than 170 mN since the rotational speed was not enough to produce a back EMF that could be measured.

6.5.4 Software Design

Control of the propulsive force can be achieved through the PWM signals issued by the Arduino microcontroller output, which are applied to the ESC of each thruster to get the magnitude of the forces (see Figure 5.43 in Chapter 5). Underwater movement is achieved through the combination of the forces of four thrusters.

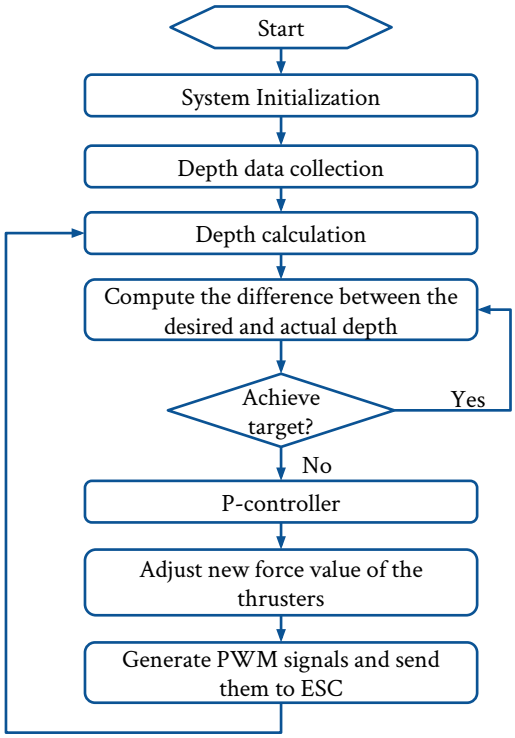

Figure 6.7 Schematic representation of the control strategy and the software structure

The direction and gain of the thrusters was controlled through a proportional P-controller (through the identification system), which also helped to make the thrusters more flexible. The flow chart of the control strategy is illustrated in schematic form in Figure 6.7. Within the context of a particular task, the first procedure undertaken by the robot was initializing its system, whereby the sensors were activated and calibrated. The next procedure was computing the initial depth and position. A comparison between existing and desired parameters was subsequently undertaken by the robot. If discrepancies were found between the two sets of parameters, the robot computed an appropriate trajectory to minimize those discrepancies through upwards or downwards movement.

6.5.5 Setup of Dynamic Model Identification

Estimation of the parameters m_t and d_l is necessary so that the dynamic model in Equation 6.7 can be used to derive a feedback control law. Manual trimming of the AUV to neutral buoyancy was undertaken during the identification experiment, giving a value of 0 to $m_i g$. The open loop experiment of SEMBIO is unfortunately

not successful due to the integral behaviour of the system, where SEMBIO dives down to the ground or rise to the surface of the rain barrel. This obstacle is disbanded by using a closed loop experiment. A P-controller was employed to carry out a closed-loop test (see Figure 6.8). Thus, the proportional feedback gain K_P is required for the extension of the heave model.

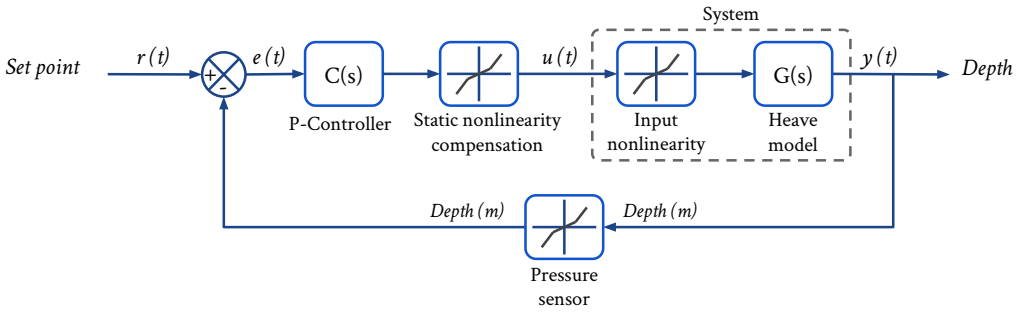

Figure 6.8 Feedback control loop

$$G_{\mathrm{cl}}(s) = \frac{K_P}{s(s\, m_t + d) + K_P} \tag{6.8}$$

High performance requirements are not demanded for this control system. The identification algorithm is concerned to gather the input and output signals from the system, and therefore effects such as oscillations towards the set point can be tolerated.

The thrusters were subjected to a minimal force, due to the dead zone in the thruster curve (Figure 6.6), to further ensure the linearity of the system during the identification experiment. The minimal body force $\tau_{z,min}$ was established to be 700 mN, since the minimum possible downwards force of one thruster is 170 mN.

$$\tau_z = \begin{cases} \tau_{z,min} & 0 < \tau_z < \tau_{z,min} \\ -\tau_{z,min} & -\tau_{z,min} < \tau_z < 0 \\ \tau_z & \text{otherwise} \end{cases} \tag{6.9}$$

When the minimal force rather than the estimated feedback is applied, adjustment of the controller inputs is necessary in order to maintain a proportional ratio between the controller input and output. To achieve this, the model input (i.e., the setpoint) was altered so that $\tau_{z,min}$ or $-\tau_{z,min}$ was obtained from multiplying the resulting error by the gain K_P. The controller linearity and, implicitly, the linearity of the augmented heave model could thus be maintained (Equation 6.8).

6.5.6 Dynamic Model Identification-Motion Scenario Experiments

Three available testing facilities were appropriate for the heave control experiments. These facilities were a rain barrel with a 70 cm diameter and 80 cm depth, a swimming pool with the dimensions 25 m x 15 m x 2 m, and the Wakenitz river in the vicinity of the university. Testing in the rain barrel produced negative results because of the disturbance water current produced by the external flow water of the thruster nozzle, which had an impact on the vehicle's movement.

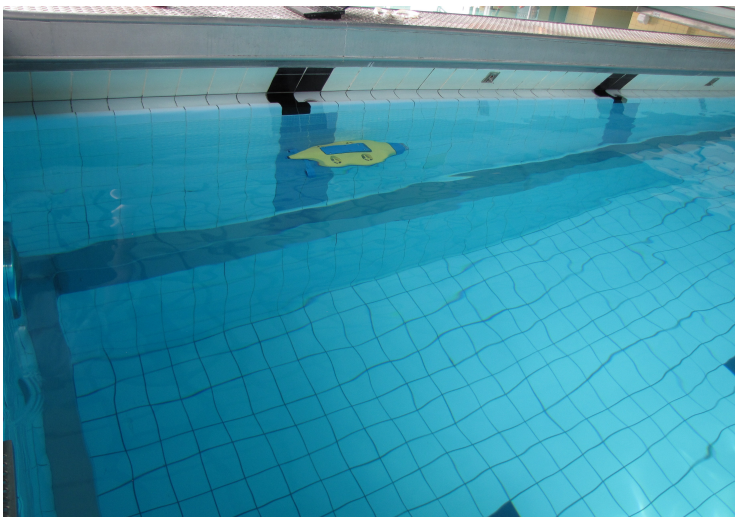

Figure 6.9 The field test (swimming pool) for system identification process

The least squares method for linear models is used to identify the parameters. External disturbances were negligible and thus disturbance model was not needed. To obtain distinct datasets for identification of the parameters and assessment of the resulting closed-loop model, a number of test runs was performed in a swimming pool containing fresh water with a temperature of 28 °C (Figure 6.9). In the experimental tests, two kinds of inputs were employed, namely, step and staircase (series of steps) setpoint inputs. Staircase function of different depths constituted the input. Due to the fact that the water surface was not modeled as a physical barrier, which would have produced erroneous parameters, the test data of the emerged vehicle were cut off.

To increase the analysis of the behavior and the response of the heave model, different input signals for the closed-loop model G_{cl} were applied. Figure 6.10 illustrates the first set of experimental results of the closed-loop model G_{cl} for the two-step input of 0.8 and 1.6 m. A two-step or two-depth input was conducted for several P-control values (K_P was 30, 40, 50, and 60, respectively). Pressure readings are stored in the embedded system SD card and were accessed after each experiment.

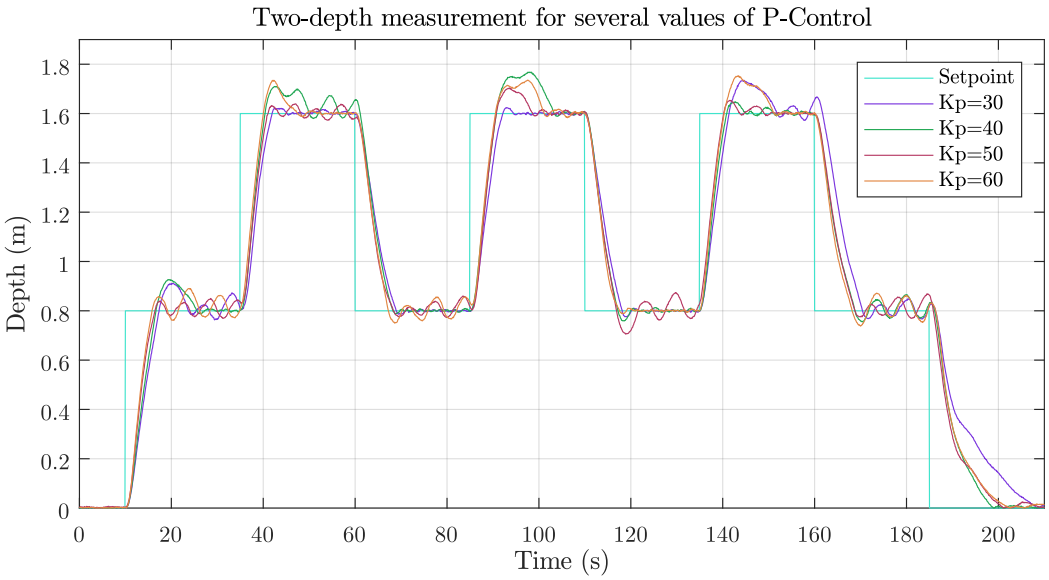

Figure 6.10 Experimental results for system identification illustrate the closed-loop response for which the input signal was a two-depth control

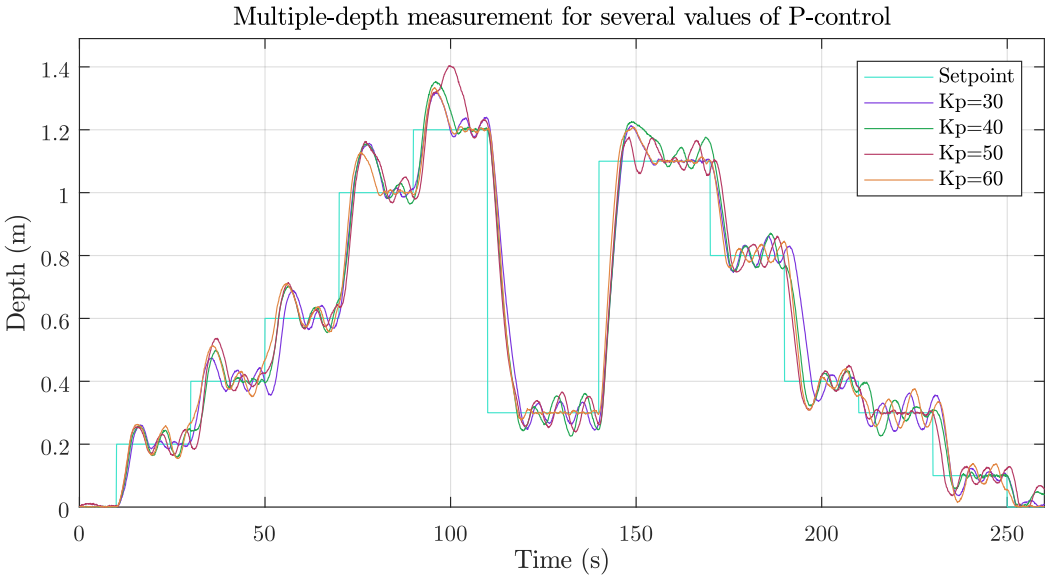

Figure 6.11 Experimental results for system identification illustrate the closed-loop response for which the input signal was multi-depth control

In the same manner, Figure 6.11 illustrates the second set of experimental results for the closed-loop model for multi-depth inputs of 0.2, 0.4, 0.6, 1.0, 1.2, 0.3, 1.10, 0.8, 0.4, 0.3, and 0.1 m.

Various noises, such as the water waves of the swimming pool, influenced the previous results, which led to what appeared to be a different positive overshoot and undershoot.

The system identification toolbox in MATLAB was used to create the closed-loop model from the measured input-output data. The second set of experimental results were the best to describe the behavior of the heave model, and for this reason they were selected.

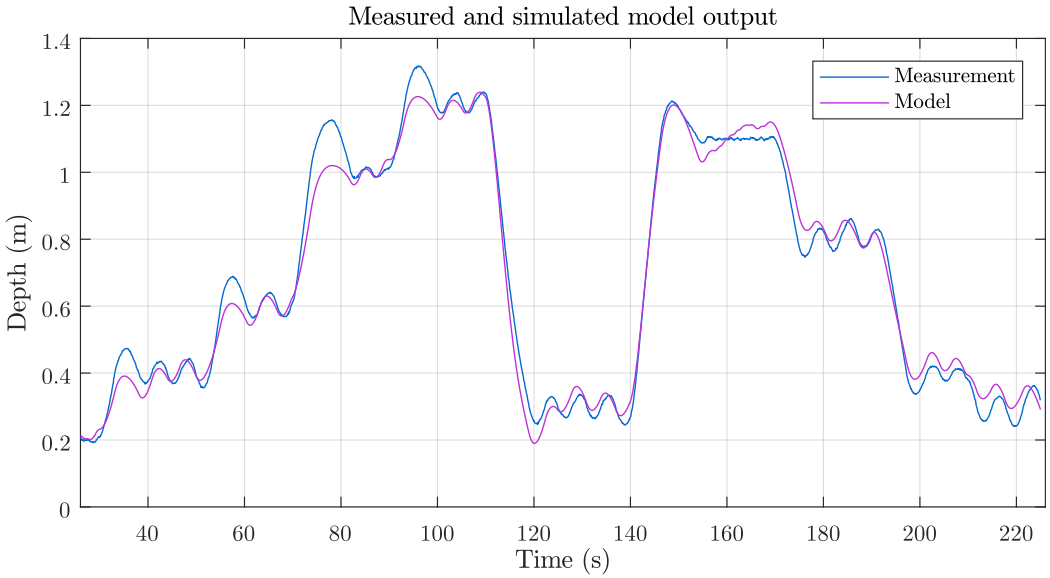

Figure 6.12 Comparison between the measurement and output of the identified closed-loop model

The output of the identified model G_{cl} is compared with a validation dataset in Figure 6.12. The model had a goodness of FIT of 0.8748 and the maximum deviance between the model output and measurements was $|e|_{\text{max}} = 0.137\,\text{m}$ (see Figure 6.13). This uncomplicated model failed to identify certain high-frequency dynamics, as suggested by the oscillations with overshooting occurring after every step. Nevertheless, the model successfully characterized the low-frequency movement.

The dive experiment fostered an explanation for the unmodeled oscillations. During upward or downward movement, the AUV has a tendency to pitch. Oscillating rotations have an impact on the depth measurement due to the positioning of the depth sensor in the front region. Consequently, such measurements are not indicative of the actual heave movement, but rather of the pitch angle. Despite

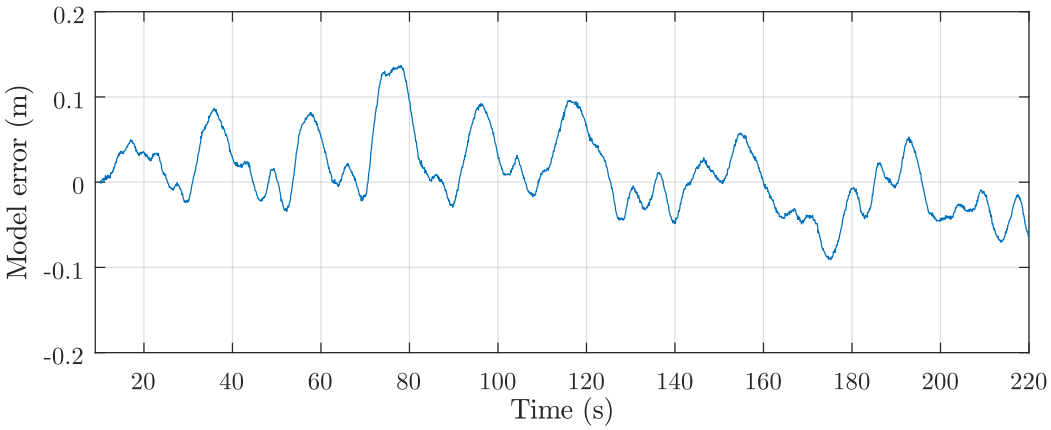

Figure 6.13 Model error illustrating the deviance between the model output and measurements

the derivation of a second-order model (Equation 6.8), there is the possibility to expand this model to model the pitch dynamic. As indicated in Table 6.1, a linear model that provides a precise characterization of these oscillations is not achieved by increasing the model order.

Model order	FIT
1	0.63
2	0.87
3	0.86
4	0.89

Table 6.1 Various model orders compared in terms of goodness of FIT

According to the results of the identification process (Figure 6.12), the total mass including the added mass is $m_t = 24.14\,\text{kg}$ and $d_l = 9.970\,\text{N}\,\text{s}\,\text{m}^{-1}$. The combined mass was accepted, confounding expectations that the mass parameter and the weight would not differ significantly, where the body mass is $m_b = 7\,\text{kg}$ [75]. The heave model that was obtained is as follows:

$$G_o = \frac{1}{24.14s^2 + 9.97s} \tag{6.10}$$

Figure 6.14 shows the placement of the two poles of this model.

6.6 Control Design Implementation and Evaluation

In this section, a basic description of SMC is presented and then applied to our heave model of SEMBIO. In addition, a comparison between the SMC and PID

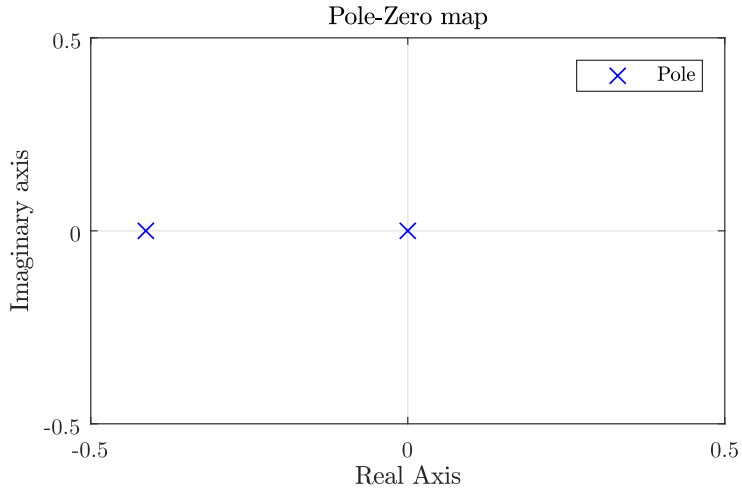

Figure 6.14 Illustrates how the two poles of the heave motion model are positioned.

with and without noises are conducted and illustrated. Finally, the real experiments of SEMBIO using SMC in a rain barrel and a swimming pool are implemented and illustrated.

6.6.1 Basic concept of Sliding Mode Control

The fundamental concept of the SMC system is to attract the system states in the direction of a surface known as the sliding surface. This is appropriately selected, and a stabilizing control law is created which retains the system states upon a surface of this kind. A variable structure control switches from separate control laws on the basis of the system state in comparison with a PID controller which uses a continuous control law. A switching controller of this type does not have the disadvantage of the thrusters' dead zone, provided that the controller output constantly exceeds the minimal feasible thruster force; consequently, this is appropriate for our specific application.

SMC that switches between two control laws by employing a switching surface $s(x)$, which is dependent upon state x of the controlled system $\dot{x} = Ax + Bu$, is a variable structure controller subclass, where the system matrix is denoted by A, control matrix is denoted by B, and the control input is denoted by u. The control laws direct the system trajectories to the switching surface. On reaching the surface, high-frequency switching commences and the system is forced along the switching surface by the controller to the equilibrium point $x = 0$. The switching surface is also known as the sliding surface.

Premature deterioration within the actuators is a likely disadvantage of variable structure control, the cause of which is high-frequency switching. Although many

solutions to this difficulty have been suggested, none of these is relevant here, since the SEMBIO control loop is clocked at 10 Hz, at which rate BLDCs may be operated safely. SMC's strength against parameter variations in the course of the sliding phase can be regarded as advantageous.

The SMC design involves locating a switching surface, normally linearly defined as $s(x) = r^T x$, being the foundation of the feedback control law.

$$u(x) = \begin{cases} u_+ & \text{for} \quad s(x) > 0 \\ u_- & \text{for} \quad s(x) < 0 \end{cases} \tag{6.11}$$

This directs the system trajectories onto the sliding surface within finite time. Usually, the surface can be defined as the hyperplane $s(x) = r^T x$ where the vector of coefficients is denoted by r. Therefor, for the second order model which is used in our case, r is defined as

$$r = \begin{bmatrix} 1 \\ c \end{bmatrix} \tag{6.12}$$

We find that the switching surface is a straight line with gradient c. The required condition of the surface being reached is given by

$$\dot{s}(x) < 0 \quad \text{for} \quad s(x) > 0 \tag{6.13}$$
$$\dot{s}(x) > 0 \quad \text{for} \quad s(x) < 0 \tag{6.14}$$

or in another formula is defined as

$$s(x)\dot{s}(x) < 0 \tag{6.15}$$

According to $s(x) = r^T x$ the derivation is defined as

$$\dot{s}(x) = r^T \dot{x} \tag{6.16}$$

An additional condition, which these conditions do not necessarily attain is that there is a requirement to reach the sliding surface within finite time [6, 211].

6.6.2 Controllers Design

Equation 6.7 that describes the heave model of SEMBIO can be written as state space model as:

$$\begin{aligned} \dot{x} &= \begin{bmatrix} 0 & 1 \\ 0 & -\frac{d}{m} \end{bmatrix} x + \begin{bmatrix} 0 \\ \frac{1}{m} \end{bmatrix} u \\ y &= \begin{bmatrix} 1 & 0 \end{bmatrix} x \end{aligned} \tag{6.17}$$

State variables of depth and heave velocity are denoted as $x_1 = z$, $x_2 = v$ respectively. Thus the linear switching surface $r = \begin{bmatrix} 1 \\ c \end{bmatrix}$ is defined as

$$s(x) = \begin{bmatrix} c & 1 \end{bmatrix} \begin{bmatrix} x_1 \\ x_2 \end{bmatrix}$$

$$= cx_1 + x_2 \tag{6.18}$$

then with the derivative

$$\dot{s}(x) = \begin{bmatrix} c & 1 \end{bmatrix} \begin{bmatrix} x_2 \\ -\frac{d}{m}x_2 + \frac{1}{m}u \end{bmatrix}$$

$$= \left(c - \frac{d}{m} \right) x_2 + \frac{1}{m}u \tag{6.19}$$

this leads to the selection of

$$c = \frac{d}{m} \tag{6.20}$$

The control is dependent on the switching surface $s(x)$, which in turn is dependent on the system state x. Furthermore, due to the the system parameters being not related to the derivative it can be controlled with the input u

$$\dot{s}(x) = \frac{1}{m}u \tag{6.21}$$

The existence condition for a sliding surface is achieved by selecting the input $u = -k \cdot \text{sgn}(s)$

$$s(x)\dot{s}(x) = s(x)\frac{-k}{m}\text{sgn}\left(s\left(x\right)\right) \tag{6.22}$$

$$= -\frac{k}{m}|\left(s\left(x\right)\right)| < 0 \tag{6.23}$$

As it can be shown also for small values of $|s(x)|$ that $\dot{s}(x)$ is changed between $\frac{k}{m}$ and $-\frac{k}{m}$, the switching surface is reached in finite time and the system is asymptotically stable for all $k > 0$.

The comparison of the responses of the PID (fine-tuned PID controller) and SMC controller to a multi-depth input obtained by simulations with MATLAB are illustrated in Figure 6.15. The simulated results are acceptable for both in this case, where the vehicle is not exposed to any noises or disturbances. Furthermore, the results show a slight preference for the SMC controller, as it did no overshoot in its response and stabilized the system at the desired depth (satisfying the goals),

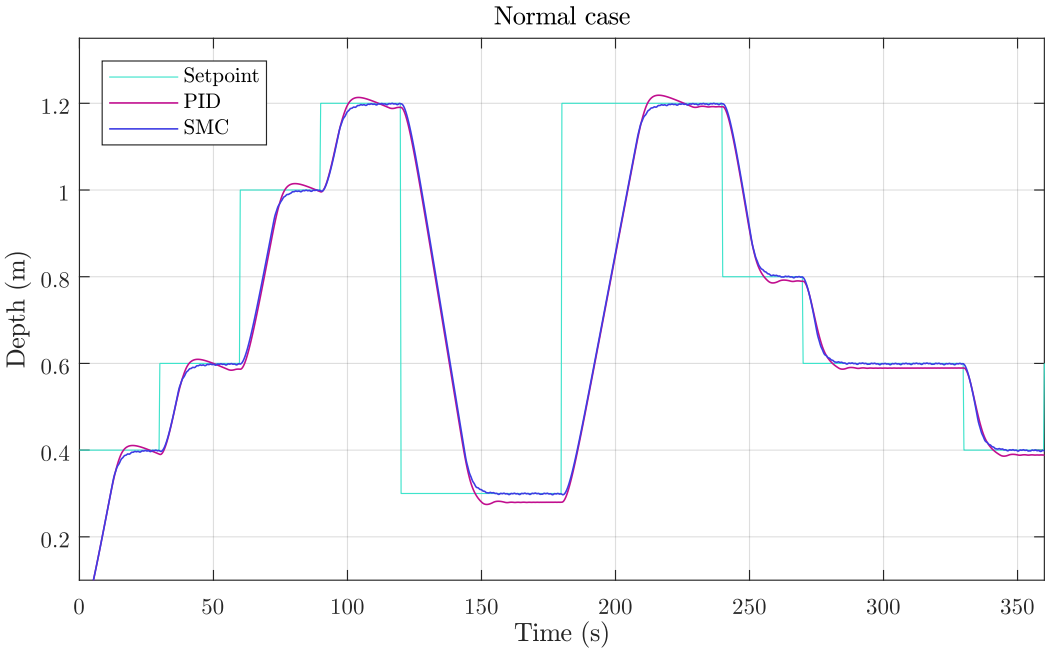

Figure 6.15 Comparison of PID and SMC without noises and disturbances

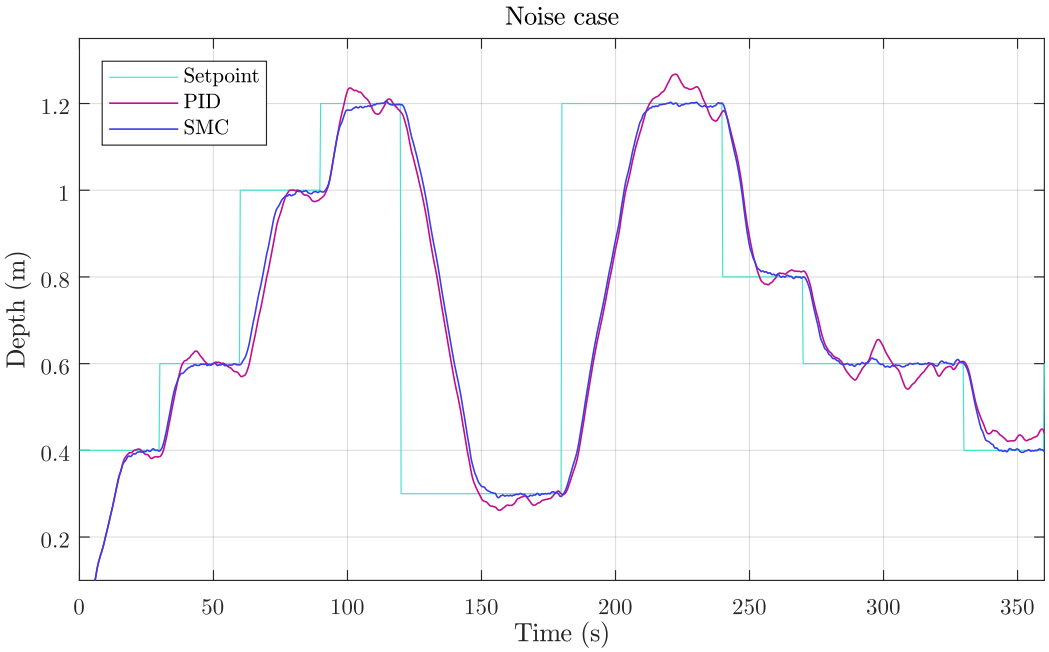

Figure 6.16 Comparison of PID and SMC with noises and disturbances

while the PID controller exhibited overshoot and did not stabilize the system at the desired depth within the small error bound because small regulating values have no effect. In addition, a steady stats error caused by the imbalanced buoyancy force can be observed in the PID controller results [75], meaning that the SMC controller is a better fit than the PID controller as shown in Figure 6.15.

To illustrate the robustness of the closed-loop system for both controllers, white noises and disturbances are added (see Figure 6.16). Clearly, the SMC controller, which is classed as robust and is suited to dealing with disturbances, is more robust than the PID controller in this case. The results illustrated that the PID controller has a big overshoot with unstable depth. According to the simulation results illustrated in Figure 6.15 and Figure 6.16, the SMC controller was selected to be used in the practical experiments of SEMBIO.

6.6.3 Experiments and Results

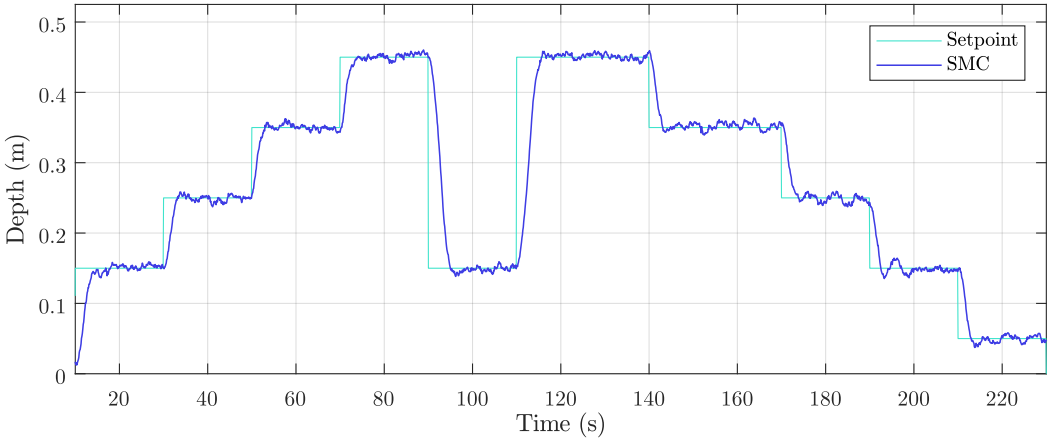

Figure 6.17 Experimental result showing the SMC controller's response to multi-depth input

The SMC controller is implemented on SEMBIO and the experiment conducted in the 0.8 m tank (rain barrel), however, the rain barrel was excluded from the identification system experiments because of the disturbance water current produced by the external flow water from the thruster nozzle, which had an impact on vehicle movement. But this issue was an incentive to test the robustness of the SMC controller. The buoyancy force was adjusted to be SEMBIO slightly positively buoyant.

Testing the SMC in the rain barrel produced positive results despite the disturbance water current. Figure 6.17 shows the results of the SMC controller, which show that the response to the multi-depth input is stable and more robust against the disturbance water. The oscillations are very small and have not impacted the

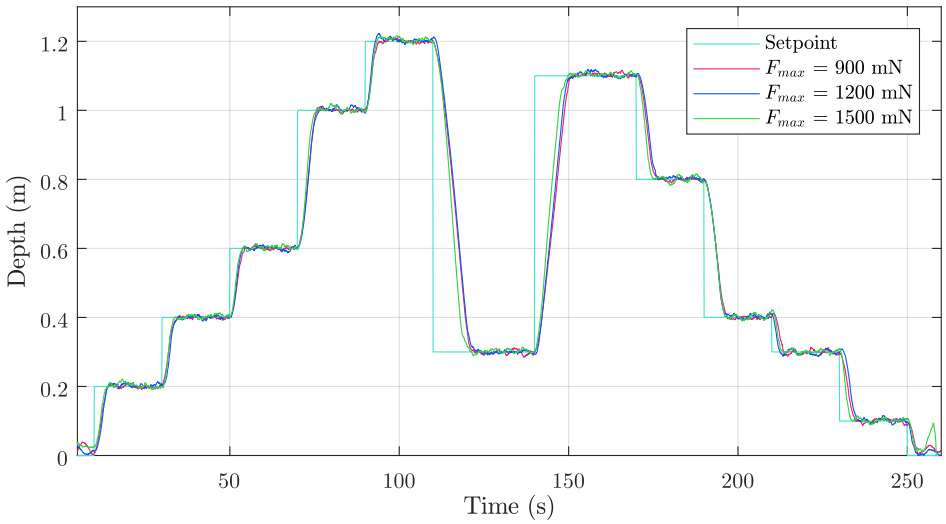

Figure 6.18 Experimental result of swimming pool showing the SMC controller response to multi-depth input

stability of the response. The vehicle reached the setpoint without or with a slight overshoot. In addition, SEMBIO reached the setpoint and remained at that level within a Root Mean Square (RMS) error of 0.491 cm and a maximal error of 1.43 cm. The mean absolute error was 0.394 cm, and the variance was 0.241 cm^2.

Further experiments were conducted in a swimming pool with 26 °C. SMC controllers with changing the maximum force $k = F_{max}$ was implemented on SEMBIO to illustrate and analyze the impact on the controller. Figure 6.18 illustrates the results of the swimming pool experiments. It can be seen that the performance of SMC controller is not affected by different values of the maximal force of the input, the response was with no overshoot. In addition, changing the maximal force of the input has only very light effects on the robustness of the controller.

6.7 Summary

The control strategies of PID and SMC were the main focus of the present chapter. Alongside these strategies, the movement equations for an AUV were outlined, and the creation of control systems for the movement of SEMBIO in the vertical plane was discussed. This chapter also presented the system identification and the derivation of a depth controller for SEMBIO, addressing the nonlinearities of the thrusters. Simulation of the controllers prior to their implementation in the prototype vehicle was made possible by the development of an extensive model in MATLAB. In addition, an evaluation of a control strategy of greater reliability in the form of an SMC was conducted as well. It was noted that, by comparison to the PID controller, performance was improved when the SMC was applied.

7 Solar and Energy Management System (SEMS)

The power module is one of the most important components of an AUV's electrical design [99]. The AUV's propulsion, sensors, and processing are usually powered by batteries. However, batteries cannot provide a great deal of energy, which influences the AUV's range and mission objectives, and, implicitly, its level of autonomy.

For small and micro AUVs, longer endurance is a key aim and a desirable feature for practical applications.

In Chapter 5, the design of the prototype micro AUV with full functionality was discussed, with particular emphasis on the design and methods for enhancing the streamlined body of SEMBIO. Such a streamlined body would not only minimize drag but also reduce the energy consumption.

Although the enhancement of energy sources and storage performance is beyond the scope of the present study, attention must be paid not only to the performance of the on-board energy source, but also to the amount of energy that is required overall. Thus, the present chapter investigates the energy management, from the perspective of electrical and power system design, as an alternative to the mechanical design perspective of Chapter 5 for reducing the amount of energy consumption by SEMBIO during operation. Parts of this chapter were published in [15, 90].

7.1 Introduction

Unlike tethered ROVs that receive their power from the mission vessel, untethered vehicles are restricted in their duration of operation by their on-board power system. For the majority of existing AUVs, the system is based on batteries that provide a limited amount of energy [242].

For autonomous vehicles intended for long-duration missions, the essential design components are the on-board energy source and storage [99]. Autonomous vehicles will be able to endure longer if the amount of on-board energy per unit weight is high, irrespective of additional factors.

The hardware or software structure of underwater robots was improved in a number of projects as a way of the extending mission duration, as in the case of the Solar-powered Autonomous Underwater Vehicle (SAUV) [55].

Weighing of 200 kg, SAUV II is equipped with a 2 m^2 solar panel on its top surface. The vehicle can operate at night, as it is powered by lithium ion batteries that are charged with solar energy during the day. On the downside, to be recharged, SAUV II has to float during the daytime, and climate conditions, such as the presence of clouds, determine the duration of the recharging. Even so, the mission duration is considerably expanded by daylight recharging. However, swarm formation is challenging because the SAUV II is so large.

A different measurement and simulation infrastructure project involved the measuring and recording of the electrical currents for all the components of a Slocum Glider [234]. A special measurement board enabled the Slocum Glider to formulate tradeoff decisions, such as between the length of a mission and the amount of energy consumption. Links were established between such tradeoffs and supply resources for probable future events.

The energy resource constitutes an important factor in the context of swarm robotics. The purpose of the swarm robotics strategy is to establish coordination among multiple robots that feature sensing, actuation, processing, and cognition abilities to cooperate on the achievement of a common task [110, 181, 182]. Therefore, AUVs are the main ingredient or the key component to creating underwater swarms. One study proposed a strategy for extending the mission duration based on load-balancing behavior for multi-AUVs with energy and fault tolerance being taken into account, as will be discussed later on in Chapter 8 [16, 17].

Energy management is so important in the case of AUVs because they are battery-powered, meaning that the energy amount available to them is limited, which has implications for the duration of operation and the types of missions that can be undertaken. To achieve optimal regulation of power usage, numerous tradeoffs between data processing, active sensing, navigation, and communication are necessary. Therefore, given that the management and control of AUV energy resources is of such significance, a system capable of measuring the power used by every AUV component and reducing energy consumption whenever possible to prolong the mission time has to be developed.

The features of the SEMBIO power system are discussed in the following section, with particular emphasis on the management of the overall on-board power based on an energy management system capable of monitoring all data regarding energy consumption and the mission time [15, 90]. Furthermore, to enable vehicle localization and retrieval in emergency situations, and to provide a backup for the primary energy system, a solar system was constructed [91].

7.2 Power System Design

Figure 7.1 presents the sample power system created for SEMBIO. The components of this system include a primary battery powering the electronic components, a power switch high-current relay for switching between the charger and the battery, a power switch linking the battery to the external charger via a tether, a magnetic switch, and a DC-DC converter for power conversion into 11.1V, 5V, and 3.3V, according to the requirements of the various electronic components.

Significant difficulties were posed by battery charging. To enable the batteries to be charged within the hull, a power switch board was designed. A pair of diodes and relays were included in the developed circuit board, which also had an extension cable linking it to the external connector to ensure the availability of a charger or an external source. Four of the eight pin positions on a circular connector positioned on SEMBIO's tail end were used by the charger, while the other pin positions facilitated transferring the data between the robot and a computer. Due to the ease of plugging in and charging the vehicle prior to a mission or work in the preparatory stage in extreme conditions, such a feature is useful for the work between missions.

The figure below presents SEMBIO's power resource comprising batteries and a solar panel.

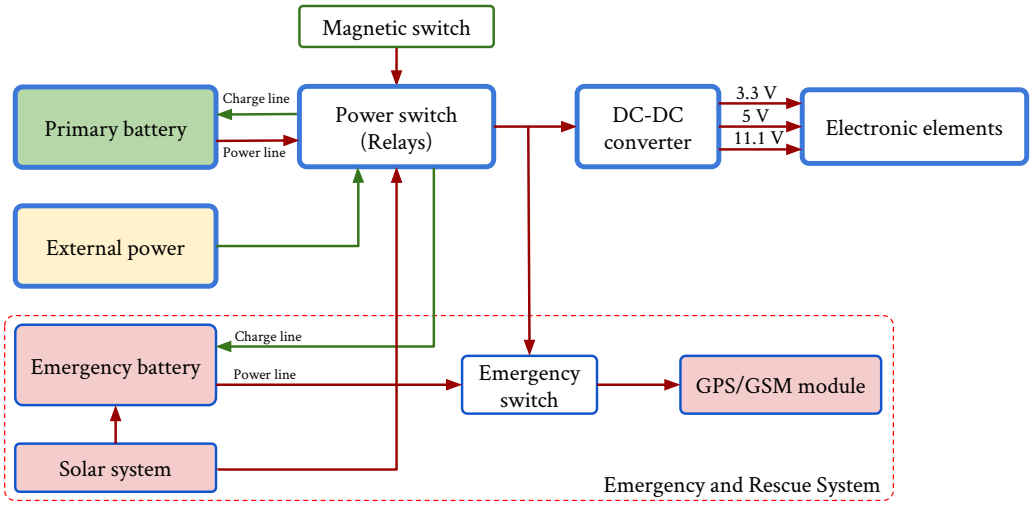

Figure 7.1 Schematic illustration of the power system

An emergency and rescue system was also incorporated in SEMBIO's power system (see Section 7.5)

7.2.1 SEMBIO's Batteries

SEMBIO was equipped with two batteries, namely, the primary battery and the emergency battery, which are used respectively in regular and emergency conditions. For the application, the emergency battery could be more significant if it could be charged during the mission.

The comparison of the wide range of existing types of batteries resulted in the decision to use Li-Po batteries due to such advantages as broad availability, ease of procurement, varying package dimensions and capacities, as well as cost-effectiveness. Li-Po cells represent Lithium-Ion (Li-Ion) cells containing the electrolyte in an absorbing material that affords them the property of pressure compensation. Compared to Li-Ion cells, these cells are believed to supply a better energy density. Batteries incorporating this technology have been recently launched on the market by Bluefin Technologies [233]. If they become successful in the field, they will likely become the most suitable batteries for AUVs.

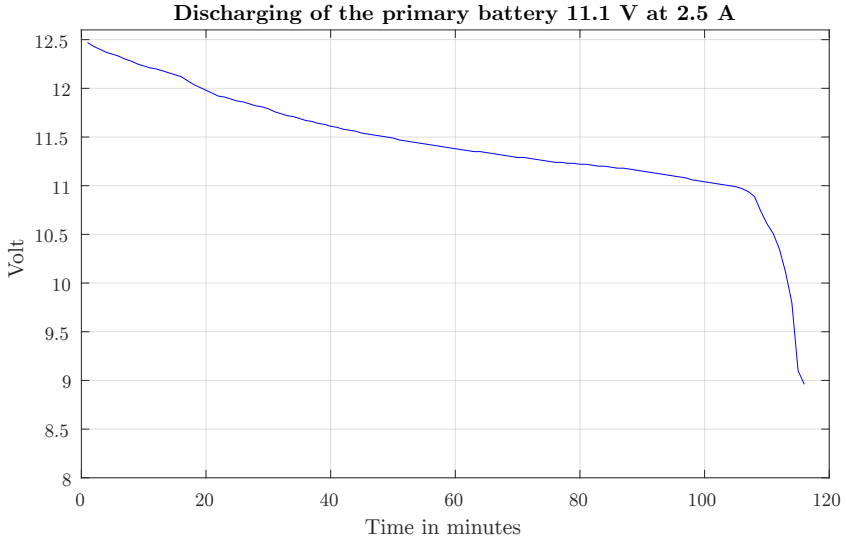

Figure 7.2 Discharge of the primary battery at a constant current of 2.5 A, a capacity of 5 Ah, 11.1 V, and a cut-off of 10.8 V at 20 ℃

The specific energy, expressed in (Wh/kg), constitutes the main requirement for batteries powering missions of long duration. The specific energy of the primary battery (comprising two batteries in parallel connection, with a capacity of 5 Ah, 11.1 V, and a weight of 360 g) and SEMBIO's emergency battery are indicated in Table 7.1. SEMBIO has an overall power capacity of around 120 Wh. The discharging processor of one of the primary batteries is shown in Figure 7.2 (5 Ah or 55.5 Wh). The discharging time is calculated by dividing the Ah or Wh rating by the current or power (the relationship between power and consumption is time, energy consumption Wh = power (W) × time (h)). For a discharging current of

2.5 A or 27.75 W, the real/practical discharging time was acceptable (1.86h = 112 minutes) and similar to the ideal/theoretical discharging time (2h = 120 minutes), with approximately 93% efficiency and a cut-off at 10.8 V. Hence, SEMBIO's power system had a discharging time of (12.7 Ah ÷ 2.5 A) × 0.93 = 4.72 h.

Battery type	Voltage	Capacity	Weight	Specific energy
Primary	11.1 V (3S)	10 Ah (111 Wh)	720 g	155 Wh/kg
Emergency	3.7 V (1S)	2.7 Ah (10 Wh)	50 g	185 Wh/kg

Table 7.1 The battery specification of SEMBIO's power system

7.2.2 Solar Energy

Solar energy produced by photovoltaic cells could represent one potential source of energy. Photovoltaic or solar cells generate electricity from solar energy and a range of such types of cells are available, differing according to the material and the manufacturing method. The majority of photovoltaic cells are made of silicon, which is an affordable and widely available material.

At present, compared to non-concentrator photovoltaic cells, multifunction concentrator photovoltaic cells are significantly more efficient (34.1% vs 43.5%).

SEMBIO should be equipped with a solar system to prolong mission duration and to enable vehicle retrieval in the event of a power system error or energy exhaustion.

Owing to the choice of location of the photovoltaic cells on the top surface of the hull, it was necessary to use types of cells demonstrating flexibility.

The flexible solar panel shown in Figure 7.3 was chosen for use in the solar power system [5], as it is capable of supplying around 6 V DC in direct sunlight at up to 1 W or about 160 mA. Although it presents cost efficiency, ease of maintenance, and ease of use, unfortunately this solar panel is not as efficient as other alternatives.

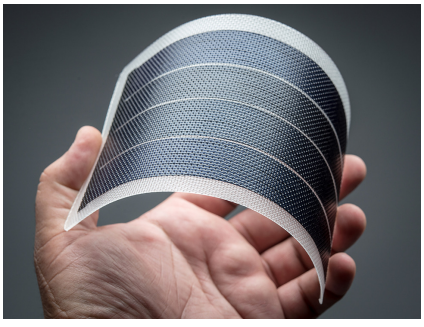

Figure 7.3 Solar cell demonstrating flexibility [5]

7.3 Solar and Energy Management System

This section focuses on an energy management system capable of overseeing the entire AUV operation, from the initial phases of the AUV component development to mission management, and AUV performance and power usage monitoring.

The Solar and Energy Management System (SEMS) was developed to ensure that the on-board energy source was used effectively by keeping track of the energy consumption of each component in the electrical system. The creation of SEMS was justified by the need to control AUV energy resources to reduce power usage and thus enhance battery life, thereby prolonging mission endurance or time. An additional objective of SEMS is to minimize the complexity of AUV operational procedures for researchers and other users to make it easier to use such vehicles for different missions.

7.3.1 SEMS Concept

Unlike the traditional approach of transmitting a mission to a robot, which involves the functions of every robot component throughout the mission, SEMS was designed to divide a mission into tasks and subtasks. The subtask is the lowest level of the mission structure that controls and measures the energy consumption of every component of the AUV. For example, the subtasks monitor the power usage of cameras, acoustic communication, pressure sensors, thrusters, and processing units. The major constituents of SEMS are SEMS-Communication, SEMS-Embedded-Board, SEMS-Solar, and SEMS-Mission-Planner.

The components of the SEMS hardware and software structure needed to control vehicle energy consumption are shown in Figure 7.4.

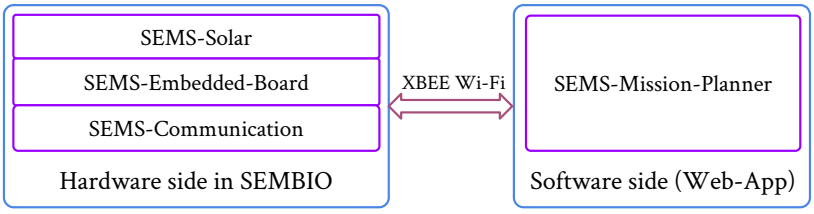

Figure 7.4 SEMS-Mission-Planner sends packet data for the whole mission (control code) to the robot. The data are processed by the robot's on-board system to initiate the mission and perform the tasks.

A Graphical User Interface (GUI) permits mission development over the Internet (Figure 7.5). The initial stage is the creation of a database comprising information about all of the robot components. In the second stage, the subtasks, tasks, and mis-

sion are planned. The SEMS-Mission-Planner underpinning these two stages subsequently produces the mission packet data (control code), which is transmitted to the robot, specifically to the SEMS-Embedded-Board, via SEMS-Communication. Measurement data are gathered and transmitted by the SEMS-Embedded-Board to the SEMS-Mission-Planner in the form of feedback so that the latter can inspect and plot them. The vehicle software is pre-installed for packet data interpretation and subsequently performs its task based on four modules or sub-function codes, which are respectively responsible for vehicle component management according to the control code, smart energy management, measurement of component energy consumption, and data collection and monitoring.

In the absence of SEMS, the robot would adhere to the normal controlling path, running every component in a traditional manner. By contrast, SEMS enables the use of the controlled energy-management pathway comprising two routes, namely, a route functioning on the basis of a control code discussed later on and a route based on smart management, which undertakes the data analysis and processing related to every component, identifies the environment of the operation, and uses the environmental data for energy management. For example, if the robot descends to a depth of 2 m, the depth is measured by smart management based on the pressure sensor feedback, and the device chooses to deactivate the GPS, since it is not functional underwater. In the present project, smart management was not implemented but was considered only as a concept. The other SEMS components are discussed next.

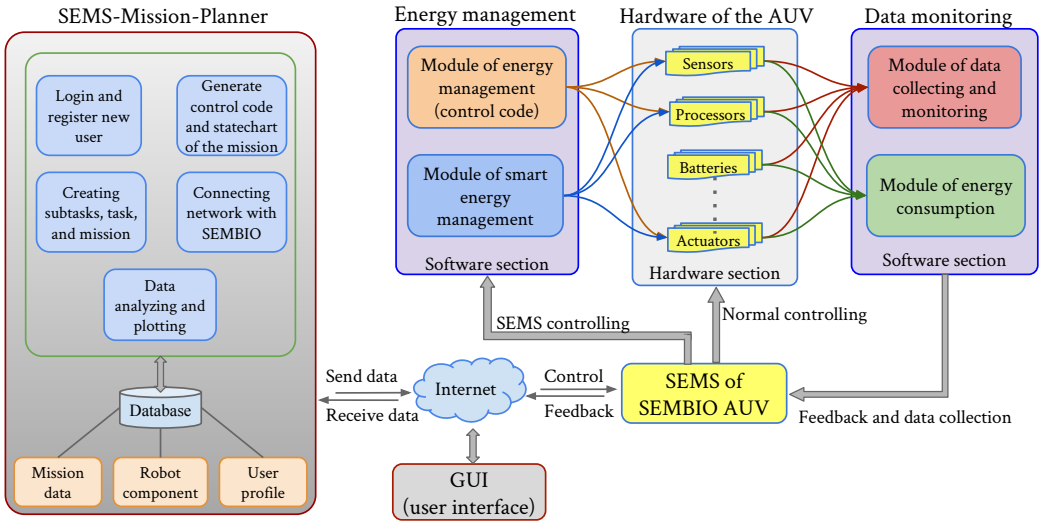

Figure 7.5 The concept of SEMS integrated into SEMBIO

SEMS was incorporated into SEMBIO's electrical design to measure and record the currents and the energy consumption from every robotic component throughout the

operation. SEMS employs a smart algorithm to improve energy efficiency and thus prolong mission duration.

7.3.2 SEMS-Communication

Online communication between a user and SEMBIO is mediated by SEMS-Communication through the Xbee module. This SEMS component has an AUV side and a server side, respectively representing the client and the host. To manage the communication between the two sides, the Xbee module was chosen (see Section 5.6.1). The mission codes from the PC are sent to the AUV by the SEMS-Communication, from which it obtains measurements of the component energy consumption during the operation.

7.3.3 SEMS-Embedded-Board

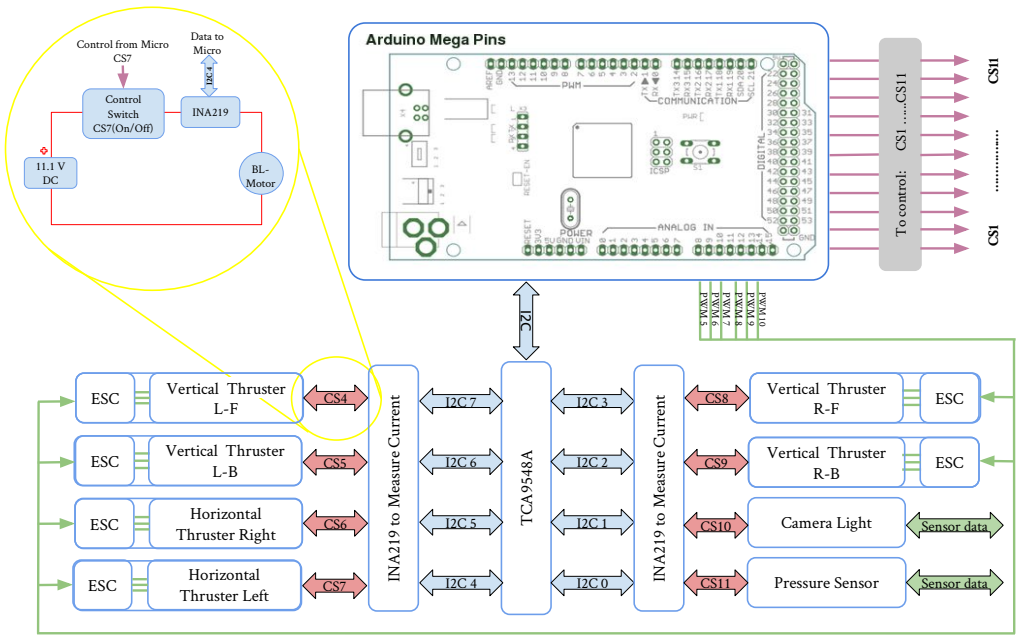

Figure 7.6 Illustration of the incorporation of the propulsion system and certain electrical system sensors with SEMS

The SEMS-Embedded-Board is installed in a shield of Arduino Mega to lead the energy management processes on-board the vehicle. After receiving a mission alongside a control code, it begins to manage every robot component. In idle mode, numerous components consume significant energy, and, therefore, a Solid State Relay (SSR) is used to perform the switching processes and prevent excessive energy

consumption. The incorporation of SEMS into the main electrical system is illustrated in Figure 7.6. The propulsion system receives the speed signal from processor 1 (Arduino Mega) through its connection to the PWM port. The incorporation of SEMS leads to the creation of a novel communication channel (via I2C) to allow the INA219 [102] current sensor to measure the thruster currents and transmit the data to the processor. Furthermore, a control signal (CS) from the processor allows the SSR to turn the thruster on or off. For example, PWM 10 indicates the speed of the vertical thruster at the right front side, the current of which is measured by the I2C 3 channel, and it is turned on or off by SSR on the basis of the CS8 issued by processor 1. This is applicable to every sensor, actuator, and processor in SEMBIO. An example is the pressure sensor: An I2C channel is used by the pressure sensor linked to the electrical system to transmit data to the processor, while a current measurement is performed by an other I2C channel (I2C0), and control signal CS11 issued by processor 1 enables the SSR to turn it on or off.

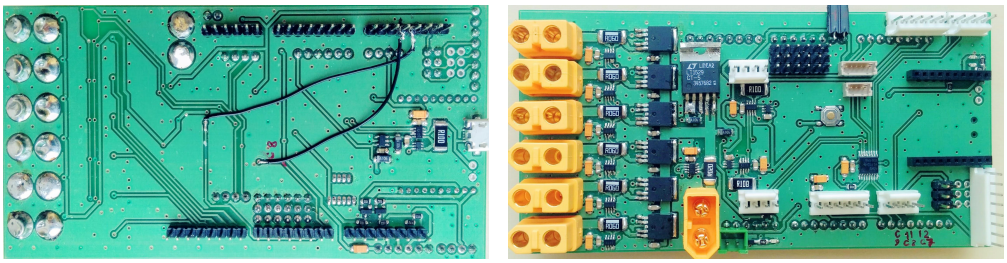

Figure 7.7 The original prototype of the SEMS-Embedded-Board (top and bottom are the right and left side, respectively)

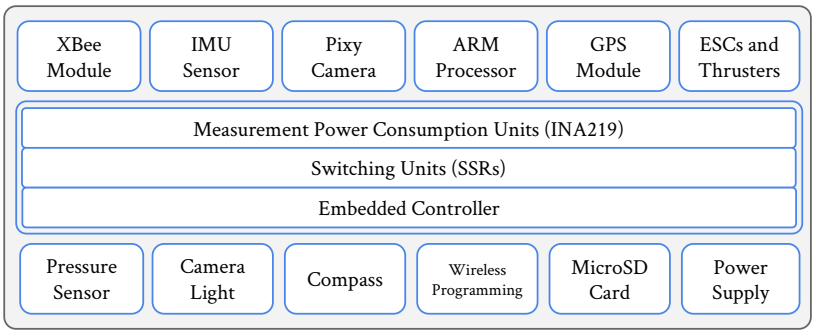

Figure 7.8 Diagram showing the functional components of the SEMS-Embedded-Board

The power consumption of some sensors or components is so low that a SSR is not necessary, as they turn on or off simply based on the control signals of the output pins of processor 1.

Figure 7.7 and Figure 7.8, respectively, illustrate the SEMS-Embedded-Board prototype and its components. The design of this board takes the form of a standard Arduino shield, representing a modular circuit board that extends the abilities of Arduino PCB when plugged above the latter. Both the manufacturing and mounting of the shield are usually straightforward (Figure 7.7).

The INA219 sensors enable the SEMS-Embedded-Board to measure the current of all components. By employing the I2C bus, the SEMS-Embedded-Board can run and manage numerous components, thereby attaining a high scalability. For example, the 54 pins of the Arduino Mega and the extensible I2C connection (using TCA9548A multiplexer) make it possible for processor 1 to run more than 36 components.

7.3.4 SEMS-Solar

On the surface, the SEMS-Solar component partly provides SEMBIO's main power system. As it is positively buoyant, SEMBIO can float to a certain location at the surface in the event of a malfunction of the primary power system or a depletion of its batteries. If exhausted, the emergency battery is charged by the solar panel at the surface, powering the rescue system (see Section 7.5) and enabling it to transmit its location information for recovery. This allows SEMBIO to be recovered more quickly than it would be possible otherwise.

7.3.5 SEMS-Mission-Planner

The development of a mission consisting of multiple tasks is achieved by the web-application platform SEMS-Mission-Planner by connecting it to the SEMS-Embedded-Board via SEMS-Communication.

Every real-time vehicle measurement is performed by the SEMS-Mission-Planner. In this project, a web application was created rather than a desktop application, since the former enables greater flexibility regarding the configuration of the communication between a central server/computer and the AUV, as well as simplifying the task allocation to the AUV and performance monitoring by facilitating accessibility from a local network or Internet connection. Furthermore, greater convenience is afforded by the existence of a central database comprising every component specification, existing task, mission, and history records of an AUV. Additionally, the option of account creation affords user independence in mission development.

The web application technologies Node.js, MongoDB, AngularJS, HTML, and CSS helped develop the SEMS-Mission-Planner in an open source environment, it was designed by T.Alamiri. Since the software design is beyond the scope of the present study, only a brief description will be given, with the full focus and the consideration being only on how to use it in SEMS.

As shown in Figure 7.9, the visual interface provided by this web application allows the user to develop the AUV components, including sensors, actuators, processors, and batteries through the allocation of their connection ports and power usage in both active and power saving mode. Moreover, on an interactive dashboard, the application provides real-time analytics associated with the energy usage of the actuators, sensors, and processors, as well as mission runtime and estimated amount of battery capacity left. A data log of AUV missions is also kept by the SEMS-Mission-Planner, and reports are issued to better understand how power is consumed and how the vehicle can be made to perform better.

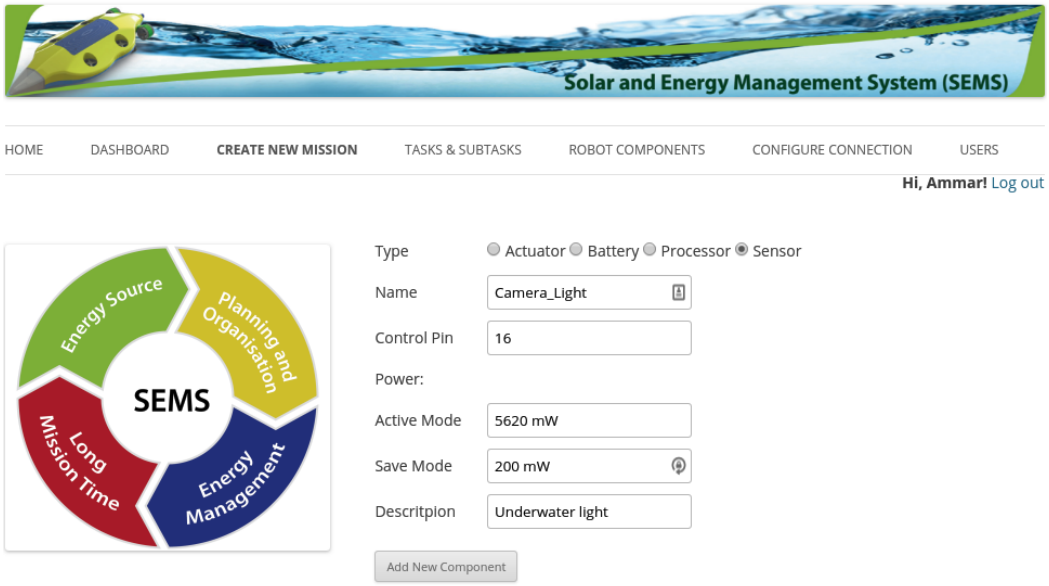

Figure 7.9 A screenshot of a computer-run SEMS-Mission-Planner, responsible for the mission development and transmission of the mission control code to the vehicle

In the traditional strategy of transmitting a mission to a robot, all components are run throughout the mission. By contrast, the SEMS-Mission-Planner consists of three layers preceding the components, including the mission, which is divided into tasks and in turn comprises different subtasks, as shown in Figure 7.10. The subtasks are linked to the robot components, enabling or disabling them according to the requirements and the type of the tasks and mission. As a result of this structure, the robot components do not all run at the same time, but only when they are activated, thus reducing energy consumption. Furthermore, the tasks and subtasks are prioritized by the SEMS-Mission-Planner. For example, apart from the sensors necessary for the robot to return to its homebase, all other sensors are switched off when the amount of energy left is less than 10%.

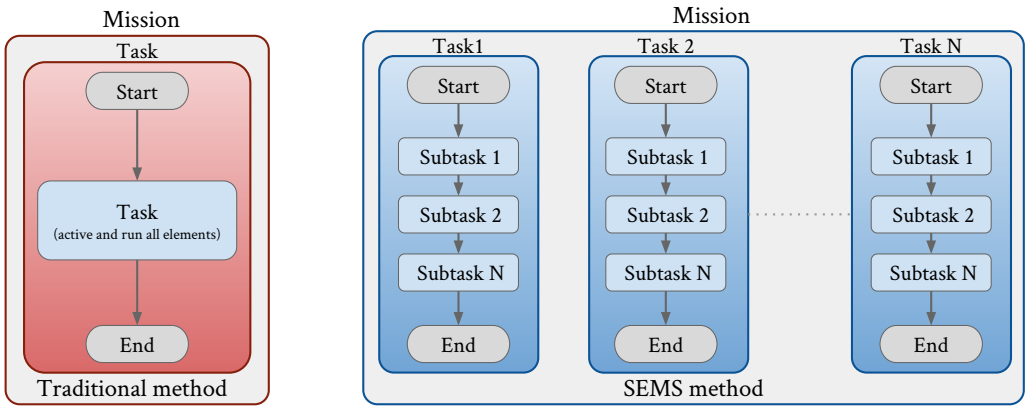

Figure 7.10 The different structures of a mission's execution

All robot components should have a profile characterizing them to supply relevant information (Figure 7.9). Prior to the mission design, it was determined that the profile of every component should specify is component type and name, component control pin linking the component to the SEMS-Embedded-Board, and its average energy consumption. Subsequently, component lists should be divided into groups (e.g., list of sensors). Once these matters are settled, the mission development can begin, entailing the formulation of a minimum of one task, which in turn necessitates the formulation of a minimum of one subtask. The subtasks are primarily centered on the management of the thrusters, batteries, processor units, and sensors of the robot. Furthermore, a control code specifying the components included in the subtask has to be created as part of subtask development.

The Control Code

Components are activated in accordance with the SEMS control code, a binary value that is transmitted to the robot. The code is produced to frame the mission and is transmitted to the SEMS-Embedded-Board to instruct the robot how to tackle that mission. There are many principles that can underpin a mission, task, and subtask. One interesting principle is the I2C port, which is extendable and highly efficient, although it requires an identification address to be allocated to every component and presents a high level of complexity (software issues). Another relevant principle is the multiplexer, which requires a significant amount of hardware. A more straightforward strategy for the evaluation of SEMS, which was employed in this project, is the use of the existing Arduino Mega pins.

Of the 54 pins of the SEMS-Embedded-Board, 36 are free. Therefore, in this project, 32 pins (4 bytes or 2 words) were chosen to be linked to the 32 components of the robot, therefore resulting in 32 bits available to deal with the components.

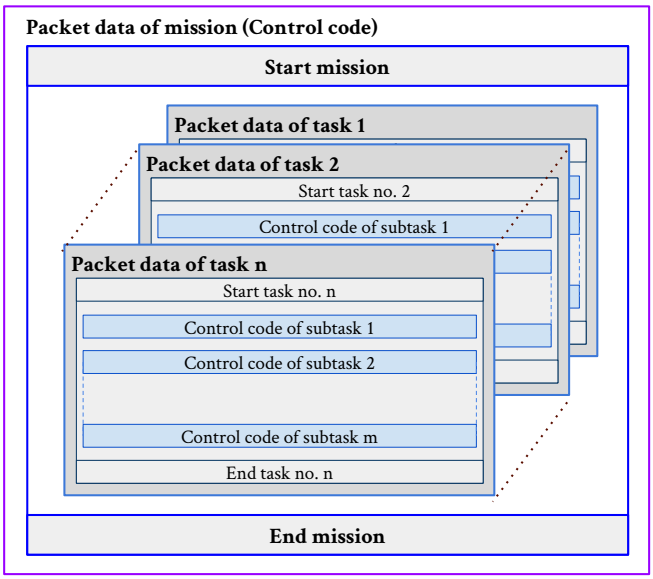

Figure 7.11 The configuration of the mission control code

The configuration of the mission control code is shown in Figure 7.11. The SEMS-Mission-Planner can devise a mission by generating tasks and subtasks, thereby making it possible to auto-generate the mission control codes while simultaneously allocating start- and end-points for each subtask to enable a transmission between subtasks alongside the creation of a task/mission flowchart. The initial control code produced prior to the mission formulation is indicated in the first row of Table 7.2, while the control code associated with a particular subtask is indicated in the second row, with 1 denoting that the component linked to the pin in question is active and 0 denoting that the component is inactive.

Initial control code	0000 0000 0000 0000 0000 0000 0000 0000
Control code for a certain subtask	0100 1001 1000 0000 0000 0001 1000 0101

Table 7.2 The size of the control code for every subtask

7.4 Measurement of Component Power Consumption

The overall energy requirement or consumption of a mission can be approximated through measuring the amount of energy consumed by every component. SEMS evaluation can also be conducted based on the development of a database of com-

ponent energy consumption. SEMS tries to use a high range of energy efficiency since certain components (e.g., thrusters) possess this range.

SEMS itself is used for the measurement of power, beginning by connecting a certain component to the equivalent pin on the SEMS-Embedded-Board which is plugged into Arduino Mega, and possesses 32 addressed pins for SEMS. Subsequently, SEMS sends 0 to all components to switch them off before employing the INA219 current sensor to measure their current consumption. An independent current sensor is included in the input of certain pins. Many current sensors are incorporated in the SEMS-Embedded-Board for linking to components such as cameras and RPi, the current usage of which is prioritized by SEMS.

To keep measuring probes and errors down to a minimum, the measurement of all components is performed for 10 minutes, during which 10 measurements of the power (current×volt) are conducted per second, with a calculation of the average time once the 10 minutes are up. Furthermore, to ensure that the measurement of energy consumption is reliable, the procedure is carried out five times.

7.4.1 Results of the Processor Unit Measurement

Arduino Mega and RPi are the two processor units of SEMBIO, as discussed in Section 5.6.3. Owing to differences in voltage sources, power consumption rather than current consumption is addressed from now on. Power consumption in Arduino was conducted in idle mode, normal loading mode, and high loading mode. In the normal loading mode, a straightforward code was uploaded to run and blink an LED. The high loading mode involved the activation of a greater number of peripherals, with data being transmitted from the Arduino to a computer at a BAUD rate of 9,600 Hz/UART. The transfer and decoding of an XML file on Arduino were performed as well.

The power consumption of Arduino Mega is presented in Figure 7.12. Minor differences exist between idle mode and normal mode. The former can be disregarded, as it is similar to the normal mode. Thus, to eliminate the energy consumption in idle mode, Arduino Mega must be linked to a pin with an SSR for activating or deactivating it. In this project, SEMBIO's Arduino Mega could be used by SEMS as well, although, to remain active throughout the empirical work, SEMS was also implemented on a second Arduino Mega.

The power consumption of RPi2 is shown in Figure 7.13. The measurement of RPi's power was repeated five times in two distinct settings, although both settings involved RPi with an initial CPU clock and pre-installed Ubuntu 14.04 throughout the measurements. The second setting involved using the RPi camera to turn on the video watching with 1920x1080 resolution. Since it was relatively high, the idle mode was disregarded and a SSR was introduced.

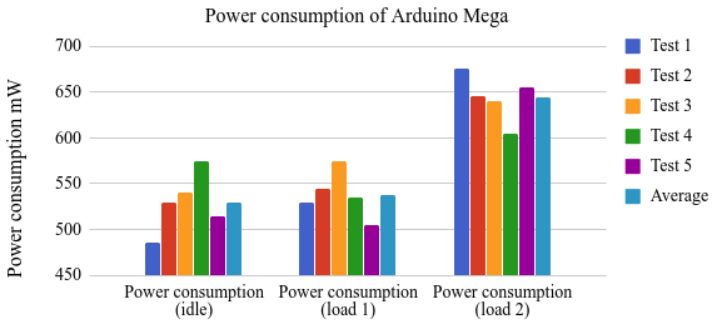

Figure 7.12 Measurement of the power consumption of Arduino Mega in three settings

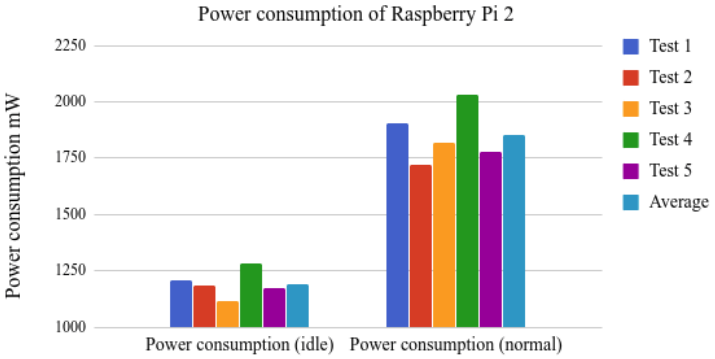

Figure 7.13 Measurement of the power consumption of RPi2 in two settings

7.4.2 Results of the Sensors Measurement

Serving as the vision sensor, Pixy represents SEMBIO's second camera (see Section 5.6.5). The measurement of Pixy was conducted in three distinct settings. The first setting involved measuring Pixy's power consumption in idle mode (i.e., no image transmission), and the second setting measured Pixy's power consumption during transmission of images with a resolution of 640x400 at 50 Hz. The third setting measured Pixy's power consumption during the transmission of images with a resolution of 1280x800. Figure 7.14 presents the results.

The navigation system was based on the GPS module discussed in Section 5.6.2. The results obtained in both idle mode and active mode are shown in Figure 7.15. In active mode, signal data reached the GPS at a 10Hz frequency.

The other sensors and components were measured in the same way. Table 7.3 provides the results obtained.

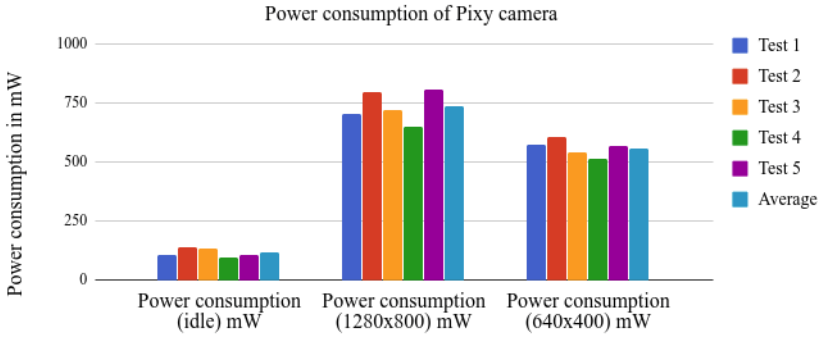

Figure 7.14 Measurement of the power consumption of the Pixy camera

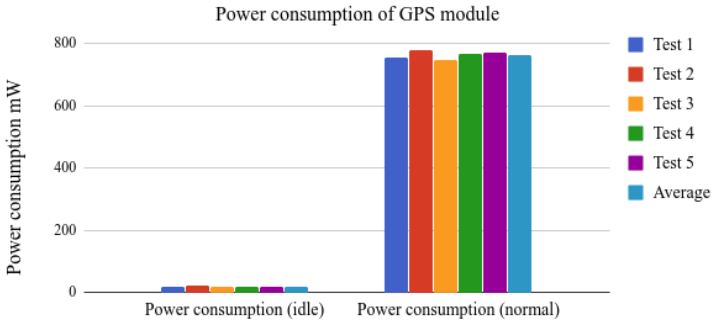

Figure 7.15 Measurement of the power consumption of the GPS module

7.4.3 Results of the Thruster Measurement

Thruster unit power consumption measurement was undertaken in Chapter 4. The following section focuses on how and where consumption occurred and how the measurement results could be employed to improve performance while minimizing consumption.

	Idle mode (W)	Active Mode (W)
Compass kit	-	0.4
Camera light	0.2	5.62
Pressure sensor	-	0.01
PXFmini	0.13	0.41
XBee	0.27	0.97

Table 7.3 The amount of power used by the sensors and other components

As in most other AUVs, no other SEMBIO component consumes more power than the thrusters. An ESC was used to drive each thruster and uses power itself as well. An 11.1 V Li-Po battery was used to perform the measurement. Figure 7.16 shows how thrust and power consumption are correlated. The use of SEMS is supported by how successfully the power consumption of the thrusters was managed. Based on the analysis of the results provided in Section 4.5.3 and Figure 7.16, it can be summarized that the efficiency zone of the thrusters allows them to thrust the vehicle with minimal power consumption, while in the saturation zone the current increases without significantly increasing the produced force. The two zones are of great importance for SEMS to determine the optimal approach to vehicle thrusting with a high energy efficiency and to avoid the saturation zone. The saturation zone underwent an extension from 73% to 100% in both directions and, therefore, its use was not recommended. The second zone underwent an extension from 20% to 60%, exhibiting an efficiency of over 80% in the forward direction, the same as the zone in the backward direction, which extended from 20% to 48%. Owing to these high efficiency zones, each thruster was capable of a thrust of 0.25-2.3 N.

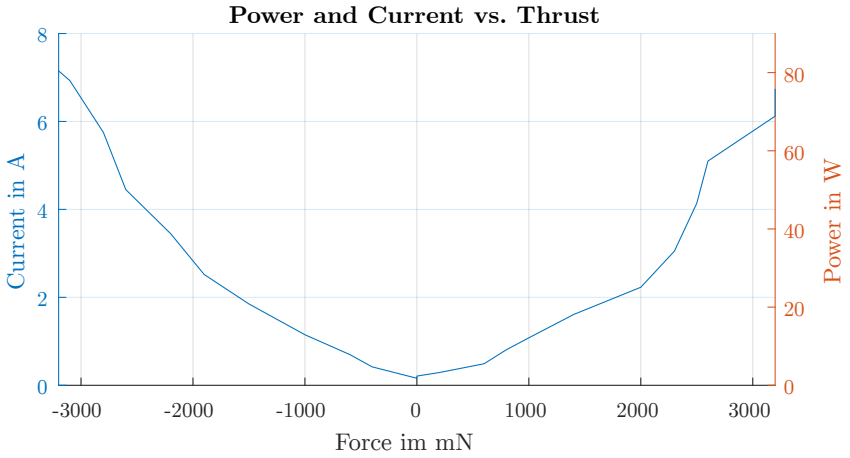

Figure 7.16 Diagram showing how the required power and the produced thrust are correlated

Thus, the power consumption of the thrusters in the efficiency zone and in the saturation zone were respectively 2-50 W and up to 78 W.

In the efficiency zone, SEMBIO's two forward direction thrusters produced a combined thrust of up to 4.6 N, giving the vehicle a speed of around 0.8 m/s (5.3 N and around 58 W produced a speed of 1 m/s). Therefore, a speed of 0.5 m/s requiring around 28 W was established for the forward direction.

The efficiency zone was used more actively for the four thrusters for diving. A thrust of 2 N was necessary for adequate diving (see Section 5.3.5), with 0.5 N produced by each thruster necessitating around 4.8 W, which totaled 18 W for all four thrusters in the diving direction.

Both the thrusters and the ESC driving the thrusters exhibited a "no-load current", meaning that each thruster used around 1.7 W even when they were not rotating. SEMS can address this issue by giving a stop signal to SSR instead of ESC to deactivate the thrusters and their drivers.

7.5 Emergency and Rescue System

Emergency call, or eCall, is a type of emergency and rescue system [151] based on a straightforward mechanism. For example, in the event of a car accident, the system activates an emergency call that transmits information to a rescue center about time, location, and direction of travel, as well as the number of people in the car, if the vehicle allows it. Despite the fact that more than half of the AUVs are lost due to power deficiency, not many AUVs are equipped with an emergency system [136]. Locating a large AUV on the open sea with numerous drifts and waves is challenging and time-consuming, much less however for a small or micro AUV.

Similar to eCall, is the Emergency and Rescue System (ERS) incorporated into SEMBIO. The ERS can support long-range communication based on Global System for Mobile (GSM) communication (Figure 7.1). Upon ERS activation, the emergency devices necessary for the transmission of location information to aid the AUV search and retrieval are sufficiently powered by the emergency battery. The system is beneficial both financially, as a loss of an AUV and the data it gathered could have significant implications, as well as scientifically, as it affords a simple and cost-effective system to link the micro AUV to the homebase.

Any error or malfunction that could cause an energy depletion or a loss of main power can trigger the ERS, with emergency electronic devices comprising primarily GPS and GSM being powered by an emergency battery [3].

7.6 Experiments and Results

To evaluate the performance of SEMS-Solar, ERS, and SEMS, experiments were conducted and are illustrated in this section.

7.6.1 Experiments and Results of SEMS-Solar

To conduct the solar cell experiments, the SEMBIO cover was used to create a SEMS-Solar prototype. To ensure its impermeability and for protection against environmental factors, a transparent epoxy was used to coat the flexible solar panel.

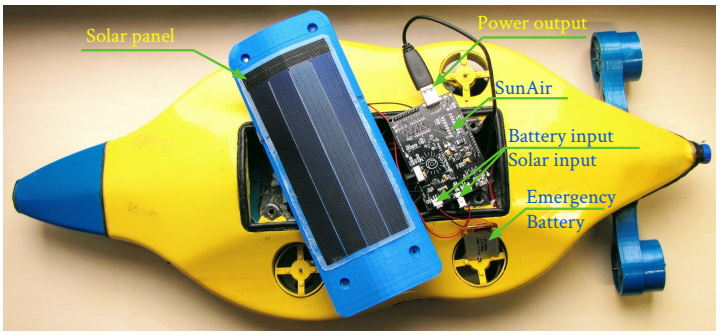

Figure 7.17 The setup for the experiment with SEMS-solar

For integration into the energy system, special development of the solar cells was necessary. To enable the ERS emergency battery and SEMBIO's primary battery to be charged, the energy from the solar cells was extracted with the SunAir-Plus [199] board. The solar charging control of the SunAir-Plus board is responsible for charging the batteries, along with a voltage booster for boosting the default 3.7-4.2 V output of the emergency battery to 5 V. INA219 current sensors were employed to measure the SEMS-Solar's current and voltage. The data from the solar logging platform was generated and stored on an SD card. The experimental configuration of SEMS-Solar is shown in Figure 7.17.

Three different climatic conditions were measured to ensure authentic results. The measurement was started at eight o'clock in the morning until seven o'clock in the evening, and an SD card was used to store the current measurement every minute through the Arduino. When the measurement was finalized, the processing of the data was conducted.

The correlation between the generated current or power and direct solar irradiation is indicated by the dashed red line in Figure 7.18. The accuracy and reliability of the results were limited because the measurement was conducted at a time with cloudy and fluctuating climatic conditions. The measurement conducted on a sunny and warm summer day (18 ℃) is indicated by the dashed green line in Figure 7.18. By comparison to the earlier figure, the curve that was produced provided favorable results, yet the desired power of 1 W was not achieved. At the ideal time, around 380 mW were generated at 6 V.

The measurement undertaken in ideal climatic conditions is indicated by the dashed blue line in Figure 7.18. The result fell short of the desired 1 W, reaching only about 650 mW for a short period of time. Therefore, owing to the climatic conditions and poorly effective solar cells, the SEMS-solar results were suboptimal and SEMBIO's primary battery was not charged. Furthermore, charging the emergency battery to 400 mAh was challenging for SEMS-Solar as well.

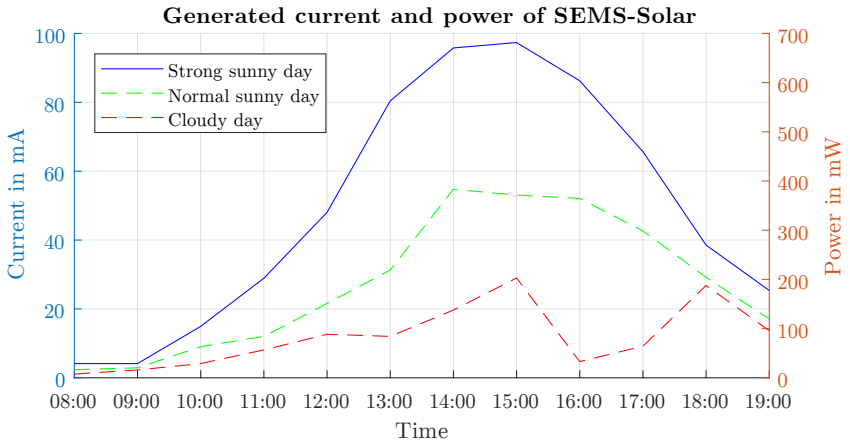

Figure 7.18 Solar power fluctuation in various sunny days

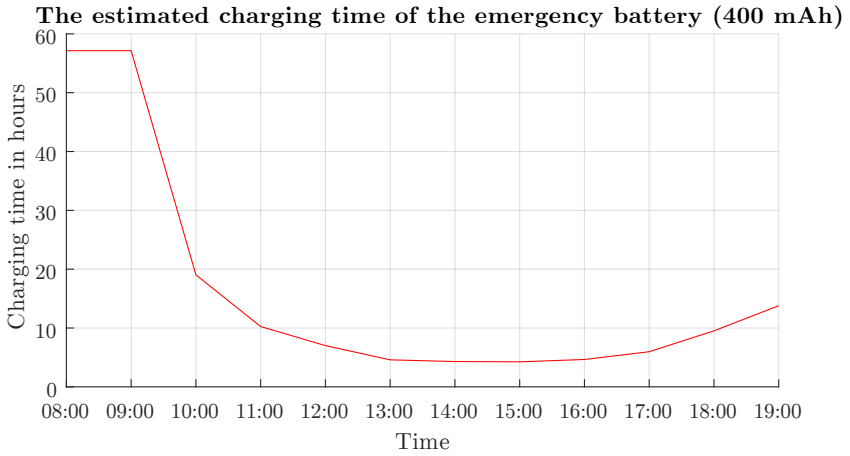

Figure 7.19 The approximate duration for charging the emergency battery

As indicated in Figure 7.19, based on the premise that the ideal results were achieved, the estimated charging time of the emergency battery was around four hours between one and four o'clock in the afternoon, meaning that there was a possibility of complete charging of the battery in that period.

7.6.2 Experiments and Results of ERS

In the event of loss or error of SEMBIO's power system, SEMBIO's ERS sent an emergency message to the homebase for vehicle retrieval. To enable communication with the satellites and GSM stations, the GSM and GPS antennas of ERS were positioned on SEMBIO's highest point, namely, its cover.

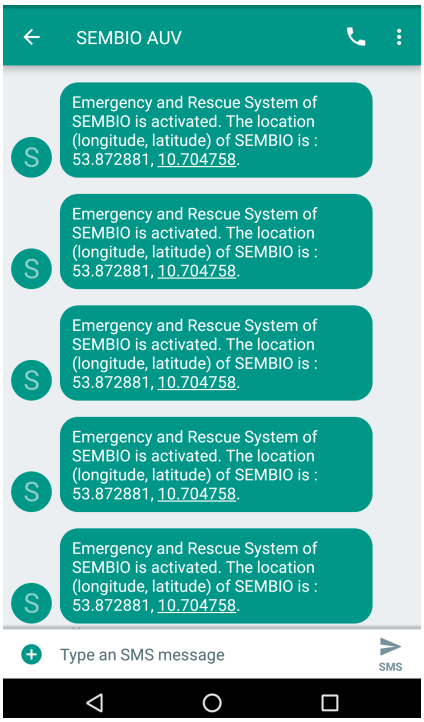

Figure 7.20 Vehicle retrieval based on SEMBIO's location found through a mobile phone message (53.872881, 10.704758)

The ERS activation required the occurrence of an error in the main power system. To this end, the procedure implemented involved the preparation of SEMBIO for a mission in the Wakenitz river at a depth of 0.5 m. SEMBIO was put into the river and moved forward slowly and without a set direction, being attached with a soft wire to prevent its loss and restore it to the starting point. SEMBIO could no longer be seen after it submerged and moved underwater for ten minutes. Consequently, Arduino's internal timer signal was issued, and a switch relay was activated to turn off SEMBIO's main power, leading to the activation of the emergency switch. This triggered ERS and, since it was positively buoyant, SEMBIO floated to the surface. The emergency battery was charged prior to commencing the mission, and thus possessed sufficient energy to support ERS. At the surface, a connection of GPS and the GSM module initiated the signal search. It took arou nd 30 sec (startup time) to process the connection and to detect the location.

The first emergency message (see Figure 7.20) providing information about the vehicle's location was delivered to a mobile phone a couple of minutes later due to the startup time and connection issues.

Although ERS is capable of transmitting one message per minute, but to increase the lifespan of the emergency battery, it was set to transmit messages every five or ten minutes to ensure that ERS stayed active until the vehicle retrieval was

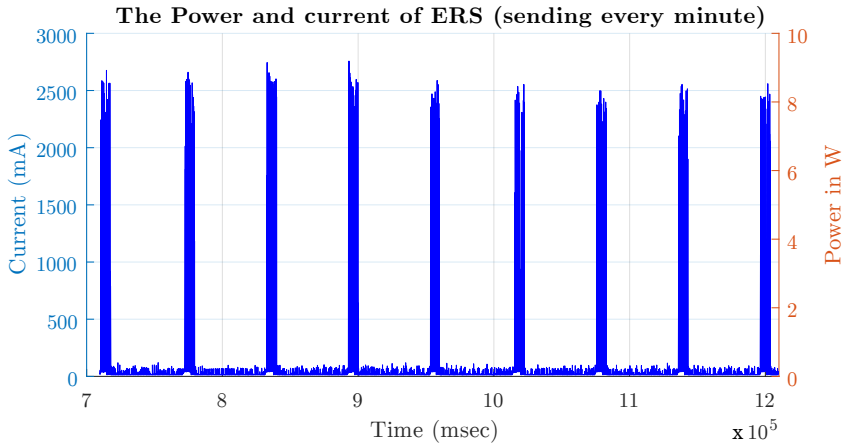

Figure 7.21 The power and current consumed by ERS to send a message per minute

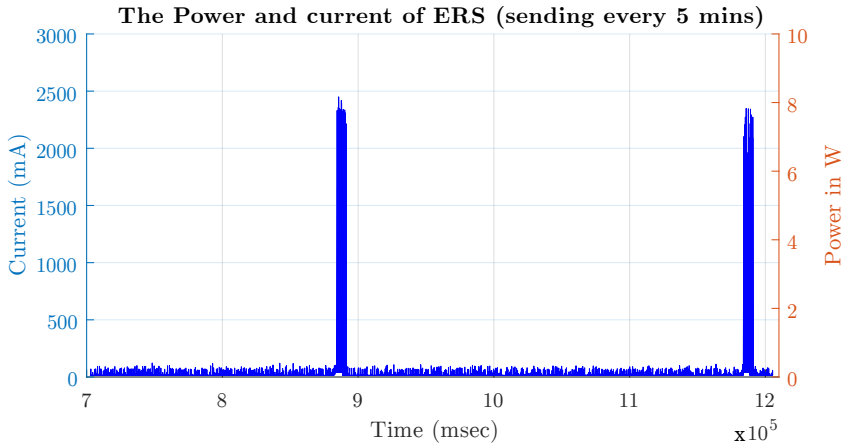

Figure 7.22 The power and current consumed by ERS to send a message every five minutes

completed. When ERS is active, its components use around 20-25 mA and when it transmits or receives data, the energy consumption can be up to 200 mA, with minor peaks of up to 2.5 A. Figure 7.21 and Figure 7.22 show the power and current consumed by ERS to send an emergency message per minute and every five minutes, respectively.

If ERS transmits a message every five minutes, it can be kept running by the emergency battery (400 mAh, 1480 mWh) for approximately 34 hours (Figure 7.23), with an energy consumption of around 48 mWh.

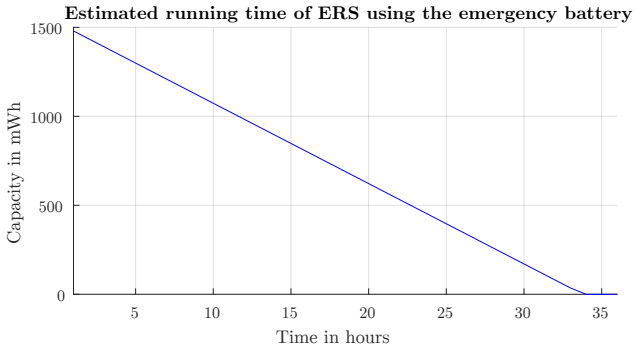

Figure 7.23 The estimated amount of ERS running time supported by the emergency battery

7.6.3 Experiments and Results of SEMS

The energy savings that can be achieved with SEMS are discussed in the following section. A mission can be planned better if the values of the vehicle's components and the amount of energy consumption are known beforehand.

In this project, SEMS was assessed by conducting a mission with SEMS and the same mission without SEMS and subsequently comparing the results.

Establishment of a Monitoring Mission

The device user determines the manner in which a mission is developed. For the purposes of this evaluation, a "monitoring mission" was undertaken to monitor and investigate a particular area underwater, as the name implies. As can be seen in the mission stages presented in Figure 7.24, which includes only one task, the monitor task comprised four subtasks: guiding the vehicle from the homebase to the established task coordinates based on GPS (navigation subtask), diving the vehicle to a given depth using pressure sensors (depth subtask), underwater exploration based on SEMBIO's vision (monitor subtask), and guiding the vehicle back to homebase (return home subtask).

Subtask creation involves the selection of components from different categories or lists (i.e., thrusters, sensors, batteries, processors) for use in the subtask and for generating a subtask code with the SEMS-Mission-Planner (Figure 7.25). Thus, the horizontal thrusters, Arduino Mega, GPS, and compass were chosen for the navigation subtasks and to guide the vehicle back to the homebase, and the pressure sensor, Arduino Mega, and vertical thrusters were chosen for the depth subtask. RPi2 and its camera, camera light, and horizontal thrusters alongside the components selected for the previous subtask were chosen for the monitor subtask. As shown in Figure 7.26, a subtask requires the components to form the basis for its emergence, just as a task requires subtasks to take form. Furthermore, task creation and mis-

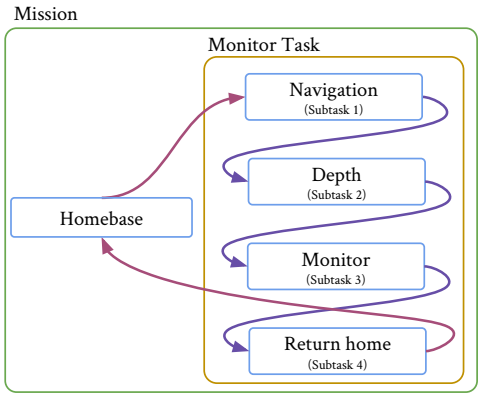

Figure 7.24 The stages included in the monitoring mission

sion planning require the specification of the start- and end-point of every subtask, in a formation that must be preprogrammed and saved in the SEMS-Embedded-Board. For the present mission, the start- and end-points of the GPS coordinates (longitude, latitude) of SEMBIO were established to be (53.853363, 10.702976) and (53.854054, 10.704120), respectively representing P0(0,0) and P1(1,1). After the diving from the surface (start-point of the depth = D0) to a depth of 50 cm (end-point of the depth = D1), then SEMBIO began monitoring the underwater environment for a quarter of an hour. This subtask was connected to time, rather than to a sensor. The creation of the monitor task comprising the preceding four subtasks was the last stage. The mission was created in the same manner as the task. Tasks are selected in accordance with the objectives of the monitoring mission to ensure that those objectives are achieved. For our experiments, a single task was included in the monitoring mission (Figure 7.27).

NAME	CONTROL CODE	DELETE
Navigation	00000000000000000000000000000000000000000011000000000011111	Delete
Depth_Control	00000000000000000000000000000000000000000100000000111100111	Delete
Monitor	00000000000000000000000000000000000000000100100001011111111	Delete
Return_Home	00000000000000000000000000000000000000000100110000000000011101	Delete

Figure 7.25 Screenshot of the generated control code after all subtasks were created

Through this procedure, the whole control code was generated and transmitted to the SEMS-Embedded-Board (Table 7.4).

The generated code is interpreted by the SEMS-Embedded-Board based on a complete software code, with 1 and 0 respectively determining is a component is active (switch on) or deactivated (switched off) for every subtask. Furthermore, more

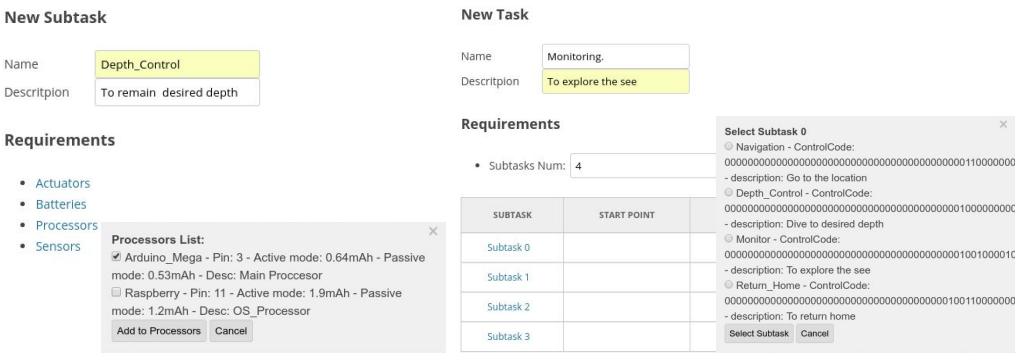

Figure 7.26 Screenshot of subtask and task with the components and subtasks used to create them, respectively

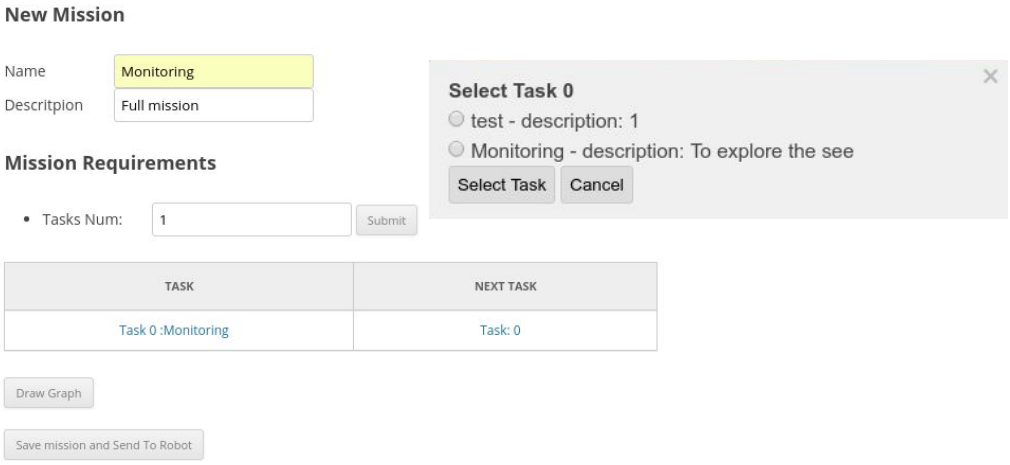

Figure 7.27 Screenshot of the monitoring mission developed on the basis of a single task

than one point is associated with the software preprogrammed data of the sensors (e.g., GPS).

This mission has only one priority case, namely, in the event of battery capacity reduction to less than 20%, the mission has to deactivate the vehicle, terminate every task and subtask, and guide the vehicle back to the homebase.

Theoretical Evaluation of the Monitoring Mission

The monitoring mission was evaluated theoretically for two reasons: (1) to support and compare it with the real evaluation of SEMS. The theoretical evaluations for each mission give us a complete overview of the energy consumption of a mission;

1;1;00000000000000011000000000011111;0;1;2;1 1;2;00000000000001000000000111100111;0:1;3;1 1;3;00000000000001001000010111111111;0:1;4;1 1;4;11001111100001101110001110111111;1:0;1;1 1;1;00000000000100110000000000011101;1:0;1;1
Interpretation of mission control array: the initial field for the first task = 1; the second field for the first subtask specifies the subtask name = 1; thus 1 is the navigation subtask, 2 is the depth control subtask, etc.. the control code of the navigation subtask = 00000000000000011000000000011111; with the status of the component on the AUV board being indicated by the value of each bit (i.e. 1 = on, 0 = off). the next two fields are the start and end point of the first subtask respectively = 0;1; the next field is the next subtask (the second subtask) = 2; the last field is the next task = 1;

Table 7.4 The control code of the monitoring mission

(2) to validate that the theoretical evaluation can be an alternative to the real evaluation, which faced challenges during the evaluation procedures. This theoretical evaluation involved a comparison between the overall energy consumption value of the components employed in every subtask with and without SEMS. For every subtask, the working premise was that the efficiency zone of the thruster remained constant both with and without SEMS. Therefore, the calculation of the navigation subtask's energy consumption (power (W) × Time (hours)) in the absence of SEMS was undertaken as follows.

The energy consumption of the navigation subtask was determined by summing up the power used by the Arduino Mega, GPS, compass, and horizontal thrusters, and the energy consumed by the vertical thrusters, sensors, and processors in idle mode.

Thus, the total power of the navigation subtask was 0.65 + 0.76 + 0.4 + 28 + (1.7x4 + 0.79 + 1.19) = 38.59 W. For one hour, the energy consumption was 38.59 Wh.

With SEMS, the same procedure was applied to calculate the overall energy consumption of the navigation subtask, which was the sum of the energy consumed by the Arduino Mega, GPS, compass, and horizontal thrusters.

Thus, the total power of the navigation task was 0.65 + 0.76 + 0.4 + 28 = 29.81 W. For one hour, the energy consumption was 29.81 Wh.

Given that SEMBIO had an energy capacity of 111 Wh, without SEMS the navigation subtask could run for 2.87 h (111 Wh ÷ 38.59 W), while with SEMS it could run for 3.72 h (111 Wh ÷ 29.81 W). This calculation is conducted to determine the run time of each subtask.

	Mission without SEMS		Mission with SEMS		
Subtasks	Power	Time	Power	Time	Percentage gain using SEMS
Navigation	38.59 W	2.87 h	29.81 W	3.72 h	29.97 %
Depth control	24.49 W	4.53 h	18.65 W	5.95 h	31.35 %
Monitor	28.45 W	3.90 h	27.85 W	3.98 h	2.05 %
Return home	38.59 W	2.87 h	13.37 W	8.30 h	189.2 %
Total sum	**130.12 W**	**0.85 h**	**89.68 W**	**1.24 h**	**45.88 %**

Table 7.5 Overview of the results of the theoretical evaluation in the absence and presence of SEMS, the time of energy consumption in all subtasks is calculated according to the energy capacity of SEMBIO, which is 111 Wh

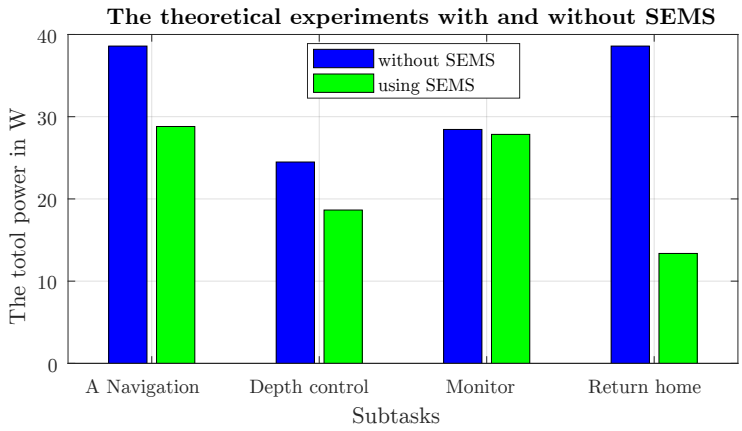

Figure 7.28 Comparison of the power consumed by the monitoring mission comprising one task and four subtasks in the absence and presence of SEMS

Based on the results obtained from the calculation of the first subtask, it was concluded that the use of SEMS in the navigation subtask increased the SEMBIO running time by one hour, which represents a percentage of 34.15 %. The other three subtasks were also calculated using the same procedure. Table 7.5 provides an overview of all the results. Furthermore, a comparison between the calculated values in the presence and absence of SEMS is provided in Figure 7.28, alongside the differences that were identified. Therefore, it can be concluded that the use of SEMS reduced the amount of energy consumed by every subtask, and in particular the navigation subtask of return to homebase, which did not involve any essential action, due to its use of the high efficiency zone of the thrusters (0.2 m/s generated from 1 N).

Although SEMS afforded a wider range of options, they were not used to maintain the mission requirements identical to the scenario without the use of SEMS. The power was observed to be almost the same in the case of the monitor subtask, due to the fact that all sensors and thrusters were activated. The use of SEMS could engender a difference, e.g., by changing the camera resolution or the thruster efficiency zone.

Experimental Evaluation of the Monitoring Mission

The procedure applied to obtain the results of SEMS for the monitoring mission was as follows. Prior to the installation of SEMS, the full software operating the vehicle was installed on-board SEMBIO and the batteries were fully charged. In the first case, each experiment was carried out in the same manner as the experiments in the absence of SEMS. It must be highlighted that, in the context of the actual experiment, the term "without or in the absence SEMS" referred to the fact that the entire output of the SEMS-Embedded-Board was switched on and every component was either active or in idle mode, whereas the term "with or in the presence of SEMS" referred to the fact that output activation was carried out in keeping with the control code of the "monitoring mission".

In the second case, SEMS was used. After receiving the control code of the "monitoring mission" from the SEMS-Mission-Planner through XBee, the SEMS-Embedded-Board proceeded to parse the control code and employ SSR to switch components on or off, depending on the requirements of the mission, tasks, and subtasks. As discussed in Section 7.3.3, INA219 sensors were used to measure the current and voltage of the components, including sensors, processors, and thrusters. An SD card stored all the measurement data on-board at a rate of 5 Hz.

Figure 7.29 The set-up and location of the real SEMS experiment

To ensure that the results were as reliable and valid as possible, the performance of the real experiments in the Waknitz river were repeated several times. No complex equipment was needed to conduct the evaluation of SEMS, the vehicle with a laptop and fishing reel (to pull the vehicle in case of any faults) being sufficient (Figure 7.29).

Figure 7.30 represents the starting point of the experiments where SEMBIO was immersed in the water to conduct some tests before the launch of the experiments.

Figure 7.30 Launch of SEMBIO into the water

The procedure adopted in the theoretical evaluation was employed in the real experiment as well in order to avoid any complication or problems. In the theoretical evaluation, two scenarios were enacted, namely, one mission with a single task and four subtasks being performed with and without SEMS, respectively. However, the experimental evaluation of SEMS encountered a number of issues. One issue was that the first subtask (i.e., the navigation subtask), was not successfully performed by SEMBIO, failing to reach the intended location at the surface of the water by relying on GPS. To put it differently, the vehicle did not follow the ideal path between P0 (53.853363, 10.702976) and P1 (53.854054, 10.704120). The solution to this issue was to ignore the fault, permitting SEMBIO to move freely at the surface of the water. However, the subtask was connected to a specific time, after which the vehicle was submerged to an established depth for a set amount of time as well. Another issue that arose was the flow and waves of the water made it impossible to measure the current accurately, since the current of the thrusters changed alongside changes in the drag force of the water. The solution to this issue presented itself in the form of taking more measurement samples of the current and producing an average of those values.

SEMS measured a number of different parameters, including the total power (W), current (A), battery voltage (V), battery capacity (Wh), and the diving depth (cm). Figure 7.31 presents the initial set of measurements conducted in the absence of SEMS until the completion of the first subtask. It can be seen in this figure that,

after a starting point of zero, the power exhibited small spikes of up to 16 W when the SEMBIO electrical system was turned on. SEMBIO remained activated for the preparing phase and the power level was around 5 W for approximately 1,000 sec. Meanwhile, the battery voltage, which did not change, and the battery capacity underwent slow changes at a significant rate when SEMBIO was introduced at the surface of the water at a depth of 2-4 cm, which varied according to the water waves. Between around 1,000 sec and 2,360 sec, the power fluctuated depending on the speed (different speeds range of 0.1, 0.15, 0.2, 0.25, and 0.3 m/s were used), leading to changes in the battery voltage and battery discharge rate (i.e., battery capacity). Between around 2,360 sec and 3,520 sec, the vehicle moved from P0 to P1 at a speed of 0.5 m/s, using approximately 44.5 W. The subtask went on for around 20 minutes, during which time it was observed that both the battery voltage and battery capacity decreased more obviously. It should be noted that the SEMS-Solar charged the emergency battery during the navigation subtask at an amount of 190 mWh or about 0.13 % of the total capacity.

The data in Figure 7.31 formed the basis for the calculation of the energy consumed in the navigation subtask. Thus, for 20 minutes of operation, the energy consumption was 14.42 Wh, meaning that for one hour, the energy consumption would be $14.42 \times 3 = 43.26$ Wh, which was almost equal to the average total power used by the navigation subtask (44.5 W), which means that for one hour the energy consumption 44.5 Wh.

There was a difference of over 6 W between the theoretical evaluation and the real evaluation (38.59 W vs 44.5 W). Potential reasons for this difference include the fact that running some of the components in idle mode was not successful or the fact that the battery voltage was changed from 11.1 V in the theoretical evaluation to 11.65-12.2 V in the real evaluation.

For the following three subtasks, an identical approach as in the case of the navigation subtask was adopted (see Figure 7.32). The second subtask of depth control involved the vehicle diving from the surface to a depth of 1 m. Given that it did not take long to accomplish this, the calculation of the amount of energy consumed (for 10 minutes) to dive to such a shallow depth was challenging due to the short distance of the water depth. The solution implemented was to permit the vehicle to repeatedly dive and float between the desired depth and the surface of the water to obtain adequate average values of the energy consumption. Figure 7.32 indicated that the depth subtask took around 10 minutes to complete, which was equivalent to energy consumption of 4.34 Wh. Thus, the amount of energy consumed in one hour would be 26.04 Wh, which was similar to the average total power associated with this subtask (26.20 W).

Compared to the other subtasks, the monitor subtask was less complicated. It involved moving the vehicle horizontally at the desired depth of 0.5 m for a period of 20 minutes (see Figure 7.32). During that time, the energy consumption of the vehicle was around 11.03 Wh, meaning that, in one hour, it consumed 33.09 Wh,

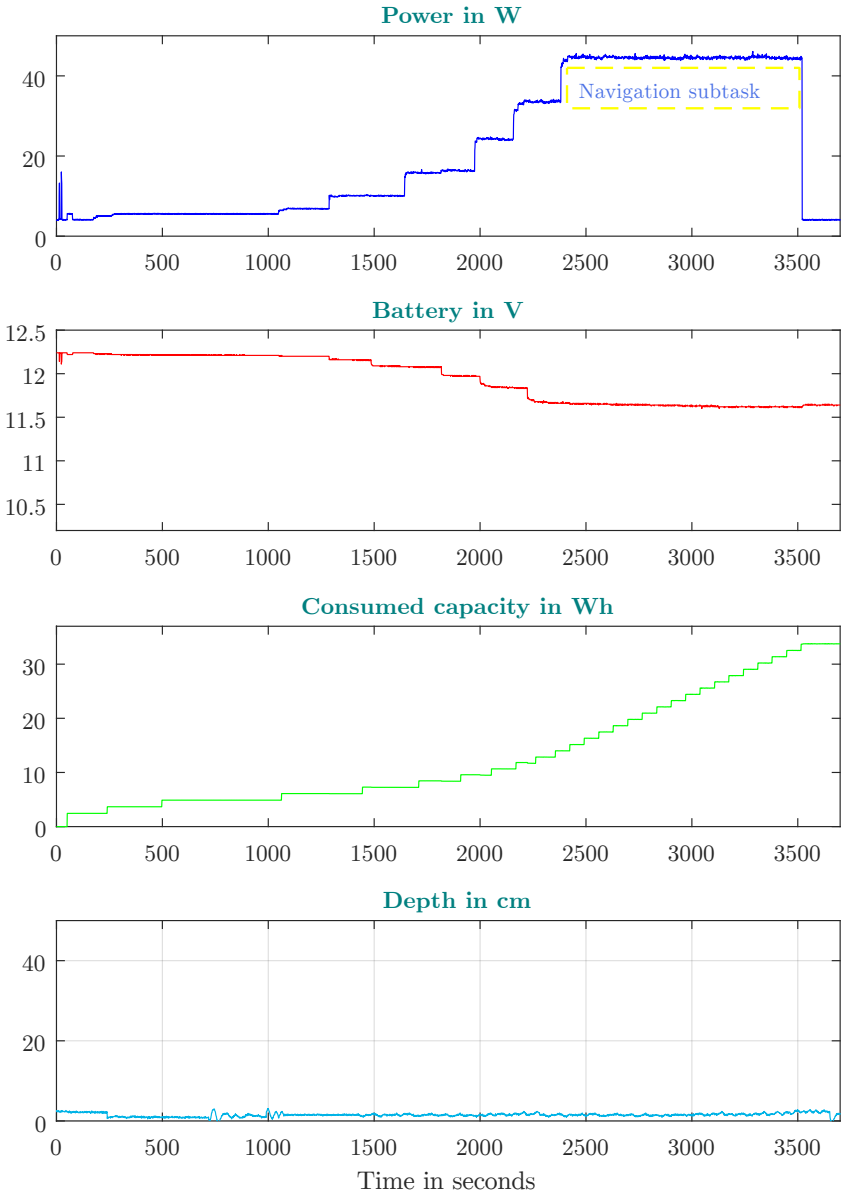

Figure 7.31 The data measurements taken for the monitoring mission with a navigation subtask in the absence of SEMS

which was very close to the average total power measured for this subtask (33.26 W).

Similar to the first subtask of navigation, the final subtask of return to the homebase involved floating the vehicle to the surface and moving it from its location to the homebase. This subtask was performed in a different way, depending on whether SEMS was used or not. In the absence of SEMS, the performance of the subtask did not differ from the performance of the navigation subtask. However, in the presence

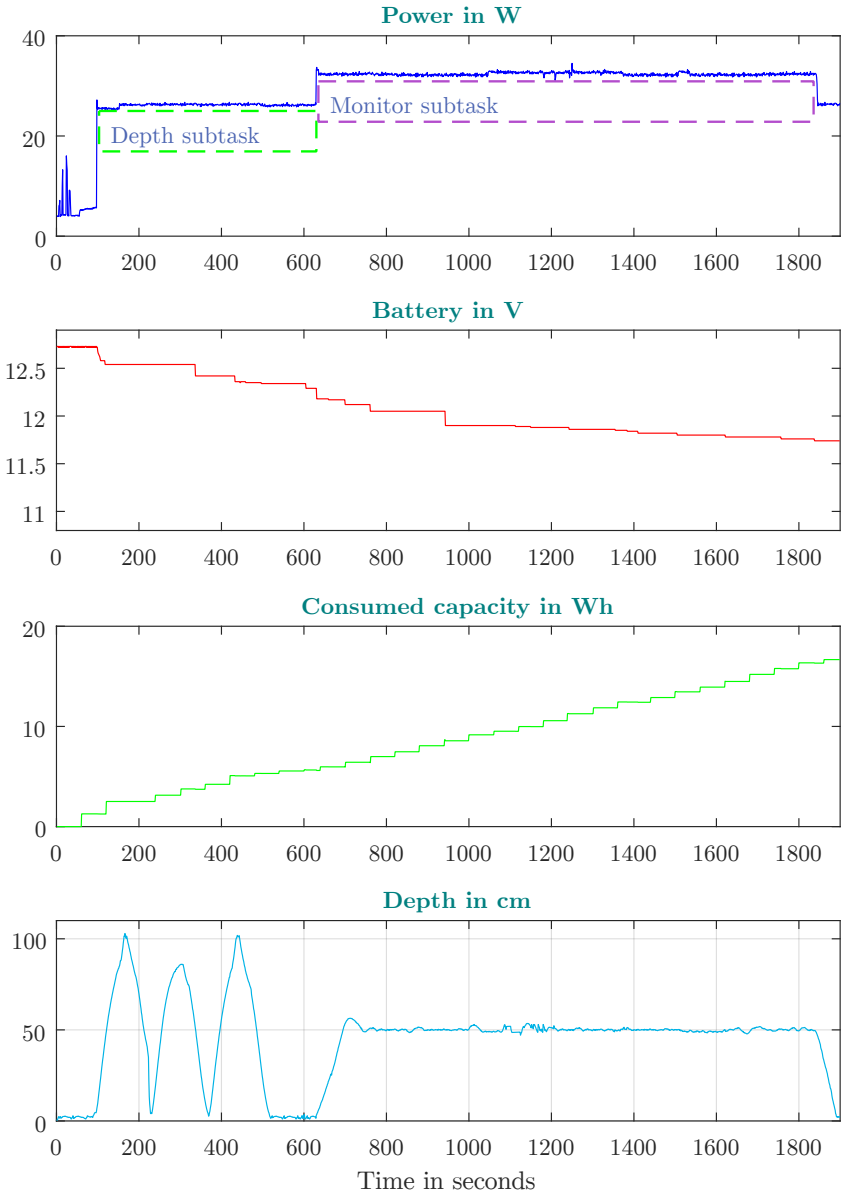

Figure 7.32 The data measurements taken for the monitoring mission with depth, monitor, and return home subtasks in the absence of SEMS

of SEMS, a slower vehicle speed was used to ensure that it was within the high efficiency zone of the energy consumption, because a high speed was unnecessary as no other subtasks were left to be completed.

In the final part of the experiments, SEMS was used, and its evaluation involved the performance of the same procedures, with the exception that the monitoring mission was initiated after the battery was completely charged and SEMS was activated.

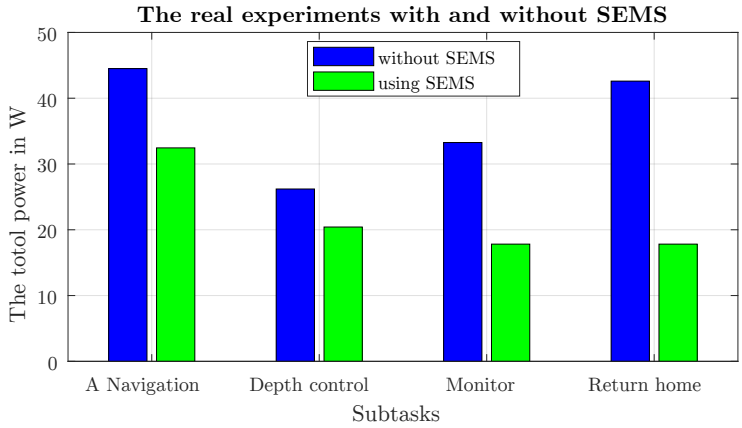

Figure 7.33 Comparison of the results of the real experiments with and without SEMS in terms of the energy consumption for a monitoring mission with one task and four subtasks

	Mission without SEMS		Mission with SEMS		
Subtasks	Power	Time	Power	Time	Percentage gain using SEMS
Navigation	44.50 W	2.49 h	32.45 W	3.42 h	37.35 %
Depth control	26.20 W	4.23 h	20.42 W	5.43 h	26.87 %
Monitor	33.26 W	3.34 h	31.70 W	3.50 h	4.79 %
Return home	42.60 W	2.61 h	17.82 W	6.23 h	138.7 %
Total sum	**146.5 W**	**0.76 h**	**102.4 W**	**1.08 h**	**42.11 %**

Table 7.6 Overview of the results of the real experiments with and without SEMS, the time of energy consumption in all subtasks is calculated according to the energy capacity of SEMBIO, which is 111 Wh

Figure 7.33 presents the differences identified when the real experiments with and without SEMS were compared. Table 7.6 provides an overview of all the results. Identical to the results obtained in the theoretical evaluation, the use of SEMS reduced the energy consumption in all subtasks in the real experiments, and the results of the real evaluation were close to the theoretical evaluation, with only slight differences. The use of SEMS was highly advantageous, not only helping to secure a gain of more than 40 % in energy usage, but also to better manage the different vehicle components.

7.7 Summary

The present chapter focused on the discussion of the basic SEMS system as a viable option for managing SEMBIO's energy consumption, reducing the consumption, and therefore prolonging the mission time by controlling the restricted on-board energy source. SEMS can achieve these objectives through its four interconnected and inter-collaborative parts. Furthermore, to enable such AUV processes as a development of mission, tasks, and subtasks, and monitoring in real-time of how the vehicle performed and consumed energy, a user interface environment was created. Moreover, to facilitate the retrieval of the micro AUV in an emergency situation, an additional system, ERS, was incorporated into the vehicle as well. The performance and analysis of SEMS, SEMS-Solar, and ERS experiments and their results were also undertaken in this chapter.

8 Load Balancing Approach to Increase Mission Time of Multiple AUVs

As specified in Chapter 1, the present study aimed to achieve the design and development of a cost-effective hand-portable AUV in a streamlined shape that could be used in swarm robotics research, especially applications of environmental monitoring both in inland and coastal waters. While this aim was discussed and accomplished in the earlier chapters, during the work phases of this project, the energy concept and the mission time were also taken into account and considered, for instance by choosing the most energy efficient propulsion system through careful selection of the most suitable propellers, minimizing the drag factor of the vehicle's hull using a streamlined shape design, or by using SEMS to manage the limited power resource on-board the vehicle.

In the present chapter, and in the same context of energy concept and mission time, a load balancing approach is suggested and implemented to increase overall mission time with consideration of energy and fault-tolerance for multiple AUV formations.

However, when this study was conducted, there were no available prototypes of acoustic modems that were affordable and of small proportions. The implementation of this approach is alternatively achieved, therefore, by using a simulator. In addition, the results of simulation are also outlined in this chapter which was partly published in [16, 17].

8.1 Introduction and Background

The underwater environment contains a rich diversity of as-yet unidentified organisms and resources. Such an environment can be explored and better understood through the deployment of AUVs [241]. A single AUV requires a high complexity of behaviors and instructions for processing data [49, 169]. Additionally, a single AUV relies on a complicated and lengthy search pattern, which is why it takes up a significant amount of time to achieve a task. By contrast, multiple AUVs can search an area much faster due to the fact that they behave as a distributed sensor network. Thus, a swarm or team of AUVs could be more advantageous than a single AUV in terms of being more efficient and completing a task quicker. For example, it took over 40 days for the REMUS 6000 AUV to identify the location of the Air

France Flight 447 that crashed in 2009 [167]. However, it must be noted that even a swarm of AUVs has a high energy consumption and takes a long time to complete a task in the case of long-term tasks comprising more than one mission. In these kinds of tasks, it is essential to consider energy consumption and management, since AUVs are typically powered by batteries, as mentioned in Chapter 7.

A number of factors determine how much energy an AUV consumes, including how complex the mission is, how much data there is to process, and the nature of the environment. It may be challenging to estimate the amount of energy required for a mission in the event of unforeseen environmental conditions and autonomous behavior of the members of an AUVs swarm. An additional issue that may arise is that some members may even malfunction, making them unable to carry out their tasks.

A number of projects have attempted to refine either the hardware or software structure of the robot to extend the duration of mission. One such project is the SAUV, which was succinctly discussed in Section 2.11.1, while its principle for long-endurance missions was addressed in Section 7.1.

The present study proposes the use of multiple AUVs based on a load balancing approach to extend the total mission duration while considering energy and fault-tolerance. The formation is separated into two layers using this type of approach. One layer remains at the surface and restricts its movements and measurements to conserve energy. Meanwhile, the other layer goes underwater and undertakes the monitoring task while exhibiting depth-holding behavior. When a submerged AUV that belongs to a second layer depletes its energy resources or malfunctions due to damage to hardware components (e.g., faulty pressure sensors or power system), it exchanges places with the first layer AUVs. To provide evidence to back up this suggested approach, a simulation was undertaken, as described in this chapter.

8.2 Pattern Formation

Formation control has been the focus of the majority of research conducted on underwater consensus control. The purpose of formation control is to mobilize agents in an organized and repetitive way to maintain a geometrical shape in their environment [36, 41]. This requires the member AUVs to comply with a number of straightforward behaviors or rules in order to achieve unison movement. Furthermore, numerous applications require multiple autonomous vehicles to follow a predefined trajectory simultaneously to maintain a specific spatial pattern formation. Movement in formation can be more advantageous than movement patterns lacking coordination. A range of control strategies were therefore introduced according to the nature of the mission or the particular task that the formation is required to undertake [48]. The main formation control approaches applicable to

independent vehicles include the behavior-based approach, vision-based approach, leader–follower approach, and virtual structure approach [48].

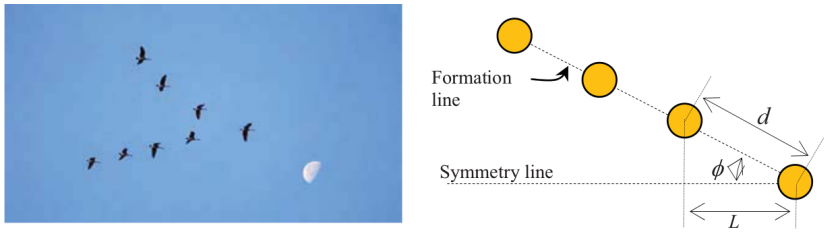

Figure 8.1 The principle of V-shaped formations [132]

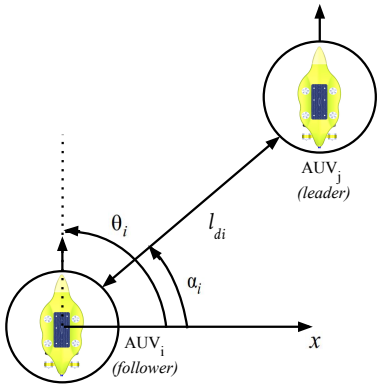

Figure 8.2 The leader–follower approach; the desired relative angle between the follower (AUV_i) and its leader (AUV_j) is denoted by α_i, while the heading direction of the follower is denoted by θ_i, and the desired distance between the follower and the leader is denoted by l_{di}

The present study attempts to develop and maintain the robotic formation by implementing the leader–follower approach in conjunction with the V-shape pattern formation [57], which is illustrated in Figure 8.1. This formation pattern was selected for a number of reasons, including the simplicity of implementing this approach underwater. Leader–follower works well in underwater implementations because it employs local sensing and minimal communication. This pattern of movement is inspired by the organization of migratory birds, which allows them to avoid the wake generated by the birds in front and thus consume less energy. The amount of energy saved is greater the more wake the follower birds can avoid [60]. Thus, the V-shape formation can enable the AUVs to cover and monitor a wider area in a time-effective manner, with minimal energy usage.

The leader–follower approach involves establishing a leader agent and moving the follower agents in a way that preserves the spacing and bearing in relation to the leader as well as to a subgroup of adjacent elements (Figure 8.2). More specifically,

a predefined trajectory is traced by the leader while the followers maintain the targeted geometric pattern with the leader. Scalability of the formation is achieved if a follower is appointed as the leader for a different vehicle. If a global leader is established, then the reference trajectory of that leader is used to shape group behavior. The control laws of each vehicle help to keep the internal formation stable based on position measurements derived from the leader.

Several difficulties are presented by the formation control of AUVs, such as poor underwater communication that makes it challenging for AUVs to exchange information with one another. Such problems are disregarded through the use of a simulator in order to simplify the V-shape creation.

8.3 Energy Load Balancing Approach

The energy load balancing approach for multiple AUVs is discussed in the following section. In Figure 8.3 the concept of swarm localization is shown, which can also be used for multiple AUV formations. This principle allows the members of the formation that are at the surface to localize themselves through GPS. However, GPS-based localization is impossible underwater, so the submerged AUVs rely on acoustic communication instead. Thus, the GPS data is received by a number of AUVs that are on the surface, and they subsequently transmit the data to the vehicles underwater through the means of an acoustic modem. The location of the underwater vehicles in relation to the GPS location of the AUVs at the surface can be determined by distance measured, based on the time of arrival of signals from various locations. In addition, failures can be overcome, and network state stability can be achieved by employing formations and grouping the vehicles in one location.

The principle underpinning this approach is explained as follows. Efficient navigation and sensing are essential due to the greater complexity of task performance underwater, such as the use of cameras to sense the movement of other AUVs [241]. As a result, the energy usage of underwater AUVs is greater compared to that of AUVs at the surface. Furthermore, as indicated in Chapter 7, submerged vehicles use a greater amount of energy than vehicles floating at the surface, particularly if the thrusters are employed at the efficiency zone. To give an example, the monitoring task requires activation of the cameras, depth pressure, and depth controller. The latter also necessitates activation of four vertical thrusters (depth-holding behavior to hold a specific depth). Meanwhile, at the surface, the floating vehicles necessitate activation of communication units, GPS, and two horizontal thrusters. Consequently, it is possible to increase the duration of the mission by introducing an exchange process between them, as presented in Section 8.3.3. Trilateration via GPS requires a minimum of three AUVs to float at the surface.

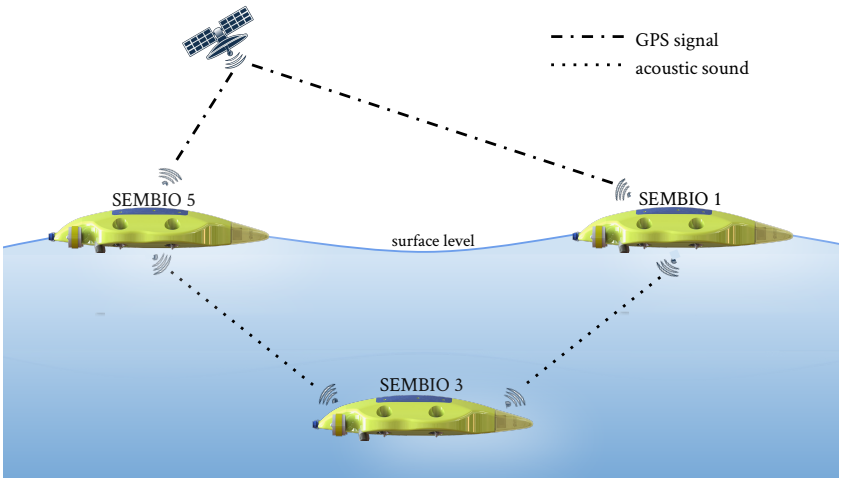

Figure 8.3 Illustration of the swarm localization concept that can be used in a V-shape formation; SEMBIO 3 is in active mode in the lower layer, having reached the desired depth, while the other vehicles stay at the surface where they serve as an energy supply. The upper layer members that employ an acoustic modem transmit their GPS data to the lower layer to enable localization

There are four phases making up the approach. The first phase involves creation of a V-shaped formation by the members at the surface. In the second phase, the formation is separated into two layers. A number of members go underwater to carry out their tasks, such as exploring, investigating, or gathering data. The rest of the members (to receive the GPS data) remain at the surface and move in conjunction with the underwater AUVs in a V-shape. The third phase consists of the exchange process between the members of the formation. The fourth phase involves the surfacing of the underwater AUVs once they have completed the mission or are running low on energy. All the AUVs can then return to the homebase. Figure 8.4 presents the entire process, and a more in-depth discussion is provided below.

8.3.1 Assembling the V-shaped Formation

Drawing on inspiration from the natural world, the V-shaped formation pattern keeps the vehicles close to one another, thus mediating communication and coordination among members [58, 129].

The principle underlying the leader–follower approach is that the follower AUV attempts to keep a certain distance and angle in relation to the leader AUV. The desired formations are achieved when every vehicle is positioned correctly.

In keeping with the leader's position, the reference trajectory of the follower is established in such a way that its position is changed by a distance l_d and an angle

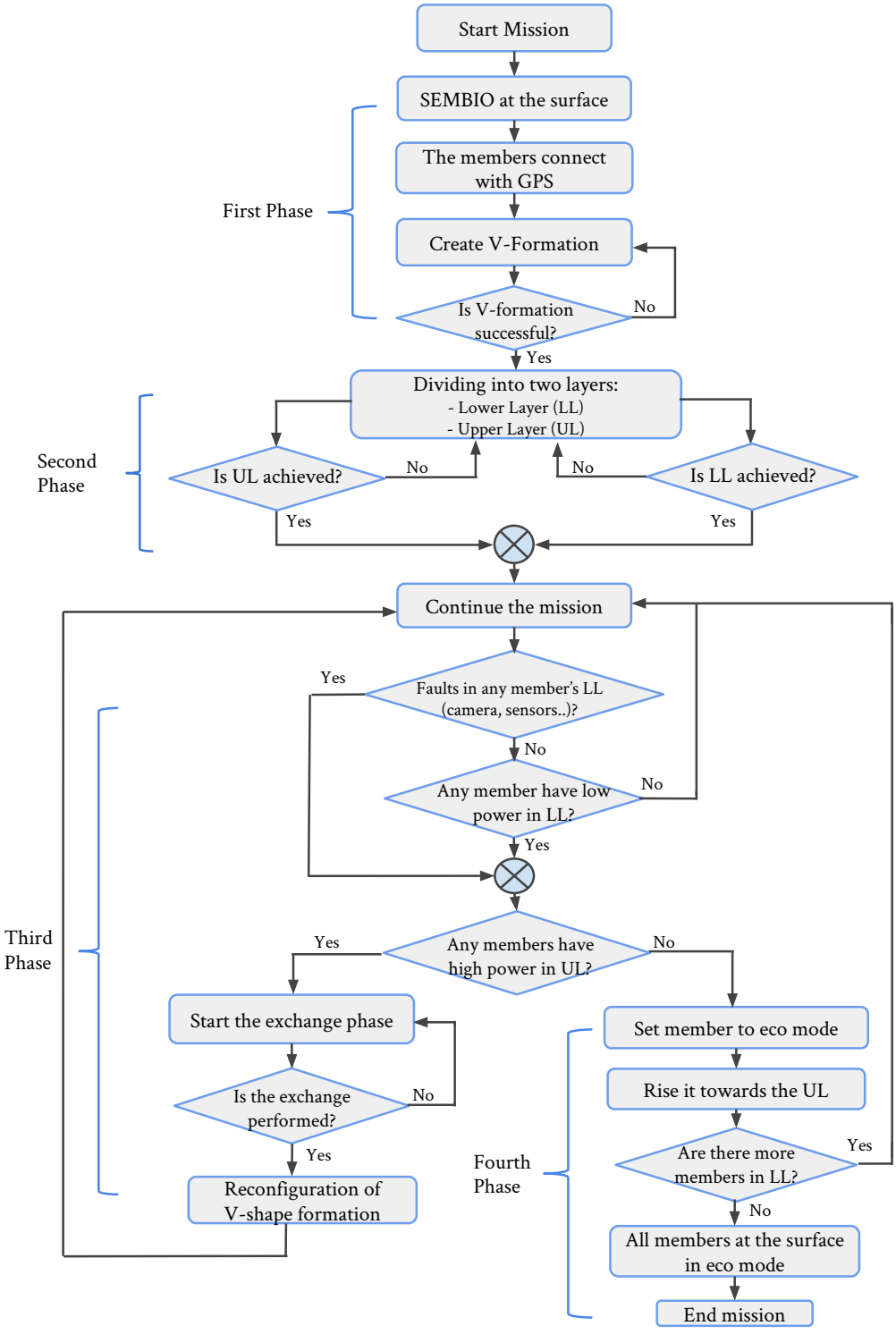

Figure 8.4 Flow chart illustrating the processes in each phase during a mission; the V-shape takes form during the first phase, while the layers are separated in the second phase; the exchange between two vehicles occurs in the third phase, and all the AUVs revert to their initial position in the fourth phase

α in relation to the leader. While the leader is cruising, the reference trajectory of the follower is set. This trajectory is traced by a virtual vehicle. The subsequent step is to devise the position tracking control for the follower to trace the virtual vehicle trajectory. The integral part of the controller to trace l_d and α is required to attain this objective. To this end, the development of the position tracking control for the members employing a PID controller is undertaken.

Syncword Start	AUVs ID	Delimiter	Data Type	Delimiter	Data1	Delimiter	.....	Data n	End
$	01	@	Energy	@	100	@	.....	n	#

Figure 8.5 A straightforward protocol for the suggested system that is employed in communication between the vehicles to obtain the relative position of submerged AUVs; the vehicle ID and a data type followed by the current data are included in every broadcast

The communication mechanism put forth involves all vehicles relying on their Unique Identification (ID) to broadcast and receive a series of sequential messages. To allow the members to exchange data amongst themselves, an uncomplicated protocol was employed that consists of the vehicle ID, data type (e.g., amount of energy or depth), and data value, as shown in Figure 8.5. The rules associated with the V-shaped formation and the use of the controller are provided below.

SEMBIO has positive buoyancy, meaning that all the vehicles can float on the surface. The initial phase involves creating a V-shaped formation of multiple AUVs at the surface based on the distances and angles among the vehicles as approximated by a GPS sensor, as shown in Figure 8.4.

More specifically, the order of the IDs of the vehicles determines the manner in which they are organized in the V-shape. Because the formation of the AUVs is not the focus of the research, the simplest rules were followed to create the V-shaped formation. The ID of each vehicle is predefined, thus, the leader fronting the vehicles towards an established aim is chosen to be the vehicle with an ID of ID1. The rest of the vehicles are followers arranged at the back of the leader at an angle of $\pm 45°$. It assumed that the angle is $+45°$in the case of vehicles with odd IDs and $-45°$in the case of vehicles with even IDs. Broadcasting the position and orientation is undertaken by all the vehicles. The distances and angles between the vehicles are maintained during the motion. The velocity of the follower will be increased if the distance between two vehicles exceeds the desired distance, while the velocity of the follower will be decreased if the distance between two vehicles is less than the desired distance.

The vehicles will exhibit avoidance behavior if confronted with obstacles. Therefore, to address this problem, the vehicles in the simulator are equipped with two infrared distance sensors to detect any obstacles in front of them.

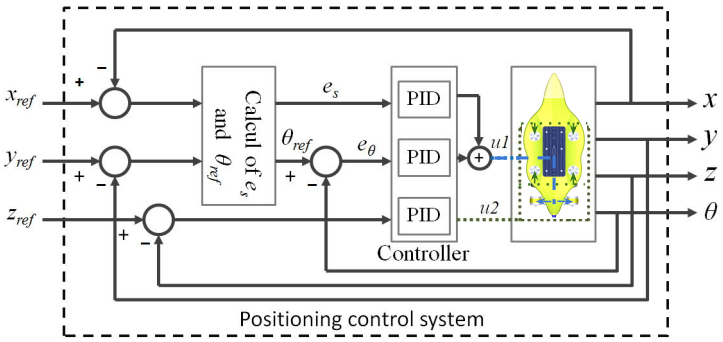

Figure 8.6 The positioning control system of all members that create the V-shape, which is made up of two sections; one section represents a distance and angle measurement associated with the employed position, while the other section comprises a PID controller for depth, a PID controller for distance, and a PID controller for angle; the obtained controller values for distance and angle are summed up and employed for the horizontal thrusters, while the depth value is reserved for the vertical thrusters

The leader starts moving in the direction of the mission target. Concomitantly, the leader informs its followers where it is located and how it is oriented. Such information is known as heading direction θ data for the followers and is used by the latter to situate themselves accordingly. To establish the desired distance between the members, the movement of the followers is slow or rapid. Furthermore, the angle of the followers must maintain the orientation between themselves and the leader, which is based on where in the formation each follower is positioned ($+45°$and $-45°$for even and odd IDs, respectively). This kind of behavior is implemented by a positioning control system, as illustrated in Figure 8.6.

The parameters of (x, y, z, θ) represent the actual position of the vehicle, while $(x_{ref}, y_{ref}, z_{ref}, \theta_{ref})$ represent the desired position that the vehicle has to follow it e.g., the position of the leader. The value of $u1$ and $u2$ represent the control output, e_s and e_θ represent the error of the distances and angles respectively.

In the present study, every vehicle was associated with three controllers, not just one; the three controllers are respectively used to establish the position, orientation, and the depth of the vehicles. To ensure that they are correctly positioned in the formation, each follower presents itself to a different follower, relying on the position of the reference vehicle to set its own position. Relative localization (i.e., relative distance and angle) is achieved as every vehicle computes the position and orientation of its forerunner in the V-shape.

The controller processes require each vehicle to deal with three values (x, y, z), with the formula (Equation 8.1) from [216] being applied to determine the desired distance and angle based on the x_{ref} and y_{ref} values. The control value for the

horizontal thrusters is subsequently determined by summing up the values from the PID controller associated with distance and the PID controller associated with orientation. The z_{ref} value is employed directly in the third PID controller for depth control via the vertical thrusters.

$$l_d = \sqrt{(x_{ref} - x)^2 + (y_{ref} - y)^2}$$
$$\alpha = tan^{-1}(\frac{y_{ref} - y}{x_{ref} - x}) \tag{8.1}$$

The feedback of vehicle depth determines the third axis. In this way, the three PID controllers maintain the angles, distances, and depths between the members of the V-shaped formation.

When they float at the surface, the vehicles are in what is known as eco (economical) mode, in which the only activated system functions are GPS, Wi-Fi, and two horizontally mounted thrusters to propel the vehicles towards the objective. This allows the members to conserve energy whilst moving towards the operation zone, thereby enhancing their total lifespan. The subsequent stage of layer separation (see the flowchart in Figure 8.4) commences once the V-shape has become stable based on a satisfactory margin of distance and orientation error, which in this case is 100 cm and 45°, respectively, and once the operation zone has been reached.

8.3.2 Layer Division

The V-shape of AUVs is separated into two layers based on the assumption that there are more than three members that created the formation pattern. Three or more AUVs should remain at the surface, constituting the upper or eco layer. These AUVs play an important role in the localization task [153]. The remaining AUVs submerge underwater, forming the second layer (lower or active layer), which is where the monitoring task will be carried out. The positioning control system illustrated in Figure 8.6 will enable the submerged vehicles to dive to the target depth z_d. Due to the fact that they will undertake the monitoring tasks involving depth maintenance and use of camera and image processing devices, the submerged vehicles employ not only their sensing capacities to a greater extent, but also more actuation. For SEMBIO, depth is controlled by four vertically oriented thrusters, which is why the submerged members have greater energy requirements compared to the members at the surface. In addition, the environmental conditions that the two layers have to deal with are different, with a higher drag in the lower layer. Thus, the two layers do not use the same amount of energy. More specifically, the energy consumption of the AUVs in the lower layer is higher than that of the AUVs in the upper layer. The subsequent stage addresses this difference in energy usage to extend the duration of the mission via load balancing.

8.3.3 Exchange

The number of vehicles in the upper layer determines how many exchanges can be performed. For instance, three exchanges can be done in the case of the V-shaped formation made up of five SEMBIOs, two of which are submerged and three which are floating at the surface. The higher the number of exchanges, the longer the duration of the mission will be. The current section discusses when the exchange is carried out and the underlying mechanisms, as well as the ideal behavior of the load balancing approach. As noted earlier, the vehicles rely on their unique ID to broadcast and receive a series of sequential messages. Among these messages is one that provides the latest AUV energy level, as shown in Figure 8.5. Hence, after every broadcast, the energy levels of all AUVs are known to all other members. As previously mentioned, the AUVs in the lower layer usually have higher levels of energy consumption compared to the AUVs in the upper layer, because they undertake their tasks in the active rather than eco mode. Therefore, the upper layer constitutes an energy reservoir for the lower layer. Two conditions must be fulfilled for an exchange to take place between two members:

- The energy level of one of the submerged vehicles must be lower than an established threshold, such as 15%. SEMBIO keeps track of its own battery, so it is aware of its energy level. The low-level percentage is set based on the amount of energy needed to complete the desired task in eco mode and return to homebase (see Section 8.3.4 for further information).

- The energy level of one of the vehicles at the surface must have enough energy to enable an exchange; in other words, it should be higher than 25% (see the third phase in Figure 8.4).

Upon fulfillment of these two conditions, an available vehicle in the upper layer is accepted to carry out the exchange with a vehicle with a low energy level. A straightforward criterion is applied in the selection process. Essentially, the neighborhood takes precedence over the energy level; in the event of availability of two vehicles in the upper layer, the closest one will be selected for the exchange.

To give an example, a vehicle is established in a position by x and y, and the target depth of the vehicle is established by z. The process of exchange taking place between SEMBIO 2 and SEMBIO 4 is presented in Figure 8.7. SEMBIO 2, the submerged vehicle with the low energy level, and SEMBIO 4, the floating vehicle with the high energy level, trade places, keeping with the V-shape. After the determination of which vehicles will exchange places, SEMBIO 2 decreases its speed and floats to the surface behind SEMBIO 4. In doing so, it avoids collisions into the other members. When it surfaces, SEMBIO 2 switches its active mode to eco mode and waits for a GPS update and localization. Subsequently, it broadcasts and receives information about its status to the upper layer through Wi-Fi and to the lower layer through acoustic modem. The message issued by SEMBIO 2 informs the group that it has reached the surface. SEMBIO 4 subsequently submerges and

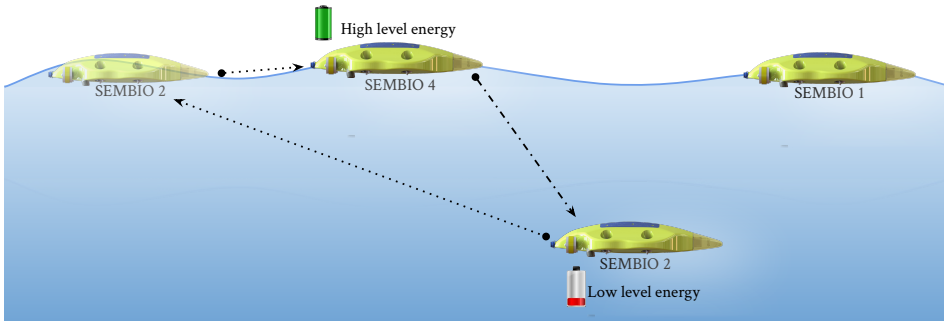

Figure 8.7 The exchange taking place between SEMBIO 2 and SEMBIO 4; the submerged vehicle decreases its speed to surface behind SEMBIO 4, after which the latter dives to replace SEMBIO 2 in its original position

adopts the position that was previously occupied by SEMBIO 2. In addition, it switches its eco mode into active mode and appropriates the new functions necessary to complete the underwater tasks. Thus, the process of exchange is finalized with success. The V-shape is then adjusted to achieve the desired distance and orientation of the members from the initial phase by the positioning and control system. Additional AUVs in active mode undergo the exchange process when their energy levels are low. In this way, the overall duration of the mission is increased, and errors caused by a low voltage supply to the sensors and actuators are prevented. Apart from low energy levels, the process of exchange is triggered by the need to attain fault-tolerance as well, such as in cases where a system component (e.g., vertical thrusters or pressure sensors) does not function properly.

For this reason, system function verification and broadcasting of basic status messages are undertaken by all vehicles. Such status messages reflect vehicle condition so that they can be deemed as health signals [130]. If a vehicle in the lower layer exhibits improper function in one of its system components, it will undergo a process of exchange with a vehicle floating at the surface. This ensures that the system is more robust against faulty vehicles.

The pressure sensor served as the health signal generator in the current behavior simulation experiment. The sensor was considered to be malfunctioning if the pressure sensor values were outside a valid range, which was established based on the datasheet of the sensor. SEMBIO's pressure sensor does not go further than 13 bar. Thus, this was taken as the threshold above which values indicated improper functioning of the sensor or risks to the actual vehicle. The sensor was also considered to be malfunctioning if the values were not published or were published with delay. Figure 8.8 illustrates how a likely malfunctioning pressure sensor can be detected.

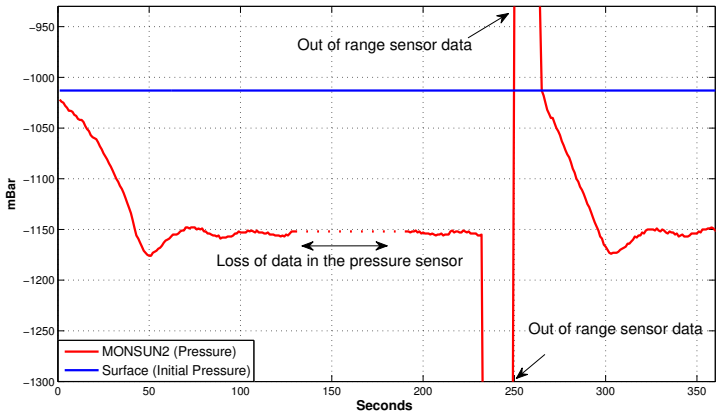

Figure 8.8 Representation of the health condition of the pressure sensor data, shown in red; the pressure sensor can be considered to be malfunctioning in the absence of data, as indicated by the dotted red line; the sensor is also deemed to be malfunctioning if values are less than or over an established threshold (normal range is from the datasheet of the sensor)

8.3.4 Mission End

The number of members with levels of energy high enough to permit them to submerge is diminished with each exchange that takes place in the third phase. In the configuration employed in this study, three was the maximum number of exchange processes that were possible. Depletion of this number means that every vehicle in the upper layer will be left with a low energy level of less than 15%. This results in the initiation of the final phase (see Figure 8.4). As highlighted above, the messages that the members broadcast amongst themselves inform on the energy levels each member possesses. The leader then decides that, at this point, initialization of the exchange process between members would be redundant. Instead, this process is deferred until a vehicle in the lower level completes its task or its level of energy decreases below 15%. If this threshold is reached, the leader transmits a message to the submerged vehicle in question that the swarm has no sufficient energy reserves in the upper layer to enable the process of exchange. Therefore, the submerged vehicle is ordered by the leader to surface and assume its position in the V-shape formation. Upon receiving this order, the submerged vehicle deactivates its vertically directed thrusters and rises to the surface, as facilitated by SEMBIO's positive buoyancy. Once it surfaces, the submerged vehicle switches its active mode to eco mode. The leader begins to go back to the homebase after every submerged vehicle has surfaced. It is necessary for the vehicles to have enough energy left for the return. The homebase constitutes a predefined location where every member has to congregate once the mission is completed. Determination of

the amount of energy required to return to the homebase can be calculated based on the energy consumption used to reach the target position from the homebase.

8.4 Simulation and Results

The MArine Robotics Simulator (MARS)[1] for marine robotics was employed to evaluate the energy load balancing approach [206]. MARS provides a Hardware-in-the-Loop real-time simulation environment that is particularly intended for AUVs. An additional advantage of MARS is that it can support more than one AUV and is capable of simulating energy consumption. A physical behavior that demonstrates realism both underwater and at the surface of the water is made possible by several factors: the water currents in conjunction with waves, determination of the center of buoyancy, and determination of volume. MARS is compatible with an arbitrary application, thanks to its simple TCP/IP interface, which allows for a connection on the basis of a straightforward request response protocol. MARS facilitated the evaluation of the employed load balancing approach because it supports a ROS interface. Since the approach is coded and written in C++, its implementation with ROS was easy.

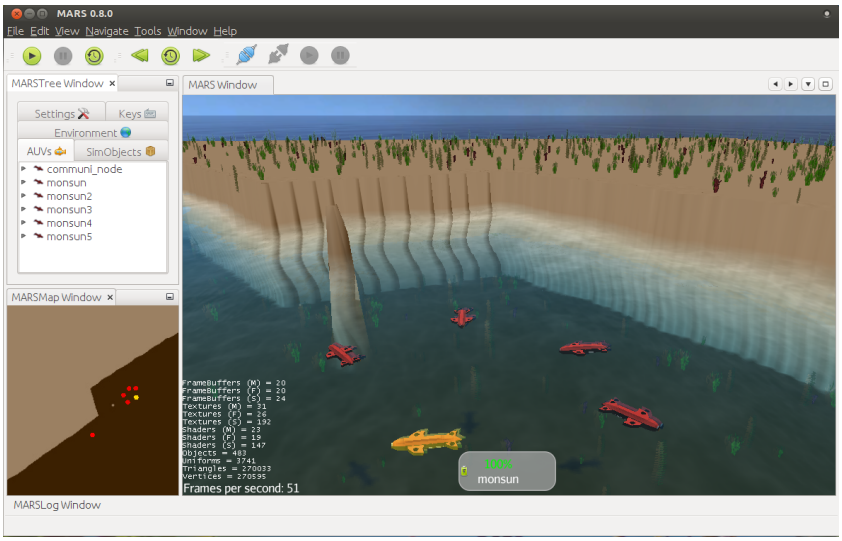

Figure 8.9 A snapshot of MARS showing a number of five MONSUNs; the vehicles are presented in the first phase, when they are in the process of creating the V-shape at the surface of the water

Owing to the update required by MARS to make use of using SEMBIO, MONSUN was used instead to carry out the simulation in this study. This substitution had no impact on the results, due to the fact that the simulator does not differentiate

[1] http://www.iti.uni-luebeck.de/en/research/mobile-robotics/mars.html

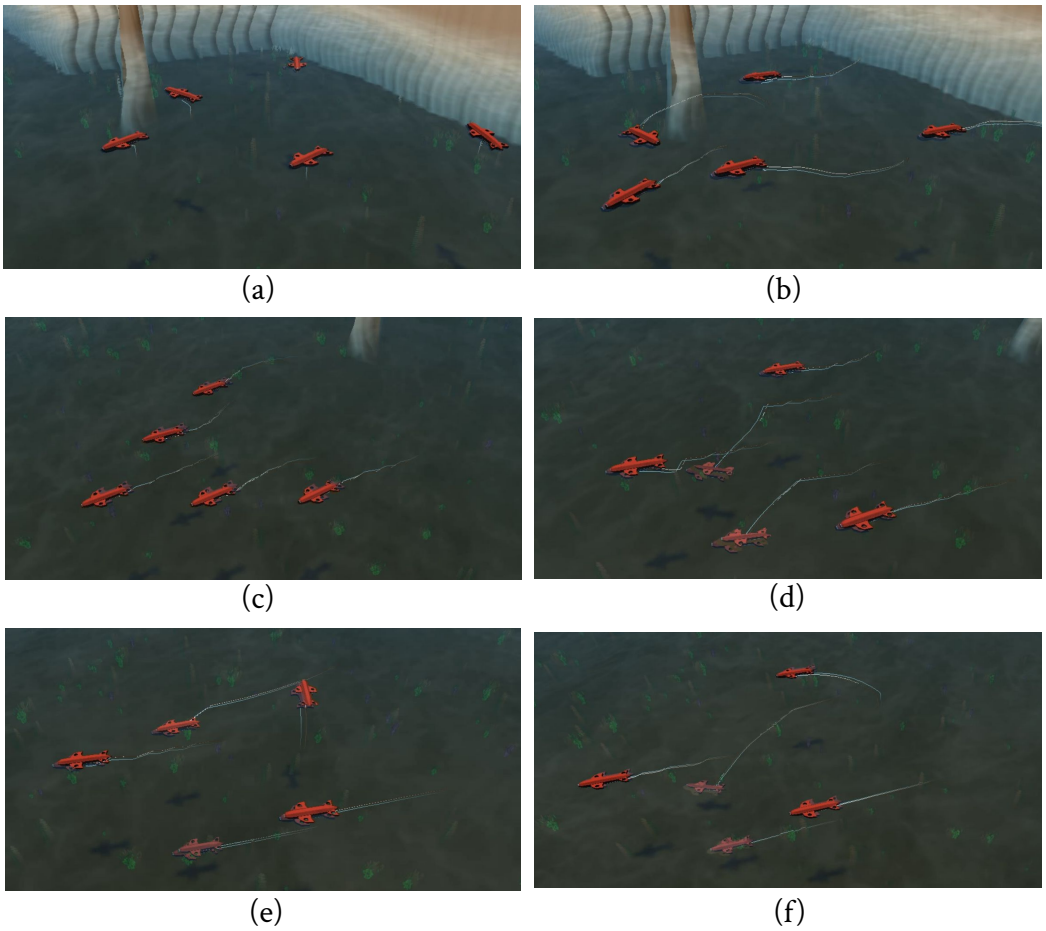

Figure 8.10 The snapshot of the simulation scenario. (a) free distribution of five vehicles at the surface; (b) the vehicles are starting to create the formation; (c) the stability of the V-formation is achieved; (d) two vehicles are submerged to the desired depth, (e) and (f) one vehicle with low energy is emerged and takes the position of the surface vehicle, and the surface vehicle takes the position of the emerged vehicle

between the two types of vehicles and disregards dynamic properties like drag or fluid hydrodynamics. Figure 8.9 provides a snapshot of MARS, where it can be seen that the MONSUNs are arranged at random at the surface of the water in eco mode and are about to commence the first phase. Furthermore, the level of energy of every MONSUN is maximal.

The amount of energy consumption and the force generated by the SEMBIO thruster were added to the simulator in order to make the results more accurate and to achieve an energy drain that was as realistic as possible. The thruster efficiency

zone was employed, and, moreover, a reduction by a constant factor in the battery capacity of each vehicle was performed with the purpose of diminishing the simulation time.

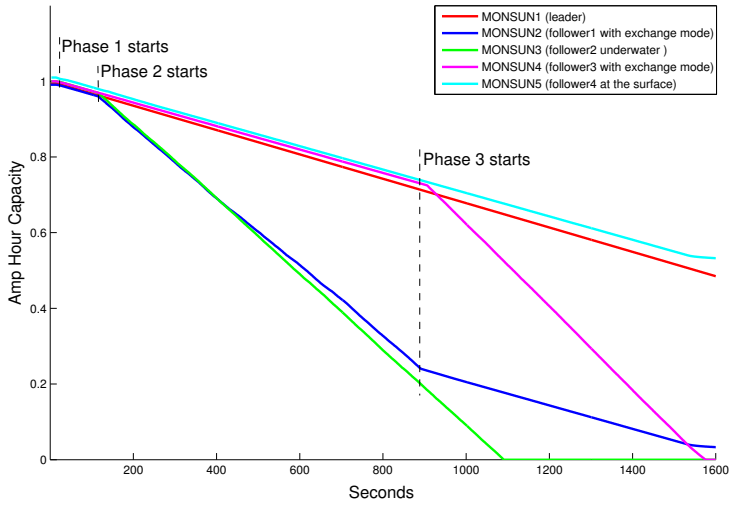

Figure 8.11 The capacity of the accumulator for all MONSUNs in the V-shaped formation; MONSUN 1 and MONSUN 5 rely on two horizontal thrusters to move at the surface with navigation sensors, while MONSUN 3 uses all its sensors with six thrusters to move whilst submerged; two horizontal thrusters also propel the movement of MONSUN 4 until the third phase, when it takes the place of MONSUN 2 and begins to use all the thrusters underwater; MONSUN 2 began using all six thrusters in the second phase until the third phase also then using two horizontal thrusters

The scenario of the simulation is built to illustrate the same sequence of the approach. Figure 8.10 is a snapshot of the simulation scenario for the first three phases. The results according to the energy consumption of the V-shape formation are illustrated firstly. The capacity of the accumulator that supplied every MONSUN thruster with energy through the entire mission is indicated by the results presented in Figure 8.11. During the mission, MONSUN 1 and MONSUN 5 remained at the surface in eco mode. MONSUN 3 submerged and worked in active mode in the lower layer, whereas MONSUN 2 and MONSUN 4 functioned both in eco mode and in active mode to illustrate the exchange process. MONSUN 3 did not participate to illustrate the case of the energy consumption in the absence of the process of exchange; its energy source was the first exhausted. In addition, MONSUN 3 determines the time mission in normally case which support us to calculate the slop and then to define the enhancing mission time.

The four phases of the results of Figure 8.11 are as follows. In phase one, all the vehicles moved at the surface, using only two horizontal thrusters and having

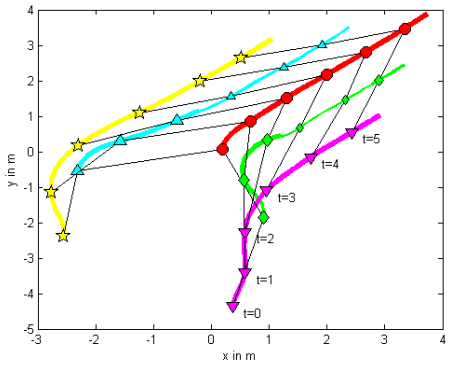

Figure 8.12 The different positions of the vehicles at the beginning of the V-shaped formation

more or less equal energy consumption. In phase two, MONSUN 2 and MONSUN 3 switched to active mode and submerged to the desired depth by relying on two horizontal and four vertical thrusters. The remaining vehicles floated at the surface. Based on the slope from the energy usage of MONSUN 3 and MONSUN 5, it was determined that the consumption of the vehicles in active mode was 2.8 times greater compared to the vehicles in eco mode. This difference in energy consumption enabled exchange of vehicles between the upper and lower layers, thus increasing mission duration. In phase three, the exchange occurred between MONSUN 2 and MONSUN 4, enhancing mission duration (calculated by using the slope) by 32% thanks to being in eco mode where only two vertical thrusters, GPS, compass, IMU, and Wi-Fi are activated, while in active mode all the thrusters, camera, IMU, and pressure sensor are activated.

The entire mission is presented from the positioning perspective in Figure 8.13. The mission involved all four phases, which were carried out sequentially, with the leader establishing the trajectory to start the mission. The information supplied by the leader enabled the members to adjust their movement accordingly to create the V-shape formation as shown in Figure 8.12. A three-dimensional representation of the mission whereby the swarm attempted the development of a V-shaped formation from MONSUNs with arbitrary positions is shown in the upper portion of Figure 8.13. Once the V-shaped formation reached the operation zone, MONSUN 2 and MONSUN 3 submerged in order to carry out their monitoring tasks.

MONSUN 2's energy level began to decrease after a time interval of 890 seconds. When its energy level became low, MONSUN 2 broadcasted a message to all members to let them know about its energy status and to request the initialization of an exchange with MONSUN 4 or MONSUN 5 that were positioned in the upper layer. MONSUN 2 made the decision that the process of exchange would take place with MONSUN 4 because it was physically the closest.

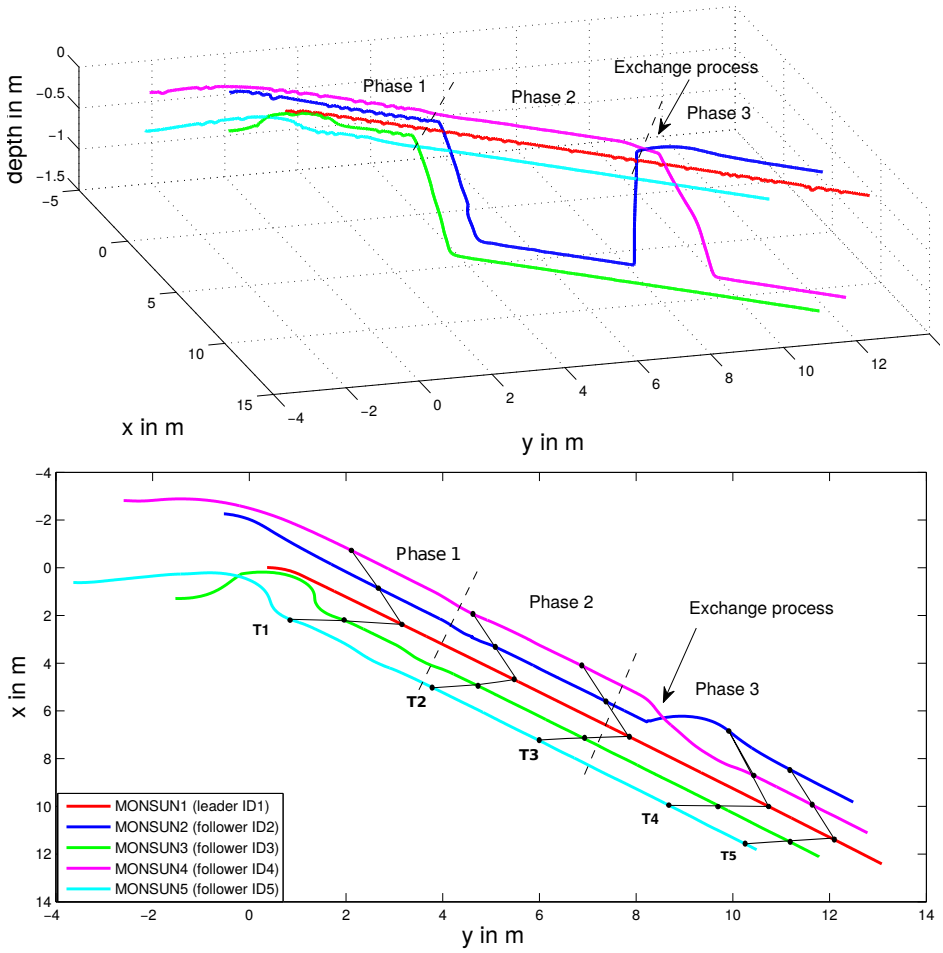

Figure 8.13 The trajectory of the mission is represented in the top figure, which is shown in 3D. The bottom figure shows that, in the first phase, the members succeeded in creating a V-shape; the top figure shows that, in the second phase, MONSUN 2 and MONSUN 3 submerged to carry out their monitoring tasks; both figures show that, in the third phase, the process of exchange was initiated as the level of energy of MONSUN 2 became low after a period of activity; the exact position where the exchange took place between MONSUN 2 and MONSUN 4 is highlighted by the arrow

8.5 Summary

The present chapter focused on the proposed energy load balancing approach for multiple AUV formations to facilitate longer performance of underwater exploration tasks and environmental monitoring. This approach demonstrated that it could enhance the duration of a mission by up to 32% based on the process of exchange

between the members of the V-shape formation. MARS was the simulator that was employed to conduct the evaluation. The simulation outcomes revealed that the members succeeded in creating a V-shape and a number of the members submerged to the lower layer to conduct monitoring tasks. The exchange was initiated when one member displayed a low energy level, thus enabling the successful completion of the mission.

9 Conclusion and Future Work

The following chapter sets out the main findings, outputs and conclusions realized by the research reported in this thesis. The study aimed to assess the viability of a small or micro AUV that could be utilized to produce a swarm of AUVs for environmental monitoring applications. The scope of the research covered the mechatronic aspects of the vehicle. These included the body, propulsion systems and the associated control circuitry, and basic motion control systems.

The research undertaken can be considered successful. It enabled the design of a streamlined, practical micro AUV, into which a comprehensive sensor suite can be incorporated. As far as the researcher is aware, this innovative micro AUV is the first of its kind in terms of its streamlined shape in form of a guitar fish. It also has the functionality of a traditional AUV, but it also incorporates an acoustic communication system to produce and apply swarm behavior.

9.1 Conclusion

It was realized that there were no suitable AUVs taking account of energy consumption that could be utilized in the study of a swarm of AUVs. This is especially relevant for environmental monitoring functions in many inland and coastal waters. This pointed to the need for a new vehicle to be designed and constructed.

This study carried out and tested the mechanical design, drawing, building, 3D printing, and assembly of a micro AUV called SEMBIO. The vehicle was equipped with a bespoke propulsion system, electrical design, sensing function, and embedded system. All of these components were selected carefully to fit with the overall design of the micro AUV.

SEMBIO was mostly constructed with components that were inexpensive and already available. The propellers, motors, sensors, and the discrete components for the PCBs were all standard, while the hull and its seal, motor mounting ring and PCBs were customized. One of the requirements was to incorporate an acoustic modem, but this was not implemented, because the relevant modem equipment was unavailable at the time of the research. The estimated cost of the mechatronic components was less than 780 €, excluding including labor for construction.

Nature, specifically an organism known as a guitarfish, was the initial influence for creating the flattened and streamlined form of SEMBIO, including the optimal

shape of the hull. This flattened and streamlined shape was accomplished and optimized through use of CFD and SolidWorks, allowing a hydrodynamic analysis of the micro AUV to determine possible enhancements to the hull. After many versions of the hull were produced, an ideal version was achieved, with minimal drag, and consequently, low energy consumption.

The propulsion system is important in aiding vehicle motion in both the horizontal and vertical planes with minimal energy consumption. A review of propulsion systems for small-scale vehicles was conducted. This research found that propellers linked to BLDC electric motors would be most appropriate for use in SEMBIO. No suitable small, low-power, linear actuators were available to use with a micro AUV. An interesting part of the research was devising propeller-based thruster units to achieve the optimal propeller for the thruster and the necessary thrust with the highest performance, i.e., maximum productive thrust with minimum energy consumption.

SEMBIO contained six thrusters that provided high maneuverability in five DOFs. This enabled the vehicle to move in many directions and to operate in hard-to-reach and poorly defined areas, making it better suited for environmental monitoring. However, closed-loop control was implemented and achieved in the heave model.

Movement in the vertical axis is independent of movement in the horizontal plane. System identification was undertaken to determine the heave model of SEMBIO. A model was devised to perform controller development for the vehicle, and the controllers identified as most suitable for this study were PID and SMC.

It was established that the PID controller was more affected by noise than the SMC controller. The latter controller performed better in terms of overshoot and steady-state error and oscillations. It was concluded that the SMC was the most simple, robust, and appropriate option for micro AUVs. Testing was carried out effectively with the heave controller. An experiment with an RMS error of 0.491 cm and a maximal error of 1.43 cm demonstrated that SEMBIO had the same capacity for movement as a traditional AUV.

SEMBIO has a horizontal clearance of 70 cm and a vertical clearance of 10 cm, and it weighs 7 kg, thus attaining the mechatronic requirement of a small, handy sized vehicle. This micro AUV is sufficiently small to limit the cost of its transport to the site of use. The tests demonstrated that it could be manually operated with ease from a shore or a boat. Moreover, the vehicle's micro size means that it can be manufactured cost effectively in large quantities.

The vehicle was supported with SEMS. This is a simple system for controlling the restricted in-vehicle energy source, so as to reduce energy consumption and extend mission time. SEMS achieves this through its integrated parts, which worked together. The researcher assumes a system that assists practitioners in building AUV components, and in defining missions, tasks, and subtasks. In addition, to aid the retrieval of the micro AUV in emergency circumstances, a further system,

ERS, was built into SEMBIO. Trials were conducted to assess the performance of both systems. It was evident from the findings that, when utilizing SEMS, the micro AUV consumed less power up to 42%. This resulted in extended battery life and the vehicle accomplishing more tasks before it had to be returned to the base for a battery recharge.

SEMBIO was powered by Li-Po rechargeable batteries, realizing the vision of battery recharge without it needing to be removed from the vehicle. A power switchboard was devised to connect the batteries to an external charger through the data connector. This connector can also used to transfer data between the micro AUV and a computer via a tether.

The load-balancing approach was employed to maximize the energy efficiency and lengthen the operational period of multiple AUVs. An evaluation was undertaken in the MARS simulator. The findings indicated that the AUVs grouped effectively in a V-shape and that several vehicles could dive into the desired depth to conduct monitoring activities. The exchange of vehicles within the V-shape formation could extend overall mission duration by up to 32%. Exchange was activated after the energy supply of one vehicle was almost consumed, and then progressed to a successful conclusion.

9.2 Future Work

Despite its successes, the micro AUV SEMBIO that was proposed and developed in this research is still far from perfect. Experimental vehicle field testing will be accorded greater priority in future expansions of this research. Some design features remain unfinished, such as the incorporation of the acoustic communication system, which would enable not only the testing of a complete three-dimensional closed-loop control, but also communication with base stations and other vehicles, thus facilitating transmission of sensor data to the operator. Achievement of this will permit the next step of the vehicle re-design to make the vehicle more market appropriate.

Navigating and guiding the vehicle during environmental monitoring is the main aspect that future study should address. The development and incorporation of an obstacle detection system would be necessary to allow for optimal swarm formation. For this purpose, either acoustic transducers or lasers could be employed as sensors. The minimum working range of acoustic transducers is 0.5 m, meaning that objects nearer than this could be missed due to ringing in the transducers. Lasers could be used instead of acoustic transducers or alongside them to detect objects in a close range. Water turbidity would determine how effective lasers could be [126, 244].

Future research could explore in more depth robot vision as well. Due to reduced detection ranges and low visibility, cameras have not attracted much interest as underwater sensors. Nevertheless, underwater sensing could benefit from camera-

generated visual data and cameras could particularly help to detect objects at close range. High-resolution information about how nearby objects and terrain are shaped and what their range is based on video images together with specialized machine vision algorithms would be useful.

State estimation needs to be studied in greater depth as well. Other projects have employed Kalman filters more or less successfully. Non-linear observers could be considered a different option to Kalman filters. The yaw DOF should be modelled more precisely, and the use of a digital compass in conjunction with rate gyroscope demands more research. However, the compass is affected by magnetic interference and does not function adequately in turbulent water. Thus, it is worth endeavoring to determine how and when the rate gyroscope should be used instead of the compass, and obstacle detection sensors may be necessary for this shift. Attention could be paid to gyroscope recalibration during the mission to diminish drift.

Regarding energy concepts and management, future research should focus on expanding the SEMS concept to integrate a range of AUV types and produce a manifest file mapping the AUV components with main board pins to verify the components prior to mission launch. The subject of smart energy management also demands consideration so that vehicle components can be controlled according to environmental conditions and mission characteristics.

Another interesting topic is the development of inductive charging for underwater use. Preliminary exploration of inductive charging revealed that this approach may lack practicality due to system inefficiencies producing significant heat and the complex nature of the necessary circuits. However, a related and interesting challenge would be to develop recharge stations to prolong vehicle operation time.

Last, but not least, for future work, a range of applications could benefit from the technology intended for environmental facility monitoring. For example, the AUVs could be deployed in facilities, such as in water and wastewater industries or in reservoirs.

Personal Publications

- Amory, A., Maehle, E. Modelling and CFD Simulation of a Micro Autonomous Underwater Vehicle SEMBIO. Proceedings of OCEANS 2018 MTS/IEEE Charleston, USA, 2018.

- Behrje, U., Amory, A., and Maehle, E. System identification and sliding mode depth control of the micro AUV SEMBIO. In 50th International Symposium on Robotics (ISR 2018), Munich, Germany 2018.

- Amory, A., Maehle, E: SEMBIO - A Small Energy-Efficient Swarm AUV. Proceedings of OCEANS 2016 MTS/IEEE Monterey, USA, 2016.

- Amory, A., Maehle, E.: SEMBIO: An Energy Efficient Underwater Swarm Robot for Environmental Monitoring. International Conference on Intelligent Robots and Systems (IROS), IEEE/RSJ, Hamburg, Germany 2015.

- Amory, A., Tosik, T., and Maehle, E. A load balancing behavior for underwater robot swarms to increase mission time and fault tolerance. In Parallel Distributed Processing Symposium Workshops (IPDPSW), 2014 IEEE International (May 2014), pp. 1306-1313.

- Renner, C., Meyer, B., Bimschas, D., Gabrecht, A., Ebers, S., Tosik, T., Amory, A., Maehle, E., Fischer, S.: Poster Abstract: Hybrid Underwater Environmental Monitoring. 12th ACM Conference on Embedded Networked Sensor Systems, ACM, Memphis, TN, USA 2014

- Amory, A., Meyer, B., Osterloh, C., Tosik, T., and Maehle, E. Towards fault-tolerant and energy-efficient swarms of underwater robots. In Parallel and Distributed Processing Symposium Workshops and PhD Forum (IPDPSW), 2013 IEEE 27th International (2013), IEEE, pp. 1550-1553.

- Osterloh, C., Meyer, B., Amory, A., Pionteck, T., and Maehle, E. MONSUN II-towards autonomous underwater swarms for environmental monitoring. In International Conference on Intelligent Robots and Systems (IROS), Workshop on Robotics for Environmental Monitoring, Vilamoura, Algarve, Portugal. (2012), pp. 7-12.

Indices

List of Tables

List of Figures

List of Acronyms

ABS Acrylonitrile Butadiene Styrene

AUG Autonomous Underwater Gliders

AUV Autonomous Underwater Vehicle

BAUV Biomimetic Autonomous Undersea Vehicle

BLDC Brushless DC electric motor

CFD Computational Fluid Dynamics

CSI Camera Serial Interface

CTD Conductivity Temperature Depth

DC Direct Current

DOF Degrees Of Freedom

EMF Electromotive Force

ESC Electronic Speed Controller

ERS Emergency and Rescue System

ESH Embedded System Hardware

FEA Finite Element Analysis

GPS Global Positioning System

GSM Global System for Mobile

GRP Fibre-glass Reinforced Plastic

GSM Global System for Mobile

GUI Graphical User Interface

I2C Inter-Integrated Circuit or I square C

IMU Inertial Measurement Unit

LED Light-Emitting Diodes

LES Large Eddy Simulation

ID Unique Identification

Li-Ion Lithium-Ion

Li-Po Lithium-Polymer

LTI Linear Time Invariant

MISO Multiple Input Single Output

MIMO Multiple Input Multiple Output

PCB Printed Circuit Board

PID Proportional Integral Derivative

PLA Poly Lactic Acid

PWM Pulse Width Modulation

RANS Reynolds-averaged Navier-Stokes

Re Reynolds number

ROS Robot Operating System

ROV Remotely Operated Vehicle

RMS Root Mean Square

RPi Raspberry Pi

SAUV Solar-powered Autonomous Underwater Vehicle

SEMS Solar and Energy Management System

SISO Single Input Single Output

SIMO Single Input Multiple Output

SMC Sliding Mode Control

SPI Serial Peripheral Interface

SSR Solid State Relay

St Strouhal number

TF Transfer Function

UART Universal Asynchronous Receiver/Transmitter

USV Unmanned Surface Vehicles

UUV Unmanned Underwater Vehicles

UV Underwater Vehicle

Wi-Fi Wireless Networking Technology

Bibliography

[1] Chapter 10 - Underwater vehicles. In *The Maritime Engineering Reference Book*, A. F. Molland, Ed. Butterworth-Heinemann, Oxford, 2008, pp. 728 – 783.

[2] Aage, C., and Smitt, L. W. Hydrodynamic manoeuvrability data of a flatfish type AUV. In *OCEANS'94.'Oceans Engineering for Today's Technology and Tomorrow's Preservation.'Proceedings* (1994), vol. 3, IEEE, pp. III–425.

[3] Adafruit. Adafruit FONA 808 breakout. Http://www.adafruit.com/product/2542, 2015. [Online; accessed 04-June-2017].

[4] Adafruit. Bluefruit EZ-Link-bluetooth serial. Http://www.adafruit.com/product/1588, 2015. [Online; accessed 27-Aug-2015].

[5] Adafruit. Flexieble solar panel. Http://www.adafruit.com/product/1485, 2015. [Online; accessed 19-Aug-2015].

[6] Adamy, J. *Nichtlineare Regelungen*. Springer-Verlag, 2009.

[7] Agrawal, A., Prasad, B., Viswanathan, V., and Panda, S. K. Dynamic modeling of variable ballast tank for spherical underwater robot. In *2013 IEEE International Conference on Industrial Technology (ICIT)* (Feb 2013), pp. 58–63.

[8] Alam, K., Ray, T., and Anavatti, S. G. Design of a toy submarine using underwater vehicle design optimization framework. *IEEE SSCI 2011: Symposium Series on Computational Intelligence - CIVTS 2011: 2011 IEEE Symposium on Computational Intelligence in Vehicles and Transportation Systems*, November 2015 (2011), 23–29.

[9] Alam, K., Ray, T., and Anavatti, S. G. A new robust design optimization approach for unmanned underwater vehicle design. *Proceedings of the Institution of Mechanical Engineers, Part M: Journal of Engineering for the Maritime Environment 226*, 3 (2012), 235–249.

[10] Allen, B., Stokey, R., Austin, T., Forrester, N., Goldsborough, R., Purcell, M., and von Alt, C. REMUS: a small, low cost AUV; system description, field trials and performance results. In *OCEANS '97. MTS/IEEE Conference Proceedings* (Oct 1997), pp. 994–1000 vol.2.

[11] Allotta, B., Bartolini, F., Conti, R., Costanzi, R., Gelli, J., Monni, N., Natalini, M., Pugi, L., and Ridolfi, A. MARTA: An AUV

for underwater cultural heritage. *Proceedings of the underwater acoustics 2014* (2014).

[12] Allotta, B., Costanzi, R., Ridolfi, A., Colombo, C., Bellavia, F., Fanfani, M., Pazzaglia, F., Salvetti, O., Moroni, D., Pascali, M. A., et al. The ARROWS project: adapting and developing robotics technologies for underwater archaeology. *IFAC-PapersOnLine 48*, 2 (2015), 194–199.

[13] Alvarez, A., Bertram, V., and Gualdesi, L. Hull hydrodynamic optimization of autonomous underwater vehicles operating at snorkeling depth. *Ocean Engineering 36*, 1 (2009), 105–112.

[14] Amory, A. Identification and modeling of static diving system of AUV-MONSUN II and PID controller design. Master's thesis, Institute of Computer Engineering - University of Luebeck, Luebeck, 2011.

[15] Amory, A., and Maehle, E. SEMBIO-a small energy-efficient swarm AUV. In *OCEANS 2016 MTS/IEEE Monterey* (2016), IEEE, pp. 1–7.

[16] Amory, A., Meyer, B., Osterloh, C., Tosik, T., and Maehle, E. Towards fault-tolerant and energy-efficient swarms of underwater robots. In *Parallel and Distributed Processing Symposium Workshops & PhD Forum (IPDPSW), 2013 IEEE 27th International* (2013), IEEE, pp. 1550–1553.

[17] Amory, A., Tosik, T., and Maehle, E. A load balancing behavior for underwater robot swarms to increase mission time and fault tolerance. In *Parallel Distributed Processing Symposium Workshops (IPDPSW), 2014 IEEE International* (May 2014), pp. 1306–1313.

[18] Anderson, J. M., and Chhabra, N. K. Maneuvering and stability performance of a robotic tuna. *Integrative and comparative biology 42*, 1 (2002), 118–126.

[19] Antonelli, G., and Leonessa, A. Underwater robots: motion and force control of vehicle-manipulator systems. *IEEE Control Systems Magazine* (2008), 138–139.

[20] Applied Physics Laboratory University of Washington. The self propelled underwater research vehicle (SPURV). Http://www.apl.washington.edu/about/history.php, 2017. [Online; accessed 22-March-2017].

[21] Araki, M. Control systems, robotics, and automation. *Encyclopedia of Life Support Systems (EOLSS) 2* (1993).

[22] Barngrover, C., Kastner, R., Denewiler, T., and Mills, G. The stingray AUV: A small and cost-effective solution for ecological monitoring. In *OCEANS'11 MTS/IEEE KONA* (Sept 2011), pp. 1–8.

[23] Barrett, D., Triantafyllou, M., Yue, D., Grosenbaugh, M., and Wolfgang, M. Drag reduction in fish-like locomotion. *Journal of Fluid Mechanics 392* (1999), 183–212.

[24] Barrett, N., Seiler, J., Anderson, T., Williams, S., Nichol, S., and Hill, S. N. Autonomous underwater vehicle (AUV) for mapping marine biodiversity in coastal and shelf waters: Implications for marine management. In *OCEANS 2010 IEEE - Sydney* (May 2010), pp. 1–6.

[25] Bayat, B., Crespi, A., and Ijspeert, A. Envirobot: A bio-inspired environmental monitoring platform. In *Autonomous Underwater Vehicles (AUV), 2016 IEEE/OES* (2016), Ieee, pp. 381–386.

[26] Behrje, U., Amory, A., and Maehle, E. System identification and sliding mode depth control of the micro AUV SEMBIO. In *50th International Symposium on Robotics (ISR 2018)* (Munich, Germany, June 2018).

[27] Behrje, U., Isokeit, C., Meyer, B., and Maehle, E. A robust acoustic-based communication principle for the navigation of an underwater robot swarm. In *OCEANS–Kobe, 2018* (2018), IEEE.

[28] Bellingham, J. Autonomous underwater vehicles (AUVs). In *Encyclopedia of Ocean Sciences*. Elsevier BV, 2001, pp. 212–216.

[29] Bellingham, J. G. New oceanographic uses of autonomous underwater vehicles. *Marine Technology Society. Marine Technology Society Journal 31*, 3 (1997), 34.

[30] Bellingham, J. G., Goudey, C., Consi, T., Chryssostomidis, C., et al. A small, long-range autonomous vehicle for deep ocean exploration. In *The Second International Offshore and Polar Engineering Conference* (1992), International Society of Offshore and Polar Engineers.

[31] Bellingham, J. G., Zhang, Y., Kerwin, J. E., Erikson, J., Hobson, B., Kieft, B., Godin, M., McEwen, R., Hoover, T., Paul, J., et al. Efficient propulsion for the Tethys long-range autonomous underwater vehicle. In *Autonomous Underwater Vehicles (AUV), 2010 IEEE/OES* (2010), IEEE, pp. 1–7.

[32] Blidberg, D. R. The development of autonomous underwater vehicles (AUV); a brief summary. In *IEEE ICRA* (2001), vol. 4.

[33] Bonin-Font, F., Massot-Campos, M., Negre-Carrasco, P. L., Oliver-Codina, G., and Beltran, J. P. Inertial sensor self-calibration in a visually-aided navigation approach for a micro-AUV. *Sensors 15*, 1 (2015), 1825–1860.

[34] Botelho, S., Neves, R., and Taddei, L. Localization of a fleet of AUVs using visual maps. In *Europe Oceans 2005* (June 2005), vol. 2, pp. 1320–1325 Vol. 2.

[35] Bovio, E., Cecchi, D., and Baralli, F. Autonomous underwater vehicles for scientific and naval operations. *Annual Reviews in Control 30*, 2 (2006), 117–130.

[36] Brambilla, M., Ferrante, E., Birattari, M., and Dorigo, M. Swarm robotics: a review from the swarm engineering perspective. *Swarm Intelligence 7*, 1 (2013), 1–41.

[37] Burguera, A., González, Y., and Oliver, G. The UspIC: Performing scan matching localization using an imaging sonar. *Sensors 12*, 12 (jun 2012), 7855–7885.

[38] Bushnell, D. M., and Moore, K. Drag reduction in nature. *Annual Review of Fluid Mechanics 23*, 1 (1991), 65–79.

[39] Button, R. W., Kamp, J., Curtin, T. B., and Dryden, J. *A survey of missions for unmanned undersea vehicles.* Rand national Defense Research Inst., Santa Monica, 2009.

[40] Camilli, R., and Hemond, H. Nereus/kemonaut, a mobile autonomous underwater mass spectrometer. *TrAC Trends in Analytical Chemistry 23*, 4 (2004), 307–313.

[41] Cao, Y., Yu, W., Ren, W., and Chen, G. An overview of recent progress in the study of distributed multi-agent coordination. *IEEE Transactions on Industrial informatics 9*, 1 (2013), 427–438.

[42] Carlson, A. Implementing precision control for rc submarine, 2016. [Online; accessed 11-March-2018]. Http://www.eetasia.com/news/article/implementing-precision-control-for-rc-submarine.

[43] Carreiro, L. G., and Burke, A. A. Unmanned underwater vehicles. In *7th Annual SECA Workshop and Peer Review Meeting* (2006).

[44] Carrier, J. C., Musick, J. A., and Heithaus, M. R. *Biology of sharks and their relatives.* CRC press, 2012.

[45] Charmed. Pixy CMUcam5. Http://charmedlabs.com/default/pixy-cmucam5/, 2015. [Online; accessed 18-Sep-2015].

[46] Chemori, A., Kuusmik, K., Salumae, T., and Kruusmaa, M. Depth control of the biomimetic U-CAT turtle-like AUV with experiments in real operating conditions. In *2016 IEEE International Conference on Robotics and Automation (ICRA)* (May 2016), pp. 4750–4755.

[47] Chen, M., and Chen, W.-H. Sliding mode control for a class of uncertain nonlinear system based on disturbance observer. *International Journal of Adaptive Control and Signal Processing 24*, 1 (2010), 51–64.

[48] Chen, Y. Q., and Wang, Z. Formation control: a review and a new consideration. In *Intelligent Robots and Systems, 2005.(IROS 2005). 2005 IEEE/RSJ International Conference on* (2005), IEEE, pp. 3181–3186.

[49] Chitre, M. Teamwork among marine robots–advances and challenges. In *Workshop on Marine Robotics* (2013).

[50] Chong, C. W., Zhong, Y., Zhou, C. L., Low, K. H., Gerald, S. G. L., and Lim, H. B. Can the swimming thrust of bcf biomimetics fish be enhanced? In *2008 IEEE International Conference on Robotics and Biomimetics* (Feb 2009), pp. 437–442.

[51] Christensen, L., Kampmann, P., Hildebrandt, M., Albiez, J., and Kirchner, F. Hardware ROV simulation facility for the evaluation of novel underwater manipulation techniques. In *OCEANS 2009-EUROPE* (2009), IEEE, pp. 1–8.

[52] Clark, R. P., and Smits, A. J. Thrust production and wake structure of a batoid-inspired oscillating fin. *Journal of fluid mechanics 562* (2006), 415–429.

[53] Clarke, M. E., Whitmire, C., Fruh, E., Anderson, J., Taylor, J., Rooney, J., Ferguson, S., and Singh, H. Developing the SeaBED AUV as a tool for conducting routine surveys of fish and their habitat in the Pacific. In *Proceedings of* (2010).

[54] Connectivity, T. Pressure Sensors. Http://www.te.com/usa-en/product-CAT-BLPS0013.html, 2014. [Online; accessed 11-Jun-2014].

[55] Crimmins, D., Patty, C., Beliard, M., Baker, J., Jalbert, J., Komerska, R., Chappell, S., and Blidberg, D. Long-endurance test results of the solar-powered AUV system. In *OCEANS 2006* (2006), pp. 1–5.

[56] Cruz, N. A., and Alves, J. C. Ocean sampling and surveillance using autonomous sailboats. In *IRSC 2008 International Robotic Sailing Conference* (2008), p. 30.

[57] Cui, R., Ge, S. S., How, B. V. E., and Choo, Y. S. Leader–follower formation control of underactuated autonomous underwater vehicles. *Ocean Engineering 37*, 17 (2010), 1491–1502.

[58] Cui, S., Wu, L., Zhao, L., and Bing, Z. Research on method of multi-agent formation control. In *Power Electronics and Design (APED), 2010 Asia-Pacific Conference on* (2010), pp. 59–62.

[59] Curtin, T. B., Bellingham, J. G., Catipovic, J., and Webb, D. Autonomous oceanographic sampling networks. *Oceanography 6*, 3 (1993), 86–94.

[60] Cutts, C., and Speakman, J. Energy savings in formation flight of pink-footed geese. *Journal of Experimental Biology 189*, 1 (1994), 251–261.

[61] Diercks, A. R., Woolsey, M., Jarnagin, R., Asper, V. L., Dike, C., D'Emidio, M., Tidwell, S., and Conti, A. Site reconnaissance surveys for oil spill research using deep-sea AUVs. In *2013 OCEANS - San Diego* (Sept 2013), pp. 1–5.

[62] DIGI. XBEE 2.4 GHz series of modules. Http://www.digi.com/products/xbee-rf-solutions/2-4-ghz-modules, 2015. [Online; accessed 27-Sep-2015].

[63] Dorigo, M., and Şahin, E. Guest editorial. *Autonomous Robots 17*, 2 (2004), 111–113.

[64] Dudek, G., Jenkin, M., Prahacs, C., Hogue, A., Sattar, J., Giguere, P., German, A., Liu, H., Saunderson, S., Ripsman, A., Simhon, S., Torres, L. A., Milios, E., Zhang, P., and Rekletis, I. A visually guided swimming robot. In *2005 IEEE/RSJ International Conference on Intelligent Robots and Systems* (Aug 2005), pp. 3604–3609.

[65] Ehlers, K., Meyer, B., and Maehle, E. Full holonomic control of the omni-directional AUV SMART-E. In *ISR/Robotik 2014; 41st International Symposium on Robotics; Proceedings of* (2014), VDE, pp. 1–6.

[66] Endicott, D., and Kuhl, G. The fast area search system (fass). a feasibility study. Tech. rep., DTIC Document, 1992.

[67] Eriksen, C. C., Osse, T. J., Light, R. D., Wen, T., Lehman, T. W., Sabin, P. L., Ballard, J. W., and Chiodi, A. M. Seaglider: a long-range autonomous underwater vehicle for oceanographic research. *IEEE Journal of Oceanic Engineering 26*, 4 (Oct 2001), 424–436.

[68] Erlerobotics. PXFmini Board. Http://docs.erlerobotics.com/brains/pxfmini, 2015. [Online; accessed 12-Sep-2016].

[69] Fantone, S. J., Leitermann, O., Austin-Breneman, J., Eastment, A. S., and Crumlin, E. The autonomous underwater vehicle" pipsqueak". In *OCEANS'02 MTS/IEEE* (2002), vol. 4, IEEE, pp. 2497–2501.

[70] Fish, F., and Lauder, G. Passive and active flow control by swimming fishes and mammals. *Annu. Rev. Fluid Mech. 38* (2006), 193–224.

[71] Fish, F. E. Imaginative solutions by marine organisms for drag reduction. In *Proceedings of the International Symposium on Seawater Drag Reduction* (1998), Newport, Rhode Island, pp. 443–450.

[72] Fish, F. E., and Beneski, J. T. *Evolution and Bio-Inspired Design: Natural Limitations*. Springer London, London, 2014, pp. 287–312.

[73] Fish, F. E., Lauder, G. V., Mittal, R., Techet, A. H., Triantafyllou, M. S., Walker, J. A., and Webb, P. W. Conceptual design for the construction of a biorobotic AUV based on biological hydrodynamics. In *13th International Symposium on Unmanned Untethered Submersible Technology, Durham, NH, Aug* (2003), pp. 24–27.

[74] Fish, F. E., and Rohr, J. Review of dolphin hydrodynamics and swimming performance. Tech. rep., Space and naval warfare systems commandSan Diego CA, 1999.

[75] Fossen, T. I. *Guidance and Control of Ocean Vehicles*. JOHN WILEY & SONS INC, 1994.

[76] Fossen, T. I. *Handbook of marine craft hydrodynamics and motion control*. John Wiley & Sons, 2011.

[77] Freitag, L., Grund, M., Singh, S., Partan, J., Koski, P., and Ball, K. The whoi micro-modem: an acoustic communications and navigation system for multiple platforms. In *Proceedings of OCEANS 2005 MTS/IEEE* (Sept 2005), pp. 1086–1092 Vol. 2.

[78] Freitag, L., Johnson, M., Grund, M., Singh, S., and Preisig, J. Integrated acoustic communication and navigation for multiple UUVs. In *OCEANS, 2001. MTS/IEEE Conference and Exhibition* (2001), vol. 4, IEEE, pp. 2065–2070.

[79] Gao, T., Wang, Y., Pang, Y., and Cao, J. Hull shape optimization for autonomous underwater vehicles using cfd. *Engineering Applications of Computational Fluid Mechanics 10*, 1 (2016), 599–607.

[80] Gomáriz, S., Masmitjà, I., González, J., Masmitjà, G., and Prat, J. GUANAY-II: an autonomous underwater vehicle for vertical/horizontal sampling. *Journal of Marine Science and Technology 20*, 1 (2015), 81–93.

[81] Gould, W. J. From swallow floats to argo-the development of neutrally buoyant floats. *Deep Sea Research Part II: Topical Studies in Oceanography 52*, 3 (2005), 529–543.

[82] Griffiths, G., Birch, K., Millard, N., McPhail, S., Stevenson, P., Pebody, M., Perrett, J., Webb, A., Squires, M., Harris, A., et al. Oceanographic surveys with a 50 hour endurance autonomous underwater vehicle. In *Offshore Technology Conference* (2000).

[83] Guan, Z., Gao, W., Gu, N., and Nahavandi, S. 3D hydrodynamic analysis of a biomimetic robot fish. *11th International Conference on Control, Automation, Robotics and Vision, ICARCV 2010* (2010), 793–798.

[84] Guo, J. Maneuvering and control of a biomimetic autonomous underwater vehicle. *Autonomous Robots 26*, 4 (May 2009), 241–249.

[85] Hagen, P. E., Storkersen, N., Vestgard, K., and Kartvedt, P. The HUGIN 1000 autonomous underwater vehicle for military applications. In *Oceans 2003. Celebrating the Past ... Teaming Toward the Future (IEEE Cat. No.03CH37492)* (Sept 2003), pp. 1141–1145 Vol.2.

[86] Han, X., and Neubauer, M. A research on the switching control laws for synchronised switch damping on inductor technique. *International Journal of Mechatronics and Automation 2*, 3 (2012), 207–216.

[87] Hanff, H., Schmid, K., Kloss, P., and Kroffke, S. μAUV 2-development of a minuscule autonomous underwater vehicle. *International Conference on Informatics in Control, Automation and Robotics (ICINCO-2016)* (2016).

[88] Heine, C. *Mechanics of Flapping Fin Locomotion in the Cownose Ray, Rhinoptera Bonasus (Elasmobranchii, Myliobatidae)*. Duke University, 1992.

[89] Heiszwolf, J. J. Submarine dive technology. Http://www.heiszwolf.com/subs/tech/tech01.html, 2017. [Online; accessed 22-March-2017].

[90] Hennings, S. Energy management system for autonomous underwater vehicle. Bachelor's thesis, Institute of Computer Engineering - University of Luebeck, Luebeck, 2016.

[91] Hennings, S. Rescue system for sembio. Master's thesis, Institute of Computer Engineering - University of Luebeck, Luebeck, 2018.

[92] Hiller, T., Steingrimsson, A., and Melvin, R. Positioning small AUVs for deeper water surveys using inverted USBL. In *Proceedings Hydro12 - Taking care of the sea, Hydrographic Society Benelux* (November 2012).

[93] Hobson, B., Schulz, B., Janét, J., Kemp, M., Moody, R., Pell, C., and Pinnix, H. Development of a micro autonomous underwater vehicle for complex 3-D sensing. In *OCEANS, 2001. MTS/IEEE Conference and Exhibition* (2001), vol. 4, IEEE, pp. 2043–2045.

[94] Hobson, B., Schulz, B., Pinnix, H., Moody, R., Kemp, M., and Pell, C. Low-cost UUVs for task specific and expendable missions. In *13th International Symposium on Unmanned Untethered Submersible Technology [C/CD]. New Hampshire, USA: New Hampshire University Press* (2003).

[95] Horner, D. P., Healey, A. J., and Kragelund, S. P. AUV experiments in obstacle avoidance. In *Proceedings of OCEANS 2005 MTS/IEEE* (Sept 2005), pp. 1464–1470 Vol. 2.

[96] Houghton, E., and Carpenter, P. *Aerodynamics for Engineering Students*. Elsevier Science, 2003.

[97] Hu, H. Biologically inspired design of autonomous robotic fish at essex. In *proceedings of the IEEE SMC UK-RI chapter conference* (2006), pp. 1–8.

[98] Hussein, A.-A., Govindu, V., and Nigusse, A. G. M. Evaluation of groundwater potential using geospatial techniques. *Applied Water Science* (2016), 1–15.

[99] Hyakudome, T. Design of autonomous underwater vehicle. *International Journal of Advanced Robotic Systems 8*, 1 (2011), 9.

[100] Hydro-International. AUVs: A view of the autonomous underwater vehicle market. *Hydro International* (2013).

[101] Hylands. Nanoseeker micro AUV, 2016. [Online; accessed 14-March-2016]. URL: http://www.huv.com/nanoSeeker/pics/index.html.

[102] INA219. Current sensor. Http://www.ti.com/lit/ds/symlink/ina219.pdf, 2015. [Online; accessed 13-Sep-2015].

[103] IntegratedThruster. A propeller design and optimise company. Http://www.tsltechnology.com/docs/PA-THR-DS-0008.pdf, 2017. [Online; accessed 29-April-2017].

[104] Jagadeesh, P., Murali, K., and Idichandy, V. Experimental investigation of hydrodynamic force coefficients over AUV hull form. *Ocean Engineering 36*, 1 (2009), 113–118.

[105] Jain, N., and Alleyne, A. G. Comparison of SISO and MIMO control techniques for a diagonally dominant vapor compression system. In *American Control Conference, 2009. ACC'09.* (2009), IEEE, pp. 1580–1585.

[106] Jakab, P. L. *Visions of a flying machine: The Wright brothers and the process of invention.* Smithsonian Institution, 2014.

[107] Jalbert, J., Baker, J., Duchesney, J., Pietryka, P., Dalton, W., Blidberg, D., Chappell, S., Nitzel, R., and Holappa, K. A solar-powered autonomous underwater vehicle. In *Oceans 2003. Proceedings* (2003), vol. 2, IEEE, pp. 1132–1140.

[108] Javaid, M. Y., Ovinis, M., Nagarajan, T., and Hashim, F. B. Underwater gliders: A review. In *MATEC Web of Conferences* (2014), vol. 13, EDP Sciences, p. 02020.

[109] Jiang, Y., Wang, S., Ishida, K., Ando, T., and Fujie, M. G. A novel direction control method for walking support with an omnidirectional walker. *International Journal of Mechatronics and Automation 1*, 3-4 (2011), 244–252.

[110] Joordens, M. A., Shaneyfelt, T., Nagothu, K., Jaimes, A., and Jamshidi, M. Applications and prototype for system of systems swarm robotics. In *Systems, Man and Cybernetics, 2008. SMC 2008. IEEE International Conference on* (Oct 2008), pp. 2049–2055.

[111] Joung, T., Sammut, K., He, F., Lee, S.-K., et al. A study on the design optimization of an AUV by using computational fluid dynamic analysis. In *The Nineteenth International Offshore and Polar Engineering Conference* (2009), International Society of Offshore and Polar Engineers.

[112] Kalantar, S., and Zimmer, U. R. Contour shaped formation control for autonomous underwater vehicles using canonical shape descriptors and deformable models. In *OCEANS '04. MTTS/IEEE TECHNO-OCEAN '04* (Nov 2004), vol. 1, pp. 296–307 Vol.1.

[113] Kalantar, S., and Zimmer, U. R. Scale-adaptive polygonal formations of submersible vehicles and tracking isocontours. In *Intelligent Robots and Systems, 2008. IROS 2008. IEEE/RSJ International Conference on* (2008), IEEE, pp. 3146–3151.

[114] Khan, J. U., and Cho, H.-S. Data-gathering scheme using AUVS in large-scale underwater sensor networks: A multihop approach. *Sensors 16*, 10 (2016), 1626.

[115] Klemas, V., and Pieterse, A. Using remote sensing to map and monitor water resources in arid and semiarid regions. In *Advances in Watershed Science and Assessment*. Springer, 2015, pp. 33–60.

[116] Kokegei, M., He, F., and Sammut, K. *Fully coupled 6 degree-of-freedom control of an over-actuated autonomous underwater vehicle*. INTECH Open Access Publisher, 2011.

[117] Kongsberg-Maritime. Autonomous underwater vehicle-REMUS 100. Https://www.km.kongsberg.com, 2017. [Online; accessed 22-March-2017].

[118] Kottege, N., and Zimmer, U. R. Relative localisation for AUV swarms. In *2007 Symposium on Underwater Technology and Workshop on Scientific Use of Submarine Cables and Related Technologies* (April 2007), pp. 588–593.

[119] Kudo, K. Overseas trends in the development of human occupied deep submersibles and a proposal for japan's way to take. *Sci. Technol. Trends 26* (2008), 104–123.

[120] Last, P. R., and Stevens, J. D. *Sharks and rays of Australia*. Australia: CSIRO; ISBN: 0-643-05143-0, 1994.

[121] Lee, F. Y., Jun, B. H., Lee, P. M., and Kim, K. Implementation and test of ISiMI100 AUV for a member of AUVs fleet. In *OCEANS 2008* (Sept 2008), pp. 1–6.

[122] Lermusiaux, P. Estimation and study of mesoscale variability in the Strait of Sicily. *Dynamics of Atmospheres and Oceans 29*, 2 (1999), 255–303.

[123] Li, M., Guo, S., Hirata, H., and Ishihara, H. Design and performance evaluation of an amphibious spherical robot. *Robotics and Autonomous Systems 64* (2015), 21–34.

[124] Linke, P., and Lackschewitz, K. Autonomous underwater vehicle ABYSS. *Journal of large-scale research facilities JLSRF 2* (2016), 79.

[125] Listak, M., Martin, G., Pugal, D., Aabloo, A., and Kruusmaa, M. Design of a semiautonomous biomimetic underwater vehicle for environmental monitoring. In *Computational Intelligence in Robotics and Automation, 2005. CIRA 2005. Proceedings. 2005 IEEE International Symposium on* (2005), IEEE, pp. 9–14.

[126] Liu, J., Jia, Y., and Xi, N. Identification of road surface conditions based on laser scanning. In *2013 IEEE International Conference on Robotics and Biomimetics (ROBIO)* (Dec 2013), pp. 2476–2481.

[127] Ludvigsen, M., Ellingsen, I., Odegaard, O. T., and Sortland, B. Model supported AUV freshwater distribution surveys in the upper layers of deep fjords. In *Oceans 2003. Celebrating the Past ... Teaming Toward the Future (IEEE Cat. No.03CH37492)* (Sept 2003), vol. 4, pp. 1969–1975 Vol.4.

[128] Lutz, T., and Wagner, S. Numerical shape optimization of natural laminar flow bodies. In *Proceedings of 21st ICAS Congress* (1998).

[129] López-Sánchez, M., and Cerquides., J. Formation maintenance for autonomous robots by steering behaviour parameterization. *book: Recent Advances in Control Systems, Robotics and Automation (ISBN: 88-901928-0-1). Ed. S. Pennacchio. InternationalSAR* (2006), 134–139.

[130] Maas, R., and Maehle, E. Fault tolerant and adaptive path planning in crowded environments for mobile robots based on hazard estimation via health signals. *Lecture Notes in Informatics (LNI) - Proceedings, Volume P-200, ISBN 978-3-88579-294-9, Bonner Köllen Verlag* (2012), 221–232.

[131] MacIver, M. A., Fontaine, E., and Burdick, J. W. Designing future underwater vehicles: principles and mechanisms of the weakly electric fish. *IEEE Journal of Oceanic Engineering 29*, 3 (July 2004), 651–659.

[132] Majid, M., and Arshad, M. Hydrodynamic effect on v-shape pattern formation of swarm autonomous surface vehicles (ASVs). *Procedia Computer Science 76* (2015), 186–191.

[133] Mallios, A., Ridao, P., Carreras, M., and Hernández, E. Navigating and mapping with the SPARUS AUV in a natural and unstructured underwater environment. In *OCEANS 2011* (2011), IEEE, pp. 1–7.

[134] Marthiniussen, R., Vestgard, K., Klepaker, R. A., and Storkersen, N. HUGIN-AUV concept and operational experiences to date. In *OCEANS '04. MTTS/IEEE TECHNO-OCEAN '04* (Nov 2004), pp. 846–850 Vol.2.

[135] Massey, B., and Ward-Smith, J. *Mechanics of Fluids, Seventh Edition*. Taylor & Francis, 1998.

[136] Meng, L., and Qingyu, Y. Enhanced safety control and self-rescue system applied in AUV. In *Intelligent Computation Technology and Automation (ICICTA), 2010 International Conference on* (2010), vol. 2, IEEE, pp. 212–215.

[137] Meyer, B., Ehlers, K., Isokeit, C., and Maehle, E. The development of the modular hard-and software architecture of the autonomous underwater vehicle MONSUN. In *ISR/Robotik 2014; 41st International Symposium on Robotics; Proceedings of* (2014), VDE, pp. 1–6.

[138] Meyer, B., Isokeit, C., Maehle, E., and Baschek, B. Using small swarm-capable AUVs for submesoscale eddy measurements in the Baltic Sea. In *OCEANS–Anchorage, 2017* (2017), IEEE, pp. 1–5.

[139] Meyer, B., Renner, C., and Maehle, E. Versatile sensor and communication expansion set for the autonomous underwater vehicle MONSUN. In *Advances in Cooperative Robotics*. World Scientific, 2016, pp. 250–257.

[140] Meyer, D. Glider technology for ocean observations: A Review. *Ocean Science Discussions* (jul 2016), 1–26.

[141] Michel, J.-L., and Le Roux, H. Epaulard:-deep bottom surveys now with acoustic remote controlled vehicle-first operational experience. In *OCEANS 81* (1981), IEEE, pp. 99–103.

[142] Mindell, D., and Bingham, B. New archaeological uses of autonomous underwater vehicles. In *OCEANS, 2001. MTS/IEEE Conference and Exhibition* (2001), vol. 1, IEEE, pp. 555–558.

[143] MIT Sea Grant AUV Lab. The Odyssey II class of AUV. Https://auvlab.mit.edu/, 2017. [Online; accessed 22-March-2017].

[144] Moored, K. W., Fish, F. E., Kemp, T. H., and Bart-Smith, H. Batoid fishes: inspiration for the next generation of underwater robots. *Marine Technology Society Journal 45*, 4 (2011), 99–109.

[145] Myring, D. A theoretical study of body drag in subcritical axisymmetric flow. *Aeronautical quarterly 27*, 03 (1976), 186–194.

[146] National Maritime Research Institute. Prototype fish robot, PF-600 designed to study propulsion performance. Http://www.nmri.go.jp/eng/khirata/fish/experiment/experimente.htm, 2016. [Online; accessed 28-March-2017].

[147] Newman, P. Unmanned vehicles for shallow and costal waters. Http://www.thsuk.org/documents/ths.org.uk/downloads/shallowwater_auv_and_usv.pdf, 2010. [Online; accessed 14-June-2015].

[148] Nicholson, J., and Healey, A. The present state of autonomous underwater vehicle (AUV) applications and technologies. *Marine Technology Society Journal 42*, 1 (2008), 44–51.

[149] Niu, H., Adams, S., Lee, K., Husain, T., Bose, N., et al. Applications of autonomous underwater vehicles in offshore petroleum industry environmental effects monitoring. *Journal of Canadian Petroleum Technology 48*, 05 (2009), 12–16.

[150] O'Dwyer, A. *Handbook of PI and PID controller tuning rules*. World Scientific, 2009.

[151] Oorni, R., and Goulart, A. In-vehicle emergency call services: eCall and beyond. *IEEE Communications Magazine 55*, 1 (2017), 159–165.

[152] Osterloh, C., Litza, M., and Maehle, E. Hard-and software architecture of a small autonomous underwater vehicle for environmental monitoring tasks. *Advances in Robotics Research* (2009), 347–356.

[153] Osterloh, C., Meyer, B., Amory, A., Pionteck, T., and Maehle, E. MONSUN II-towards autonomous underwater swarms for environmental monitoring. In *International Conference on Intelligent Robots and Systems (IROS), Workshop on Robotics for Environmental Monitoring, Vilamoura, Algarve, Portugal.* (2012), pp. 7–12.

[154] Osterloh, C., Pionteck, T., and Maehle, E. MONSUN II: A small and inexpensive AUV for underwater swarms. In *ROBOTIK 2012; 7th German Conference on Robotics* (May 2012), pp. 1–6.

[155] Ozog, P., Troni, G., Kaess, M., Eustice, R. M., and Johnson-Roberson, M. Building 3d mosaics from an autonomous underwater vehicle, doppler velocity log, and 2d imaging sonar. In *2015 IEEE International Conference on Robotics and Automation (ICRA)* (May 2015), pp. 1137–1143.

[156] Paduan, J. D., and Rosenfeld, L. K. Remotely sensed surface currents in Monterey Bay from shore-based hf radar (Coastal Ocean Dynamics Application Radar). *Journal of Geophysical Research: Oceans 101*, C9 (1996), 20669–20686.

[157] Pailhas, Y., Brown, K., Lane, D., Valeyrie, N., and Capus, C. Developing new sensing capabilities for archaeological operations using wideband sonar systems. In *OCEANS 2016 - Shanghai* (April 2016), pp. 1–4.

[158] Patch, D. A. *A solar energy system for long-term deployment of AUVs.* Autonomous Undersea Systems Institute, 2000.

[159] Pennel, V., Veitch, B., hawboldt, K., and Ferguson, J. Use of autonomous underwater vehicle for environmental effect monitoring. *13th International Symposium on Unmanned Untethered Submersible Technology, Durham, NH, U.S.* (August, 2003).

[160] Petersen, E. E., Kidd, R. W., and Pearce, J. M. Impact of diy home manufacturing with 3d printing on the toy and game market. *Technologies 5*, 3 (2017), 45.

[161] Petrich, J., and Stilwell, D. J. Model simplification for AUV pitch-axis control design. *Ocean Engineering 37*, 7 (2010), 638–651.

[162] Phillips, A., Turnock, S., and Furlong, M. The use of computational fluid dynamics to aid cost-effective hydrodynamic design of autonomous underwater vehicles. *Proceedings of the Institution of Mechanical Engineers, Part M: Journal of Engineering for the Maritime Environment 224*, 4 (2010), 239–254.

[163] Pilskaln, C. H., Lehmann, C., Paduan, J. B., and Silver, M. W. Spatial and temporal dynamics in marine aggregate abundance, sinking rate and flux: Monterey Bay, central California. *Deep Sea Research Part II: Topical Studies in Oceanography 45*, 8 (1998), 1803–1837.

[164] Prahacs, C., Saudners, A., Smith, M. K., McMordie, D., and Buehler, M. Towards legged amphibious mobile robotics. *Proceedings of the Canadian Engineering Education Association* (2004).

[165] Prasad, B., Agrawal, A., Viswanathan, V., Yadav, P., Kumar, R., and Panda, S. K. Energy-efficient optimal thrust allocation for spherical underwater robot. In *2013 IEEE International Symposium on Industrial Electronics* (May 2013), pp. 1–6.

[166] Prestero, T. Development of a six-degree of freedom simulation model for the REMUS autonomous underwater vehicle. In *MTS/IEEE Oceans 2001. An Ocean Odyssey. Conference Proceedings (IEEE Cat. No.01CH37295)* (2001), vol. 1, pp. 450–455 vol.1.

[167] Purcell, M., Gallo, D., Packard, G., Dennett, M., Rothenbeck, M., Sherrell, A., and Pascaud, S. Use of REMUS 6000 AUVs in the search for the Air France Flight 447. In *OCEANS 2011* (2011), pp. 1–7.

[168] Purcell, M., Gallo, D., Sherrell, A., Rothenbeck, M., and Pascaud, S. Use of REMUS 6000 AUVs in the search for the Air France Flight 447. In *OCEANS'11 MTS/IEEE KONA* (Sept 2011), pp. 1–7.

[169] Ray, P., O'Rourke, M., and Edwards, D. The ontological status of autonomous underwater vehicle fleets. In *OCEANS 2009, MTS/IEEE Biloxi - Marine Technology for Our Future: Global and Local Challenges* (Oct 2009), pp. 1–7.

[170] Read, M., Möslinger, C., Dipper, T., Kengyel, D., Hilder, J., Thenius, R., Tyrrell, A., Timmis, J., and Schmickl, T. Profiling underwater swarm robotic shoaling performance using simulation. In *Conference Towards Autonomous Robotic Systems* (2013), Springer, pp. 404–416.

[171] Renner, C., Gabrecht, A., Meyer, B., Osterloh, C., and Maehle, E. Low-power low-cost acoustic underwater modem. In *Quantitative Monitoring of the Underwater Environment*. Springer, 2016, pp. 59–65.

[172] Renner, C., and Golkowski, A. J. Acoustic modem for micro AUVs: design and practical evaluation. In *Proceedings of the 11th ACM International Conference on Underwater Networks & Systems* (2016), ACM, p. 2.

[173] Ribas, D., Ridao, P., MagÃ, L., Palomeras, N., and Carreras, M. The Girona 500, a multipurpose autonomous underwater vehicle. In *OCEANS 2011 IEEE - Spain* (June 2011), pp. 1–5.

[174] Ribas, D., Ridao, P., and Neira, J. *Design and Development of the Ictineu AUV*. Springer Berlin Heidelberg, Berlin, Heidelberg, 2010, pp. 23–35.

[175] Ridao, P., Carreras, M., Ribas, D., and Garcia, R. Visual inspection of hydroelectric dams using an autonomous underwater vehicle. *Journal of Field Robotics 27*, 6 (2010), 759–778.

[176] Rodríguez, P., and Piera Fernández, J. Mini AUV, a platform for future use on marine research for the spanish research council? *Instrumentation ViewPoint, 2005, Autumn, núm. 4* (2005).

[177] Rosenberger, L. J. Pectoral fin locomotion in batoid fishes: undulation versus oscillation. *Journal of Experimental Biology 204*, 2 (2001), 379–394.

[178] Rudnick, D. L., Davis, R. E., Eriksen, C. C., Fratantoni, D. M., and Perry, M. J. Underwater gliders for ocean research. *Marine Technology Society Journal 38*, 2 (2004), 73–84.

[179] Russo, R., Blemker, S., Fish, F., and Bart-Smith, H. Biomechanical model of batoid (skates and rays) pectoral fins predicts the influence of skeletal structure on fin kinematics: implications for bio-inspired design. *Bioinspiration & biomimetics 10*, 4 (2015), 046002.

[180] Şahin, E. Swarm robotics: From sources of inspiration to domains of application. In *International workshop on swarm robotics* (2004), Springer Berlin Heidelberg, pp. 10–20.

[181] Şahin, E. Swarm robotics: From sources of inspiration to domains of application. In *International workshop on swarm robotics* (2004), Springer Berlin Heidelberg, pp. 10–20.

[182] Sahin, E., Girgin, S., Bayindir, L., and Turgut, A. E. Swarm robotics. *Swarm intelligence 1* (2008), 87–100.

[183] Sattar, J., Dudek, G., Chiu, O., Rekleitis, I., Giguere, P., Mills, A., Plamondon, N., Prahacs, C., Girdhar, Y., Nahon, M., and Lobos, J. P. Enabling autonomous capabilities in underwater robotics. In *2008 IEEE/RSJ International Conference on Intelligent Robots and Systems* (Sept 2008), pp. 3628–3634.

[184] Schill, F., Zimmer, U. R., and Trumpf, J. Towards optimal tdma scheduling for robotic swarm communication. *Proceedings Towards Autonomous Robotic Systems* (2005).

[185] Schmickl, T., Thenius, R., Moslinger, C., Timmis, J., Tyrrell, A., Read, M., Hilder, J., Halloy, J., Campo, A., Stefanini, C., et al. CoCoRo–the self-aware underwater swarm. In *Self-Adaptive and Self-Organizing Systems Workshops (SASOW), 2011 Fifth IEEE Conference on* (2011), IEEE, pp. 120–126.

[186] Schneider, S. H., and Mastrandrea, M. D. *Encyclopedia of Climate and Weather*, vol. 1. Oxford University Press, 2011.

[187] Schulz, B., Hobson, B., Kemp, M., Meyer, J., Moody, R., Pinnix, H., and Clair, M. S. Multi-UUV missions using ranger microUUVs. *Proc. Unmanned Untethered Submersible Tech* (2003).

[188] Sfakiotakis, M., Lane, D. M., and Davies, J. B. C. Review of fish swimming modes for aquatic locomotion. *IEEE Journal of oceanic engineering 24*, 2 (1999), 237–252.

[189] Shaari, M. F., Samad, Z., Jun, C., Husaini, A., and Omar, A. M. Conceptual design and preliminary analysis on bio-inspired squid micro AUV. In *Mechatronics and Automation (ICMA), 2013 IEEE International Conference on* (2013), IEEE, pp. 1594–1598.

[190] Sharma, K., Singh, S., Singh, N., and Kalla, A. Role of satellite remote sensing for monitoring of surface water resources in an arid environment. *Hydrological sciences journal 34*, 5 (1989), 531–537.

[191] Sherman, J., Davis, R. E., Owens, W. B., and Valdes, J. The autonomous underwater glider "spray". *IEEE Journal of Oceanic Engineering 26*, 4 (Oct 2001), 437–446.

[192] Shome, S., Sen, D., Biswas, D., Banerjee, D., Pankaj, A., Tyagi, A., and Raheja, L. Preliminary design of india's first AUV. *Advanced Manufacturing and Robotics* (2004), 141–148.

[193] Shtessel, Y., Edwards, C., Fridman, L., and Levant, A. Introduction: Intuitive theory of sliding mode control. In *Sliding Mode Control and Observation*. Springer, 2014, pp. 1–42.

[194] Slater, P., Pandey, M., and Sherbourne, A. Finite element analysis of buckling of corroded ship plates. *Canadian Journal of Civil Engineering 27*, 3 (2000), 463–474.

[195] Slotine, J.-J. E., Li, W., et al. *Applied nonlinear control*, vol. 199. Prentice hall Englewood Cliffs, NJ, 1991.

[196] Stephens, B., Azimi, P., Orch, Z. E., and Ramos, T. Ultrafine particle emissions from desktop 3d printers. *Atmospheric Environment 79* (2013), 334 – 339.

[197] Stilwell, D. J., and Bishop, B. E. Platoons of underwater vehicles. *IEEE control systems 20*, 6 (2000), 45–52.

[198] Stokey, R. P., Roup, A., von Alt, C., Allen, B., Forrester, N., Austin, T., Goldsborough, R., Purcell, M., Jaffre, F., Packard, G., et al. Development of the REMUS 600 autonomous underwater vehicle. In *OCEANS, 2005. Proceedings of MTS/IEEE* (2005), IEEE, pp. 1301–1304.

[199] Switchdoc. SunAirPlus solar power controller. Http://www.switchdoc.com/sunairplus-solar-power-controllerdata-collector/, 2015. [Online; accessed 17-Feb-2015].

[200] Tan, H.-P., Diamant, R., Seah, W. K., and Waldmeyer, M. A survey of techniques and challenges in underwater localization. *Ocean Engineering 38*, 14 (2011), 1663–1676.

[201] Tang, M., Zhang, Z., and Xing, Y. Analysis of new developments and key technologies of autonomous underwater vehicle in marine survey. *Procedia Environmental Sciences 10* (2011), 1992 – 1997.

[202] Teledyne Webb Research. Slocum Glider. Http://www.teledynemarine.com/slocum-glider, 2016. [Online; accessed 14-April-2016].

[203] the U.S. Navy. *The Navy Unmanned Undersea Vehicle (UUV) Master Plan.* November, 2004. [Online; accessed 18-Des-2016], Http://www.navy.mil/navydata/technology/uuvmp.pdf.

[204] Tian, B., Zhou, W., Li, L., and Yao, Z. Research on realization mechanisms of multifunctional hybrid glider. In *OCEANS 2016 - Shanghai* (April 2016), pp. 1–5.

[205] Tokiwa, Y., Calabia, B. P., Ugwu, C. U., and Aiba, S. Biodegradability of plastics. *International Journal of Molecular Sciences 10*, 9 (2009), 3722–3742.

[206] Tosik, T., and Maehle, E. Mars: A simulation environment for marine robotics. In *Oceans-St. John's, 2014* (2014), IEEE, pp. 1–7.

[207] Triantafyllou, M. S., and Triantafyllou, G. S. An efficient swimming machine. *Scientific american 272*, 3 (1995), 64–71.

[208] Uhrich, R., and Watson, S. Deep-ocean search and inspection: Advanced unmanned search system (auss) concept of operation. Tech. rep., DTIC Document, 1992.

[209] Ulsoy, A. G., Peng, H., and Çakmakci, M. *Automotive control systems*. Cambridge University Press, 2012.

[210] Ultimaker. Software-all platforms. Http://ultimaker.com/en/products/cura-software/, 2016. [Online; accessed 18-July-2016].

[211] Utkin, V. Variable structure systems with sliding modes. *IEEE Transactions on Automatic control 22*, 2 (1977), 212–222.

[212] Vaganay, J., Elkins, M., Esposito, D., O'Halloran, W., Hover, F., and Kokko, M. Ship hull inspection with the HAUV: US navy and NATO demonstrations results. In *OCEANS 2006* (Sept 2006), pp. 1–6.

[213] Vaidyanathan, S., and Lien, C.-H. *Applications of Sliding Mode Control in Science and Engineering*, vol. 709. Springer, 2017.

[214] Vasudev, K., Sharma, R., and Bhattacharyya, S. A multi-criteria decision based robust optimization model for design of AUVs. In *Proceedings of the 7th International Conference on Advanced Computing and Communication Technologies-India. ICACM (India)-2013. Inderscience, UK, ISBN* (2013), vol. 1152615797, pp. 7–12.

[215] Vasudev, K. L., Sharma, R., and Bhattacharyya, S. K. A CAGD+CFD integrated optimization model for design of AUVs. In *OCEANS 2014 - TAIPEI* (April 2014), pp. 1–8.

[216] Vieira, F. C., Medeiros, A. A. D., and Alsina, P. J. Position and orientation control of a two-wheeled differentially driven nonholonomic mobile robot. In *ICINCO (2)* (2004), pp. 256–262.

[217] Vogel, S. *Life's devices: the physical world of animals and plants*. Princeton University Press, 1988.

[218] Vogel, S. *Life in moving fluids: the physical biology of flow*. Princeton University Press, 1994.

[219] von Alt, C. Autonomous underwater vehicles. In *Autonomous Underwater Lagrangian Platforms and Sensors Workshop* (2003), vol. 3.

[220] Von Kármán, T. *Aerodynamics: Selected Topics in the Light of Their Historical Development*. Dover Books on Aeronautical Engineering Series. Dover Publications, 2004.

[221] Vukić, Z., and Mišković, N. State and perspectives of underwater robotics-role of laboratory for underwater systems and technologies. *Pomorski zbornik*, 1 (2016), 15–27.

[222] Walchko, K. J., Novick, D., and Nechyba, M. C. Development of a sliding mode control system with extended kalman filter estimation for subjugator. *Con. on Recent Advances in Robotics, Florida* (2003).

[223] Walker, D. Micro autonomous underwater vehicle concept for distributed data collection. In *OCEANS 2006* (Sept 2006), pp. 1–4.

[224] Webb, D. C., Simonetti, P. J., and Jones, C. P. SLOCUM: an underwater glider propelled by environmental energy. *IEEE Journal of Oceanic Engineering 26*, 4 (Oct 2001), 447–452.

[225] Wernli, R. L. AUVs-the maturity of the technology. In *OCEANS'99 MTS/IEEE. Riding the Crest into the 21st Century* (1999), vol. 1, IEEE, pp. 189–195.

[226] Westwood, J. The AUV market place. *Douglas-Westwood Ltd, Oceanology International, London* (2010).

[227] Whitcomb, L. L. Underwater robotics: out of the research laboratory and into the field. In *Proceedings 2000 ICRA. Millennium Conference. IEEE International Conference on Robotics and Automation. Symposia Proceedings (Cat. No.00CH37065)* (2000), vol. 1, pp. 709–716 vol.1.

[228] Whitcomb, L. L., Jakuba, M. V., Kinsey, J. C., Martin, S. C., Webster, S. E., Howland, J. C., Taylor, C. L., Gomez-Ibanez, D., and Yoerger, D. R. Navigation and control of the nereus hybrid underwater vehicle for global ocean science to 10,903 m depth: Preliminary results. In *2010 IEEE International Conference on Robotics and Automation* (May 2010), pp. 594–600.

[229] Wikipedia. Shovelnose guitarfish — Wikipedia, the free encyclopedia. Http://en.wikipedia.org/w/index.php?title=Shovelnose%20guitarfish&oldid=790332930, 2015. [Online; accessed 27-July-2015].

[230] Wildscreen Aktive. Guitarfish. Http://www.arkive.org/shovelnose-guitarfish/rhinobatos-productus/, 2015. [Online; accessed 02-July-2015].

[231] Wilga, C. D., and Motta, P. J. Feeding mechanism of the atlantic guitarfish rhinobatos lentiginosus: modulation of kinematic and motor activity. *Journal of Experimental Biology 201*, 23 (1998), 3167–3183.

[232] Williams, S. B., Pizarro, O., Webster, J. M., Beaman, R. J., Mahon, I., Johnson-Roberson, M., and Bridge, T. C. L. Autonomous underwater vehicle-assisted surveying of drowned reefs on the shelf edge of the Great Barrier Reef, Australia. *Journal of Field Robotics 27*, 5 (2010), 675–697.

[233] Wilson, R. A., and Bales, J. W. Development and experience of a practical, pressure-tolerant, lithium battery for underwater use. In *OCEANS 2006* (2006), IEEE, pp. 1–5.

[234] Woithe, H. C., Chigirev, I., Aragon, D., Iqbal, M., Shames, Y., Glenn, S., Schofield, O., Seskar, I., and Kremer, U. Slocum glider energy measurement and simulation infrastructure. In *OCEANS 2010 IEEE - Sydney* (May 2010), pp. 1–8.

[235] Woithe, H. C., and Kremer, U. Trilobiteg: A programming architecture for autonomous underwater vehicles. In *ACM SIGPLAN Notices* (2015), vol. 50, ACM, p. 14.

[236] Wynn, R. B., Huvenne, V. A., Bas, T. P. L., Murton, B. J., Connelly, D. P., Bett, B. J., Ruhl, H. A., Morris, K. J., Peakall, J., Parsons, D. R., Sumner, E. J., Darby, S. E., Dorrell, R. M., and Hunt, J. E. Autonomous underwater vehicles (AUVs): Their past, present and future contributions to the advancement of marine geoscience. *Marine Geology 352* (2014), 451 – 468.

[237] Yan, E., Milewski, A., Sultan, M., Abdeldayem, A., Soliman, F., and Abdel Gelil, K. Remote sensing based approach to improve regional estimation of renewable water resources for sustainable development. In *Proceedings of US-Egypt workshop on space technology and geo-information for sustainable development, Cairo, Egypt* (2010), pp. 14–17.

[238] Yoerger, D., and Slotine, J. Robust trajectory control of underwater vehicles. *IEEE Journal of Oceanic Engineering 10*, 4 (1985), 462–470.

[239] Yoon, H. K., Son, N. S., and Lee, G. J. Estimation of the roll hydrodynamic moment model of a ship by using the system identification method and the free running model test. *IEEE Journal of Oceanic Engineering 32*, 4 (2007), 798–806.

[240] Yue, C., Guo, S., and Li, M. ANSYS FLUENT-based modeling and hydrodynamic analysis for a spherical underwater robot. In *2013 IEEE International Conference on Mechatronics and Automation* (aug 2013), Institute of Electrical and Electronics Engineers (IEEE).

[241] Yuh, J. Design and control of autonomous underwater robots: A survey. *Autonomous Robots 8*, 1 (2000), 7–24.

[242] Yuh, J., and Choi, H.-T. Unmanned underwater vehicles. *Wiley Encyclopedia of Electrical and Electronics Engineering* (2015).

[243] Yuh, J., Marani, G., and Blidberg, D. R. Applications of marine robotic vehicles. *Intelligent Service Robotics 4* (2011), 221–231.

[244] Zhang, Y., Wei, Y. G. H., Lou, L., Song, H., Yang, P., and Liu, C. Influence of water on underwater distance measurement by a laser range finder. In *OCEANS 2017 - Aberdeen* (June 2017), pp. 1–5.

[245] Ziegler, J. G., and Nichols, N. B. Optimum settings for automatic controllers. *trans. ASME 64*, 11 (1942).

[246] Zimmer, U. R., and Kottege, N. Acoustical methods for azimuth, range and heading estimation in underwater swarms. *Journal of the Acoustical Society of America 123*, 5 (2008), 3007.